UNCLASSIFIED

AD NUMBER

AD828853

LIMITATION CHANGES

TO:

Approved for public release; distribution is unlimited.

FROM:

Distribution: Further dissemination only as directed by Air Force Cambridge Research Labs., Bedford, MA, OCT 1967, or higher DoD authority.

AUTHORITY

AFCRL ltr 29 Apr 1969

THIS PAGE IS UNCLASSIFIED

AD No. AD828853
DDC FILE COPY

00088

AFCRL-67-0631

RESEARCH TOWARD FEASIBILITY OF AN INSTRUMENT FOR MEASURING VERTICAL GRADIENTS OF GRAVITY

Robert L. Forward

Principal Investigator

Hughes Research Laboratories
3011 Malibu Canyon Road
Malibu, California 90265

Contract No. AF 19(628)-6134

Project No. 8607
Task No. 860703
Work Unit No. 86070301

FINAL REPORT

Period Covered: 15 July 1966 through 14 September 1967

October 1967

Contract Monitor: David Anthony
Terrestrial Sciences Laboratory

This document may be further distributed by any holder only with specific prior approval of AFCRL (CRJL), L.G. Hanscom Field, Bedford, Massachusetts 01730

Prepared for

AIR FORCE CAMBRIDGE RESEARCH LABORATORIES
OFFICE OF AEROSPACE RESEARCH
UNITED STATES AIR FORCE
BEDFORD, MASSACHUSETTS 01730

DDC

Best
Available
Copy

Form 1473

(18) AFCRL-67-0631 (19)

(6) RESEARCH TOWARD FEASIBILITY OF AN INSTRUMENT FOR MEASURING VERTICAL GRADIENTS OF GRAVITY

(10) Robert L. Forward

~~Principal Investigator~~

Hughes Research Laboratories
3011 Malibu Canyon Road
Malibu, California 90265

(15) Contract No. AF 19(628)-6134

(16) AF [redacted] 8607

[redacted] 03

(17) 860703

Work Unit [redacted] 01

(9) FINAL REPORT.

[redacted] 15 Jul [redacted] 66 [redacted] 14 Sep [redacted] 67,

(11) Oct [redacted] 67 (12) 223p.

Contract Monitor: David Anthony
Terrestrial Sciences Laboratory

This document may be further distributed by any holder only with specific prior approval of AFCRL (CRJL), L.G. Hanscom Field, Bedford, Massachusetts 01730

Prepared for

AIR FORCE CAMBRIDGE RESEARCH LABORATORIES
OFFICE OF AEROSPACE RESEARCH
UNITED STATES AIR FORCE
BEDFORD, MASSACHUSETTS 01730

mlw

(172 600) DC

TABLE OF CONTENTS

SECTION PAGE

ABSTRACT

The theories for the determination of the Newtonian gravitation constant (G) and the earth's gravitational constant (GM) have been examined. Two experiments have been considered for determining the Newtonian constant, one of which appears to be capable of improving the accuracy of measurement of G by at least one order of magnitude. Measurement of GM by gradient techniques does not, however, appear to yield any improved accuracy.

Experimental tests have demonstrated that the rotating gravitational gradient sensor concept is capable of measuring static gravitational gradients in the 1 g environment of the earth and that the sensor designs have the accuracy needed for useful measurements (0.5×10^{-9} sec^{-2}). A design of a prototype transportable gradiometer system has been completed and a program for fabrication and test has been established.

A study of sensor applications indicates that these sensors can aid in airborne gravimetry surveys by improving the guidance system performance and by obtaining a real time measurement of local gravity anomalies.

SECTION I

INTRODUCTION

The following were the three over-all objectives of the research work:

1. Design engineering plans and drawings for a transportable vertical gradiometer

2. Study the application of terrestrial vertical gravity gradients for the accurate determination of the earth's gravitational constant (GM)

3. Investigate experiments for the accurate determination of the Newtonian gravitational constant (G).

The people who devoted a significant percentage of their time to the contract are:

Principal Investigator	Dr. Robert L. Forward
Sensor Development Engineer	Mr. Curtis C. Bell
Analyst	Mr. David Berman
Electronic Engineer	Mr. Larry R. Miller
Application Studies	Mr. E. Hose
Designer	Mr. Stanley V. Pope
Technician	Mr. Donald D. Boswell
Geophysical Consultant	Prof. J. C. Harrison, U. of Colorado
Newtonian Experiment Consultant	Prof. Hermon M. Parker U. of Virginia

PRECEDING PAGE BLANK - NOT FILMED.

SECTION II

GRADIOMETER DESIGN

A gradiometer capable of measuring vertical gradients of the earth's gravitational force field has been designed. Experimental testing has been performed on a breadboard model of the sensor head, which demonstrated a calibration threshold limit of less than 0.2×10^{-9} sec^{-2} (0.2 E.U.). More importantly, the experimental tests also demonstrated that the rotating gravitational gradient sensor concept is capable of measuring static gradients in the noisy 1 g environment of the earth. The magnitude of static gradient signal measured in these tests was 600 E.U. The noise level was 200 E.U. and was primarily the result of stray magnetic fields coupling to the central flexure and electronic noise in the transmitter; both problems have been corrected in the prototype design. For a detailed discussion of the static tests, see Section V.

An investigation of internal mechanical noise generation in rotating gravitational gradient sensors has been completed and a Scientific Report on the work has been submitted (see Appendix A). The results of the analysis show that the sensor can be operated equally well on a stiff mount at a low rotation frequency and on a soft mount at a high rotation frequency. In addition, we found that it is necessary for three different fabrication errors to be present for internally generated noise to affect the gravity sensing mode of the sensor. The amount of noise generated depends upon the amount of rotor unbalance and the amount of bearing anisoelasticity. This noise affects the sensor in an amount proportional to the sensor construction errors. Our results indicate that the balancing requirements for 0.5 E.U. in a typical sensor are 0.02%; these are well within the capabilities of good mechanical design and fabrication techniques.

A 12-month prototype development program has been proposed which will result in an assembled vertical gravity gradiometer with suspension system and electronics capable of sensing vertical gradients in the low E.U. region. If desired, a continuation of this effort to include refinements in design should result in a sensor system which is capable of sensing 0.5 E.U. or better.

The vertical gradiometer design is discussed in Appendix B and the proposed prototype development program is discussed in detail in Section VI.

Considerations for gravity gradiometer application have established the need for predicting gradiometer response to mass distributions of particular interest. A digital computer program has been developed to simulate the rotating gravitational mass sensor, and to map the gradient contours of the gravitational field created by an arbitrary mass distribution (see Appendix C). The analysis in Appendix C demonstrates the interaction of the gradiometer with second and higher order gravitational gradients. The information about the mass distribution of an object was found to increase with the gradient order. This treatment gives a basic introduction to gravitational tensors as well as a mathematical formulation of the gradiometer model. Computer results are included which demonstrate the gravitational gradient contours associated with some selected mass distributions.

SECTION III

DETERMINATION OF THE EARTH'S GRAVITATIONAL CONSTANT (GM)

The investigation into the feasibility of utilizing vertical gravity gradients on the ground to determine the earth's gravitational constant (GM) has resulted in an essentially negative finding (see Appendix D). Despite some initial optimism expressed in Quarterly Status Report No. 1, the analysis has encountered the difficulty discussed in the Hughes proposal for this contract, i.e., that gravitational gradients come primarily from nearby objects. An analysis using a spherical earth would indicate that GM can be separated from R by measuring the gravitational acceleration $g = GM/R^2$ and its vertical gradient $\Gamma = 2\,GM/R^3$. However, the R measured by g is related to the radius of the earth, while the R in Γ is essentially the average radius of curvature of the earth at the point of measurement. This is only indirectly related to the over-all radius.

PRECEDING PAGE BLANK - NOT FILMED.

SECTION IV

DETERMINATION OF THE NEWTONIAN GRAVITATIONAL CONSTANT (G)

Scientific Reports have been written on experiments for determining the Newtonian gravitational constant G. The first experiment is a dynamic Cavendish experiment using two rectangular solids, one of which is rapidly rotating and the other suspended on a resonant mount. The second experiment uses a mass which oscillates inside a tunnel bored through a larger mass. The expected accuracies of the two experiments are compared with the present accuracy of G and the accuracy expected from the experiment conducted at the University of Virginia.

According to the NBS Technical News Bulletin, October 1963, the presently accepted value for the Newtonian gravitational constant is $6.670 \pm 0.015 \times 10^{-11}$ m^3 kg^{-1} sec^{-2} (three standard deviations), which indicates an accuracy of only one part in 500.

This value for the constant was obtained from the "time of swing" experiment of Heyl.* This experiment consists of two concentric torsion balances similar to those used in the Cavendish apparatus. One balance is held stationary while the other is excited into a pendulum torsional mode oscillation. When the two balances are aligned in parallel, the period of swing is less than when they are aligned at right angles. In the former position, the gravitational attraction between the two balances adds to the torsional spring restoring force; and in the latter position, it subtracts from it. The gravitational constant is obtained from measurement of the difference in periods between the near and far positions. The periods were on the order of a half hour, and could be measured to 0.1 sec.

A method of determining G to higher accuracy currently is being tested at the University of Virginia (see Appendix E). The experiment described in Appendix E is designed to improve the knowledge of G to one part in 10^4. With future versions, accuracies greater than one part in 10^5, and possibly one part in 10^6, should be attainable. This experiment also consists of two concentric torsional balances. One balance is free to rotate under the attraction of the second, while the second is motor-driven and servo-controlled to maintain constant angular position with respect to the first. Hence, both balances will rotate through 360^o while a constant torque is being maintained on the free balance. The angular displacement, after many hours, determines the gravitational constant.

*P.R. Heyl, "A Redetermination of the Constant of Gravitation," Bur. Std. J. Res. 5, 1243-1290 (1930).

In trying to push the gravitational constant to higher accuracy, we ultimately approach the limitation of precision in the determination of mass separation distances and homogeneity of density within the masses themselves. It is these limitations that form the basis of discussion of the rotating flat plate experiment and the vertically tunneled sphere experiment.

A. THE ROTATING FLAT PLATE EXPERIMENT

The rotating flat plate experiment utilizes the gravitational interaction between two optically flat and parallel rectangular solids, one rotating at constant speed and the other suspended on a resonant mount (see Appendix F). In Appendix F we have established the experimental system schematic, which consists of (1) a torsional suspension system for the resonant plate, (2) a suspension system and drive for the rotating plate, (3) an optical detection system to measure angular deflection, and (4) a vacuum and external disturbance isolation system for the entire apparatus. We have also established that the gravitational interaction between the two plates is a second-order gravitational gradient and that the dynamic interaction will be at twice the rotation frequency. The magnitude of this gradient is on the order of 10 E.U., and depends only on the density of the plate for fixed dimension ratios. When all external disturbances are eliminated, the accuracy of the experiment is limited by internal thermal noise. For a plate of typical dimensions (50 x 5 x 0.5 cm) and a signal-to-noise of 10^6, a system time constant of half a day is required.

B. THE VERTICALLY TUNNELED SPHERE EXPERIMENT

The vertically tunneled sphere experiment is based on a suggestion of Professor J. W. M. DuMond of the California Institute of Technology. The experiment utilizes the fact that a mass moving freely through a tunnel bored in a sphere will oscillate about the midpoint of the tunnel at a period determined by the density of the sphere. To counteract the large forces of the earth in the vertical position, it is necessary to bore two tunnels and measure the net response of two masses suspended from the level arm of a balance. A measurement of the change in the period of the balance when the sphere is put in place will then be proportional to the density of the sphere. Limitations on the accuracy of the experiment will be in attainable tolerances in manufacture of the balance, sphere, and tunnels, as well as in detection of extremely small changes in period. The analysis indicates that inaccuracies in the manufacture of the experimental apparatus will introduce measurement errors of appreciable magnitude. It does not appear that this experiment, in the configuration analyzed, can significantly improve our knowledge of the Newtonian gravitational constant at this time (see Appendix G).

SECTION V

EXPERIMENTAL WORK

It was realized early in the study program that the cruciform sensor design developed earlier in a NASA program would not be suitable for a terrestrial vertical gradiometer because its four-arm, multiple piezoelectric transducer design made it susceptible to the 1 g acceleration field of the earth through nonlinearities in the transducers. We have therefore devised a two-arm torsional type sensor which has many advantages, such as easier balancing and matching of the mechanical components and a single torsional transducer for readout. We have analyzed the behavior of this type of sensor, studying various designs of the mechanical configuration and methods of balancing and matching.

Many elements of the gradiometer design require advances in the present state of the art, such as the magnetic support system and microdyne force measuring system; therefore, it was necessary for the development of the instrument to proceed along experimental as well as theoretical and design lines. During July through September 1967, a parallel experimental program was conducted to test the feasibility of a breadboard model of the torsional type sensor head. Funding for this experimental work was a separate general research program using company-owned equipment and hardware.

A torsional type sensor (Figure 1) was constructed and calibrated by means of our dynamic gravitational gradient generator (see Figure 2). Sensitivity of the sensor under these conditions was 16 nV/E.U. The measured threshold of the sensor was 0.2 E.U. The predominant noise sources observed were front end electronic noise and thermal noise (0.05 E.U.)

The sensor was then tested while rotating, and demonstrated for the first time an observable response to a static gravitational gradient field. The sensor was subsequently recalibrated with the dynamic gravitational gradient generator. The results of this calibration test verified that the sensor response was indeed due to gravitational excitation.

M 5704

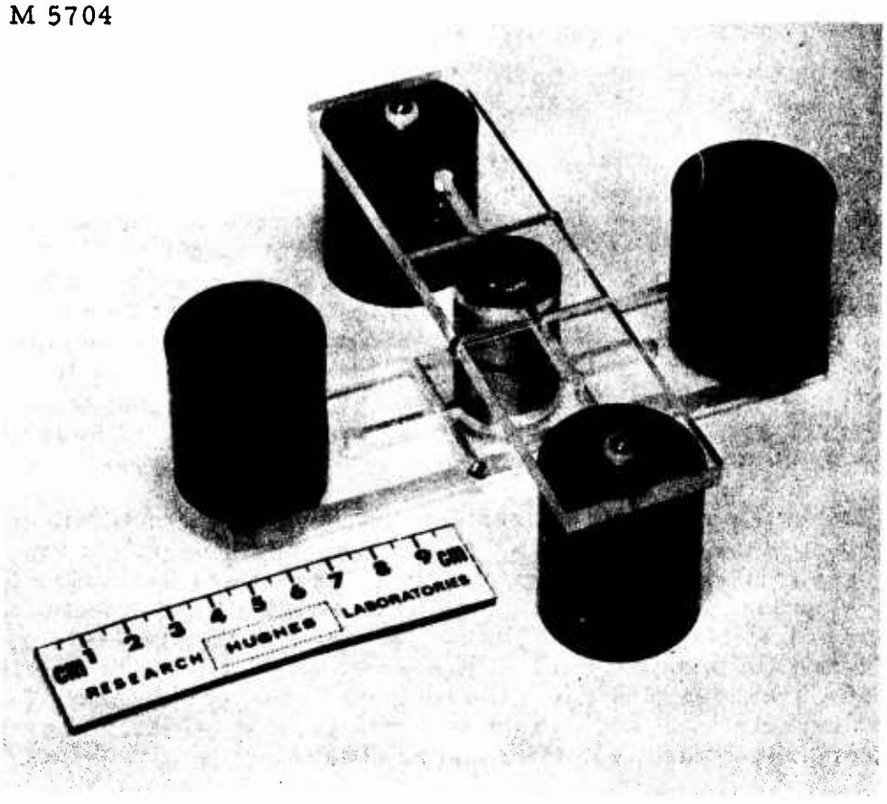

Fig. 1. Torsional sensor.

M 4181

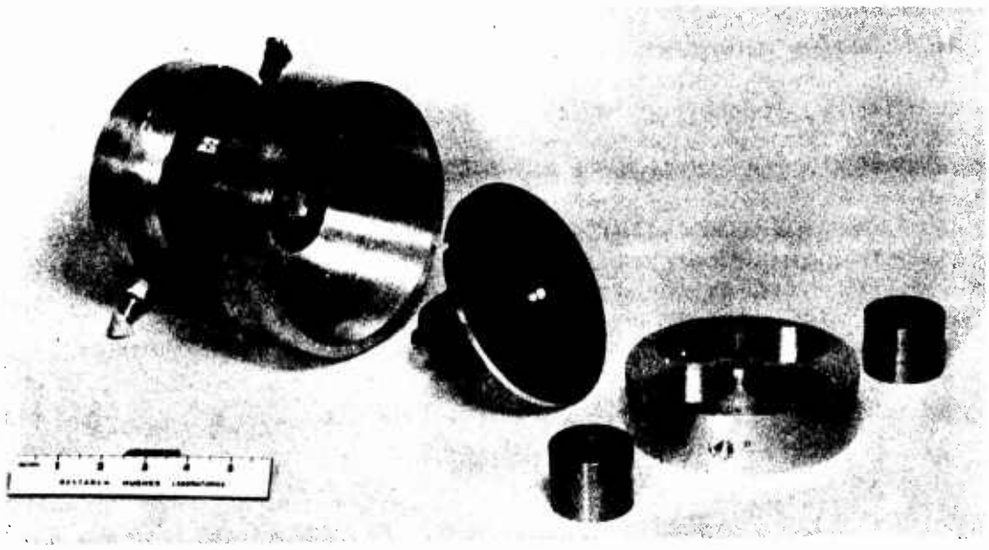

Fig. 2. Dynamic gravitational gradient field generator.

A. STATIC MASS TEST

The laboratory test of August 25 consisted of exciting the operating rotating gravitational gradient sensor by two 80 lb cylindrical lead test masses; each was at a radial distance of 26 cm from the center of the rotating gravitational gradient sensor, but on opposite sides. In this condition the gravitational gradients of the two masses add.

We define the static gradient excitation (Γ_s) as the calculated resonant mode gravitational torque produced by the test masses divided by the sensor moment of inertia. Γ_s is proportional to the gravitational gradient of the test masses and is given by

$$\Gamma_s = \frac{3GM}{R^3} \ (\text{sec}^{-2}) \qquad (1)$$

where G is the gravitational constant, M is the total test mass, and R is the distance between the sensor and each test mass.

The assumptions implied in eq. (1) are that the test masses lie in the plane of sensor rotation and that R is much larger than the sensor radius. Actual test conditions introduce errors of less than 1% in the above.

Using the values discussed above,

$$\Gamma_s = \frac{3(6.67 \times 10^{-8})(2 \times 80 \times 454)}{(26)^3} = 825 \text{ E.U.}$$

where $1 \text{ E.U.} = 10^{-9} \text{ sec}^{-2}$.

When these test masses were in the proximity of the sensor, the sensor output increased 15 ± 5 μV. The sensor scale factor of the static test k_s was, therefore:

$$k_s = \frac{15 \pm 5 \ \mu V}{825 \text{ E.U.}} = \boxed{18 \pm 6 \text{ nV/E.U.}}$$

The uncertainty of $\pm$ 5 μV (200 E.U.) in this test was primarily due to FM transmitter noise.

B. DYNAMIC CALIBRATION TEST

The dynamic calibration was performed by rotating two test masses under the (nonrotating) sensor. In the static test the sensor signal is broadcast through an FM transmitter to the signal analyzing electronics; in the dynamic test direct cabling is used.

A separate transmitter gain test was therefore performed to relate the instrumentation variation between the two gravitational tests. In this gain test the sensor was excited acoustically and output data were obtained for both transmitter instrumentation and cabled instrumentation.

Results of this test indicate that the transmitter instrumentation produces 3.1 times the output of the cabled instrumentation for the same input.

The equivalent gravitational excitation (Γ_d) in the dynamic gravitational test is given by

$$\Gamma_d \cong \frac{3\,GMd^2}{R^5}\left[1 + \frac{35}{12}\,\Lambda^2 + \frac{1155}{128}\,\Lambda^4\right] (\sec^{-2})^* \qquad (2)$$

where

$M \equiv$ total test mass

$d \equiv$ one-half the separation distance between the rotating test masses

$R^2 = d^2 + h^2 + \ell^2$

$h \equiv$ distance between plane of the sensor and plane of the test masses

$\ell \equiv$ sensor radius

$\Lambda = \ell d/R^2$.

For this calibration test

$M = 2 \times 1212$ g

$d = 4$ cm

$h = 7.5$ cm

$\ell = 6.35$ cm

---

*Robert L. Forward and L. R. Miller, "Generation and detection of dynamic gravitational gradient fields," J. Appl. Phys. 38, 512-518 (1967).

and the equivalent gradient excitation

$$\Gamma_d = \frac{3(6.67 \times 10^{-8})(2 \times 1212)(4)^2}{\left[(4)^2 + (7.5)^2 + (6.35)^2\right]^{5/2}} \left[1 + 0.17\right] = 65 \text{ E.U.}$$

The sensor output during this test was 340 nV or, related to the static test by the FM instrumentation gain, (340 x 3.1) = 1050 nV (equivalent). Therefore, the equivalent sensor scale factor (k_d) for the dynamic test is

$$k_d = \frac{1050 \text{ nV}}{65 \text{ E.U.}} = \boxed{16 \text{ nV/E.U.}}$$

The close agreement between the static and dynamic scale factors verifies that the sensor was indeed responding to the gravitational gradient field of the static test masses.

The high noise level observed in the static tests will be eliminated in the final design by means of an improved telemetry circuit. (See Figure 11 in Appendix B.) Additional noise resulting from magnetic interactions will be eliminated by replacing the steel flex pivot with a flexure made of quartz.

SECTION VI

CONCLUSIONS AND RECOMMENDATIONS

The studies of the experiments to determine the Newtonian gravitational constant (G) have demonstrated that improved precision of measurement is achievable. The analysis of the rotating flat plate experiment indicates that it is potentially capable of improving our knowledge of G by one to two orders of magnitude. Therefore, it is recommended that this experiment be investigated in further detail, both analytically and experimentally.

Although determination of the earth's gravitational constant (GM) does not appear feasible using gravity gradiometer techniques, the rotating gradiometer can be helpful in the field of airborne gravimetry as outlined in Appendix H. In addition, experimental tests have already demonstrated that the rotating gravitational gradient sensor is capable of measuring static gradients on the earth. It is therefore recommended that the vertical gradiometer design portion of the program be continued according to the proposed future program outlined in Section VII.

PRECEDING PAGE BLANK - NOT FILMED.

SECTION VII

PROPOSED FUTURE PROGRAM

We propose a 12-month experimental prototype development program for the fabrication and test of a transportable vertical gravity gradiometer, as outlined below and in Figure 3.

The program will begin with the manufacture of some prototype central flexures of quartz and/or beryllium copper. These flexures will be calibrated and tested using the breadboard torsional sensor arms already fabricated. Magnetic noise will be checked while running.

The Cambridge Thermionic Corporation has been requested to submit a quotation on a three-axis suspension system. Preliminary information has indicated an estimated cost of $40,000. This system will be ordered at the beginning of the contract.

Fabrication and assembly will then proceed on the sensor head vacuum chamber and telemetry. Careful dynamic calibration tests will be run and full calibration curves will be recorded.

The sensor head will then be mounted in its vacuum chamber and subjected to resonant torsional vibrational inputs. The quadrupole inertias will be adjusted to match both of the support spring-inertia ratios. This condition is indicated by a minimum response to torsional noise.

The sensor will then be tested for noise and gradient sensitivity while rotating in a horizontal plane. The data processing electronics will be manufactured and, upon receipt of the three-axis magnetic bearing, the entire system will be assembled, calibrated, and tested while rotating in a vertical plane.

Calibration threshold of the experimental prototype design using rotating proof masses will be less than 0.2×10^{-9} sec^{-2} (this threshold has already been reached in the breadboard model). The operating threshold of the experimental prototype should easily be better than 5×10^{-9} sec^{-2}. If desired, a continuation of the 12-month experimental prototype program to include design refinements based on experience gained in prototype fabrication should result in a sensor operating threshold approaching the calibration limit (0.2×10^{-9} sec^{-2}).

D702-1

TASKS	J	F	M	A	M	J	J	A	S	O	N	D	
MANUFACTURE OF PROTOTYPE FLEXURES	▲ BUY $4,000		▲ RECEIVE										
ASS'Y & TEST OF FLEXURES			1										
MANUFACTURE PROTOTYPE SENSOR HEAD ASS'Y	1	1											
ASSEMBLE TELEMETRY	1	1											
ASSEMBLE SENSOR			2	1									
TORSIONAL VIBRATION & INERTIA MATCHING				2	1								
CALIBRATION TESTS					2								
HORIZONTAL OPERATING TESTS						3							
PURCHASE 3-AXIS MAGNETIC BEARING	▲ BUY $40,000						▲ RECEIVE						
CHECK & TEST OF 3-AXIS MAGNETIC BEARING							2						
ASS'Y OF DATA READOUT ELECTRONICS	1	1	1	1	1	1	2						
ASS'Y OF SENSOR SYSTEM ON BEARING							1	2					
SYSTEM BALANCING								2					
SYSTEM CHECKOUT & CALIBRATION								1	2				
OPERATING TESTS									2	2			
FIELD TESTS & PACKAGING										1	2	2	
REPORTS												3	
	3	3	4	4	4	4	5	5	4	3	2	5	TOTALS
MTS	1	1.5	2.5	2.5	2.5	2.5	4	4	3	2	2	2	29.5
TE	1	1	1	1	1	1	1	1	1	1			10
GE	1	0.5	0.5	0.5	0.5	0.5						3	6.5

Fig. 3. Manloading schedule of prototype gradiometer development.

APPENDIX A

INTERNAL MECHANICAL NOISE GENERATION IN A ROTATING GRAVITY GRADIOMETER

(Prepared by D. Berman)

SUMMARY

A rotating gravity gradiometer measures the mass of an object by detecting its gravitational force gradient. If properly balanced, the device can demonstrate a high level of accuracy and sensitivity. Various unbalances in the gradiometer system give rise to internal mechanical noise. This paper identifies the major sources of unbalance and establishes the degree of manufacturing exactness required to control noise generation. The dynamic gradiometer is a rotating device and is subject to shaft translations caused by misalignment of the rotor and the rotating center of mass. An elliptical shaft translation will be induced by anisoelasticity in the gradiometer bearings. Such motion generates anomalous excitations by coupling through any further unbalance internal to the gravity sensitive mechanism. We have found that the internal mechanical noise is directly proportional to the product of these three unbalances. In addition, for operation above shaft resonance the noise coupling is independent of rotational speed. Below resonance, noise is proportional to the fourth-power of speed. Near future gradiometer application requires a gravitational gradient sensitivity level of 0.5 EU ($\sim 10^{-11}$ g/ft). Using presently available suspension, drive, and electronic systems, all three balancing requirements will lie between 0.1% and 0.01%.

I. INTRODUCTION

We are presently engaged in the design, construction, and test of a rotating gravity gradiometer for sensitive measurement of the earth's vertical gradient. These sensors can also be used on spinning lunar orbiters to measure the mass distribution of the moon, and on spinning deep space probes to measure the mass of the asteroids.

A rotating gradiometer can measure the mass of an object at a distance by using a rotating system of masses and springs to detect the gravitational force gradient field of the object.[1] The dynamic (or rotating) gradiometer, in its simplest form, consists of one or more low level accelerometers mounted to a rotating frame with the sensitive axes perpendicular to the centrifugal force.[2] When this is done, the output of the accelerometers will be found to contain dynamic components at multiples of the rotation frequency which are driven by the various gradients of the field. In particular, the components of the n^{th} order gradient, when examined in the rotating reference frame of a sensor, will be found to have time-varying coefficients which are at n times the rotational frequency of the sensor.[3] For example, if a simple spring-mass is rotated in a static gravitational field, the gravitational force gradient of the field (second rank gravitational tensor) will induce dynamic forces in the sensor with a frequency which is <u>twice</u> the rotation frequency of the sensor.[4]

The basic idea behind the operation of these sensors is an old one in electronics – the concept of chopping. This is used extensively in dc amplifiers, where the low level dc signal is chopped, transformed into an ac signal, and then amplified and measured by phase sensitive detectors. In the gravitational sensors, the chopping of the static gravitational field is accomplished by physically rotating the sensor so that its response to the gravitational field varies with time.[5]

Because the dynamic gradiometer is a rotating device, it has certain design problems common to a precision gyro, particularly noise generation caused by rotating unbalances. Indeed, of the several types of noise associated with the operation of a rotating gradiometer, internal mechanical noise is potentially the most limiting. Thermal and external mechanical noise can theoretically be separated from the gravity signal because it is random and thus phase-incoherent. Other types of nongravitational noise, such as acoustic and electromagnetic, can be eliminated by shielding. However, internal mechanical noise resulting from center of mass misalignments and bearing anisoelasticity is phase-coherent and at the same frequency as gravitational excitation (2Ω).

Internal mechanical noise is the result of the combination of the following three unbalances and is generated even if constant angular speed is maintained:

- Sensor head unbalance: Deviation between the geometric center of the sensor head and its center of mass
- Rotor unbalance: Deviation between the rotor geometric center and the center of mass of the entire suspended system
- Bearing unbalance: Circumferential variations in the stiffness of the bearing-shaft combination (anisoelasticity).

It is well known that when the geometric center and center of mass of a rotating body do not coincide, the geometric center will describe a circle in space. The radius of the circle will be defined by the frequency of rotation relative to the natural frequency of the shaft-suspension system. However, if there is any bearing unbalance such that the restoring force is not constant as a function of circumferential position, the path described will be elliptical rather than circular (Fig. A-1).[1] An elliptic motion can generate excitations in the rotating coordinate system of the sensor, which are at the same frequency as gravitational excitation. Any unbalances in gradiometer fabrication will allow this nongravitational noise to couple in and distort the gravity signal.

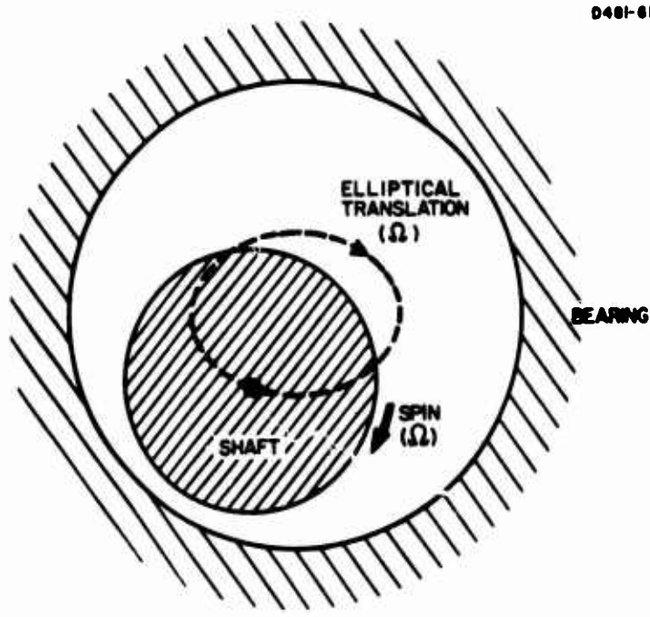

Fig. A-1. Elliptic motion of the shaft caused by bearing anisoelasticity.

The amount of coupling produced by the nongravitational forces on the sensor arms is a function of the sensor unbalance. An ideally balanced sensor will not respond to such forces.[7] The translational force is introduced to the arm through its geometric center. If its center of mass does not coincide, then the applied force resolves into a translational force at the center of mass plus a torsional couple. Thus, the mechanical noise is also a linear function of the deviation between the sensor center of geometry and center of mass.

In order to obtain the required accuracy and sensitivity of a gradiometer, all noise sources must be controlled to within a tolerable magnitude. The magnitude of the anomalous gravity signal generated by internal mechanical noise may be described in terms of an "equivalent" noise gradient. The equivalent gradient may be calculated as a function of rotational speed, suspension stiffness, and the three unbalance amplitudes. Optimum design parameters and their associated balancing requirements may then be selected to reduce the equivalent gradient below the gradiometer sensitivity requirement. For most potential applications this is 0.5 EU, which would allow a 0.02% measurement of the earth's gradient field of 3000 EU.

II. SYSTEM DESCRIPTION

The complete gradiometer system is divided into three basic areas: (1) sensor head (and housing); (2) suspension system, including shaft, bearing, and rotor; and (3) motor drive.

The sensor head of the torsional gradiometer, under development by HRL, is shown in Fig. A-2. It consists of two mass quadrupoles made of brass, which are connected internally by a magnetostrictive transducer and externally by two flexural pivots whose opposite ends are joined to a mechanical bridge between them. The sensor head is 4 to 5 in. in diameter and 1 in. thick. The overall length of the bridge is approximately 4 in. The dynamic torsional stress produced by gravitational forces acting on the sensor arms torques the magnetrostrictive wire and produces a proportional ac voltage across the coil surrounding the wire. The mechanical bridge connects to the bearing and associated support system. A housing surrounding the sensor head assembly will rotate with the sensor for windage reduction. The housing also provides electrostatic and electromagnetic shielding for the sensor.

The sensor head, housing, and associated electronics are mounted on a three-axis magnetic bearing support and drive system which rotates the sensor smoothly and quietly at its operating speed. The rotation speed is controlled by a servo loop between a photoelectric pickoff on the rotor and the voltage control on the drive motor windings. The drive power is kept at a minimum to maintain constant angular velocity on the rotor. The power requirement of the bearing and drive motor will be approximately 30 W. This will provide rotation, and a support stiffness greater than 10,000 lb/in.

In developing a suspension system specifically for a gravity-gradient sensor, the principal problem is the avoidance of noise. Magnetic suspension systems are known to operate with less noise than either air or ball bearings and should compare in noise level only

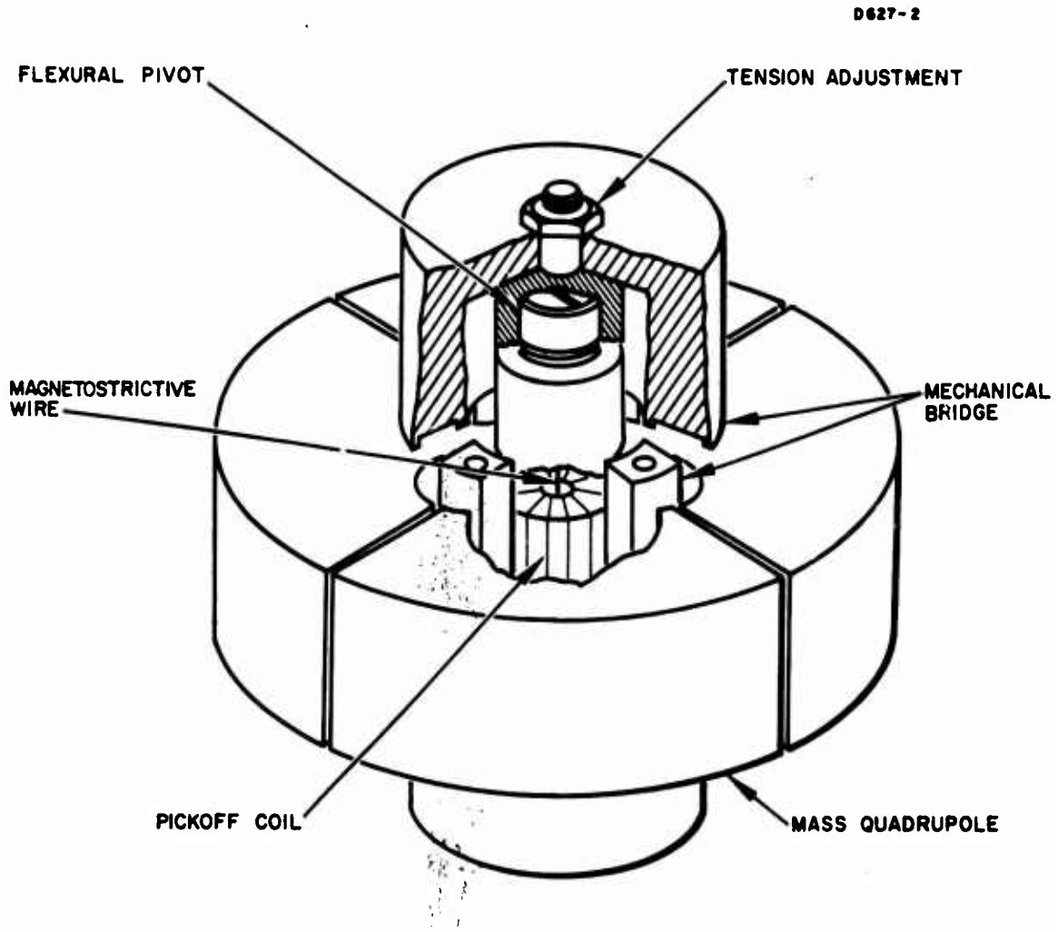

Fig. A-2. Torsional gradiometer sensor head. (Housing not shown.)

with electrostatic suspension. For a gravity-gradient sensor, the selected bearing must support 5 to 10 lb; this eliminates electrostatic bearings, which are inherently less noisy, because voltage breakdown in a vacuum system prohibits suspension of such weights.

In a magnetic bearing the shaft does not touch the outer race. The bearing mechanism consists of a magnetic field rather than solid, liquid, or gaseous bearing materials, so that full operation in a vacuum is practicable. Magnetic bearings eliminate mechanical friction and permit high speed operation over a wide temperature range. Because they do not use lubricants, they are particularly advantageous in environments which are hostile to lubricants, such as outer space.

Attachment of the drive mechanism to the shaft can be made in one of two ways: through a magnetic coupling of the motor, or a direct attachment of the armature to the shaft. Either of these will produce a satisfactory frictionless drive.

An assembled gradiometer prototype system is shown in Fig. A-3. The suspension, drive and housing are indicated; the sensor head itself cannot be seen inside the housing.

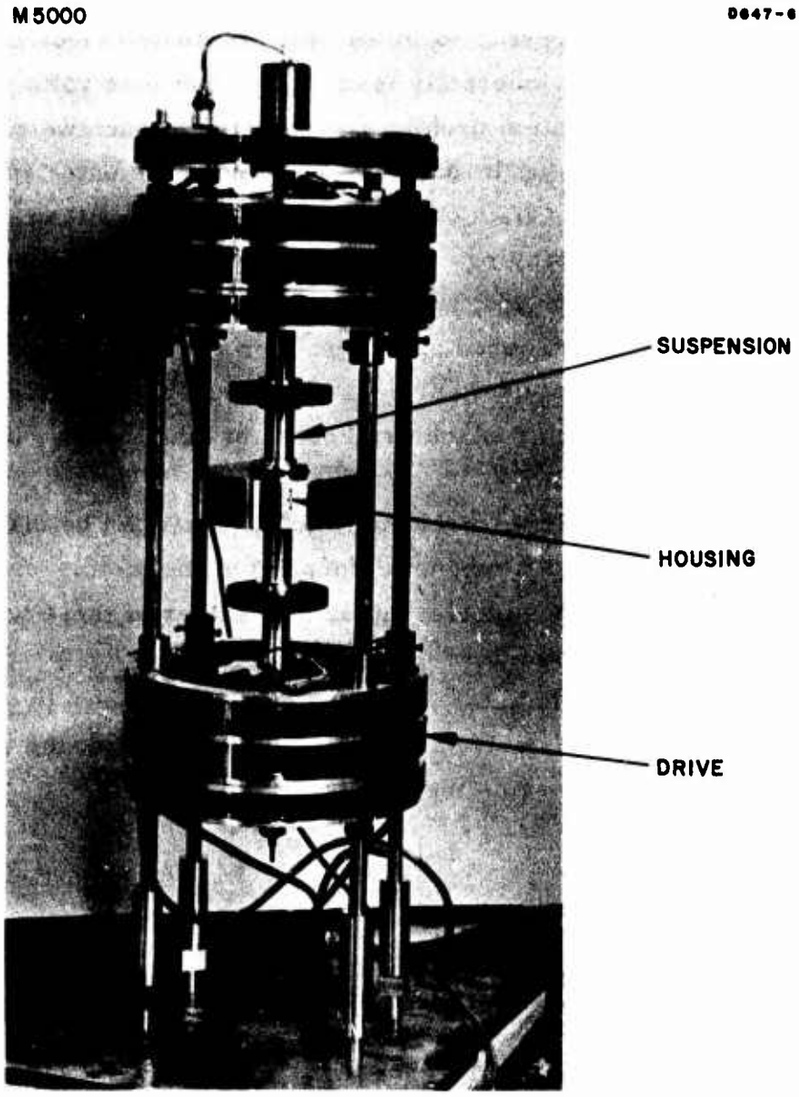

Fig. A-3. Assembled gradiometer prototype system, showing sensor housing, suspension, and drive.

III. MODEL AND COORDINATE SYSTEM

Figure A-4 is a schematic representation of the assembled gradiometer. A model of the sensor head consists of two rigid arms mounted perpendicularly on torsional springs. When they are rotated at constant angular speed, their relative motion responds ideally to the local gravitational gradient and rejects external accelerations. Also shown in the figure are the basic mechanical elements associated with suspension and drive of the gradiometer. A combination of unbalance in all of these elements gives rise to mechanical noise, as will be shown.

Figure A-5 is the coordinate system used to describe the dynamical behavior of the assembled gradiometer system. The x-y axes are fixed in space, and neither rotate nor translate. The w-z axes are attached to the housing, which rotates at constant angular speed Ω. The shaft-mounted housing also experiences a translation in the form of a negative circulation (a circular motion at the same frequency, but opposite direction of spin). The sensor head itself vibrates torsionally with respect to the rotating housing. Its displacement measured in the w-z frame is the angle α.

The sensor head therefore experiences three concurrent motions: rotation, circulatory translation, and vibration. Two of these motions are specified — rotation and translation.

The rotation is a constant spin Ω. In gradiometer operation, the platform is maintained at constant speed by external drive and servo-loop control. The translational motion is a constant negative circulation ($-\Omega$). A negative circulation will excite an unbalanced sensor head as if by a local gravitational gradient. Furthermore, any arbitrary or random motion can always be decomposed into components containing a negative circulation, Fig. A-6(a). In the case of an anisoelastic shaft, the motion will be elliptic. As will be shown later, an elliptic motion is completely described by one positive and one negative circulation.

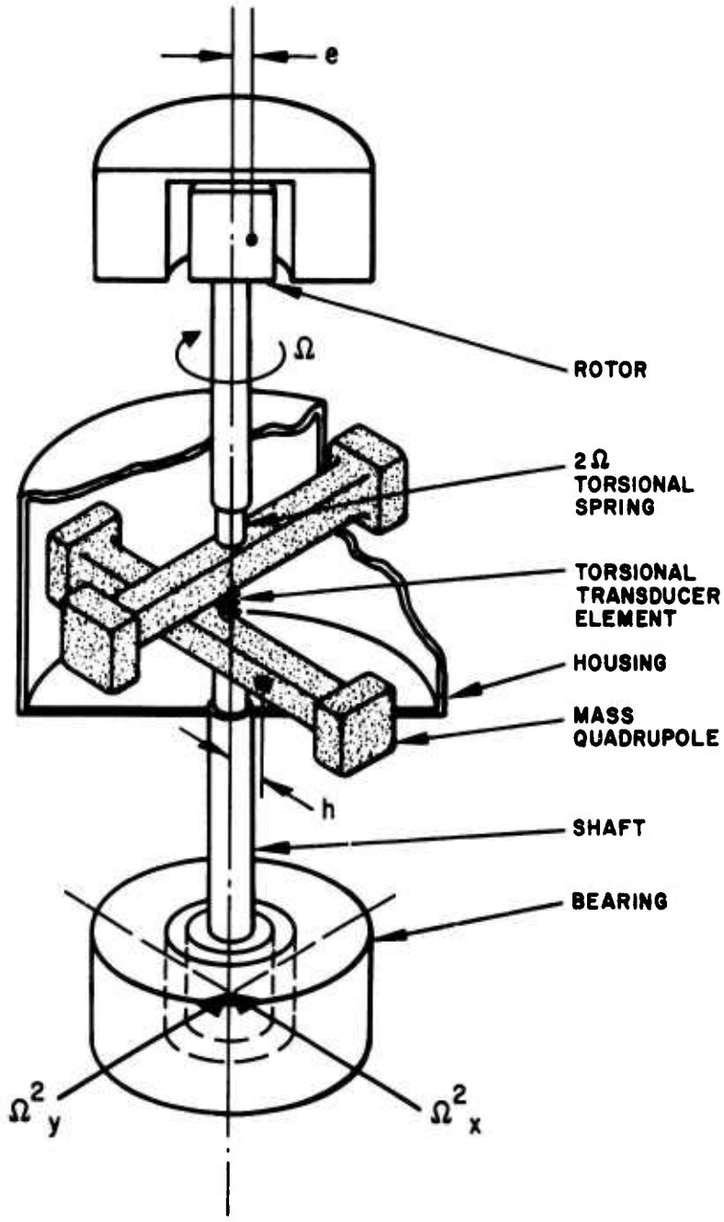

Fig. A-4. Schematic representation of rotating (torsional) gravity sensor and associated spin mechanism.

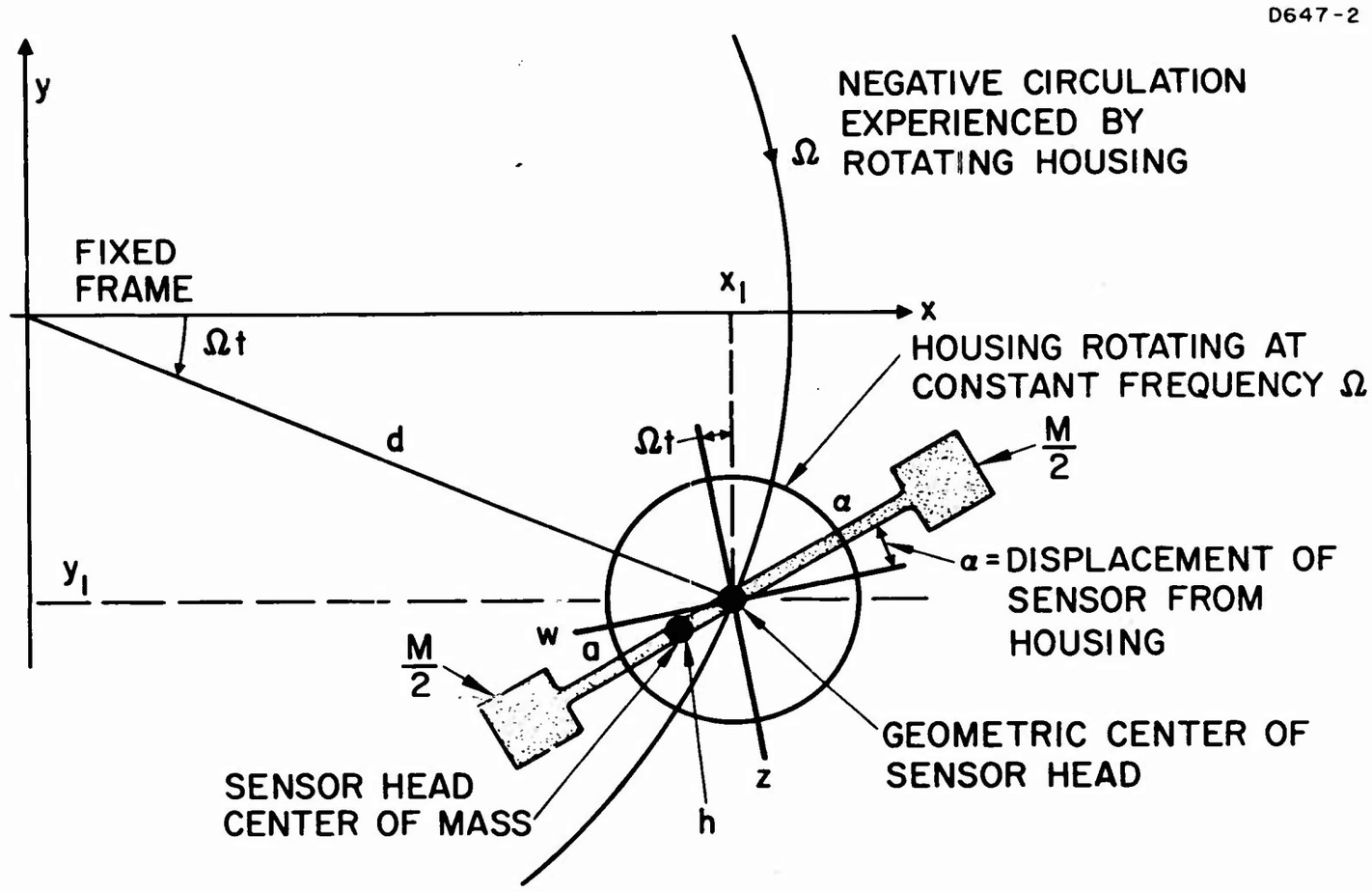

Fig. A-5. Coordinate system describing dynamic behavior of assembled gradiometer.

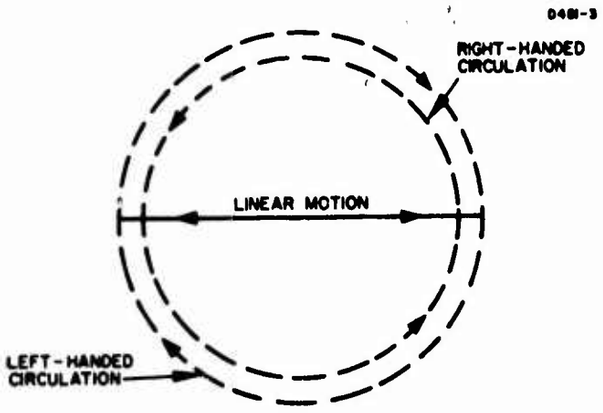

Fig. A-6(a)
Translational motion decomposes into right- and left-hand circulation.

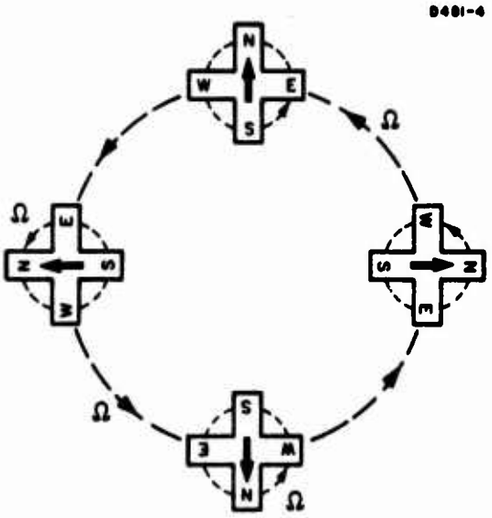

Fig. A-6(b)
Positive circulation produces no vibrational effect in rotating reference frame.

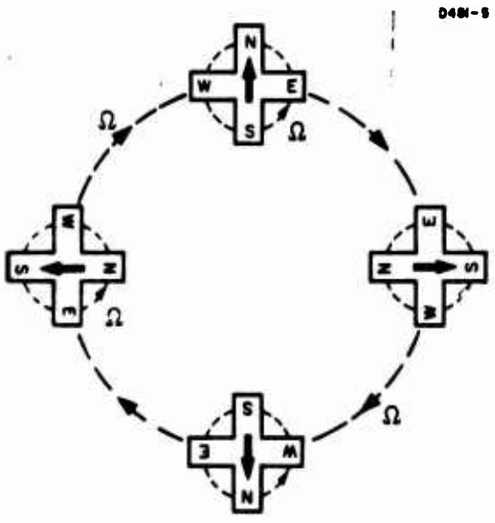

Fig. A-6(c)
Negative circulation induces a vibrational mode forcing function at twice the frequency of rotation.

The generation of anomalous gradiometer signals (or noise) from negative circulation components of translation is now demonstrated.[7] Figure A-6(b) and (c) shows the separate effects of (+) and (-) circulation on the sensor head. In the case of positive circulation, the force vector always points from S to N, regardless of the sensor orientation. The centrifugal force is constant in the rotating frame; therefore, positive circulation (of Ω) has no effect on sensor arm vibration. The arms merely experience a constant acceleration.

However, the negative circulation component is opposite to that of the spin, as shown in Fig. A-6(c). The induced force vector points sometimes from S to N and sometimes from N to S, depending on sensor orientation. In the sensor-fixed frame, the centrifugal force reverses direction twice during one complete cycle. Hence, a vibrational mode forcing function of frequency 2Ω is produced.

In ideal operation, the oscillatory displacement α of the sensor head with respect to the rotating housing is a measure of the local gravitational gradient. However, in the present case, the center of mass of the torsional sensor head does not coincide with its center of geometry. We define h as the deviation. We will shortly demonstrate that the magnitude of the anomalous gravity signal is proportional to h* (for a constant circulation).

The amount of negative circulation can be further related to the magnitude of other unbalances: rotor misalignment coupled with bearing anisoelasticity. We will separate the effects of these three unbalances by first treating the sensor head unbalance under application of a negative circulation of fixed radius d. We shall thereafter evaluate d in terms of shaft speed, natural frequency, and rotor and bearing unbalances.

---

*The sensor head actually undergoes a dual vibration of its two mass quadrupoles (Fig. A-2 or A-4), and the gravity signal is measured by their relative displacement. In the present discussion of noise, we may assume one quadrupole perfectly balanced. Otherwise, h represents the relative unbalance between the two quadrupoles.

PRECEDING PAGE BLANK - NOT FILMED.

IV. EQUATIONS OF MOTION

The equation of motion for the unbalanced vibrating sensor head, in the rotating frame and under application of negative circulation, is obtained most directly from the Lagrangian:

$$\frac{d}{dt}\left(\frac{\partial T}{\partial \dot{\alpha}}\right) - \frac{\partial T}{\partial \alpha} = F . \tag{1}$$

Here, T is the total kinetic energy of the vibrating sensor head and F represents the total forces (torques) applied. In operation, these forces contain the gravitational coupling and the torsion spring restoring and damping forces.

The total kinetic energy consists of translational energy of the center of mass, plus rotational energy about the center of mass:

$$T = \frac{M}{2}\left(\dot{x}^2 + \dot{y}^2\right) + \frac{I}{2}\left(\Omega + \dot{\alpha}\right)^2 \tag{2}$$

where M is the mass of the sensor head (half), and I is the moment of inertia of the sensor head about the axis of vibration. In order to facilitate the derivative operations in (1), we first express all variables in terms of α. The fixed x-y frame coordinates of the center of mass are related to the rotating-translating coordinate α by straightforward geometric considerations (see Fig. A-5):

$$\begin{aligned} x &= d\cos\Omega t + h\cos(\Omega t + \alpha) \\ y &= -d\sin\Omega t + h\sin(\Omega t + \alpha) \end{aligned} \tag{3}$$

with the corresponding velocity components:

$$\dot{x} = -\Omega d \sin \Omega t - h(\Omega + \dot{\alpha}) \sin(\Omega t + \alpha)$$

$$\dot{y} = -\Omega d \cos \Omega t + h(\Omega + \dot{\alpha}) \cos(\Omega t + \alpha) . \tag{4}$$

We may now write T completely in terms of α. Substituting (4) into (2) yields

$$T = \frac{1}{2}(I + Mh^2)(\Omega + \dot{\alpha})^2 + \frac{Md}{2}\left[\Omega^2 d - 2\Omega h(\Omega + \dot{\alpha}) \cos(2\Omega t + \alpha)\right] . \tag{5}$$

The required derivative operations then yield

$$\frac{\partial T}{\partial \dot{\alpha}} = (I + Mh^2)(\Omega + \dot{\alpha}) - M\Omega d h \cos(2\Omega t + \alpha)$$

$$\frac{d}{dt}\left(\frac{\partial T}{\partial \dot{\alpha}}\right) = (I + Mh^2)\ddot{\alpha} + M\Omega d h(2\Omega + \dot{\alpha}) \sin(2\Omega t + \alpha) \tag{6}$$

$$\frac{\partial T}{\partial \alpha} = M\Omega d h(\Omega + \dot{\alpha}) \sin(2\Omega t + \alpha) .$$

Substituting these expressions into (1) yields the exact equation of motion of sensor head vibration in the rotating and translating frame:

$$(I + Mh^2)\ddot{\alpha} + \Omega^2 d h M \sin(2\Omega t + \alpha) = F. \tag{7}$$

This describes the dynamic behavior of the gradiometer sensor head for constant angular speed Ω, a specified negative circulation d, and a center of mass misalignment h. No approximations have been made, and no higher-order effects have been neglected. Indeed, the results will shortly demonstrate that internal mechanical noise generation is a third-order unbalance effect. Thus it could not be identified at all if second and higher-order effects were neglected.

The moment of inertia I of the sensor head (see model, Fig. A-4) is

$$I = Ma^2 \tag{8}$$

where a is the radius. The modified moment of inertia implied by (7) may be rewritten

$$I' = Ma^2\left(1 + \frac{h^2}{a^2}\right) \quad . \tag{9}$$

Because the unbalances to be encountered will be very small ($< 1\%$), the effect of h in modifying I will be insignificant. Hence, we will neglect the slight change in I caused by the sensor head unbalance. Furthermore, the angular motion α of sensor head vibration is extremely minute, on the order of 10^{-10} rad. Therefore, it is a safe approximation to ignore the slight phase fluctuation implied in the right-hand side term of (7).

The extremely significant effect of the h-unbalance is disclosed by the second term in the left-hand side of (7). This term is driving the sensor head at its resonant gravity-sensitive frequency (2Ω), and will therefore cause an anomalous gradiometer reading. The effect will be demonstrated below.

To demonstrate the noise generating effect of the h-unbalance, we need to evaluate the generalized force F. Since α is an angle, F is a torque:

$$F/M = -\Omega_o^2 a^2 \alpha - \frac{\Omega_o}{Q} a^2 \dot{\alpha} - 3 a^2 \Gamma \sin 2\Omega t. \qquad (10)$$

In the above, the terms are, respectively, the sensor head torsional spring and damping forces, and the dynamic gravitational coupling force:

$\Omega_o \equiv$ sensor head torsional resonant frequency (2Ω)
$Q \equiv$ sensor head mechanical quality factor (amplification)
$\Gamma \equiv$ gravitational gradient (second order)*: Gm/R^3 for mass m at distance R
$G \equiv$ gravitational constant.

Substituting (10) into (7) yields (ignoring the slight moment of inertia and phase deviations, as discussed above)

$$\ddot{\alpha} + \frac{\Omega_o}{Q} \dot{\alpha} + \Omega_o^2 \alpha = -3 \left(\Gamma + \frac{\Omega^2 dh}{3a^2} \right) \sin 2\Omega t \qquad (11)$$

where we have divided by Ma^2.

Equation (11) dramatizes the influence of the sensor head unbalance (h) in producing an anomalous gravity signal. The gravitational gradient signal Γ at 2Ω is now directly coupled to a mechanical noise signal, which is proportional to both the sensor head mass unbalance and the magnitude of negative circulation. We can conveniently define the "equivalent" gradient Γ_e

*We are considering only noise in the measurement of the second-order gravitational gradient. There are really higher frequency components in F which correspond to higher-order gradients. The amplitude of these terms is much smaller than the second order gradient. Although these higher frequency terms are not disturbed by elliptical shaft translation, they would have noise due to nonlinearities.

$$\Gamma_e = \Omega^2 dh/3a^2 , \qquad (12)$$

which the gradiometer instrument would incorrectly read as a gravitational field.

The result of (12) is complete in that, for a given magnitude of negative circulation d, the required balancing h can be determined for any operational speed Ω. However, d is not an independent parameter, but also depends on rotational speed plus other unbalances. These additional unbalances are external to the sensor head, and are found in the gradiometer drive mechanism (see Fig. 4).

PRECEDING PAGE BLANK - NOT FILMED.

V. DYNAMICS OF SHAFT TRANSLATION

Rotating shaft behavior and the motion induced by rotor/bearing unbalances have received great attention. In particular, the motion of an unbalanced shaft rotating on anisoelastic bearings (with zero damping) has been previously derived[6]:

$$x_1 = \frac{er_x^2}{1 - r_x^2} \cos \Omega t$$

$$y_1 = \frac{er_y^2}{1 - r_y^2} \sin \Omega t . \qquad (13)$$

In (13), e represents the distance between the center of mass of the entire suspended shaft and the position of neutral rotor equilibrium; r_x and r_y are the inverse ratios of rotational speed Ω to the transverse components of the natural frequency of shaft suspension Ω_n:

$$r_x = \Omega/\Omega_x$$

$$r_y = \Omega/\Omega_y \qquad (14)$$

where we define a mean-square value:

$$\Omega_n^2 \equiv \Omega_x^2 + \Omega_y^2 . \qquad (15)$$

The anisoelastic shaft restoring force is shown in Fig. A-4, and the coordinates x_1 - y_1 are defined in Fig. A-5.

The trajectory described by (13) is an ellipse. As discussed above, this motion contains a negative circulation component. An elliptic motion can be decomposed into the sum of two circular motions: one positive of large amplitude, and one negative (opposite to the shaft rotation) whose amplitude is proportional to the unbalance (see Fig. A-6(a)). The component of negative circulation at 1 Ω converts into 2 Ω excitations in the rotating coordinate system of the sensor and can couple into the gravitational gradient excitation through any unbalances in gradiometer fabrication.

A positive circulation of amplitude p is expressed mathematically by

$$\begin{aligned} x_p &= p \cos \Omega t \\ y_p &= p \sin \Omega t \end{aligned} \tag{16}$$

and the negative circulation of amplitude d by

$$\begin{aligned} x_n &= d \cos \Omega t \\ y_n &= - d \sin \Omega t \ . \end{aligned} \tag{17}$$

If the net of these circulation motions is to produce the elliptical motion implied by (13), we must have

$$\begin{aligned} p + d &= e r_x^2 / \left(1 - r_x^2\right) \\ p - d &= e r_y^2 / \left(1 - r_y^2\right) \ , \end{aligned} \tag{18}$$

from which we obtain finally

$$d = \frac{e}{2} \ \frac{\left(r_x^2 - r_y^2\right)}{\left(1 - r_x^2\right)\left(1 - r_y^2\right)} \tag{19}$$

the amplitude of negative circulation.

Since the difference between the two transverse components of natural frequency will be small, we define

$$\Omega_x/\Omega_y \equiv 1 - \epsilon \tag{20}$$

where ϵ is the bearing anisoelasticity, or circumferential deviation in translational stiffness of the bearing plus shaft. Using (14), (15), and (20), eq. (19) becomes

$$d = e\,\epsilon \frac{\Omega^2/\Omega_n^2}{\left(1 - \Omega^2/\Omega_n^2\right)^2} \quad . \tag{21}$$

This expression for the amplitude of negative circulation is adequate to describe the translation of the shaft, so long as we do not allow the rotational speed Ω and natural frequency Ω_n to become comparable. In practice, this situation would always be avoided as a matter of routine. We thus consider the two regimes $\Omega < \Omega_n$ and $\Omega > \Omega_n$ and the corresponding solutions

$$d = \begin{cases} e\epsilon \dfrac{\Omega_n^2}{\Omega^2}, & \Omega_n < \Omega \\ \\ e\epsilon \dfrac{\Omega^2}{\Omega_n^2}, & \Omega_n > \Omega \quad . \end{cases} \tag{22}$$

We see from (22) that d always diminishes as the square of the frequency ratio, in either direction from the resonant condition. Thus, for operation above resonance, we would like to lower the resonant frequency as much as possible (soft-mount); below resonance, the bearings should be very stiff.

PRECEDING PAGE BLANK - NOT FILMED.

VI. EQUIVALENT GRADIENT

We are now in the position to return to (12) and express the equivalent gradient noise Γ_e completely in terms of gradiometer system unbalances: sensor head and rotor mass unbalance, and bearing anisoelasticity. Substituting (22) into (12) yields

$$\Gamma_e = \begin{cases} \frac{1}{3} \epsilon h e \Omega_n^2 , & \Omega > \Omega_n \\ \frac{1}{3} \epsilon h e \left(\frac{\Omega}{\Omega_n}\right)^2 \Omega^2 , & \Omega < \Omega_n . \end{cases} \tag{23}$$

We have dropped the factor of a^2, and will henceforth interpret both h and e as a fraction of sensor head radius. The mechanical noise is thus directly proportional to the product of the three unbalances. For the above resonance case ($\Omega > \Omega_n$), noise is independent of rotational speed and diminishes as the square of natural frequency. Below resonance ($\Omega < \Omega_n$), noise is an inverse function of natural frequency, and is also proportional to the fourth power of rotational speed.

To demonstrate the significance of these frequency regimes, we have plotted the complete equation (23) in Fig. A-7. For convenience, we have taken all of the unbalances to be identically equal to 0.01% (a lower limit on practical balancing capabilities). Hence, $e = h = \epsilon = 0.0001$. Equivalent gradient is plotted versus rotational speed, with natural frequency of suspension as a parameter. The peaks have been illustrated only to indicate to resonant condition. The actual shape of these peaks will depend on the damping characteristics of the suspension system (which are neglected in this analysis).

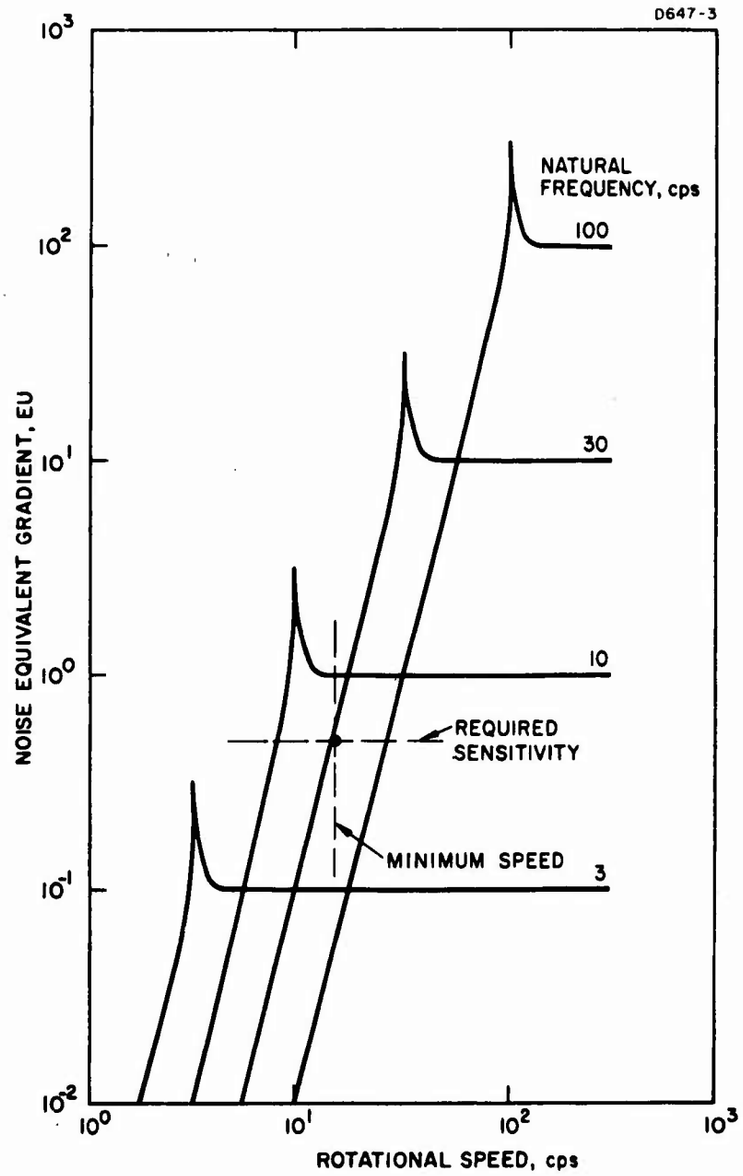

Fig. A-7. Mechanical noise generated by unbalances in gradiometer and drive mechanism: rotor bearing and gradiometer unbalances all equal to 0.01%.

For practical near future gradiometer applications, sensitivities of 0.5 EU will be required. In addition, a practical lower limit on operating frequency (because of electronic limitations) is 15 Hz. Using these values, we can obtain from Fig. A-7 the required natural frequency of shaft suspension for control of noise to below 0.5 EU. There are two answers: Ω_n = 5 Hz and 30 Hz. In other words, natural frequencies less than 10 Hz below rotation or greater than 15 Hz above rotation are satisfactory. In a practical situation, stiff support is more easily attainable. In fact, it is quite difficult to construct drive mechanisms of such low suspension stiffness as 5 Hz which would be practical for gradiometer application. Therefore, we may conclude that when possible, rotating gradiometers should be operated below the natural frequency of shaft suspension ($\Omega < \Omega_n$).

In Fig. A-7 all unbalances were assumed to be identically equal to 0.01%. It is of further interest to explore the actual balancing requirements for an optimum choice of rotational speed and natural frequency. We have seen in Fig. A-7 that the desirable mode of operation is $\Omega < \Omega_n$; therefore, the best condition is for the inequality to be maximized. The smallest practical value of rotational speed is Ω = 15 Hz, while the largest practical value for suspension frequency is Ω_n = 150 Hz. Using these values, and Γ_e = 0.5 EU, eq. (23) is plotted in Fig. A-8. The sensor head balance requirement is plotted versus maximum tolerable rotor unbalance; bearing anisoelasticity is the parameter. In Fig. A-8, the trade-off relationship among the various balancing requirements is demonstrated. For example, if bearing anisoelasticity of 0.001% could be achieved, the mass balancing requirements of both sensor head and rotor would be only 0.1%. On the other hand, if all unbalances are assumed identical, the mutual requirement is 0.02% as shown. This may be realized as a relaxation of the 0.01% mutual requirement corresponding to the suspension natural frequency of 30 Hz (Fig. A-7).

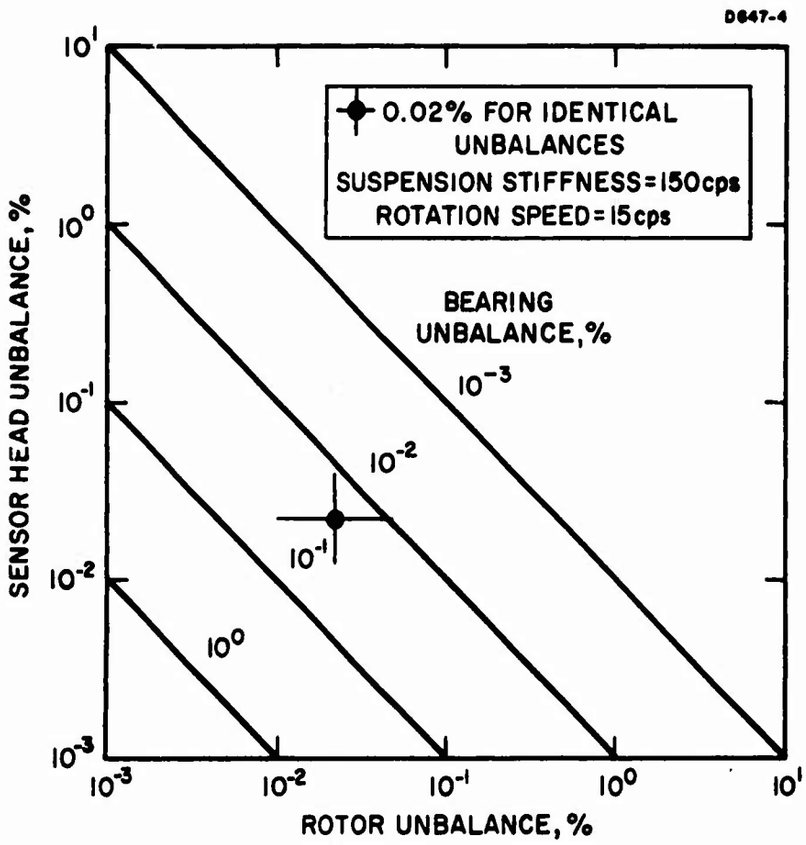

Fig. A-8 Gradiometer balancing requirement for control of internal noise generation to 0.5 EU.

To explore further the effect of natural frequency, we have plotted in Fig. A-9 the equivalent gradient Γ_e with mutual unbalance and natural frequency as variables. The rotational speed is constant at 15 Hz, while the unbalance is varied from 0.001% to 1%. The 0.5 EU requirement is shown, along with the corresponding 0.02% result at Ω_n = 150 Hz. From Fig. A-9, we observe that an order of magnitude increase in shaft suspension stiffness would be required to relax the 0.02% requirement to 0.1%. This is not feasible and balancing will need to be somewhat more critical than 0.1%.

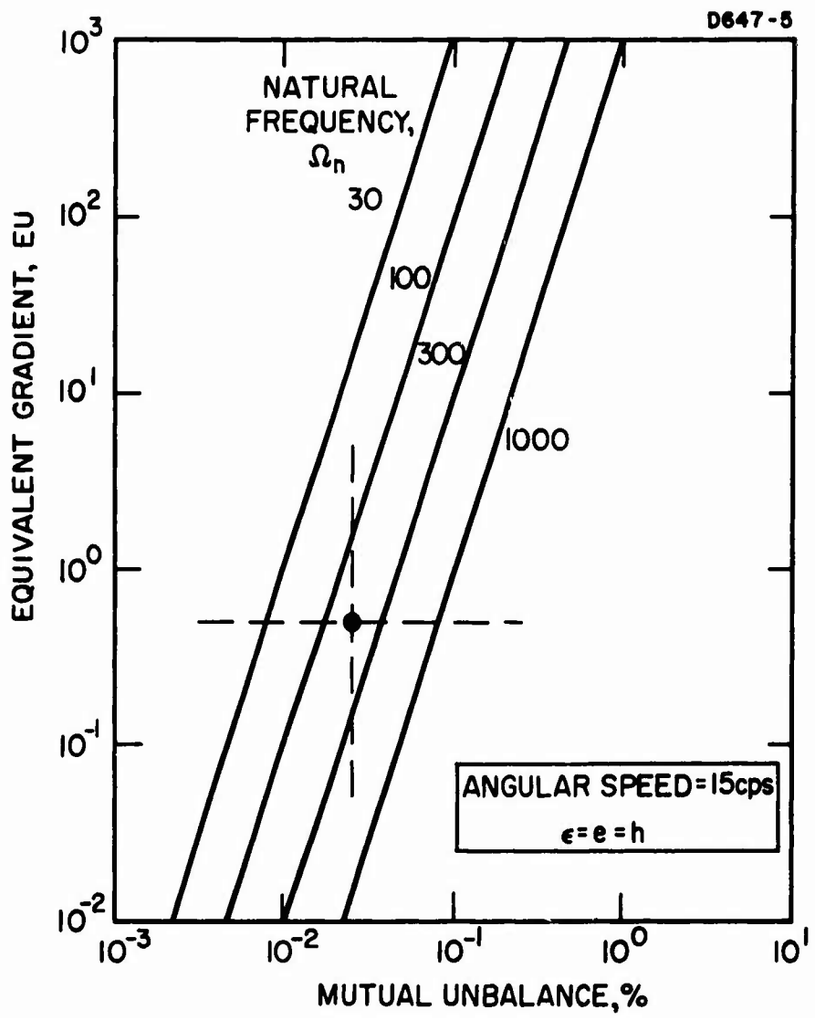

Fig. A-9. Mechanical noise generation versus identical unbalance magnitudes (angular speed = 15 cps).

VII. SUMMARY

The foregoing results demonstrate that the internal mechanical noise generation in a rotating gravity gradiometer is directly proportional to the product of three system unbalances. In addition, for operation above shaft resonance, the noise is independent of rotational speed. Below resonance, noise is heavily dependent on rotational speed, being proportional to the fourth-power.

We have established the balancing values required to control the anomalous instrument excitations to below 0.5 EU. Keeping within the practical ranges of rotational speed and shaft suspension, it is concluded that balancing to between 0.1% and 0.01% will be required. For the nominal values of 15 Hz rotational speed, and 150 Hz suspension frequency, the mutual requirement on all three sources of unbalance is 0.02%.

PRECEDING PAGE BLANK - NOT FILMED.

REFERENCES

1. R. L. Forward, "Gravitational Mass Sensor," Proc. 1963 Symposium on Unconventional Inertial Sensors, Farmingdale, New York, 18-19 November 1963; pp. 36-60.
2. J. W. Diesel, "A new approach to gravitational gradient determination of the vertical" AIAA J. 2, 1189 (July 1964).
3. R. L. Forward, "Rotating Gravitational and Inertial Sensors," AIAA Unmanned Spacecraft Meeting, Los Angeles, March 1965.
4. C. C. Bell, R. L. Forward, and J. R. Morris, "Mass Detection by Means of Measuring Gravity Gradients," AIAA paper No. 65-403, second annual meeting, July 1965, San Francisco.
5. R. L. Forward, "Rotating tensor sensors," Bull. Am. Phys. Soc. 9, 711 (1964).
6. F. S. Tse, I. E. Morse, and R. T. Hinkle, Mechanical Vibrations (Allyn and Bacon, Boston, 1963), Chap. V, p. 204.
7. D. Berman, "Nonideal Behavior of Rotating Gravitational Mass Sensors," AIAA J. 5, May 1967, pp. 1000-1008.

APPENDIX B

VERTICAL GRADIOMETER DESIGN EVALUATION REPORT

(Prepared by C.C. Bell)

SUMMARY

A rotating gravitational gradient sensor system has been designed which is capable of sensing the vertical gravitational gradient of the earth while operating on the earth's surface. The system consists of a torsional type sensor head, a magnetic support system, and associated telemetry and electronics. This report describes the considerations which went into the design choices, illustrates design features, and derives the magnitude of the noise errors present in the sensor design. Noise source analysis indicates an estimated error of 0.6×10^{-9} sec^{-2} rms (0.6 E.U.) for all noise sources for this initial prototype design.

SECTION I

INTRODUCTION

During the past year we have been engaged in work under Air Force Cambridge Research Laboratories Contract AF 19(628)-6134, "Research Toward Feasibility of an Instrument for Measuring Vertical Gradients of Gravity." We undertook the development of design engineering plans and drawings for a transportable vertical gravity gradiometer; it was desired that the instrument have the capability of attaining an ultimate accuracy and sensitivity of 0.5 E.U. (Eötvös unit = 10^{-9} sec^{-2}).

It was realized early in the study program that the cruciform design developed earlier in a NASA program would not be suitable for a terrestrial vertical gradiometer because its four arm, multiple piezoelectric transducer design made it susceptible to the 1 g acceleration field of the earth through nonlinearities in the transducers. We have therefore devised a two-arm torsional type sensor which has many advantages, such as easier balancing and matching of the mechanical components and a single torsional transducer for readout.

We have analyzed the behavior of this type of sensor, studying various designs of the mechanical configuration and methods of balancing and matching. We have constructed and operated breadboard models of these sensors which have detected the gravitational fields of nearby stationary masses, thus proving the feasibility of the concept, and have built and operated dynamic gravitational field calibration setups which have experimentally determined the threshold sensitivity.

Because many factors of the gradiometer design require advancement of the "state-of-the-art" (e.g., magnetic support system and microdyne force measuring system), the development of the instrument must necessarily proceed along experimental as well as theoretical and design lines.

Our current laboratory testing is directed toward measuring static gradients and comparing sensor response with the expected response based on sensor calibration tests.

Our laboratory test of August 25 demonstrated for the first time the response of our rotating gravitational gradient sensor to a static gravitational gradient field. To verify that the sensor response is a result of gravitational excitation, the sensor was subsequently calibrated with the dynamic gravitational gradient generator. The results of this calibration test verified that the sensor was indeed responding to gravitational gradient excitation.

The static gradient test consisted of exciting an operating rotating gravitational gradient sensor by two 80 lb cylindrical lead test masses, each at a radial distance of 26 cm from the center of the rotating gravitational gradient sensor but on opposite sides. In this condition the gravitational gradients of the two masses add.

Sensor scale factor as determined by the static gradient test was 18 ± 6 nV/E.U., while the dynamic calibration test indicated a scale factor of 16 nV/E.U. The noise level in the static tests was approximately 200 E.U., primarily as a result of FM transmitter noise. The transmitter has since been redesigned, and the new design is described in this report.

In line with the above discussion, the design of the vertical gradiometer is sufficiently flexible to accommodate modifications which may prove necessary as a result of later experimental work.

SECTION II

BASIC CONCEPT

The basic concept of the rotating gravitational gradient sensor is as follows. If a system of proof masses is rotated in the static gravitational field of an object, the gravitational force gradient of this field will induce dynamic forces on the proof masses with a frequency which is twice the rotation frequency of the system, while inertial effects caused by accelerations of the proof mass mounting structure will induce forces with a frequency at the rotational frequency. The strength and direction of the gravitational force gradient can be determined independently of the inertial forces by measuring the amplitude and phase of the vibrations induced in these proof masses at the doubled frequency. Analysis shows that the sensing of the gravitational gradient will still occur if the proof mass system is in free fall.

More specifically, the proof mass system used is a system of masses coupled together with springs in a geometry which becomes a rotating differential accelerometer.

Because of the tensoral nature of the gravitational gradient field, there are several different sensor geometries which could be used (see Figure B-1). These geometries fall into two basic types.

- Radial sensors – sensors which sense differential forces toward and away from the sensor axis of rotation (Figure B-1(a), (b)).
- Tangential sensors – sensors which sense differential forces in directions perpendicular to the sensor radius (Figure B-1(c), (d)).

The basic advantage of the tangential type of sensor over the radial is that the centrifugal reactions of the sensor masses are perpendicular to the vibrational direction of the spring, reducing any angular velocity-resonant frequency interactions of the sensor.

The pattern of tangential forces which occur at twice the rotational frequency is shown in Figure B-2 and is given by the following equations

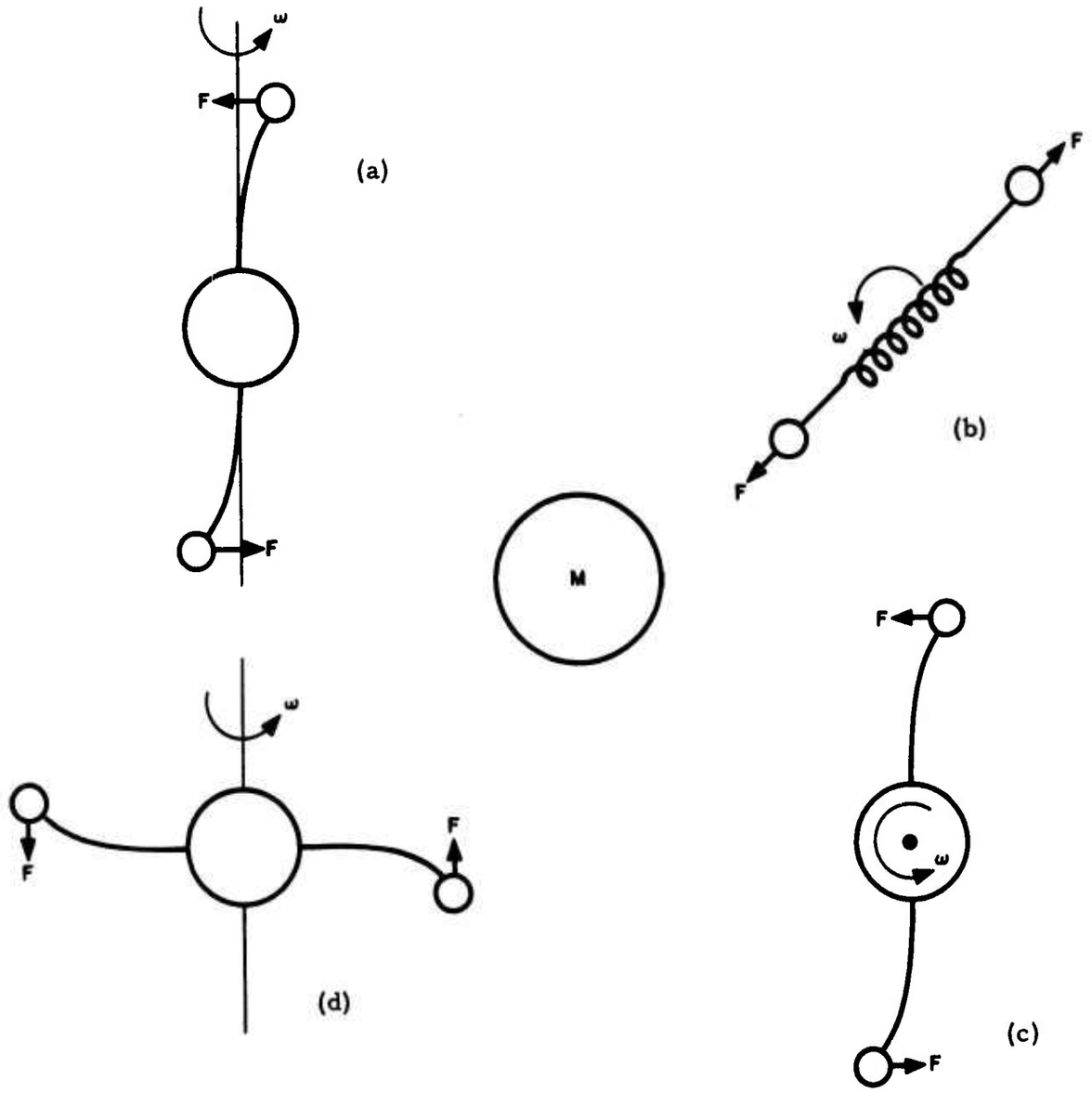

Fig. B-1. Possible sensor configurations.

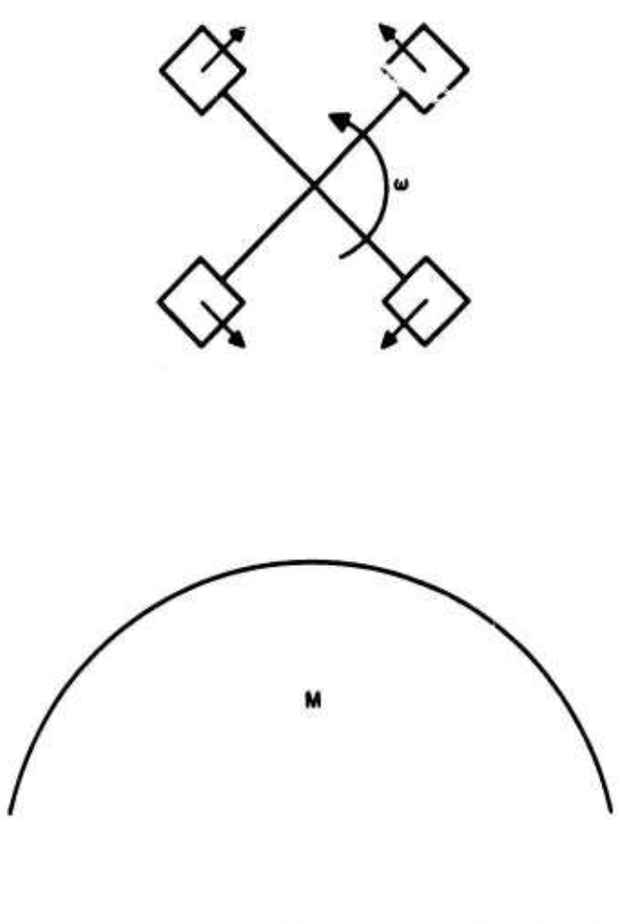

Fig. B-2. Phase of 2 ω tangential vibrations.

$$F_1 = F_3 = -\frac{3}{2}\frac{GM}{R^3} mr \sin 2\omega t \qquad (1)$$

$$F_2 = F_4 = +\frac{3}{2}\frac{GM}{R^3} mr \sin 2\omega t \qquad (2)$$

the positive forces are defined to cause positive (ccw) rotation and

m ≡ sensor end mass

ω ≡ sensor rotation speed

r ≡ sensor radius

$\frac{2GM}{R^3}$ ≡ radial gradient of the gravitational force field.

These forces are extremely small. For an input of $GM/R^3 = 10^{-9}$ sec^{-2}, a sensor end mass of 200 g and sensor radius of 2.5 in. (6.35 cm), these forces are 1.92×10^{-6} dyn each. The equivalent nonresonant angular displacement of the sensor arm in a sensor rotating at 15 cps is $\approx 10^{-13}$ rad. If the sensor is operated at resonance, these displacements of course will be increased by a factor of Q over the nonresonant response.

Tangential sensors may be further subdivided into two types, depending on the method of coupling between the end masses. The first type is the tuning fork, or cruciform, type of sensor shown in Figure B-3.

The coupling between the masses occurs in the connecting radii between the arms. The mode of vibration produced by the gravitational gradient forces is shown in Figure B-4(a). Figures B-4(b) and B-4(c) show two other modes of vibration which can occur in this type of design.

Although this type of sensor can be used for measuring gravitational gradients in free fall and for measuring horizontal gradients on the earth, it is not satisfactory for measuring vertical earth gradients. When the cruciform sensor is operated vertically, the vertical reactions of the supports generate forces of 8×10^5 dyn in the sensor translational mode at the frequency of rotation. Although response to this force theoretically could be filtered out, since it is not at the sensor gravitational response frequency, nonlinearities in the sensor

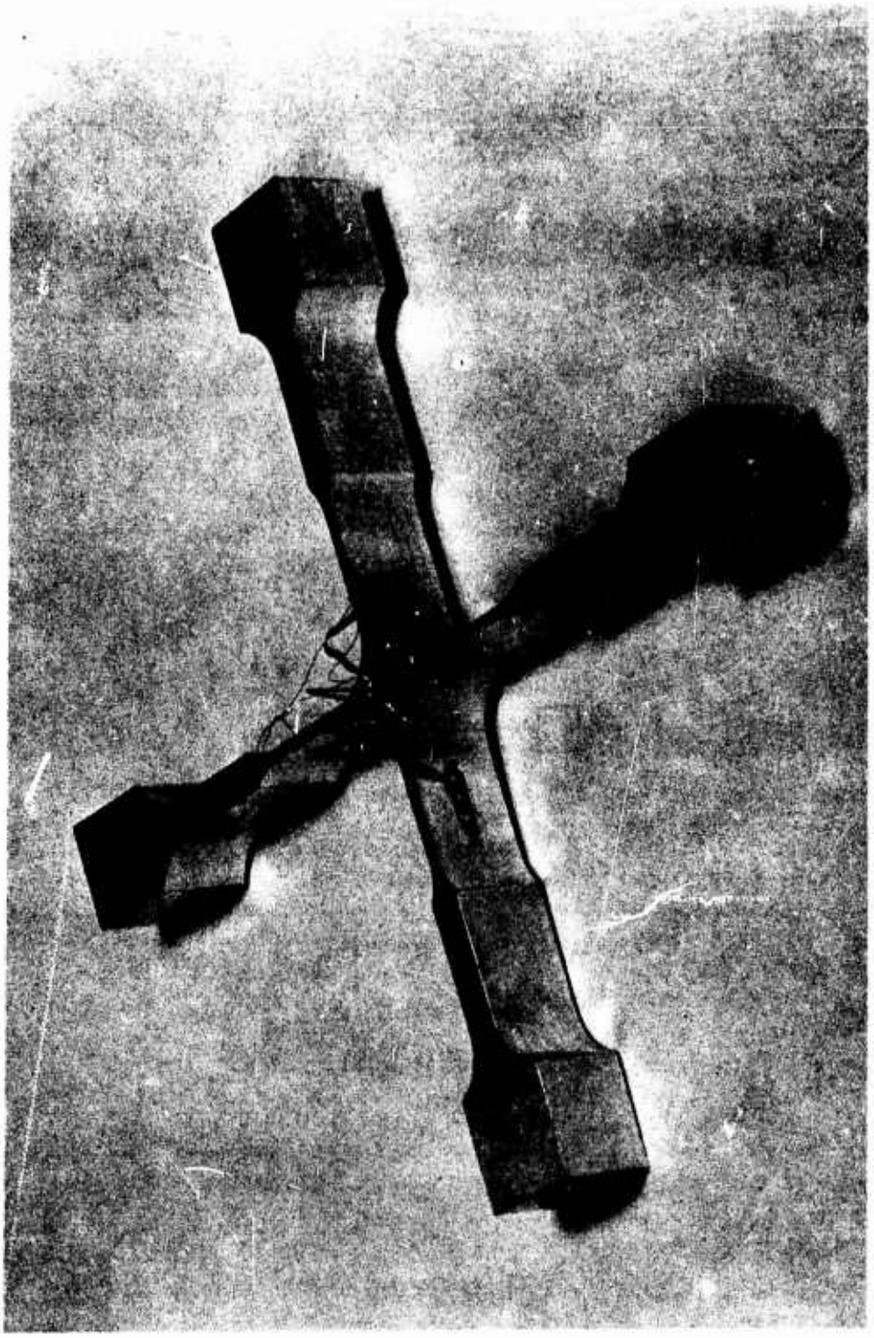

Fig. B-3. Cruciform sensor.

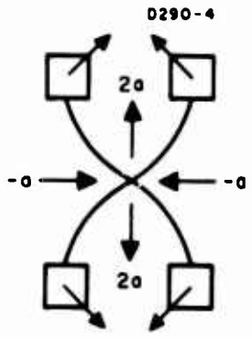

(a) gradient sensing

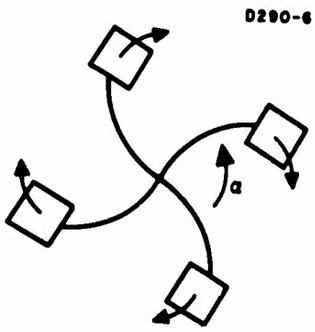

(b) rotational sensing

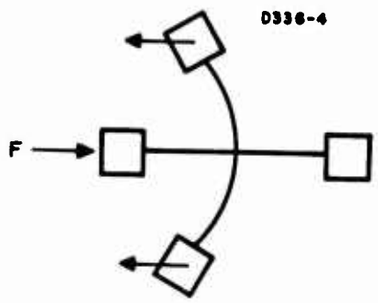

(c) translational sensing

Fig. B-4. Sensor vibrational modes.

pickoff and electronics will generate harmonics which are at the sensor response frequency. The nonlinearity of the electronics therefore would have to be held to approximately 1 part in 10^{11} to hold this noise smaller than a gradient signal of $GM/R^3 = 10^{-9}$ sec^{-2} (1 E.U.). This linearity requirement cannot be achieved with present electronic techniques.

The second type of tangential sensor, the torsionally resonant gradient sensor, is shown schematically in Figure B-5. It consists of two rigid mass quadrupoles oriented perpendicular to each other and connected at their centers with a torsionally flexible spring. When the sensor is rotated in the gravitational field of a test mass, the forces which occur between the quadrupole masses and the test mass produce torques which deflect one quadrupole with respect to the other, with restraint applied by the torsion spring.

The major advantages of this type of sensor over the cruciform type are

1. Use of a flexural member between the rigid mass quadrupoles, which is torsionally flexible but laterally rigid, assures a single mode of vibration which will be excited by gravitational gradients.

2. Use of a single flexural member coupling the quadrupoles allows the use of a single transducer and eliminates the need for matching of transducer elements.

3. A centrally located flexure with strain transducer located on the flexure itself provides the maximum strain available and consequently yields the maximum signal size.

This sensor will be made of low conductivity materials, with the central flexure made from fused quartz.

The analysis of the gravitationally induced forces is essentially the same as that for the forces produced in the cruciform type sensor. The sensor masses see gravitationally induced forces at frequencies which are 1, 2, 3, ... etc., times the rotation frequency Ω; the magnitude of the n^{th} harmonic is proportional to the n^{th} order gradient of the gravitational potential field.

Calculation of the torques on each of the quadrupoles results in cancellation of the fundamental rotation frequency and the third harmonic responses; the second harmonic torques T are found to be

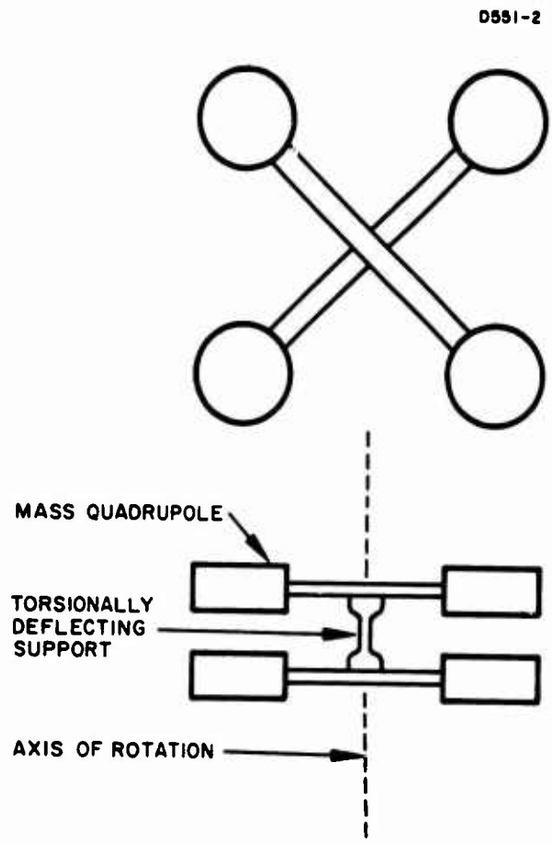

Fig. B-5. Schematic design of torsionally vibrating gradient sensor.

$$T = \frac{3GMmr^2}{R^3} \sin 2\Omega t \qquad (3)$$

where $(2GM/R^3)$ is the radial gradient of the gravitational force field, m is the end mass of the quadrupole, and r is the half-length of the quadrupole. Furthermore, the angular acceleration field produced is given by

$$\alpha = \frac{T}{I} = \frac{3GM}{R^3} \frac{mr^2}{2mr^2} \sin 2\Omega t = \frac{3}{2} \frac{GM}{R^3} \sin 2\Omega t \qquad (4)$$

where I (the quadrupole inertia) = $2mr^2$. If the sensor is made torsionally resonant at 2Ω, the angular deflection of the quadrupole from its neutral position is given by

$$\theta = \frac{\alpha Q}{(2\Omega)^2} = \frac{3GMQ}{8R^3\Omega^2} \sin 2\Omega t \qquad (5)$$

where Q is the quality factor of the sensor head and associated electronics.

The angle θ is extremely small. Surface gradients produced by the earth (3000×10^{-9} sec^{-2}) will produce angular responses of $\approx 5 \times 10^{-8}$ rad in typical torsional sensor designs (Q = 300, Ω = 80.6 rad/sec), while useful threshold signals of 10^{-9} sec^{-2} produce angular responses of $\approx 10^{-11}$ rad.

It is now necessary to transduce this mechanical motion into an electrical signal. Various types of signal transducers were considered in detail; among these were

1. Piezoelectric strain transducers
2. Magnetostrictive transducers
3. Capacitive transducers.

It was finally decided to continue the use of piezoelectric strain transducers (which were used in the cruciform sensors).

This is accomplished by using a flexural pivot as the torsional spring and affixing the strain transducer to one of the flexural spring leaves. An experimental model of this type of torsional sensor is shown in Figure B-6.

The voltage output from a piezoelectric transducer affixed to a flexural pivot is easily calculated from basic geometric considerations.

Consider one leaf of a flexural pivot which is being torqued through a total angle $2\theta_o$ (see Figure B-7). The leaf has a length λ and a thickness $2c$. When the leaf is fully flexed, it approximates an arc segment of a circle with a radius of curvature ρ (provided θ_o is very small). If we consider the centerline of the leaf as a neutral section, its length remains λ and is unstressed. However, the length of the top surface of the leaf is now $2\theta_o(\rho + c)$ and the tensile strain at this surface is

$$\epsilon = \frac{2\theta_o(\rho + c) - 2\theta_o\rho}{\lambda} = \frac{2\theta_o c}{\lambda} . \qquad (6)$$

From (5), however,

$$\theta_o = \frac{3}{2} \frac{GMQ}{R^3\omega_n^2} , \qquad (7)$$

where the resonant frequency $\omega_n = 2\Omega$; therefore,

$$\epsilon = \frac{3GMQc}{\lambda R^3\omega_n^2} . \qquad (8)$$

However, the gauge factor of the transducer is σ_g V/unit strain. Therefore, the voltage output of the sensor is

$$V = \frac{3Qc\sigma_g}{\lambda\omega_n^2} \left(\frac{GM}{R^3}\right) \text{ V/gauge} \qquad (9)$$

where (GM/R^3) is the gravitational force field gradient.

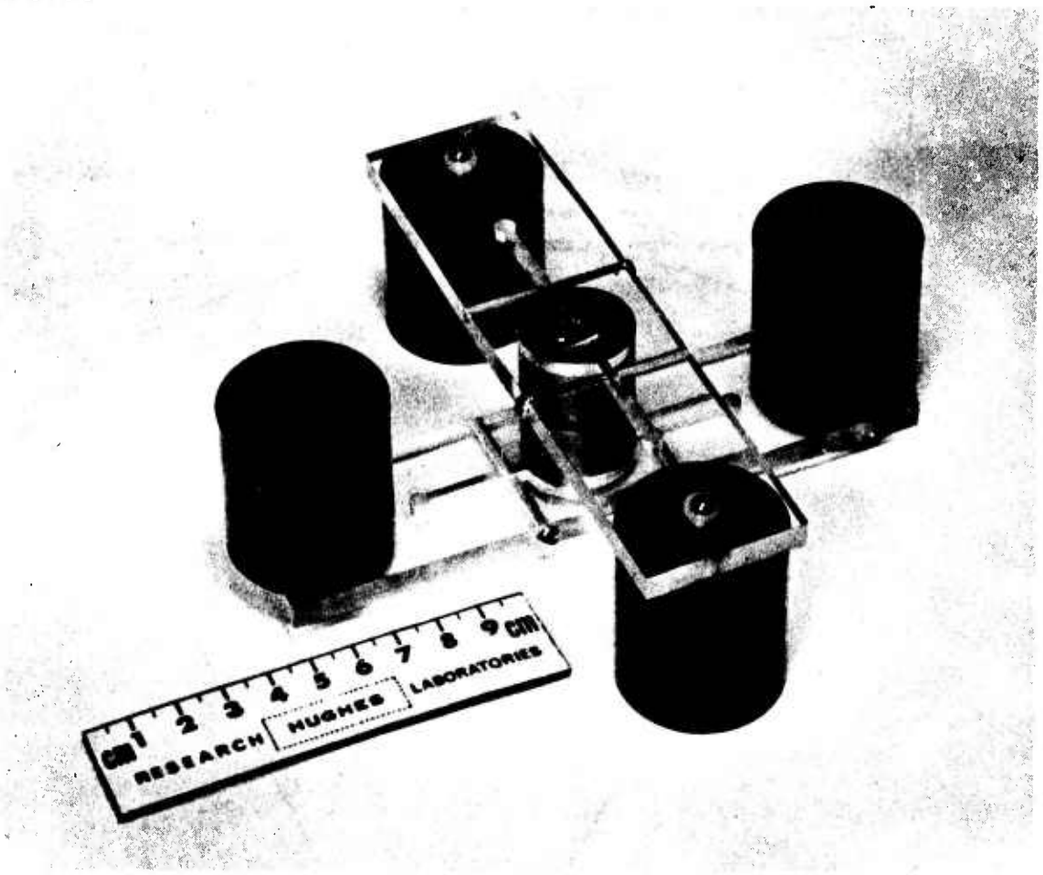

Fig. B-6. Torsionally resonant sensor experimental model.

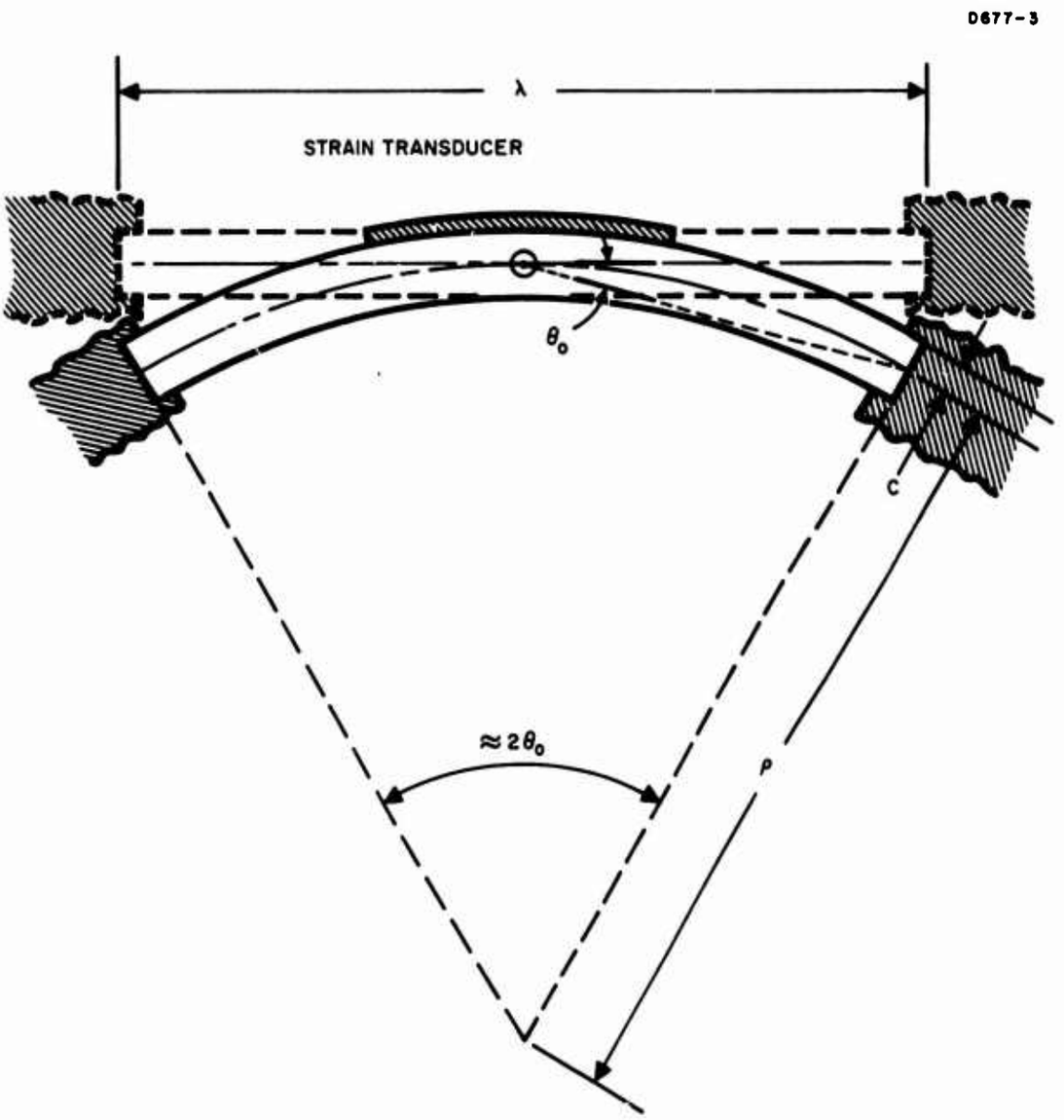

Fig. B-7. Flexural leaf bending.

The signal-to-noise energy ratio in a torsionally resonant gradient sensor is given by

$$S/N = \frac{I\omega_n^2\theta_o^2}{2\,kT} \quad ; \tag{10}$$

here kT is the thermal energy in the torsionally resonant mode and I is the total sensor head inertia. However, θ_o has been established as

$$\theta_o = \frac{3}{2}\,\frac{Q}{\omega_n^2}\,\frac{GM}{R^3} \quad . \tag{11}$$

Combining (10) and (11) and solving for (GM/R^3), therefore, we obtain

$$\frac{GM}{R^3} = \frac{2}{3}\,\frac{(S/N)^{1/2}\,\omega}{Q}\,\left(\frac{2kT}{I}\right)^{1/2} \quad . \tag{12}$$

$Q = (\tau\omega_n/2)$ and $I = 4mr^2 = m\ell^2$, and therefore

$$\frac{GM}{R^3} = \frac{4}{3}\,\frac{(S/N)^{1/2}}{\tau\ell}\,\left(\frac{2\,kT}{m}\right)^{1/2} \quad ; \tag{13}$$

here τ is the system integration time, ℓ is the center-to-center length of the quadrupole, m is a single end mass of the quadrupole, and (GM/R^3) is the minimum gradient which can be detected at the specified signal-to-noise ratio.

For the proposed torsional sensor $m = 200$ g, $\ell = 12.7$ cm, and if we assume $T = 100$ sec, $S/N = 1$, and $kT = 4 \times 10^{-21}$ J $= 4 \times 10^{-14}$ ergs, the threshold thermal noise gradient will be

$$\frac{GM}{R^3} = 5.33 \times 10^{-11}\ \text{sec}^{-2} \approx 0.05\ \text{E.U.} \tag{14}$$

This threshold can of course be improved by the use of longer integration times.

PRECEDING PAGE BLANK - NOT FILMED.

SECTION III

TORSIONALLY RESONANT GRADIENT SENSOR DESIGN

A. SYSTEM DISCUSSION

A block diagram of the complete sensor system is shown in Figure B-8. The system operates in the following manner.

The sensor head responds to the gradient of the gravitational force field through which it rotates. This response consists of minute torsional oscillations between the mass quadrupoles at twice the sensor head rotation frequency. These oscillations are detected through piezoelectric strain transducers affixed to the bending portion of the supporting flexure. The transducer signal is amplified through the low-noise preamplifier and is then used to drive the FM transmitter.

All of the above items rotate with the sensor head in an evacuated package supported by means of a separate three-axis magnetic suspension system.

The sensor head package is rotated at exactly one-half its resonant frequency by means of an asynchronous motor drive and servo system controlled by a precision reference oscillator. Sensor speed is monitored by a photoelectric pickoff and compared with the oscillator; drive oscillator voltages are then adjusted to maintain proper sensor speed.

The speed pickoff signal is also used as a frequency and phase reference for the sensor output signal which has been demodulated in the receiver and fed into the phase sensitive detector. Here the signal is filtered, matched against the reference voltage for frequency and phase, and time averaged over any specifically chosen time constant. A meter reads the voltage at the operating frequency, at any phase angle, and over any chosen integration time.

The signal amplitude read on the meter indicates the size of the gradient, while signal phase with respect to the speed reference indicates the direction of the gradient anomaly.

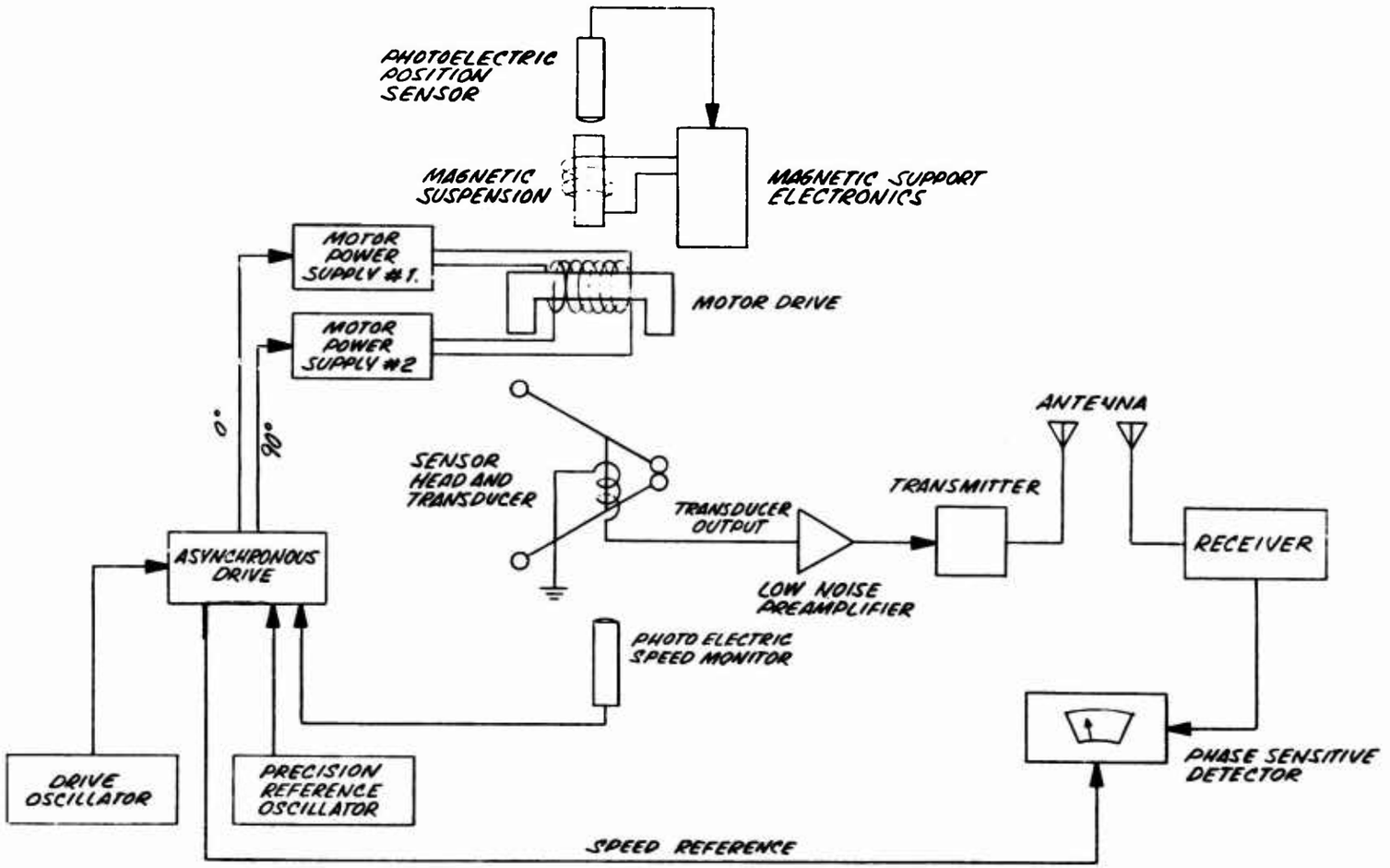

Fig. B-8. Block diagram of sensor system.

B. DETAILED DISCUSSION OF DESIGN

1. Mechanical

a. Sensor Head Assembly

The sensor head assembly is shown in Figure B-9. It consists of a central quartz flexure stack which supports two pairs of seismic masses. This central subassembly is in turn supported by two additional matched flexures to a solid supporting structure made up of four posts and two endplates. The central subassembly is non-metallic, to prevent interaction with magnetic gradient fields. The seismic masses are manufactured from a suspension of tungsten in plastic, maintaining the high density required for low thermal noise (see eq. (13)) and the high electrical resistance needed to eliminate eddy-current noise.

One or more barium titanate strain transducers are affixed to the flexing members of the central support. Torsional vibration between the two sets of masses therefore produce tensile and compressive strains in the transducers, and voltages are developed across the transducers. These voltages are then fed into the preamplifier.

b. Support and Drive System

The assembled mechanical system is shown in Fig. B-10. Here the sensor head assembly has been mounted in a vacuum chamber. The resonant circuit, preamplifier, and FM transmitter are also in this chamber but have been omitted in the drawing for clarity. The chamber is attached to a shaft supported radially by two soft iron pole-pieces which are magnetically centered by the radial positioning stators. In addition, the longitudinal position of the assembly is sensed by means of photocells No. 1 and No. 2, and servo-adjusted magnetically by the longitudinal positioning stator. The sensor rotation speed is detected by means of the speed monitoring photocell, and maintained by correction torques from the drive motor stator. The entire sensor system shown is inside a second vacuum chamber to eliminate windage on the rotor. The rotor and shaft assembly is dynamically balanced while supported in its own suspension to 0.000005 in. center of mass runout. Bearing elasticity is held constant in the radial directions to within 0.1%.

The magnetic support system will be subcontracted to the Cambridge Thermionic Corporation, a company specializing in commercial magnetic support systems.

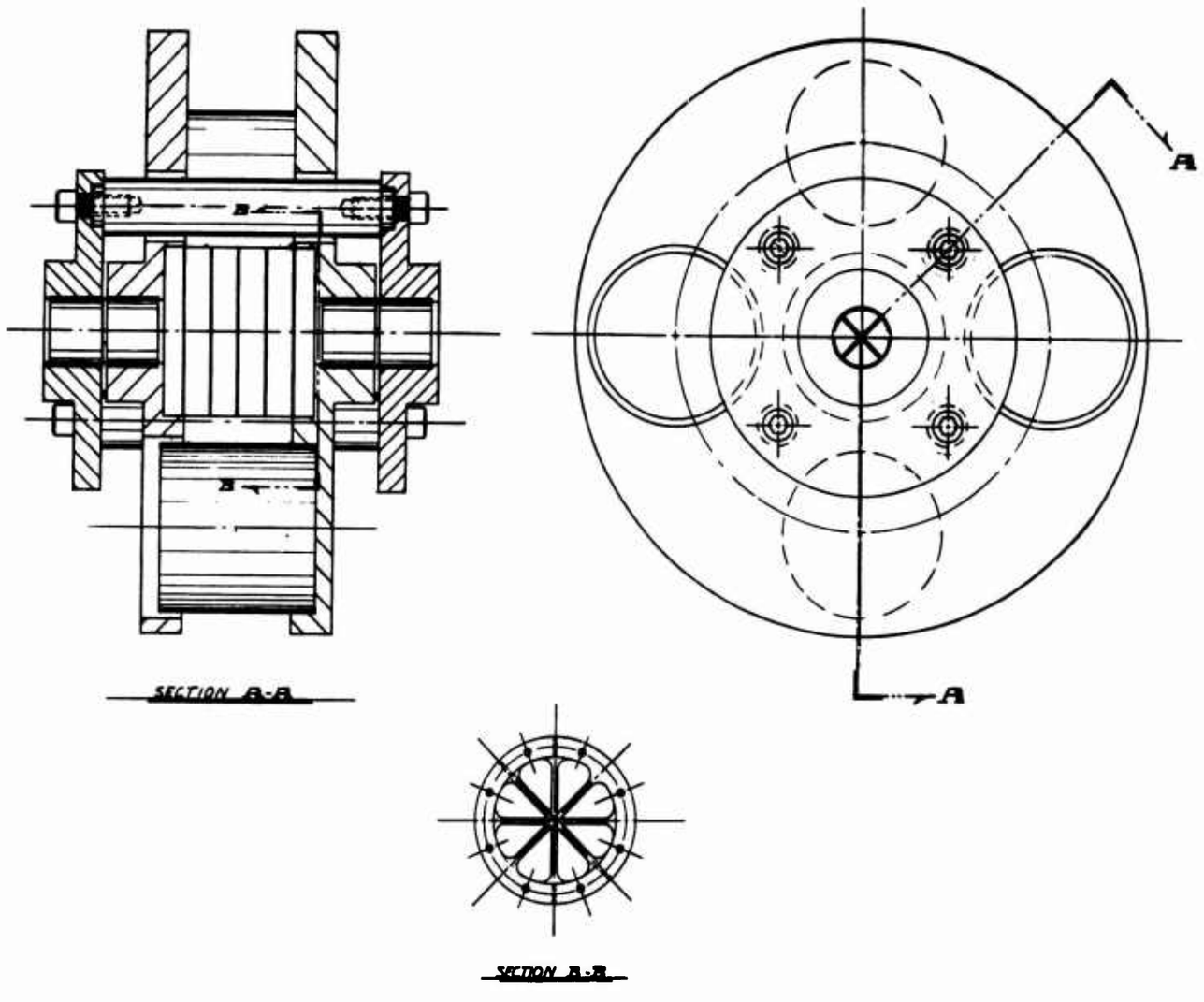

Fig. B-9. Torsional sensor head assembly.

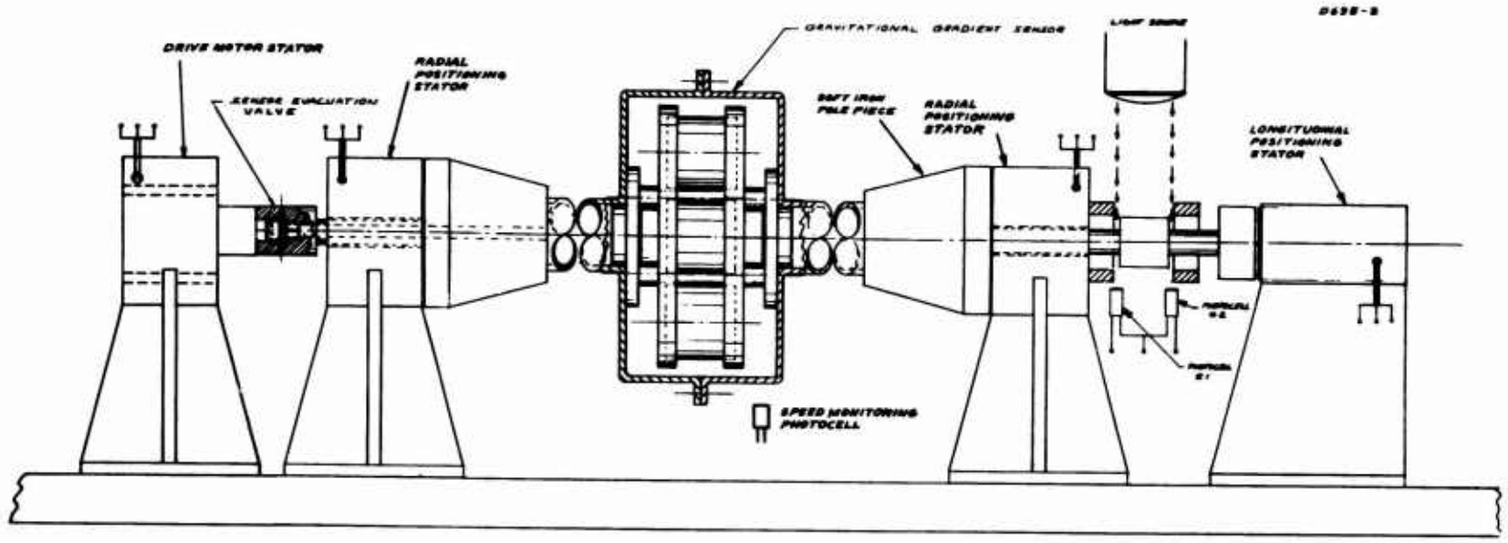

Fig. B-10. Gravitational gradient sensor system and magnetic suspension.

2. Electronics

a. Preamplifier-Transmitter

The transducer signal is preamplified, and transmitted from the rotating sensor head to the stationary receiving equipment by means of the circuit shown in Figure B-11. This transmitter has an input impedance of 22 MΩ and a front end noise of 30 nV(rms) when the data are integrated over a 100 sec time constant.

In our experimental dynamic gradient calibration tests the strain gauge signal is fed directly into the Princeton Applied Research Lock-In Amplifier where the noise level is less than 4 nV. The primary reason for this low noise figure is that this preamplifier is tube type rather than transistorized. It is estimated that additional design work on the preamplifier-transmitter should reduce the noise to less than 8 nV (0.4 E.U. equivalent).

b. Receiver

The FM receiver circuit is shown in Figure B-12. It consists of a tuned antenna and standard frequency modulation reception techniques with four-stage i.f. amplification and battery power for low noise operation.

c. Signal Processing

The demodulated telemetry signal is then fed into a phase sensitive detection system such as the Princeton Applied Research Lock-in Amplifier Model HR-8. The amplitude and phase of the desired frequency component read by the lock-in amplifier are proportional to the magnitude and direction, respectively, of the gravitational field gradient.

d. Frequency Reference

A General Radio Frequency Synthesizer, Type 1162, is used as a frequency reference for the asynchronous drive system.

e. Asynchronous Drive System

The asynchronous drive system of Figure B-13 is used to rotate the sensor at a precise angular velocity without introducing coherent electrical noise. This system compares the rotation speed of the sensor with the reference frequency and maintains the proper speed through a heavily damped servo control on the motor drive input power (see block diagram, Figure B-14).

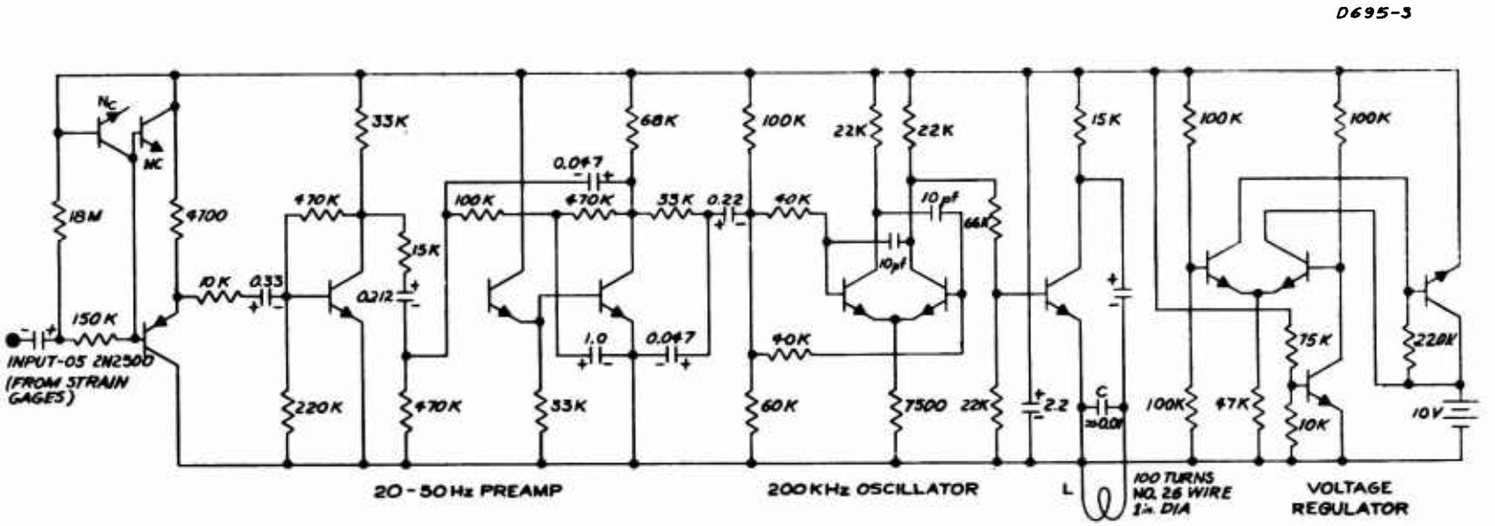

Fig. B-11. Telemetry transmitter.

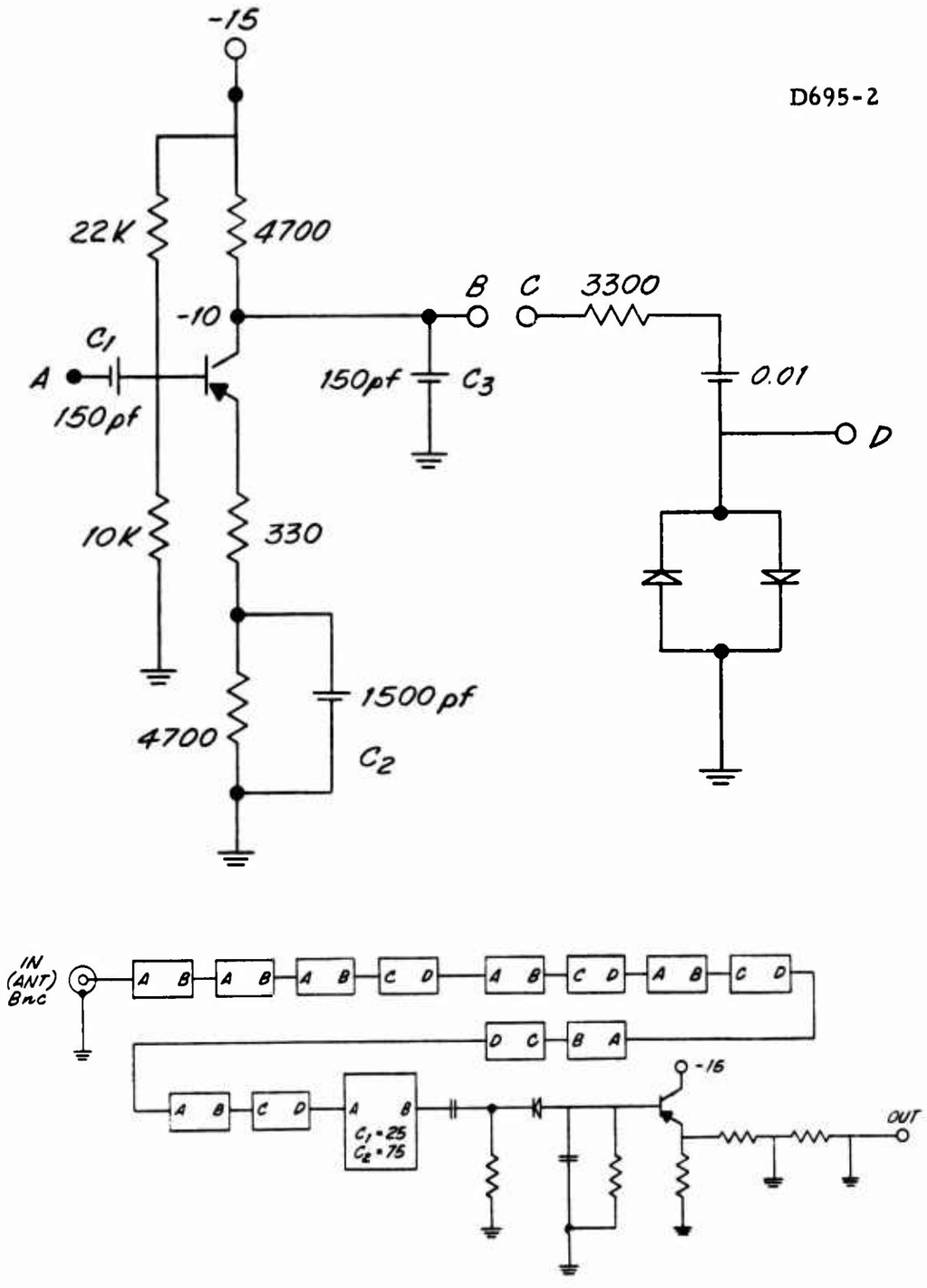

Fig. B-12. Telemetry receiver.

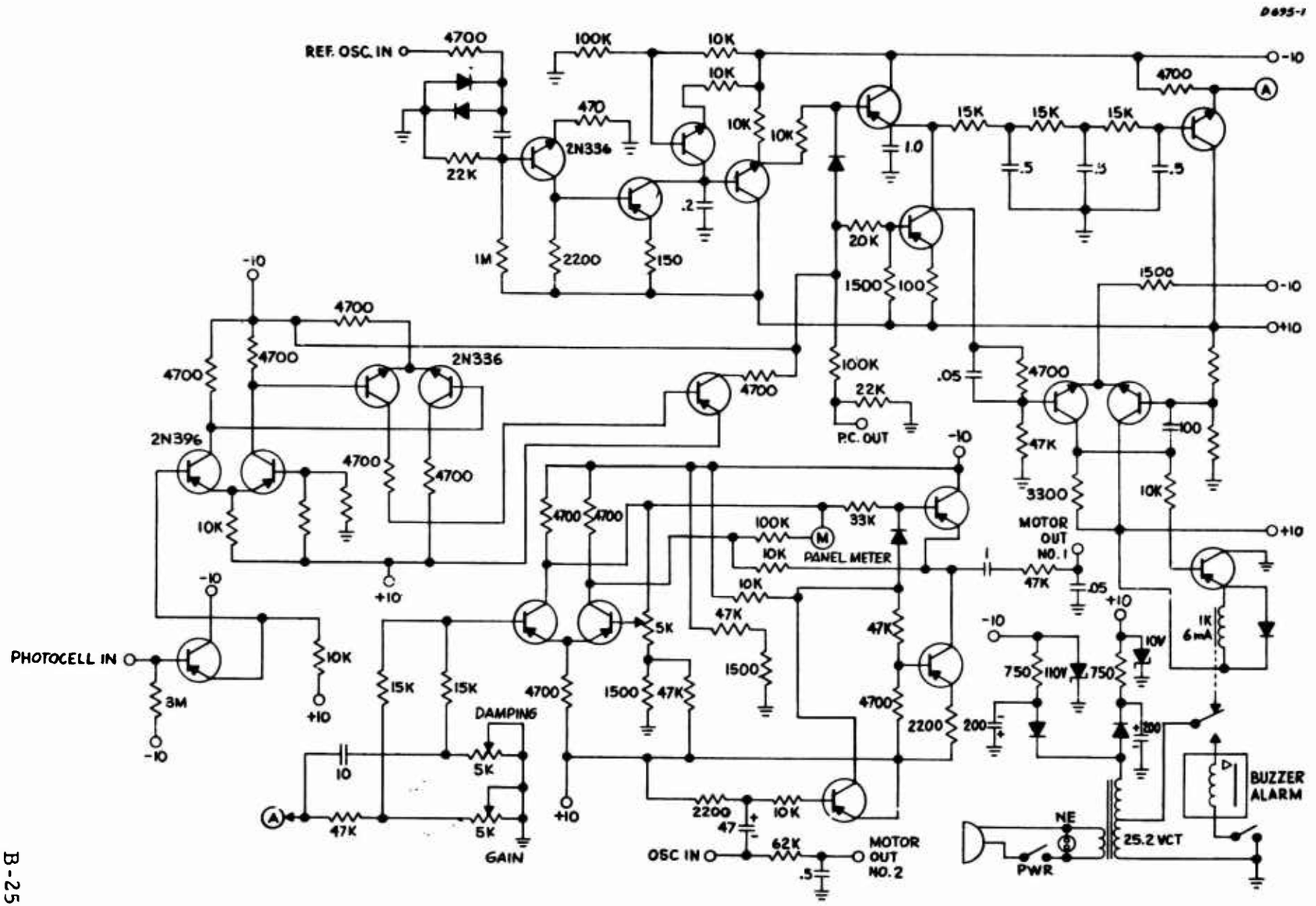

Fig. B-13. Asynchronous control.

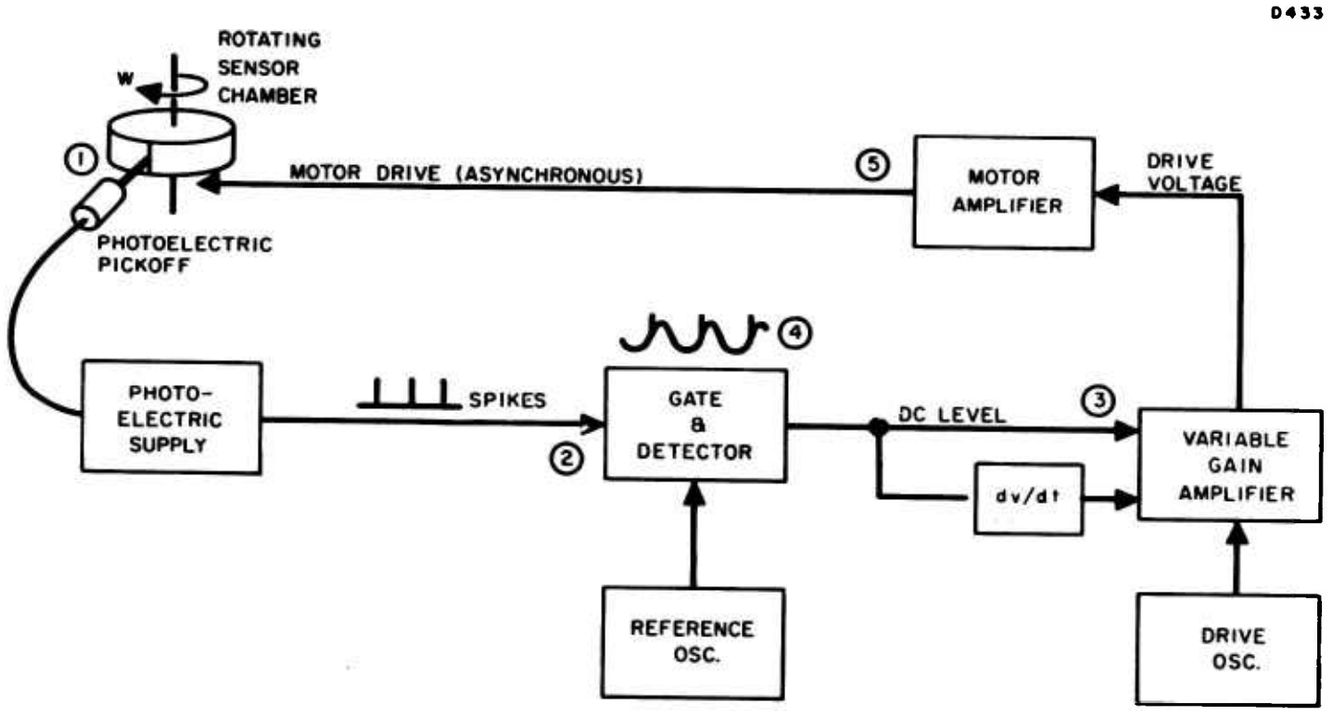

Fig. B-14. Block diagram of asynchronous drive.

SECTION IV

NOISE SOURCES

Our tests with rotating and nonrotating sensors have revealed a number of noise sources, which have been investigated. They are

- Internal mechanical noise generation resulting from fabrication errors
- Mechanical vibrations applied to the sensor mount which are generated by drive motors, air turbulence, and acoustic and vibrational sources external to the sensor and drive
- Differential forces applied directly to the sensor head which arise from coupling of the sensor arms to acoustic noise, turbulence in the residual air of the vacuum chamber, magnetic eddy current forces, and light pressure
- Pickup in the transducer leads and sensor electronics from electromagnetic coupling to stray electrostatic and magnetostatic fields, and to ac induction fields from the bearings and drive motors
- Thermal noise.

A. INTERNAL MECHANICAL NOISE

Internal mechanical noise is potentially the most limiting of the several types of noise associated with the operation of a rotating gravitational mass sensor. Thermal and external mechanical noise can theoretically be separated from the gravity signal because it is random and thus phase-incoherent. Other types of nongravitational noise, such as acoustic and electromagnetic, can be eliminated by shielding. However, internal mechanical noise resulting from center of mass misalignments in the sensor and bearings is phase-coherent and at the frequency of sensor gravitational response ($2\,\Omega$).

Figure B-15 is a schematic representation of the rotating torsional gravitational mass sensor and its associated spin mechanism. The principal construction involves two rigid arms mounted perpendicular on torsional springs. In operation, they are rotated at constant angular speed, and the relative motion responds ideally to the local gravitational gradient and rejects external accelerations. Also shown in the figure are the basic mechanical elements associated with rotation of the mass sensor. A combination of unbalance in these elements gives rise to internal mechanical noise.

There are two types of internal mechanical noise. One type is a result of deviations in rotational frequency, and is coupled into the sensor response through mismatching in the resonant frequencies of the two support torsional springs. This noise is reduced to acceptable levels in two ways:

1. The high inertia of the sensor head and heavy damping of the asynchronous drive maintain a 2Ω input torque variation of less than 0.01 dyn-cm.

2. The mass quadrupole inertias are matched to their individual support springs so that any remaining torque variations produce the same deflections in each of the sensor arms. Matching can be held within 0.01%. Therefore, the total residual torsional noise is $T_{res} = 0.01 \times 10^{-4} = 10^{-6}$ dyn-cm and the equivalent gradient signal produced by this torque $\Gamma = T_{res}/I = 10^{-6}/200(40.3) = 0.124 \times 10^{-9}$ sec^{-2}.

The other type of internal mechanical noise is generated even if constant angular speed of the housing is maintained. This is the result of the combination of the following three unbalances.

- Sensor unbalance h — Relative deviation between the geometric center of the sensor arm and its center of mass (percent of arm length)

- Rotor unbalance e — Deviation between the rotor geometric center and the center of mass of the spring (percent of arm length)

- Bearing unbalance ϵ — Circumferential variations in the stiffness of the bearing-shaft combination (percent).

It is well known that when the geometric center and the center of mass of a rotating body do not coincide, the geometric center will describe a circle in space. The radius of the circle will be defined by the frequency of rotation relative to the natural frequency of the shaft-suspension system. However, if there is any bearing stiffness unbalance

Figure B-15 is a schematic representation of the rotating torsional gravitational mass sensor and its associated spin mechanism. The principal construction involves two rigid arms mounted perpendicular on torsional springs. In operation, they are rotated at constant angular speed, and the relative motion responds ideally to the local gravitational gradient and rejects external accelerations. Also shown in the figure are the basic mechanical elements associated with rotation of the mass sensor. A combination of unbalance in these elements gives rise to internal mechanical noise.

There are two types of internal mechanical noise. One type is a result of deviations in rotational frequency, and is coupled into the sensor response through mismatching in the resonant frequencies of the two support torsional springs. This noise is reduced to acceptable levels in two ways:

1. The high inertia of the sensor head and heavy damping of the asynchronous drive maintain a 2Ω input torque variation of less than 0.01 dyn-cm.

2. The mass quadrupole inertias are matched to their individual support springs so that any remaining torque variations produce the same deflections in each of the sensor arms. Matching can be held within 0.01%. Therefore, the total residual torsional noise is $T_{res} = 0.01 \times 10^{-4} = 10^{-6}$ dyn-cm and the equivalent gradient signal produced by this torque $\Gamma = T_{res}/I = 10^{-6}/200(40.3) = 0.124 \times 10^{-9}$ sec^{-2}.

The other type of internal mechanical noise is generated even if constant angular speed of the housing is maintained. This is the result of the combination of the following three unbalances.

- Sensor unbalance h — Relative deviation between the geometric center of the sensor arm and its center of mass (percent of arm length)

- Rotor unbalance e — Deviation between the rotor geometric center and the center of mass of the spring (percent of arm length)

- Bearing unbalance ϵ — Circumferential variations in the stiffness of the bearing-shaft combination (percent).

It is well known that when the geometric center and the center of mass of a rotating body do not coincide, the geometric center will describe a circle in space. The radius of the circle will be defined by the frequency of rotation relative to the natural frequency of the shaft-suspension system. However, if there is any bearing stiffness unbalance

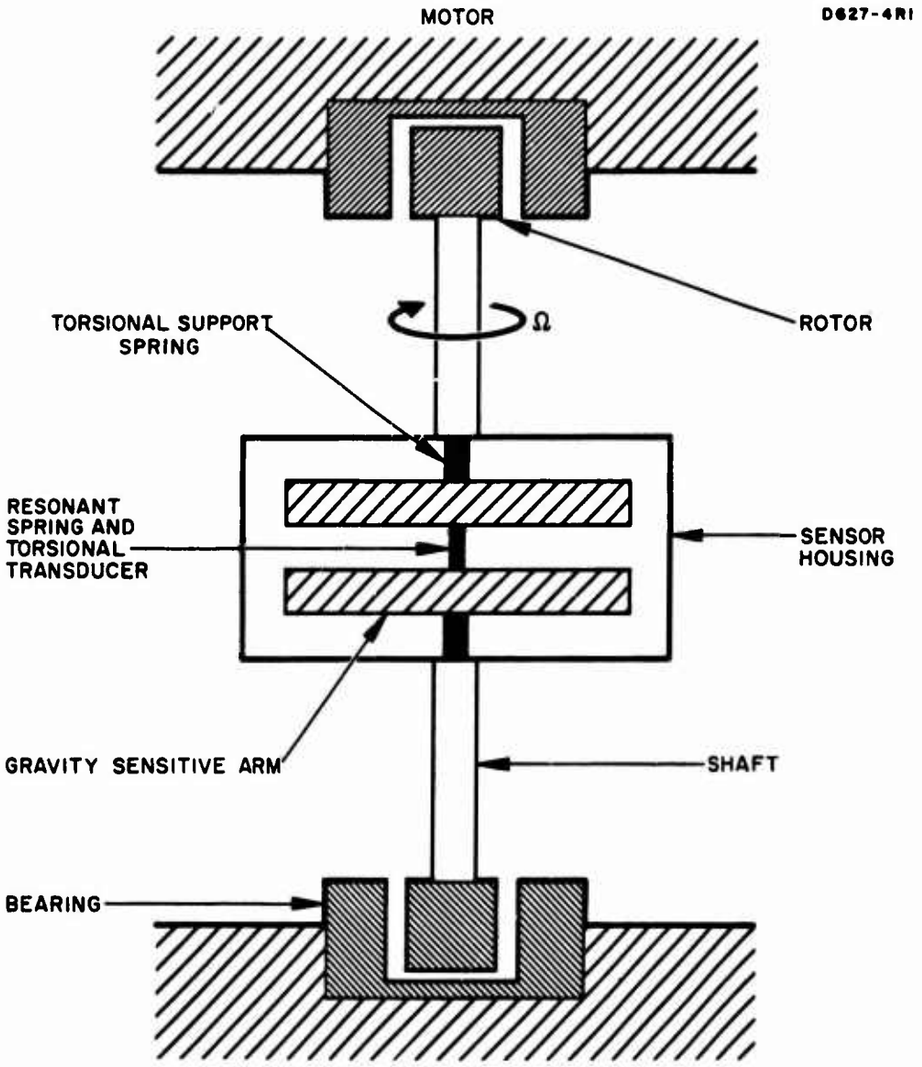

Fig. B-15. Schematic representation of rotating (torsional) gravity sensor and associated spin mechanism.

such that the restoring force is not constant as a function of circumferential position, the path described will be elliptic rather than circular. An elliptic motion can be decomposed into the sum of two circular motions: one positive and of large amplitude, and one negative (opposite to the shaft rotation) whose amplitude is proportional to the stiffness unbalance (see Figure B-16(a)).

The component of negative circulation at $1\ \Omega$ converts into $2\ \Omega$ excitations in the rotating coordinate system of the sensor (Figure B-16(c)) and can couple into the gravitational gradient excitation through the sensor fabrication errors h and e.

The amount of coupling produced by the negative circulation forces on the sensor arms is a function of the sensor unbalance. An ideally balanced sensor will not respond to such forces. The translational force is introduced to the arm through its geometric center. If the centers of mass do not coincide, the applied force resolves into a translational force at the center of mass plus a torsional couple. Thus the equivalent gradient noise Γ_e is also a linear function of the deviation between the sensor center of geometry and center of mass. The equation for the equivalent gradient noise Γ_e resulting from sensor and rotor construction errors has been derived as

$$\Gamma_e = \begin{cases} \frac{1}{3}\ \epsilon he\ \Omega_n^2, & \Omega > \Omega_n; \\ \frac{1}{3}\ \epsilon he\ \Omega^2\left(\frac{\Omega}{\Omega_n}\right)^2, & \Omega < \Omega_n\ . \end{cases} \qquad (15)$$

We see that the internal mechanical noise generation in a rotating gravity sensor is directly proportional to the product of the three unbalances. In addition, for the case of $\Omega_n < \Omega$, the noise is independent of rotational speed and proportional to the square of the suspension natural frequency. However, such low frequencies are difficult to achieve in practice. The second case ($\Omega_n > \Omega$) is more applicable to our discussion. Here, the noise is a function of rotational speed, and attenuates by the ratio $(\Omega/\Omega_n)^2$.

Therefore, by maintaining low rotational speed (15 Hz), and at the same time providing a high suspension stiffness, we may achieve very reasonable balancing specifications. The magnetic bearing manufacturer has indicated that a suspension natural frequency value as high as 150 Hz is easily attainable. Using this value, eq. (15) is plotted in Figure B-17 for the case of $\Omega_n > \Omega$ (and for a bearing anisoelasticity of 0.01%).

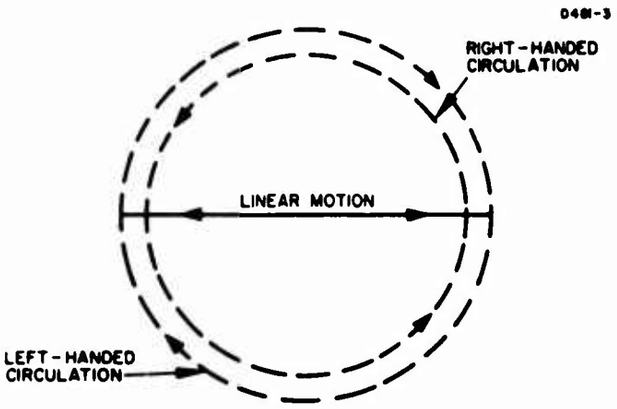

Fig. B-16(a).
Translational motion decomposes into right- and left-hand circulation.

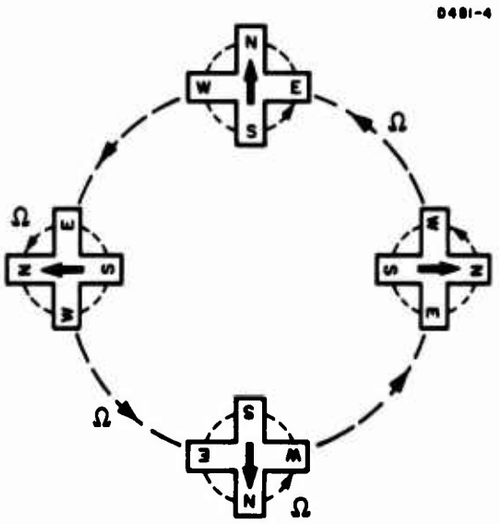

Fig. B-16(b).
Positive circulation produces no vibrational effect in rotating reference frame.

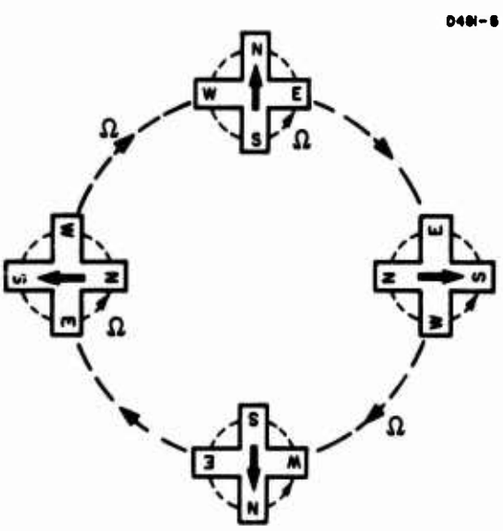

Fig. B-16(c).
Negative circulation induces a vibrational mode forcing function at twice the frequency of rotation.

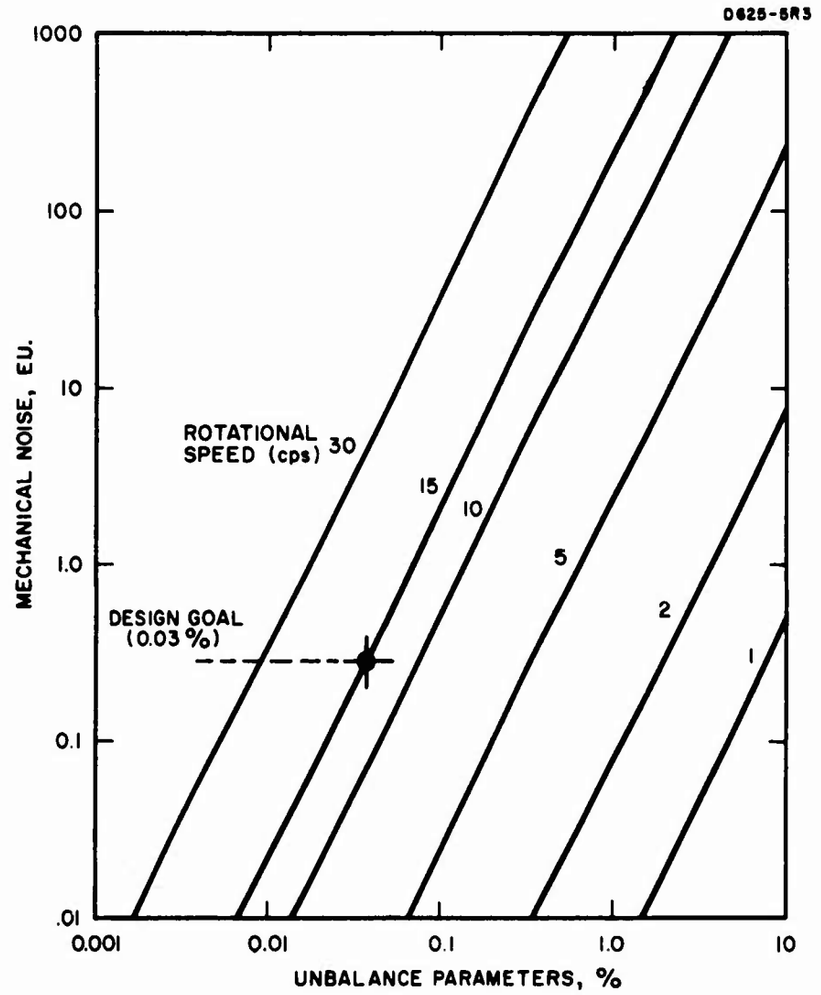

Fig. B-17. Mechanical noise generation resulting from rotor bearing sensor unbalance.

The ultimate design goal for this noise source is 0.3 E.U. The balancing requirement dictated by this sensitivity goal is shown in Figure B-17 as 0.03% for each of the three errors (h, e, and ϵ) in the system.

B. EXTERNAL VIBRATIONS

It is known from previous experience that the coupling of external acoustic noise to the sensor head will be negligible even at the very low signal levels (2 nV) attained during gravitational calibration experiments, provided that the sensor is operated in a moderate vacuum (0.010 Torr). Therefore, it does not appear to be necessary to strive for ultrahigh vacuum capabilities in our bearing and chamber designs. However, this vacuum level is not low enough to prevent differential excitation of the sensor when it is rotated inside a stationary vacuum chamber, as outlined in Section IV-C.

Other mechanical vibrations from the operational environment of the gradiometer system will depend on the particular application. In laboratory operation, no problem has been encountered. In airborne application, for example, vibration isolation techniques must be employed.

C. DIFFERENTIAL FORCES

Eddy current forces can be generated in the sensor itself only by the motion of conductive arms through a static magnetic field. The eddy current force F on a conductor of characteristic dimension ℓ moving at a velocity v through a static magnetic field B is given by

$$F = B^2 \ell^2 v/R \qquad (16)$$

where R is the resistance of the path through the conductor. This resistance is difficult to calculate accurately; however, if we assume that the end mass of the sensor has a resistance path of a few centimeters and use the resistivity of aluminum, which is 3×10^{-6} cm, the path resistance can be estimated at about 3×10^{-6} Ω. With a stray magnetic field of 5 G and a sensor arm velocity of about 2m/sec at 50 rps, the calculated eddy current force is about 30 dyn, which is many orders of magnitude higher than the calculated gravitational force level of about 0.6×10^{-3} dyn. This calculated force

level is a static force; its predominant effect on the sensor is to apply a retarding torque rather than generating noise. However, any asymmetries in the magnetic field would produce dynamically varying forces in the sensor arms at the rotation frequency and its harmonics.

For this reason, the present sensor design consists of nonconductive materials, such as quartz, etc.; such methods eliminate eddy current forces.

It has been demonstrated experimentally that the sensor responds to light pressure when a beam is directed at one side of the rotating sensor.

The force of light pressure on a reflecting object is given by

$$F = 2P/c \qquad (17)$$

where P is the light power and c is the velocity of light. The strobe flash unit used produced a beam intensity of 1.2×10^6 lm/m^2 at 1 m distance. The experiments were carried out at a distance of approximately 1 ft, with a sensor arm area of 8 cm^2. The force on the arms is calculated to be about 10^{-2} dyn, or about 20 times the calculated force due to the earth's gravitational gradient. Light pressure as a noise problem is completely eliminated when an opaque vacuum chamber is used.

The differential rotation of the sensor and chamber walls creates turbulence in the residual air in the chamber, which results in the generation of an appreciable amount of noise. This turbulence noise source is eliminated in the design by operating the sensor in a corotating vacuum chamber.

D. PICKUP

It has been found that rotation of the wire leads on the capacitive strain transducers through an electrostatic field can generate electrical pickup. Electrostatic fields observed in our test setups were found to be generated by static charges left on the teflon bumper plates when the apparatus was handled.

The removal of the teflon plates and the use of electrostatic shielding, twisted leads, and differential preamplifiers reduced the noise level from electrostatic pickup well below levels produced by other sources of noise.

When the sensor lead wires rotate through a diverging magnetic field, they generate induced currents which will depend to a large extent on the geometry of both the wire loops and the magnetic field.

The induced emf V from magnetic pickup in a wire loop of area A rotating at a speed Ω through a constant magnetic field B perpendicular to the loop is given by

$$V = B A \Omega \sin \Omega t . \qquad (18)$$

This output is at the rotation rate, of course; however, if two loops were rotating through an asymmetric field, a portion of this voltage would be proportional to the gradient of the magnetic field and at twice the rotation rate.

The residual flux level in our prototype magnetic bearing has been measured as approximately 5 G at the position of the rotating sensor. As a rough estimate, let us assume that the area of the loop in the leads is $0.1\ cm^2$ and that the asymmetries will produce 2Ω outputs which are 1% of the 1Ω outputs. At a rotation speed of 15 rps, this will give a coherent noise level of approximately 10^{-8} V (equivalent to $\approx$ 0.3 E.U.).

Electromagnetic pickup from the drive fields of the motor represented a potential noise source. However, experience with noise tests on rotating sensors has shown that this is not a major problem. With synchronous drive at high drive levels it is possible to see the effects of the drive fields; when the drive voltages are decreased to just that necessary to maintain synchronous rotation, however, the noise level decreased to that seen under free rotation operation. In any case, the use of the phase locked asynchronous drive is found to eliminate electrical pickup noise from the drive motor.

E. THERMAL NOISE LIMITS

When all the above forms of noise are eliminated, the fundamental sensitivity is determined by the thermal noise limitation. In practice, this limit can never be reached, but many systems can approach it very closely. This is especially true of low frequency devices, since the electronics available in this region has been highly developed and will contribute only a few degrees of extra equivalent noise temperature to the physical temperature of the sensor.

Near thermal noise limited sensitivity has been demonstrated repeatedly in the program for a number of the sensor-transducer-electronics configurations. The sensitivity calibration is accomplished using dynamically generated gravitational gradient fields produced by a pair of rotating 1 kg masses. A torsional sensor was calibrated using the low noise preamplifier of the HR-8 Lock-In Amplifier, and the noise level measured for a 100 sec integration time was found to be equivalent to a gravitational gradient threshold of 0.2 E.U. while the thermal noise limit is 0.05 E.U. (see eq. (14)). In this case the thermal vibrations in the sensor were contributing about one-fourth of the observed noise.

F. ESTIMATED ACHIEVABLE NOISE LEVEL

From the above discussion we can now tabulate the noise sources and estimate the total residual noise in the system (see Table B-I).

TABLE B-1

Estimate of Noise Limited Threshold

Noise Type	Caused by	Amount	Comments
Internal Mechanical	2 ω torsional input	$0.1 \times 10^{-9} sec^{-2}$	Section IV-A
	Translational balancing	$0.3 \times 10^{-9} sec^{-2}$	Section IV-A
Eddy Current	Sensor magnetic interaction	Negligible	Sensor is nonmetallic
Electrical	Static electrical fields	Negligible	Sensor is electrically shielded
Magnetic Pickup	Magnetic interaction with wires	$0.3 \times 10^{-9} sec^{-2}$	Section IV-D
Acoustic	Air turbulence	Negligible	Sensor is in corotating vacuum chamber
Electronics	Preamplifier noise	$0.4 \times 10^{-9} sec^{-2}$	Section III-B-2-a
Thermal Noise	Temperature of sensor and transducer	$0.2 \times 10^{-9} sec^{-2}$	Section IV-E
Total		$1.3 \times 10^{-9} sec^{-2}$	Sum (worst case)
		$0.6 \times 10^{-9} sec^{-2}$	rms

G. TESTING PROCEDURES

1. Static Balancing

In order to reject signals which are generated in interactions between sensor asymmetries and vibrational noise inputs, the asymmetry coefficients h, e, and ϵ outlined in Section IV-A must be reduced by mechanical balancing of the sensor-bearing assembly. This will be accomplished by introducing calibrated torsional and transverse vibrational signals into the sensor head and adjusting the inertia, center of mass, and bearing parameters of the sensor arms to produce a null output from the transducer. The sensor head will also be dynamically balanced using commercial balancing practices.

2. Calibration

For static calibration we will use a generator of dynamic gradient fields. We have constructed and successfully operated such a generator in prior experimental research on gravity sensors. Our gravitational gradient field generator consists of a flat aluminum cylinder 14 cm in diameter, with four holes which can be filled with slugs of different density to create a rotating mass quadrupole moment (see Figure 18). The generator is operated at sensor rotational frequency (15 Hz). Because of the bisymmetric mass distribution, the dynamic gravitational gradient fields generated are at a frequency of twice that of rotation. The dynamic field thus simulates the resonant response of the sensor, which also responds at twice rotational speed.

The sensor will be mounted inside its evacuated vacuum chamber, the chamber will be suspended from the ceiling, and the calibrator will be placed beneath or beside the chamber. An iron shield will be used for acoustic and magnetic isolation. This has been found to be adequate in our previous experiments with dynamic gravitational fields. Data can be taken with four different mass distributions varying from 0 to 1000 g with separation distances between sensor and calibrator varying from 5 to 20 cm. Calibration procedure will therefore be capable of accurately demonstrating the sensitivity and threshold of the sensor.

M 4181

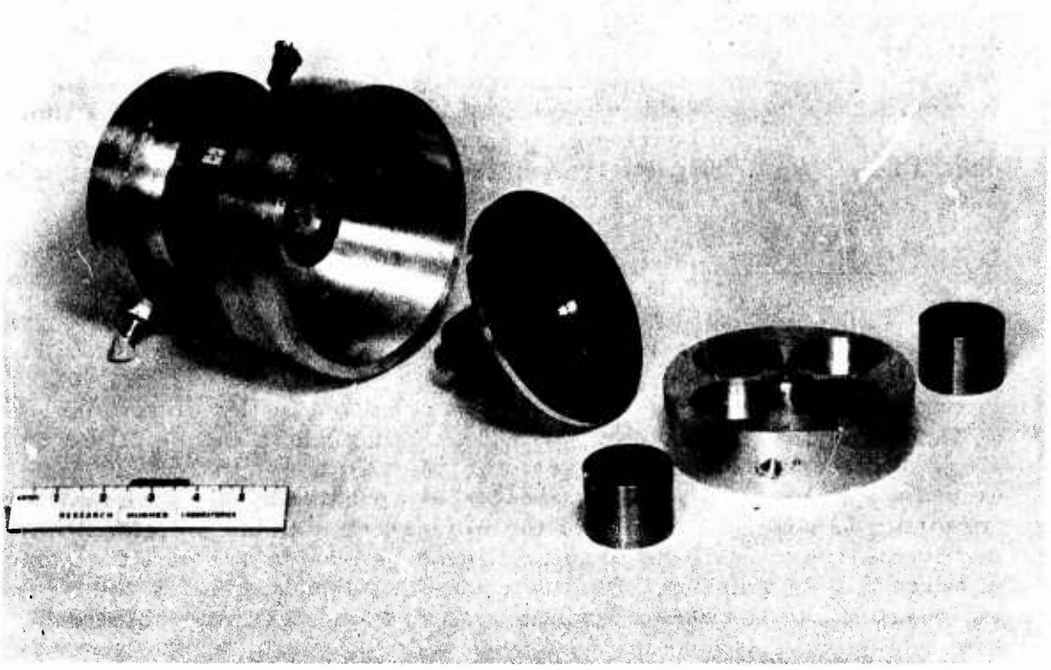

Fig. B-18. Dynamic gravitational gradient field generator.

APPENDIX C

GRAVITY GRADIOMETER COMPUTER MODEL FOR SIMULATED GRADIENT CONTOUR MAPPING

(Prepared by David Berman)

Gravity Gradiometer Computer Model for Simulated Gradient Contour Mapping*

DAVID BERMAN
Hughes Research Laboratories, Malibu, California 90265
(Received 10 May 1967; and in final form, 23 June 1967)

Considerations for gravity gradiometer application have established the need for predicting gradiometer response to mass distributions of particular interest. A digital computer program has been developed to simulate the rotating gravitational mass sensor, and to map the gradient contours of the gravitational field created by an arbitrary mass distribution. This analysis demonstrates the interaction of the gradiometer with seond and higher order gravitational gradients. The information about the mass distribution of an object was found to increase with the g ..ent order. Considered in this study is the "cruciform" mass sensor, now being developed by Hughes Research Laboratories. This rotating gradiometer is theoretically capable of measuring the second, sixth, tenth, etc., order gradient. We are presently engaged in laboratory experiments which combine with these computer results in the understanding of gradient–sensor interaction. This paper gives a basic introduction to gravitational tensors, followed by a mathematical formulation of the gradiometer model. Computer results are included which demonstrate the gravitational gradient contours associated with some selected mass distributions.

INTRODUCTION

THE gravitational field of an object can provide us with knowledge of many properties of its mass distribution.[1–3] Although the gravitational potential itself is not directly measureable, the gradients of the field are measurable. The first order gradient of the gravitational potential field is simply the gravitational force; higher order gradients are complicated tensors of high rank.

A gravitational gradient sensor measures directly the various gradients of the gravitational potential and thus enables reconstruction of the gravitational potential distribution. Present research indicates that the measurement of higher order gravitational gradients provides increasingly more information about the mass distribution of an object, and thus more accurate determination of the gravitational field detail.

Future application considerations for gravity gradiometers as well as laboratory demonstration have created a requirement for predicting the response of a gradiometer to gravitational fields of particular interest. For example, geodetic applications require the prediction of gradiometer response to the earth's gravitational field. Similar requirements are presented in our laboratory investigations of gradient sensors. For these reasons, a general computer program has been developed to map the contours of gradiometer response for an arbitrary mass distribution.

In this paper we demonstrate the contour mapping of gravitational gradients which are measurable with a gravitational gradient sensor. We have constructed a digital computer model of the rotating cruciform gravitational gradient sensor under development at the Hughes Research Laboratories. The computer program can map the gravitational gradient interaction for an arbitrary mass distribution and an arbitrary gradiometer orientation.

* This work was partially supported by the Air Force Cambridge Research Laboratories, Contract No. AF 19(628)-6134 and the Air Force Office of Scientific Research Contract No. AF 49(638)-1536. The views do not necessarily reflect those of the Air Force.

[1] R. L. Forward, "Mass Detector," Hughes Research Laboratories Internal Report RL-59 (19 March 1962).

[2] R. L. Forward, "Gravitational Mass Sensor," Proc. 1963 Symp. on Unconventional Inertial Sensors, Farmingdale, New York (18–19 November 1963), pp. 36–60.

[3] R. L. Forward, Bull. Am. Phys. Soc. 9, 711 (1964).

THE GRAVITATIONAL POTENTIAL AND ITS GRADIENTS

According to Newton's law of gravitation, a mass M characteristically sets up a field in the space around it, which interacts with other masses. If a small test mass m is placed at a distance R from the first mass, it is found that the system has a potential energy given by

$$\phi = -(GMm/R), \tag{1}$$

where $G = 6.67 \times 10^{-11}$ m³/kg sec². Strictly speaking, the above formula applies only to a spherically symmetric mass, but the concept can be extended to more complicated distributions of mass by simply adding the contributions of each part of the distribution.

The gravitational potential is not directly measurable since the point of zero reference can be changed arbitrarily. Differences in potential energy can be measured by allowing the masses to attract each other and measuring the change in kinetic energy.

The first order gradient of the potential is simply the gravitational force field. Since the inertial mass and the gravitational mass are the same for all bodies, the gravitational force field is equivalent to a gravitational acceleration field.

$$\begin{aligned} a_k &= \frac{1}{m}F_k = -\frac{1}{m}\nabla_k\phi \\ &= -[GM/(x^2+y^2+z^2)^{\frac{1}{2}}](x,y,z) \qquad \text{in Cartesian coordinates} \\ &= [-(GM/R^2), 0, 0] \text{ in spherical coordinates.} \end{aligned} \tag{2}$$

This accelerating force field can be detected by any force or acceleration measuring device such as an accelerometer or gravity meter, provided the center of mass of the sensing device and the object being investigated are not moving with respect to each other. The second order gradient of the potential is the gravitational force gradient described by the symmetric tensor

$$\Gamma_{ij}=\nabla_i\nabla_j\frac{\phi}{m}=\frac{1}{m}\begin{bmatrix}\frac{\partial^2\phi}{\partial x\partial x} & \frac{\partial^2\phi}{\partial y\partial x} & \frac{\partial^2\phi}{\partial z\partial x}\\ \frac{\partial^2\phi}{\partial x\partial y} & \frac{\partial^2\phi}{\partial y\partial y} & \frac{\partial^2\phi}{\partial z\partial y}\\ \frac{\partial^2\phi}{\partial x\partial z} & \frac{\partial^2\phi}{\partial y\partial z} & \frac{\partial^2\phi}{\partial z\partial z}\end{bmatrix}. \tag{3}$$

If we have a simple mass to measure, by proper orientation of the sensor, the measured gravitational force gradient tensor can be simplified to

$$\Gamma_{ij}=\begin{bmatrix}\Gamma_{rr} & 0 & 0\\ 0 & \Gamma_{tt} & 0\\ 0 & 0 & \Gamma_{tt}\end{bmatrix}, \tag{4}$$

which consists of the radial gravitational force gradient

$$\Gamma_{rr}=+2(GM/R^3), \tag{5}$$

and the trangential gravitational force gradient

$$\Gamma_{tt}=-(GM/R^3). \tag{6}$$

The gravitational force gradient is best known to us as the tides on the earth due to the gravitational field of the sun. Since the amplitude of the gravitational force due to the sun varies as the inverse square of the distance from the sun, and since the direction of the force vector varies with angle, the gravitational force due to the sun varies from point to point on the earth. If we look at these force vectors from the viewpoint of the center of mass of the earth, we see that after subtracting out the center of mass motion, we are left with a radial tension and tangential compression. It is important to realize that the effects of the slight angular convergence are of the same order of magnitude as the radial gradient effects. This will always be true and the angular effects must always be included for a correct calculation of gradients.[2]

There is essentially no limit to the number of higher gravitational gradients that can be measured, provided the sensor is close enough and the object under investigation is sufficiently dense that the interaction overcomes the sensor noise. These higher order gradients are complicated tensors of high rank, and sophisticated techniques and sensors may be able to obtain a great deal of information from them. Basically, they have the form[4]

$$T_{ab\cdots n}=1/m(\partial^n\phi/\partial x^a\partial x^b\cdots\partial x^n). \tag{7}$$

By measurement of the gravitational tensor components, we can theoretically reconstruct the potential field of an arbitrary mass distribution. However, the same potential field can be produced by more than one mass distribution. Consider the well known puzzle "How to distinguish between two hollow shells, one of gold, the other of silver, if their diameters and masses be alike and both be painted?" When there is radial symmetry, a gravitational gradient sensor will determine only the mass and not the distribution.

Once the potential field is known, it may be expressed as a series of spherical harmonics. These harmonics then determine the multipole moments of the potential distribution. However, there is not a one to one correspondence between these *field* moments and the moments of the *mass* distribution (moment of inertia, for example). The field moments (monopole, quadrupole, etc.) contain combinations of mass moments, so that only the combinations are determined, and not the mass moments themselves. Gravitational measurements are capable of identifying the total mass (zeroth moment) and center of mass (first moment) and also components of all higher moments. These distinguishable higher moments must contain a nonspherically symmetric characteristic length.

By going to higher order gravitational moments, increasingly more information can be obtained about the detailed structure of the object. Although the higher order moments of the mass distributions make an increasingly smaller contribution to the total potential, they produce a larger contribution to the higher order gradient. For example, consider the gravitational potential field of a relatively simple mass quadrupole (two point masses $M/2$ separated by a distance 2a)

$$\phi=GM/r(1+a^2/r^2\cos^2\theta), \tag{8}$$

where θ and r are spherical coordinates. The first term is the mass monopole moment of the distribution, and the second term is the quadrupole moment. The expression for the n^{th} order (radial) gradient of the potential is

$$\partial^n\phi/\partial r^n=GM(n!/r^{n+1})\times[1+1/2(n+1)(n+2)(a/r)^2\cos^2\theta]. \tag{9}$$

The ratio of the quadrupole to monopole moment [from Eq. (9)] is plotted in Fig. 1 as a function of the gradient order. For example, consider a sensor distance of five times the mass separation, $(a/r)^2=0.01$. In the second order gradient ($n=2$), the quadrupole moment represents

[4] R. L. Forward, "Rotating Gravitational and Inertial Sensors," presented at AIAA Unmanned Spacecraft Meeting, Los Angeles (1–4 March 1965).

only 6% of the total signal. If this 6% variation could not be detected, the doublet mass distribution could not be distinguished from a single point mass. However, in the sixth order gradient ($n=6$), the quadrupole term is 28% of the amplitude of the monopole term. Thus, the higher order gradients indicate the fine detail in the potential distribution.

GRAVITATIONAL MEASUREMENT

The simplest way to measure gravity is to use an accelerometer and measure the gravitational force (first order gradient). A single accelerometer also responds to linear accelerations induced by motion of the sensor. To make a gradiometer to measure the second order gradient, the outputs of a pair of accelerometers on the ends of a rod could be interconnected so that the acceleration due to the first order gradient or external forces is canceled out, leaving only the differential or second order gradient forces. Similarly, higher order gradients could be measured by more complex arrangements using many accelerometers.

A more sophisticated technique, considered in this paper, is that employed by dynamic (rotating) gradiometers. In its simplest form, the dynamic technique consists of mounting one or more low level accelerometers to a rotating frame with their sensitive axes perpendicular to the centrifugal force.[5] When this is done, the output of the accelerometers will be found to contain dynamic components at multiples of the rotation frequency which are driven by the various gradients of the field. The physical concept used is that forces are vectors (tensors of first rank), the gradients of forces are tensors of second rank, and higher order gradients are higher rank tensors. In general, the components of a tensor of n^{th} rank, when examined in the rotating reference frame of a sensor, will be found to have time-varying coefficients which are at n times the rotational frequency of the sensor.[4] For example, if a simple spring mass is rotated in a static gravitational field, the gravitational force gradient of the field (second rank gravitational tensor) will induce dynamic forces in the sensor with a frequency which is twice the rotation frequency of the sensor.[6,7]

The basic idea behind the operation of these sensors is an old one in electronics—the concept of chopping. This is used extensively in dc amplifiers, where the low level dc signal is chopped, transformed into an ac signal, and then amplified and measured by phase sensitive detectors. In the gravitational sensors, the chopping of the static gravitational field is accomplished by physically rotating the sensor so that its response to the gravitational field varies with time.[6]

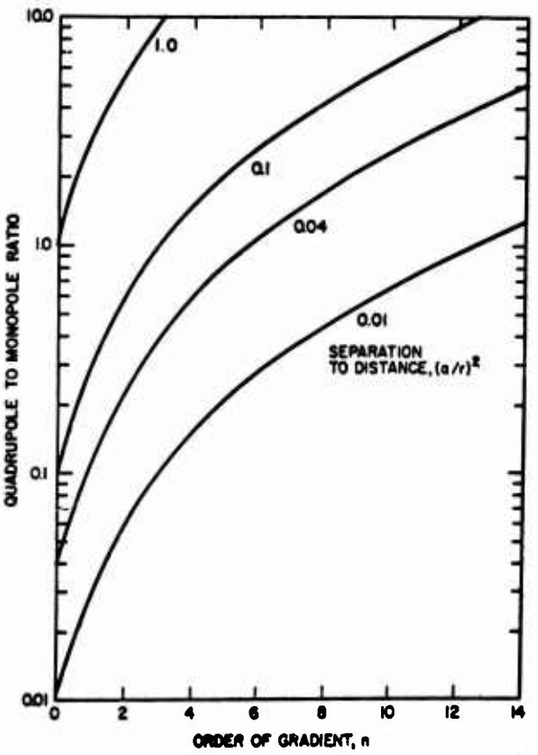

FIG. 1. Ratio of the quadrupole to the monopole moments of the gravitational potential field of a mass quadrupole.

The conversion of a static gravitational interaction into a dynamic gravitational interaction occurs because the rotation of the sensor creates a rotating reference system. From the viewpoint of the sensor, the mass to be measured is somehow whirling around the sensor, attracting it first one way and then the other.

A practical device, employing the dynamic concept, is the cruciform gradient sensor, under development by HRL (Figs. 2, 3). This device consists of four integral arms, each a spring mass system (equivalent accelerometer). Gravitational gradients excite vibrational modes of the entire integral structure. This is a large advance over the early concept of coupling the outputs of individual accelerometers which are excited independently. The cruciform sensor is computer-simulated in this paper to study the gravitational field interaction.

Figure 2 is a model of the cruciform sensor. The elementary component is a simple spring mass rotating at constant angular frequency, as described above. The system consists of four equal masses M, each at the end of a cantilever spring, rotating in the vicinity of one or more masses m_i (Fig. 2). Gravitational forces exist between

[5] J. W. Diesel, AIAA J. 2, 1189 (1964).
[6] R. L. Forward, C. C. Bell, J. R. Morris, J. M. Richardson, L. R. Miller, and D. Berman, "Research on Gravitational Mass Sensors," Final Report, NASW-1035, Hughes Research Laboratories (15 August 1966).
[7] C. C. Bell, R. L. Forward, and J. R. Morris, "Mass Detection by Means of Measuring Gravity Gradients," presented at AIAA Second Annual Meeting, San Francisco, Calif. (26–29 July 1965); also AIAA Paper 65–403.

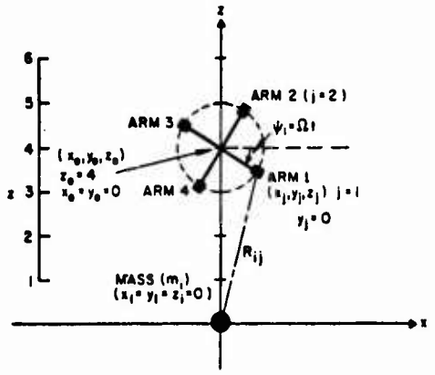

FIG. 2. Model of a dynamic gravitational gradient sensor rotating in the vicinity of a point mass.

each arm j of the sensor and each mass m_i of magnitude

$$\mathfrak{F}_{ij}=GMm_i/R_{ij}^2,\ j=1,2,3,4, \tag{10}$$

where R_{ij} is the distance between m_i and arm j. The component of this force which acts upon the cantilever spring is the tangential portion (F_{ij}) evaluated for $i=j=1$ as follows

$$F_{11}=\mathfrak{F}_{11}(R_0\sin\psi_1/R_{11}), \tag{11}$$

where R_0 is the distance to the center of the sensor. Substituting (10) into (11) yields

$$F_{11}=(GR_0Mm_i/R_{11}^3)\sin\psi_1. \tag{12}$$

Asssuming constant angular frequency, Ω of the sensor

$$F_{11}/M=(GR_0m_i/R_{11}^3)\sin\Omega t. \tag{13}$$

Evaluating

$$1/R_{11}^3=(R_0^2+b^2-2bR_0\cos\Omega t)^{-\frac{3}{2}}, \tag{14}$$

where b = sensor arm length.

If (14) is now expanded binomially, the higher power sine and cosine terms may be replaced by their corresponding multiple angle identities. All terms of like frequency are then collected, and only the terms with the lowest power of a/R are kept in each frequency. Equation (13) becomes

$$F_{11}/M=-(Gm_i/R_0^2)[\sin\Omega t+(3/2)(b/R_0)\times\sin2\Omega t+(15/8)(b/R_0)^2\sin3\Omega t+(35/16)(b/R_0)^3\sin4\Omega t+\cdots]. \tag{15}$$

Similar expressions may be obtained for the other three arms. The gravitational excitation E of a single arm is of the form [Eq. (15)]

$$E=\Sigma A_n(\partial^n\phi/\partial r^n)\sin n\Omega t, \tag{16}$$

where A_n is a constant of the sensor. Hence, the n^{th} order gradient excites a sensor arm at a frequency of n times the rotational frequency.

Equation (16) indicates the general nature of the interaction of the gravitational gradient sensor and gravitational field, although it was derived for the special case of a point mass. In general, the dynamic gradient sensor measures a combination of components in the gradient of the potential distribution. In the following section, the exact sensor-field interaction is calculated, taking account of this. The purpose of the analysis leading to Eq. (16) is only to provide a preliminary understanding of the operation of dynamic gradient sensors.

The response of a gradient sensor depends on its orientation, and many components of the n^{th} rank tensor can be obtained by a series of sensor orientations. Ideally, the potential field could be reconstructed from such measurements. The sensor excitation described by Eq. (16) corresponds to the radial components of the n^{th} rank tensor because of the particular choice of sensor orientation.

Figure 3 shows the actual cruciform gravitational mass sensor which was modeled in Fig. 2. This particular design utilized four basic spring-mass building blocks, and is capable of measuring the second, sixth, tenth, etc., order gravitational tensors. Other designs, using different numbers of arms, could be used to measure the tensors of intermediate orders.

INTERACTION OF GRAVITATIONAL FIELDS AND SENSORS

We next calculate the exact interaction of a rotating gravitational mass sensor, with the gravitational field created by an arbitrary mass distribution.

It is assumed that a mass distribution may be modeled by a three dimensional array of point masses m_i, each at an assigned coordinate (x_i,y_i,z_i). The sensor location is described by coordinates (X_0,Y_0,Z_0), which correspond to the center of gravity of the sensor.

The derived expressions shall be sufficiently general to accommodate any sensor orientation and thus shall yield all possible combinations of tensor components. In general, each of the four sensor arms is related to the coordinates of the center of gravity by the use of Euler angles. For an arbitrary orientation of the sensor (Fig. 4), the coordinates

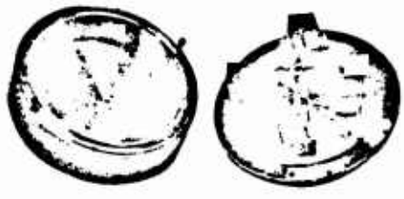

FIG. 3. 12.7 cm diam cruciform gravitational mass sensor under development at HRL.

of the four sensor arms (X_j,Y_j,Z_j) are given by

$$X_j=X_0+b(\cos\phi\cos\psi_j-\sin\phi\cos\theta\sin\psi_j),$$
$$Y_j=Y_0+b(\sin\phi\cos\psi_j+\cos\phi\cos\theta\sin\psi_j),$$
$$Z_j=Z_0+b(\sin\theta\sin\psi_j),$$

and

$$j=1, 2, 3,4. \tag{17}$$

In the above, θ is the angle made by the sensor axis of rotation with the z axis; ϕ is the angular position where the sensor plane of rotation intersects the x–y plane. The angle ψ_j describes the sensor rotation

$$\left.\begin{aligned}\psi_j&=\Omega;\\ \psi_j&=\psi_1+(j-1)\pi/2\end{aligned}\right\}j=1, 2, 3, 4, \tag{18}$$

where Ω is the rotational frequency of the sensor, and b is the arm length.

In order to determine the sensor excitation to an arbitrary mass distribution, we first need to calculate the force on arm j of the sensor due to mass i. Actually, the tangential component of this force (in the plane of rotation) is required, since the dynamic sensor responds only in the ϕ direction (Fig. 4).

The force on arm j from mass i is expressed in vector notation by

$$\mathfrak{F}_{ij}=GM(m_i/R_{ij}^3)\mathbf{R}_{ij} \tag{19}$$

where

$G\equiv$ gravitational constant,
$M\equiv$ mass of sensor arm,
$R_{ij}\equiv$ vector distance between i and j (20)
$=(X_j-x_i)\mathbf{i}+(Y_j-y_i)\mathbf{j}+(Z_j-z_i)\mathbf{k}$,

and

$\mathbf{i},\mathbf{j},\mathbf{k}\equiv$ unit vectors in the x,y,z directions, respectively.

In vector form, we may easily express the required component of $\mathfrak{F}_{ij}$. The tangential direction of arm j is identical to the radial direction of arm $j+1$. Hence,

$$F_{ij}=\mathfrak{F}_{ij}\cdot\mathbf{r}_{j+1}, \tag{21}$$

where F_{ij} is the sensor driving force and $\mathbf{r}_{j+1}$ is a unit vector describing the orientation of arm $j+1$

$$\mathbf{r}_{j+1}=(1/b)[(X_{j+1}-X_0)\mathbf{i}+(Y_{j+1}-Y_0)\mathbf{j}+(Z_{j+1}-Z_0)\mathbf{k}]. \tag{22}$$

We may thus expand $\mathbf{F}_{ij}$ using Eq. (22)

$$F_{ij}=(GM/b)(m_i/R_{ij}^3)[(X_j-x_i)(X_{j+1}-X_0)+(Y_j-y_i)(Y_{j+1}-Y_0)+(Z_j-z_i)(Z_{j+1}-Z_0)]. \tag{23}$$

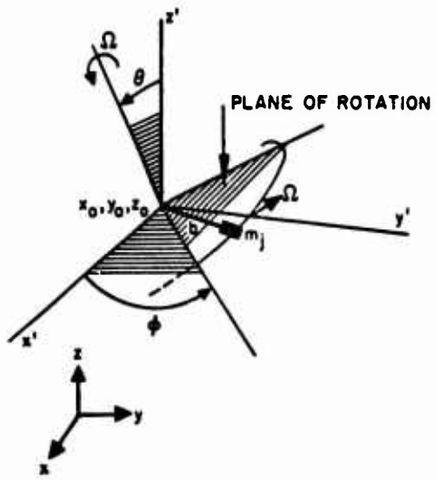

FIG. 4. Euler-angle coordinate system describing rotating gradient sensor for arbitrary position and orientation.

The total driving force on arm j resulting from all point masses in the array (N total) is

$$F_j=\sum_{i=1}^{N}F_{ij}. \tag{24}$$

The foregoing is general for any rotating gravitational gradient sensor (i.e., any number of arms). The sensor considered here has a particular vibrational mode which corresponds to a combination of individual arm motions. The gravity sensitive vibrational mode of the cruciform sensor is formed as follows[6]

$$F_\theta=\frac{1}{2}\sum_{j=1}^{4}(-1)^{j-1}F_j. \tag{25}$$

This completes all the quations necessary for constructing the sensor excitation due to any arbitrary array of point masses, and for any three-dimensional position and orientation of the sensor. At this point, it is worth while to take a simple case as an illustration of the sensor-mass interaction. In order to simplify numerical manipulation, assume all distances are multiples of the arm length b, and all point masses are multiples of a value m_0.

We now choose the special case of a single point mass at the origin, and a sensor rotating in the x–z plane with center on the positive z axis. The situation is that shown in Fig. 2 (for $Z=4$). Hence, the following values are associated with this example:

$N=1$ $\qquad$ $\phi=0$
$x_1=y_1=z_1=0$ $\qquad$ $\theta=\pi/2$
$X_0=V_0=0$
$Z_0=4$ (4×arm length).

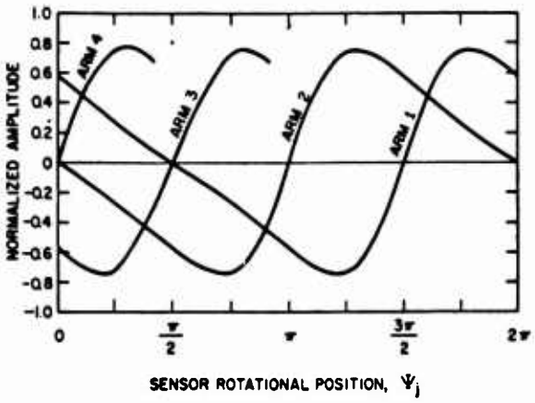

FIG. 5. Gravitational excitations of the individual arms of a gradient sensor near a point mass.

We may consider this example as two dimensional, since the plane in which the sensor rotates also contains the source mass.

Of interest first are the forces on the individual sensor arms as a function of sensor rotation ψ. These are shown in Fig. 5 [from Eq. (23), using (17) and (20)]. The calculations were facilitated by the digital computer, the programming of which is discussed below. In Fig. 5, it should be noted that all four arm excitations are identical, except for a phase shift of $\pi/2$. This is to be expected since each sensor arm follows exactly the path of the one preceding, at a separation of 90°. In Fig. 5 as well as the following figures magnitude has been normalized, in that the constants G, M, b, etc., have been ignored.

Finally, we show the gravitational mode excitation [Eq. (25)] in Fig. 6. This function appears to a first order to be a sinusoid of period π. (The period of rotation of the sensor itself is 2π.) Such information about the various frequency components of the sensor gravitational excitation is the underlying basis for determining the gradients of the gravitational field, as discussed above.

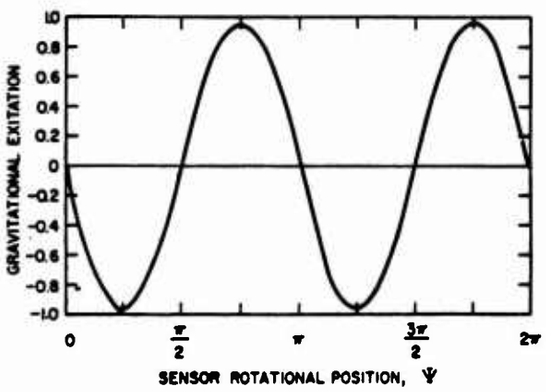

FIG. 6. Gravity-mode excitation of a cruciform gravitational gradient sensor near a point mass.

We may obtain the amplitude of each frequency component n of an arbitrary signal by use of the Fourier formulas

$$u_n = \frac{1}{\pi}\int_0^{2\pi} F_\theta \cos n\psi_1 d\psi_1$$
$$v_n = \frac{1}{\pi}\int_0^{2\pi} F_\theta \sin n\psi_1 d\psi_1. \tag{26}$$

These give the coefficients of the cosine and sine terms of

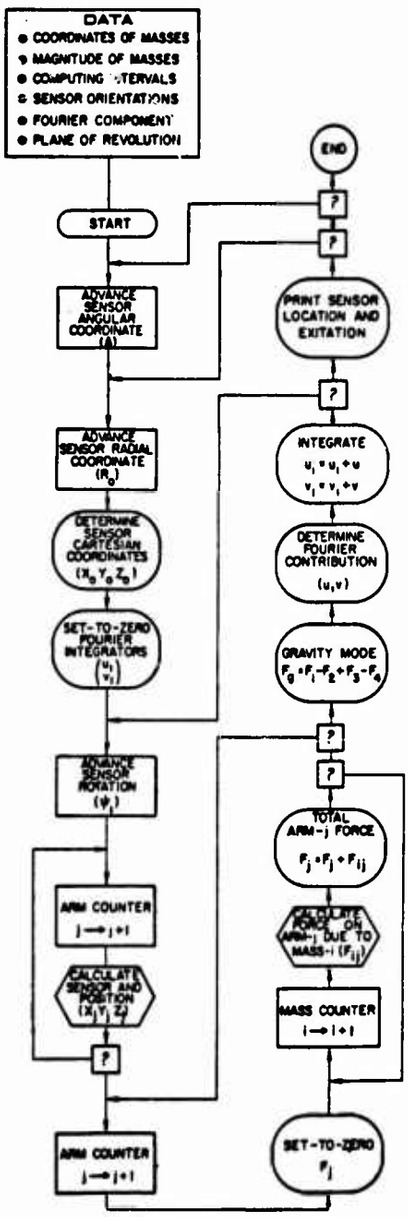

FIG. 7. Digital computer flow chart for the simulation of the gravitational field and dynamic sensor interaction.

the n^{th} frequency component. The amplitude of the excitation (E_n) is therefore

$$E_n=(u_n^2+v_n^2)^{\frac{1}{2}}. \tag{27}$$

When Fourier analysis was performed on the function in Fig. 6 (with the aid of the digital computer) it was found that there were frequency components only at $(2+4n)$ times the frequency of rotation ($n=0, 1, 2, 3$) etc. This is a property of the four-arm cruciform gravitational gradient sensor. Although Fig. 5 is the result of a very simple case (point mass), the results are general for more complex mass distributions. These findings are in agreement with elementary sensor theory.[6]

So far we have considered that the sensor is at a fixed location in the gravitational field of a mass distribution. Suppose now that the sensor moves through the field, describing a circle around the mass distribution. A plot of sensor excitation as a function of angular position is called a gradient profile of the gravitational field. We may obtain gradient profiles of various orders by using Fourier analysis to select the corresponding frequency component. In other words, we identify the n^{th} order gradient as the amplitude of the term at n-times rotational frequency. In addition, by considering various sensor orientations (θ,ϕ), we may obtain gradient profiles for many components of a high-order gradient (gravitational tensor).

COMPUTER PROGRAM

A digital computer program was constructed which is capable of mapping the contours of the gravitational

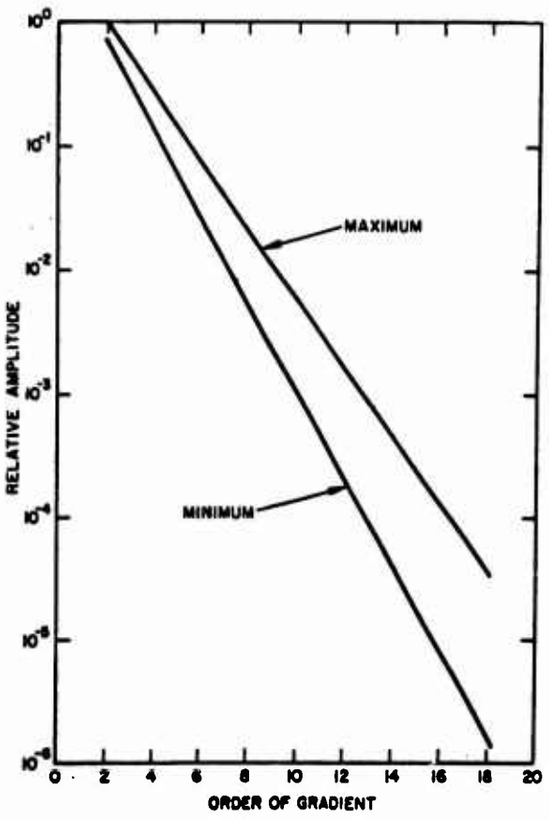

FIG. 9. Relative amplitude of the gravitational gradient signal as a function of the gradient order; cross plot of Fig. 8.

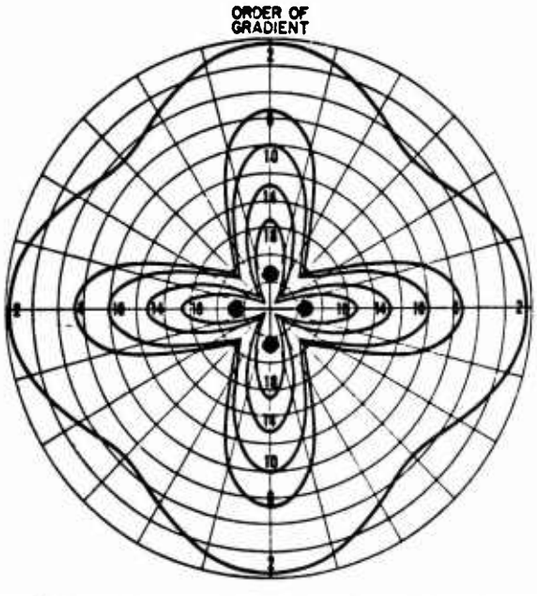

FIG. 8. Spatial distribution of the gravitational gradient signal produced by four equal, symmetric point masses. Masses are each one arm length from the origin, and sensor is three arm lengths from origin. Higher-order gradient profiles are magnified by several orders of magnitude.

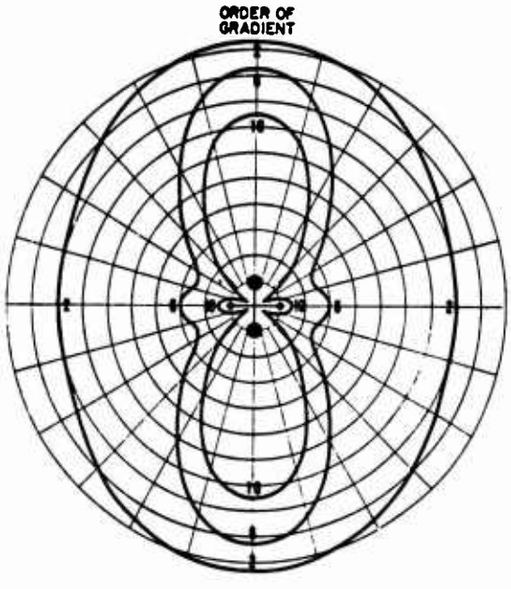

FIG. 10. Gradient profile produced by four unequal masses. Sensor distance is five arm lengths. Higher order gradients are magnified as in Fig. 8.

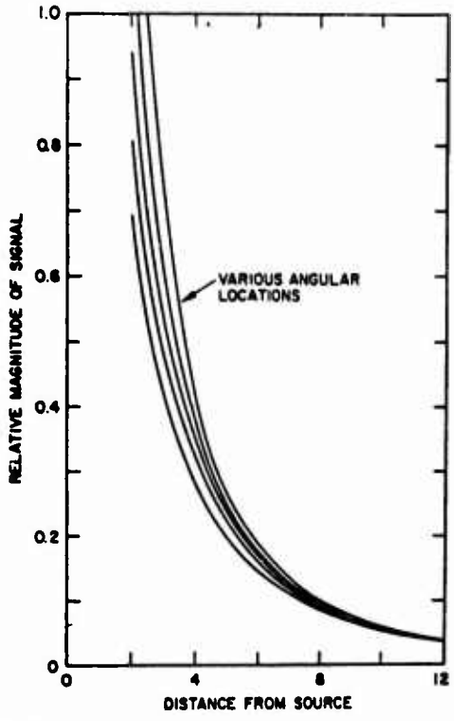

FIG. 11. Gravitational gradient signal variation with distance and angular position of sensor. Closeness of curves at increasing distances indicates lack of resolution in the gradient profile. (Second order.)

gradient interaction for an arbitrary mass distribution and an arbitrary sensor configuration. The computer program evaluates Eqs. (17) through (27) for any given mass distribution, sensor coordinate, and sensor orientation. It also automatically advances the sensor angular coordinate while maintaining constant radial coordinate. It thus calculates directly a gradient profile of any desired order (specified in the input).

Figure 7 is a detailed logic flow diagram, demonstrating the gravity gradiometer computer model, and the calculation of gradient contours. Although this particular program simulates a cruciform gradient sensor, a minor modification allows simulation of any desired sensor configuration.

Results have been obtained for several selected mass distributions. These are presented in the next section.

COMPUTER RESULTS: GRADIENT PROFILES

Gradient profiles which have been generated by the computer are presented. We have chosen several particular examples of mass distributions which demonstrate the important properties of the gravitational field and sensor interaction.

Gradient profiles corresponding to a mass distribution consisting of four symmetrically arranged equal masses are shown in Fig. 8. Each mass is at a distance of 1 from the origin and the sensor distance is 3 arm lengths. All the frequency components are shown, up to 18 times rotation. The higher frequency components correspond to higher order gradients of the gravitational field. The profiles in Fig. 8 correspond to a sensor orientation such that the plane of rotation passes through the origin.

We see that although the double frequency component gives a slight indication of the details in the mass distribution, the higher components give more and more resolution. This property of the higher order gradients was discussed above. In Fig. 8 the higher order patterns have been magnified many times. Figure 9 shows the relative magnitudes (maximum and minimum) as a function of frequency component. Because the higher order gradients become so reduced in magnitude, only the second order gradient will be of practical interest for geodesy application. It is expected that higher order gradients will be masked by instrument noise. In the laboratory, however, noise may be controlled to a much greater extent. We therefore expect, in our experimental investigation of gravitational sensors, to conduct the measurement of the higher order gradient interaction.

Figure 10 shows the gradient profile results for a different distribution; the two vertical masses are twice the size of the two horizontal masses. The sensor distance is 4.5 arm lengths. We notice here that the double-frequency component gives no indication that there are four separate masses. The sixth order component gives good resolution, and the tenth even better. Here again, the scales have been magnified successively as in Fig. 8.

As the distance from the mass distribution becomes larger, the amplitude of the tensor components diminishes. This effect is shown in Fig. 11 (for the mass distribution

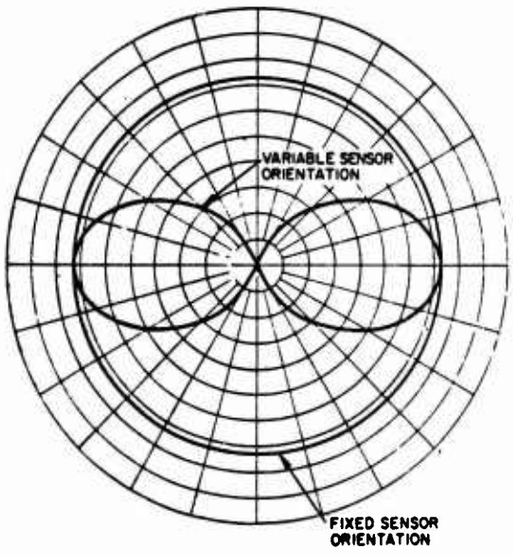

FIG. 12. Comparison of gradient profiles measured by sensors of fixed and variable orientations (point mass). Cosine-squared variation corresponds to second order gradient.

used for Fig. 10). Resolution of the gradient profile also diminishes as a function of the distance from the mass distribution, as can be observed by the lack of separation of the curves at increasing distance (Fig. 11). Lack of separation indicates that the amplitude is almost constant with angular position about the mass distribution, yielding only the monopole moment of the gravitational potential distribution.

Finally, we demonstrate the effect of sensor orientation on response. In Fig. 12 we have considered a point mass which is circled by a sensor whose axis of rotation remains pointed in a fixed direction, thus varying its orientation with respect to the point mass. Hence, the sensor orientation with respect to the mass continually changes as the sensor moves around the mass. In one extreme, the sensor experiences maximum interaction with the gravitational field, while the other extreme corresponds to a null position. The resulting figure eight was found to be a cosine-squared curve, and is indicative of second-order gradient variation.

All of the foregoing analysis is quite general, and may be used to study the interaction of sensors and the gravitational fields produced by particular objects of interest in future gradiometer applications.

APPENDIX D

DETERMINATION OF THE EARTH'S GRAVITATIONAL CONSTANT (GM)

(Prepared by J.C. Harrison, consultant
to Hughes Research Laboratories)

SUMMARY

The purpose of this study is to discover whether it is feasible to obtain a highly accurate determination of the earth's gravitational constant (GM) from measurements of the gravitational force and the gradient of the gravitational force. It has been found to be theoretically possible to determine GM for the real earth with its irregular geometry by means of Jeffreys' method for calculating the potential outside the earth. This technique involves using a surface integral over the earth's physical surface. If the observed forces or gradients do not agree with those calculated by Jeffreys' method, the geometrical shape of the earth's surface then may be modified by changing the assumed mean value for the earth's radius so that the observed and calculated gradients are brought into agreement. However, further study showed that in practice the contribution to the surface integral of the gravitational force gradient comes almost entirely from the immediate vicinity of the measurement station, and that real measurements give information of predominantly local significance and say little about the dimensions of the earth as a whole. It is concluded that an accurate determination of GM from gravitational measurements made on the earth's surface is not feasible.

I. INTRODUCTION

The purpose of this study is to determine the feasibility of obtaining the earth's gravitational constant (GM) from gravity and gravity gradient measurements taken on the earth.

Spherical Earth

A very simple relation exists between gravity and its gradient on the surface of a sphere which would make it possible to determine GM and the radius of the sphere by measuring these quantities.

For a spherical, nonrotating earth with radially symmetric density distribution, we can write the earth's gravitational field as

$$g = GM/r^2 \quad , \tag{1}$$

and the vertical gradient of the gravitational field as

$$\Gamma_{rr} = \frac{\partial g}{\partial r} = -2GM/r^3 = -2g/r \quad . \tag{2}$$

On the earth's surface we have

$$(g)_a = GM/a^2; \quad (\Gamma_{rr})_a = -2g/a \tag{3}$$

where a is the earth's radius.

Hence, if both $(g)_a$ and $(\Gamma_{rr})_a$ can be measured accurately, it is possible to determine a from the relation

$$a = -\frac{2g}{\Gamma_{rr}} \quad . \tag{4}$$

We can then substitute in the expression

$$g = GM/a^2 \tag{5}$$

to determine a value for the earth's gravitational constant (GM).

Irregular Earth

Although the relation between gravity and its gradient on the surface of a sphere is very simple and would allow GM to be determined, the earth is not spherical, but has a highly irregular and relatively unknown shape. Since the gravitational gradients are related to the local curvature of the geoid,[1] a theory based on a simple geometric shape such as a sphere or ellipsoid is clearly not adequate.

The question then is whether measurements of gravity and its gradient can be combined to give significant information about the dimensions of the real earth which in turn can be used to determine GM. Such calculations must be accurate to one part in 10^5 to confirm present determinations and to one part in 10^6 to provide a significant improvement.

Many attempts have been made in the past to determine the earth's external gravity field everywhere in space from measurements on its physical surface. The methods used in our investigation are those of the "new geodesy," deriving from a paper by Jeffreys.[2]

Jeffreys[2] theory for calculating the potential outside the earth involves using a surface integral over the earth's physical surface. This method is theoretically exact and involves only the values of observable quantities of the earth's surface. Therefore, it can be applied to an irregular body such as the earth to calculate external potential forces, or force gradients, provided the geometrical shape of the surface is known. If the observed gradients do not agree with those calculated by Jeffreys' method within the accuracy expected, the geometrical shape of the earth's surface may be modified until agreement is obtained. If the entire earth contributes moderately uniformly to the surface integral, a scale factor change in the form of a modified value of the earth's radius would be effective in bringing observed and calculated gradients into agreement. If, however, the surface integral comes almost entirely from the immediate vicinity of the station, the method gives information of purely local significance and says nothing about the dimensions of the earth as a whole.

II. DERIVATION OF JEFFREYS' FORMULA

In his paper[2] Jeffreys uses Green's theorem to derive an exact expression for the Newtonian gravitational potential outside the earth's surface, in terms of a surface integral over the earth's physical surface (or any surface which completely encloses the earth) and a relatively unimportant volume integral throughout the earth.

The advantage of this approach is that it is exact. It is then easy to apply any approximations made in the practical application of the theory. A summary of Jeffreys' derivation is given below.

Let U_p be the Newtonian potential due to a mass within the earth's physical surface at a point P external to that surface. R is the distance from the mass to P (see Fig. D-1).

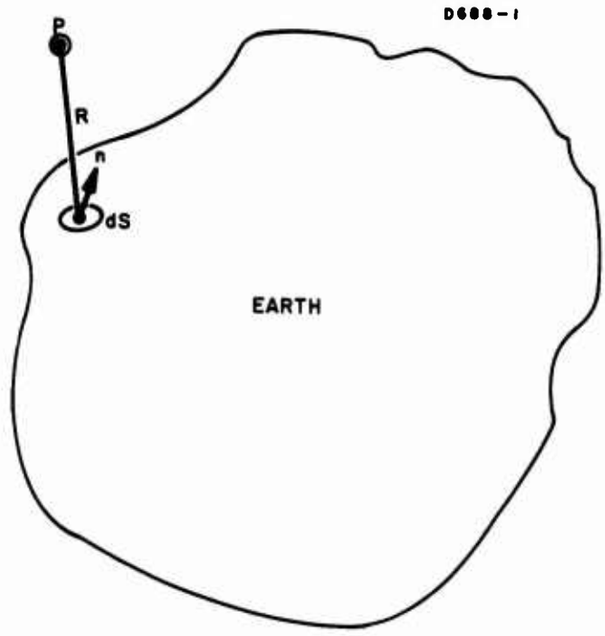

Fig. D-1.

Following Jeffreys,[2] we may apply Green's theorem

$$\iint \left(U \frac{\partial V}{\partial n} - V \frac{\partial U}{\partial n} \right) dS = \iiint (U \nabla^2 V - V \nabla^2 U) \, d\tau , \qquad (6)$$

with the volume integral being through any region and the surface integral over the same region. This is true for any functions of position U and V. In this case we let U represent the Newtonian potential and $V = 1/R$.

The region considered by Jeffreys is bounded internally by a small sphere about P and by the physical surface of the earth. In this case the right hand side is zero since $\nabla^2 V = \nabla^2 U = 0$ in this region.

On the left hand side, as the sphere around P contracts, we find that

$$\iint U \, dS/R^2 \rightarrow 4\pi U_p \tag{7}$$

leaving

$$4\pi U_p = \iint \left\{ \frac{\partial U}{\partial n} \cdot \frac{1}{R} - U \frac{\partial}{\partial n} (1/R) \right\} dS \quad . \tag{8}$$

We actually measure things on the earth with a rotating coordinate system and include the centripetal force in our measurements. We can fix this up by defining a geopotential $\Psi = U + 1/2\, \omega^2 r^2 \sin^2 \theta$ where ω = angular velocity of the earth and r, θ are spherical polar coordinates.

Substituting $U = \Psi - 1/2\, \omega^2 r^2 \sin^2 \theta$ into (8) and utilizing the fact that

$$\iint \frac{1}{2} \omega^2 r^2 \sin^2 \theta \; \frac{\partial}{\partial n} (1/R) - \frac{\partial}{\partial n} \left(\frac{1}{2} \omega^2 r^2 \sin^2 \theta \right) \frac{1}{R} \, dS = \iiint \frac{1}{R} \cdot 2\omega^2 \, d\tau \; , \tag{9}$$

we can show that

$$4\pi U_p = \iint \left\{ \frac{\partial \Psi}{\partial n} \cdot \frac{1}{R} - \Psi \frac{\partial}{\partial n} (1/R) \right\} dS + \iiint \frac{2\omega^2}{R} \, d\tau \quad . \tag{10}$$

If we compare the volume integral correction with the potential due to a uniform density earth

$$U = \iiint \frac{G\rho}{R} \, d(\mathrm{Vol})$$

we see this term is equivalent to a change in the earth's density of $1/4\pi\ (2\omega^2/G)$, or about $1/232$ of the earth's mean density. Now $\partial\Psi/\partial n$ (the component of gravity perpendicular to earth's physical surface) = $g \cos \psi$; where g is the gravity perpendicular to equipotential (level) surface and ψ is the angle between the level surface and the earth's surface therefore, eq. (11) becomes

$$4\pi U_p = \iint \left\{ \frac{g \cos \psi}{R} - \Psi \frac{d}{dn} \left(\frac{1}{R} \right) \right\} dS + \iiint \frac{2\omega^2}{R} \, d\tau \ . \qquad (11)$$

We notice that if Ψ_o is a constant,

$$\iint \Psi_o \frac{d}{dn} \left(\frac{1}{R} \right) = 0 \ .$$

Therefore, if we are only interested in the deviations from the mean potential $\Psi = (\Psi_o - \delta\Psi)$, we obtain

$$4\pi U_p = \iint \left\{ \frac{g \cos \psi}{R} + \delta\Psi \frac{\partial}{\partial n} \left(\frac{1}{R} \right) \right\} dS + \iiint \frac{2\omega^2}{R} \, d\tau \ . \qquad (12)$$

Provided that the shape of the earth is known, the quantities in eq. (12) are all determinable by physical measurement:

g ≡ magnitude of observed gravity at earth's surface

ψ ≡ slope of ground measured relative to level bubble

$\delta\Psi$ ≡ difference in potential from a standard value, i.e., value at any particular point A on the earth's surface. $\delta\Psi_B$ is then

$$\int_A^B g \, dh,$$

with g measured along a path from A to B and dh as corresponding increments in height as measured by leveling.

R, dS, $d\tau$ are all known from the geometry of the situation.

Equation (12) may be differentiated under the integral signs to obtain gradient components in any desired direction.

Evaluation of Integral

Although exact, equation (12) is not convenient because ψ and the direction represented by n (the normal to the earth's surface) vary irregularly and rapidly. The exact formula can be used in a limited region in which U_p or its required derivative is very sensitive, and an approximate form be used at greater distances. For example, at large distances we can approximate $\delta\Psi \approx gH$ and

$$\frac{\partial}{\partial n}\left(\frac{1}{R}\right) = -\left(\frac{1}{R}\right)^2 \cos\theta \approx -\frac{h}{R^2}$$

(See Fig. D-2) so that the second term in (12) becomes

$$\frac{gH\cos\theta}{R^2} \approx \frac{g}{R}\left(\frac{Hh}{R^2}\right) . \qquad (13)$$

We see from this that the second term is a very small correction term when $R > H$ and $R > h$.

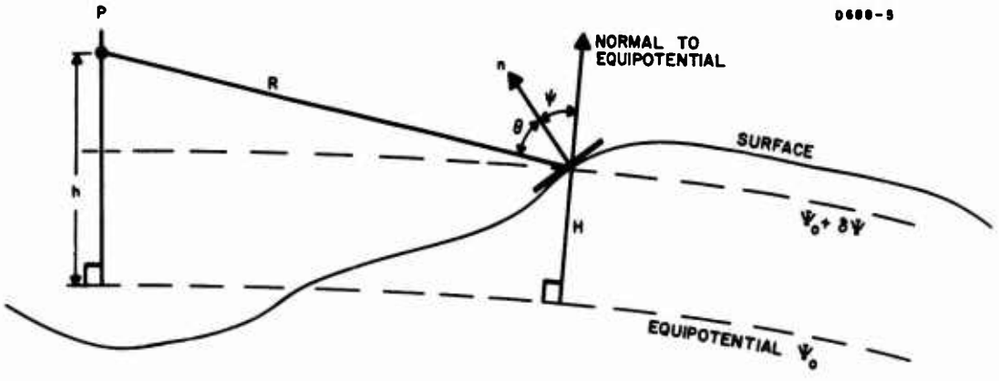

Fig. D-2.

We may also approximate dS by projecting it onto the reference surface Ψ_o with lines joining the perimeter of dS to the earth's center. In this case (see Fig. D-3)

$$dS_o = dS\cos\psi\left(\frac{r_o}{r_o + h}\right)^2 . \qquad (14)$$

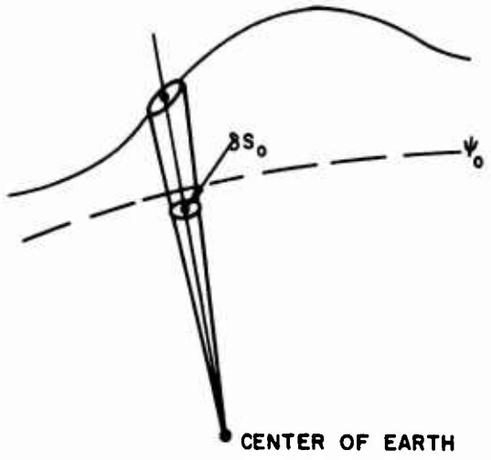

Fig. D-3.

Strictly, Ψ will have to be corrected for the angle between the reference surface Ψ_o and the radius vector; this will amount to a maximum of 12'. A correction on the basis of simple ellipsoidal shape for Ψ_o should be good enough. r_o is the radius vector to Ψ_o at the position concerned. Hence, we may replace

$$\iint g \cos \psi \, \frac{dS}{R}$$

over the physical surface by

$$\iint g \left(\frac{r_o + h}{r_o} \right)^2 \frac{dS_o}{R}$$

over an equipotential reference surface. To a lower degree of accuracy, if we put $r_o = a$ (the mean radius) and expanding $(a + h/a)^2 \approx 1 + 2h/a$, the integral above becomes:

$$4\pi U_p = \iint g \, (1 + 2h/a) \, \frac{dS_o}{R} \quad .$$

for large distances.

This theory was developed to determine the form of S_o from measurements of g. Since we wish to use it the other way around, let us assume that we know, from satellite observations, the form of the equipotential surfaces except for one scale factor. We will then use the theory to determine this scale factor.

We assume that the external potential is known in the form

$$V = \frac{GM}{r}\left[1 + \sum_{2}^{p}(a/r)^n \sum_{m=o}^{n} \overline{P}_{nm}(\sin \phi)\left\{\overline{C}_{nm} \cos m\lambda + S_{nm} \sin m\lambda\right\}\right] \tag{15}$$

where the C_{nm}, S_{nm} have been determined up to $n = p$ from satellite observations and a is the semi-major axis of the ellipsoid which fits best the earth's sea level surface.

Our reference surface is the equipotential surface passing through the ground level beneath the point of computation. The reference (sea level) potential is that given on the reference ellipsoid, i.e.,

$$U = \frac{GM}{r}\left[1 - J_2\left(\frac{a}{r}\right)^2 P_2(\sin \phi - J_4\left(\frac{a}{r}\right)^4 P_4(\sin \phi) + \ldots\right]. \tag{16}$$

The amplitudes of the smaller terms in this series are given by Cook.[3] We can determine the potential at the point below the observation point by leveling, and g measurements of (U - C) where

$$C = \int_{\text{sea level}}^{\text{point}} g\, dh \ .$$

The equipotential reference surface is given by

$$(U - C) = \frac{GM}{r}\left[1 + \sum_{2}^{p}(a/r)^n \sum \overline{P}_{nm}(\sin \phi)\left\{\overline{C}_{nm} \cos m\lambda + S_{nm} \sin m\lambda\right\}\right] \tag{17}$$

which, if GM and a are assumed, allows (a/r) to be determined.

III. APPLICATION OF JEFFREYS' FORMULA

As outlined above, by a direct application of Green's theorem, Jeffreys derives the relation (repeating (12))

$$4\pi U_p = \iint_{\substack{\text{actual earth's} \\ \text{surface}}} \left\{ (g \cos \psi)\, 1/R - \delta\Psi \frac{\partial}{\partial n} (1/R) \right\} dS + \iiint \frac{2\omega^2}{R}\, d\tau \ . \tag{18}$$

For convenience, we repeat the definitions:

U_p ≡ Newtonian potential of matter comprising the earth at a point P outside the earth's physical surface

g ≡ value of gravity at a point on the earth's surface

ψ ≡ slope of earth's surface at the point where the value of gravity is g, i.e., the angle between the normal to the surface at this point and the direction of gravity, or the slope of the surface as measured with a spirit level

$\delta\Psi$ ≡ difference in potential from some standard value Ψ_o. The value of Ψ_o is immaterial because

$$\iint_{\substack{\text{earth's} \\ \text{surface}}} \text{constant} \times \frac{\partial}{\partial n} (1/R)\, dS = 0$$

R ≡ distance from P to the point of the earth's surface

$\frac{\partial}{\partial n}$ ≡ differentiation along the normal to the earth's surface.

dS ≡ an element of area on the earth's surface.

This relation is mathematically exact with no approximations. The right hand side contains quantities which are physically determinable provided the shape of the earth's surface is known.

$g \equiv$ gravity at the earth's surface (measurable)

$\psi \equiv$ the slope of the earth's surface (measurable)

$\delta\Psi \equiv$ difference in potential (measurable by leveling in short increments in combination with gravity observations $-\ \delta\Psi = -\Sigma\, g\, dh$).

We can thus compute U and, with a small correction for rotation we can compute Ψ at all points in space. Hence, we can find gravity at all points in space, as well as its derivatives. Comparison with observations will indicate whether the integral on the right hand side has been evaluated correctly. If it has not, possible reasons could be (1) insufficiently detailed knowledge of g, ψ, or $\delta\Psi$ due to inadequate survey, or (2) incorrect values of R and dS because the wrong shape of the earth has been used.

Because observed surface gravity is an input to the right hand side of the equation, the gradient of U will provide us with the correct surface gravity, whether or not R and dS have been correctly estimated. However, measurements of the second derivatives of U do give a test of our computations of U since it is dependent on the assumed values of R and dS. It therefore tests the correctness of our knowledge about the form of the earth's surface. In principle, then, we can use a combination of gravity and its gradient to test (and hence correct) the shape of the earth's surface as deduced from survey, and use this information to determine GM.

Feasibility

Although the previous discussions show that it is theoretically possible to determine the earth's mean radius and, thereby, GM from measurements of the gravity field and its gradient, further studies have shown that it is not feasible to do this with high accuracy in a practical way.

To demonstrate this point it is not necessary to consider the whole of eq. (18). The second and third terms in (18) are small corrections to the first. The discussion will mainly center around the first term.

$$U_p = \frac{1}{4\pi} \iint \frac{g \cos \psi}{R}\, dS \quad . \tag{19}$$

Equation (19) shows that the external potential is derivable from the surface integral of an observable quantity ($g\cos\psi$) and a geometrical factor (dS/R) which has the dimensions of length. Let us assume that ($g \cos \psi$) can be determined to one part in 10^6 everywhere, and that the geometry of the earth's surface is known with the exception of a scale factor (the true radius of the earth/adopted radius). The terms (dS/R) will be in error by the same scale factor. Hence, observations of U and ($g \cos \psi$) will allow the scale factor to be determined with the same accuracy as ($g \cos \psi$). This term can be measured to one part in 10^6 if ψ is not large, because g can be measured to one part in 10^6 and $\cos \psi \approx (1 - 1/2\, \psi^2)$ for small ψ, so that extraordinary accuracy for ψ is not required.

U cannot be measured directly since there is no direct way of measuring potential with this accuracy. However, we can measure derivatives of U directly; in particular, we can measure the vertical derivative of U $\partial/\partial\nu$ where $\partial/\partial\nu$ is differentiation along the vertical:

$$g \cos \psi \left\{ \frac{\partial}{\partial \nu} \left(\frac{1}{R} \right) \right\} dS = - \frac{g \cos \psi}{R^2} \left(\frac{\partial R}{\partial \nu} \right) dS \qquad (20)$$

Since $(\partial R/\partial \nu)$ is dimensionless, as is dS/R^2, the factor by which we multiply ($g \cos \psi$) is independent of the scale of the survey. Therefore, we cannot determine the scale factor by comparing measured gravity values with those derived from application of (18). This is to be expected; since we are using observed gravity values to compute a value of the potential at a particular point, we may expect to compute gravity correctly from this potential regardless of the scale factor of our survey.

However, we can determine this scale factor by comparing measured gravity gradients with those derived from application of the second derivatives of (18). The weighting factors for ($g \cos \psi$) are of the form dS/R^3, have dimensions (1/Length), and depend on the scale factor of the survey.

If ($g \cos \psi$) can be measured over the surface of the earth, and the shape of the earth's surface is known with the uncertainty of a scale factor (which could be the major axis of the ellipsoid of best fit to the sea level surface) then this scale factor may be determined with the same order of accuracy as ($g \cos \psi$).

The next question is, "What scale factor do we determine?" If the contributions to the surface integral come almost uniformly from the earth's entire surface, then we may determine a scale factor which indeed refers to the earth's radius. However, if the integral comes almost entirely from within 100 miles of the observation point and is thus almost independent of the remainder of the earth, we can then hope to determine only the geometry of the earth's surface within 100 miles. This is not closely related to the shape of the earth as a whole, and therefore tells us nothing about the earth as a whole.

IV. SOLUTION FOR SPHERICAL EARTH

In order to investigate the relative contribution to the surface integral of the various parts of the earth it is not necessary to consider the exact shape of the earth. For this problem an adequate first approximation would involve assumption of a nonrotating body made up of uniform concentric shells. The external surface of the body is spherical and equipotential, and its g is constant on the surface. Since this is true for the earth to within 1%, this model is suitable for a first order calculation of the relative importance of the contributions to the vertical gravity gradient surface integral from the field through the areas on the surface at different distances. The model, shown in Fig. D-4 is a sphere of radius a and center O. The gradient is calculated at the point P which is at a height h above the surface. The differential area considered is the ring on the surface, so that the angle POQ is a constant for all points on the ring.

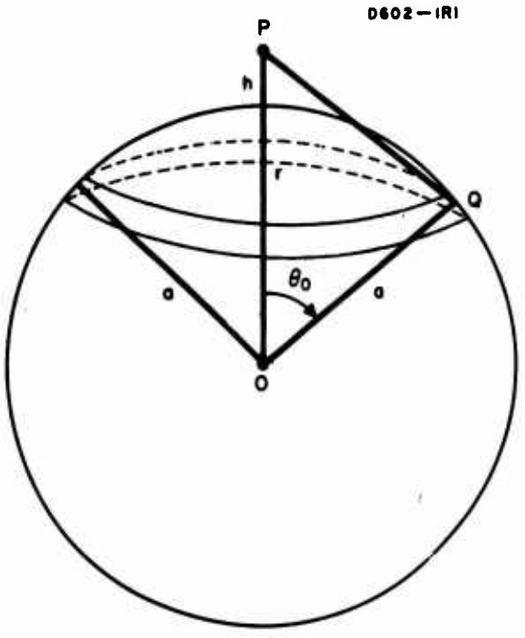

Fig. D-4. Model used for calculation of vertical gravity gradient surface integral.

In this simplified model, $\psi = 90^{\circ}$, g = constant, and $\delta\psi$ and ω are 0. Under these conditions, the equation for the gravitational potential (22) simplifies to the first term (see eq. (23)). The second order gradient of this potential (vertical gravity gradient) is then given by

$$\frac{\partial^2 U}{\partial h^2} = \frac{g}{4\pi} \iint \frac{\partial^2}{\partial h^2} \left(\frac{1}{R}\right) dS \qquad (21)$$

where $R^2 = (a + h)^2 + a^2 - 2a(a + h) \cos \phi$. Evaluating,

$$\frac{\partial^2}{\partial h^2} \left(\frac{1}{R}\right) = - \frac{1}{R^3} + \frac{3(a + h - a \cos \phi)^2}{R^5}$$

and $dS = 2\pi a^2 \sin \phi \, d \phi$. Hence,

$$4\pi \left(\frac{\partial^2 U}{\partial h^2}\right) = 2\pi a^2 g$$

$$\times \int_0^{180^\circ} \frac{(a^2 + 2h^2 + 3 a^2 \cos^2 \phi + 4 ah - 4 a^2 \cos \phi - 4 ah \cos \phi)}{\left\{(a + h)^2 + a^2 - 2a (a + h) \cos \phi\right\}^{5/2}} \sin \phi d\phi \qquad (22)$$

or the contribution from a cap of radius θ may be determined from the above integral over the limits from 0 to θ. This integral may be transformed by writing $x = \cos \phi$:

$$- 2\pi a^2 g \int_1^{\cos \theta} \frac{\{(a^2 + 2h^2 + 4ah) - (4a^2 + 4ah) x + 3r^2 x^2\}}{\{(a + h)^2 + a^2 - 2a(a + h) x\}^{5/2}} dx$$

$$= - 2\pi a^2 g \int_1^{\cos \theta} \frac{f - 2bx + cx^2}{(d - bx)^{5/2}} dx$$

$$= \frac{-2\pi a^2 g}{b^3} \left[- 2c\sqrt{d - bx} + \frac{4(b^2 - dc)}{\sqrt{d - bx}} + \frac{2}{3} \frac{(fb^2 + cd^2 - 2b^2 d)}{(d - bx)^{3/2}} \right]_1^{\cos \theta} \qquad (23)$$

where

$f = a^2 + 2h^2 + 4ah$

$b = 2a(a + h)$

$c = 3a^2$

$d = 2a^2 + 2ah + h^2$

$a \equiv$ radius of sphere

$h \equiv$ height of point above sphere

$x = \cos\theta$

$\left(\frac{\partial^2 U}{\partial h^2}\right)_{\theta_o} \equiv$ contribution to calculated vertical gravity gradient from inside a cap of radius θ_o (see Fig. D-4).

To evaluate (23) it was rewritten with $y = (1 - x)$.

After simplification, eq. (23) becomes

$$\left(\frac{\partial^2 U}{\partial h^2}\right)_{\theta_o} = \frac{-a^2 g}{(a+h)^3}\left[\frac{2h^3 - 2y(a^3+h^3) - 3a(a+h)^2 y^2}{2\{h^2 + 2a(a+h)y\}^{3/2}}\right]_o^{y_o} \tag{24}$$

$$= \frac{a^2 g}{(a+h)^3}\left[1 - \frac{1}{2}\,\frac{2h^3 - 2(a^3+h^3)\,y_o - 3a(a+h)^2 y_o^2}{\{h^2 + 2a(a+h)\,y_o\}^{3/2}}\right].$$

where $y_o = 1 - \cos\theta_o$. This may be written in the form

$$\left(\frac{\partial^2 U}{\partial h^2}\right)_{\theta_o} = \frac{a^2 g}{(a+h)^3} \cdot F \tag{25}$$

where $F = 2$ when the integral is evaluated over the entire earth, i.e., $\theta_o = 180^o$.

Values of F were computed for $h = 0.1$ to 10,000 km and for $\theta_o = 5^o$ to 180^o. The results are given in Table D-1.

For small values of θ_o we may use the plane approximation for small h:

$$\left(\frac{\partial^2 U}{\partial h^2}\right)_{\theta_o} \approx g/a \left(1 + \frac{1}{2\theta_o}\right) . \qquad (26)$$

Hence, a 1^o cap contributes $g/a[1 + (57.3/2)] = 29.65\ g/a$.

The difficulties in using gradients are now plain. Consider a point close to the earth's surface (the table of F shows the values to be very little affected by h until $h > 100$ km). The contribution from a small cap below the point of observation is very large. The contribution decreases as the size of the cap increases out as far as 70^o, but there is very little contribution to the gradient from the region beyond 30^o. If the integration were stopped at 30^o, the calculated gradient would be $2.16\ g/a$ as against the true value of $2.00\ g/a$. Hence, the earth beyond 30^o has only altered the computed gradient by $0.16\ g/a$ or 8%. On the other hand, the zone between 1^o and 5^o contributes $(29.65 - 6.76)\ g/a$ or $22.89\ g/a$, 127 times as much as the earth beyond 30^o. The computations of gradient are almost independent of the distant parts of the earth and are extremely sensitive to the part close to the point of measurement. A near surface measurement of the gravity gradient is thus extremely sensitive to local density fluctuations and is a poor method of trying to determine any quantity which relates to the earth as a whole. It is inconceivable that it could be used to give a determination of the earth's radius to the accuracies desired (parts in 10^5 or better).

Even at a point 1000 km above the surface, over 90% of the gradient originates from within a 10^o cap around the point directly below the measurement. Only at 10,000 km is the contribution spread reasonably uniformly over the earth's surface. At this height, however, the gradient is reduced to 0.055 of its surface value, creating a severe measurement problem.

TABLE D-1

Relative Contribution to Gravitational Gradient
(Ratio of g/a) by Portion of Earth Out to Angle θ

θ (deg) / Height (km)	5	10	20	40	60	80	100	120	140	160	180
0.1	6.764	3.934	2.570	1.987	1.875	1.871	1.901	1.938	1.971	1.992	2.000
1.0	6.763	3.933	2.570	1.987	1.875	1.871	1.901	1.938	1.971	1.992	2.000
10.	6.748	3.927	2.567	1.986	1.874	1.870	1.901	1.938	1.971	1.992	2.000
100.	6.368	3.833	2.533	1.972	1.866	1.866	1.898	1.936	1.970	1.992	2.000
1,000.	0.997	1.810	1.962	1.801	1.779	1.815	1.869	1.921	1.963	1.991	2.000
10,000.	0.017	0.065	0.234	0.689	1.092	1.398	1.625	1.793	1.909	1.977	2.000

PRECEDING PAGE BLANK - NOT FILMED.

V. CONCLUSIONS

In conclusion, although it is theoretically possible to determine the earth's gravitational constant by measurement of the gravity field and its gradient, combined with Jeffreys' method of calculating the field, it is not technically feasible to do this with a high degree of accuracy because of the strong dependence of the gravity gradient on local density fluctuations.

PRECEDING PAGE BLANK - NOT FILMED.

REFERENCES

1. R.J. Bomford, Geodesy, 2nd ed. (Oxford University Press, London, 1962), p. 409.

2. H. Jeffreys, Beit. Geophys. 31, 378-386 (1931).

3. H. Cook, Geophys. J. 2, 199-214 (1959).

APPENDIX E

DISCUSSION AND ANALYSIS OF THE UNIVERSITY OF VIRGINIA NEWTONIAN GRAVITATIONAL CONSTANT EXPERIMENT

(Prepared by H.M. Parker, consultant
to Hughes Research Laboratories)

SUMMARY

This Scientific Report is one portion of a program to find a new experimental method of improving our knowledge of the Newtonian gravitational constant (G). According to the NBS Technical News Bulletin (October 1963), the presently accepted value is $6.670 \pm 0.015 \times 10^{-11}$ $m^3 kg^{-1} sec^{-2}$ (three standard deviations). The University of Virginia experiment, which is now in progress, utilizes a standard Cavendish mass arrangement operated in a rotating reference frame which undergoes angular acceleration proportional to the gravitational interaction. Because this experiment shows promise of improving our knowledge of G, it is necessary that the new experimental designs considered in our studies show promise not only of improving on the known value of G, but also of at least equalling, if not surpassing, the accuracy expected in the University of Virginia experiment. The purpose of this report is to present the current status of the theoretical and experimental work on the University of Virginia project, to give a reasonable prediction of the accuracy which will result from the present project, and to estimate the potential accuracy of the method if a major effort were devoted to it. The conclusions are that the present apparatus will have an accuracy of about one part in 10^4. It is anticipated that a reasonable ultimate experiment should attain accuracies greater than one part in 10^5, perhaps approaching one part in 10^6. The primary limitations are metrology, density inhomogeneities, and determination of precise revolutions, as well as the usual problems such as temperature variations and drifts, external vibrations, alignment, and thermal fluctuations.

I. INTRODUCTION

The basic method of the University of Virginia experiment for a precision determination of the Newtonian gravitation constant may be described as follows.* The experimental apparatus is the standard Cavendish arrangement mounted on a massive precision rotating table (see Fig. E-1). The small analysis system schematically a small dumbbell, is suspended either magnetically or by the weakest possible torsion fiber from a mount rigidly attached to the table. Two large masses also rest on and rotate with the table. A light-beam Jones balance system fixed on the table detects a change in angle between the small mass system and the table (and hence the large mass system); its output is the error signal for the control system which drives the table. Thus the angle between the lines joining the small masses and the line joining the large masses is held (nearly) constant. Consequently, a torque on the small mass system about the vertical axis gives it (and the table because of the control system) an angular acceleration about the vertical axis. In principle, G may be determined from the result if

- A large fraction of the angular accleration of the system results from the gravitational interaction of the small mass system and the large mass system
- The tare acceleration is constant during a time in which the system is operated with and without the large masses
- The masses and geometry of the small and large mass systems are known
- The angular velocity of the table as a function of time is observed and the table follows the motion of the small mass system sufficiently closely.

The purpose of this report is to present the current status of the theoretical and experimental work, to give a reasonable prediction of the accuracy which will result from the present project, and (undoubtedly with less confidence) to estimate the potential accuracy of the method if a major effort were devoted to it.

---

*See H.M. Parker, R.A. Lowry, A.R. Kuhlthau, and J.W. Beams, Bull. Am. Phys. Soc. 11, 850 (1966).

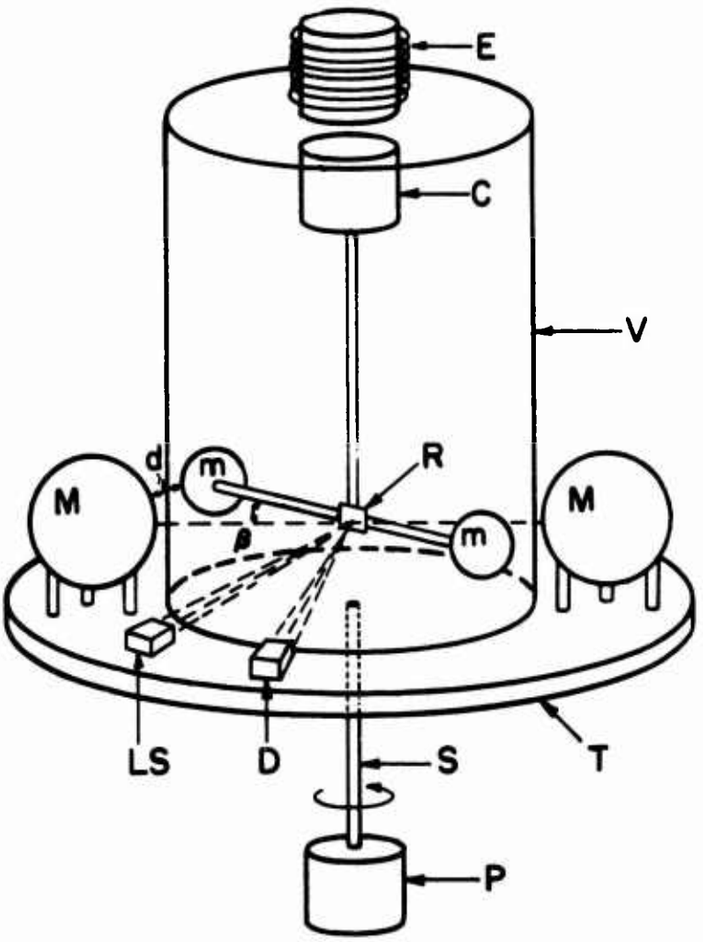

Fig. E-1. Schematic of apparatus.

II. SIMPLIFIED THEORY OF THE ARRANGEMENT

The dominant characteristics of the method may be illustrated by a model of the arrangement in which the small mass system is replaced by two perfect uniform spherical masses connected by a rigid massless rod and the two large masses are perfect uniform spheres (the lines joining their centers bisect each other at the angle β) as shown in Fig. E-2. It is a straightforward process to calculate the gravitational torque on the small mass system and the angular acceleration it produces (for the model $I = 2mr^2$). The result is

$$\dot{\omega}_{grav} = \frac{GM}{\ell_1^3} \frac{\sin\beta}{x} \left\{ [1 + x^2 - 2x\cos\beta]^{-3/2} - [1 + x^2 + 2x\cos\beta]^{-3/2} \right\} \tag{1}$$

where $x = (r_1/\ell_1)$.

Several important characteristics may be deduced from this expression. $\dot{\omega}_{grav}$ has a maximum with respect to β for some value between 0 and $\pi/2$, the precise value depending on the value of x. As x becomes very small, β_{max} approaches $\pi/4$; for larger values of x, β_{max} is somewhat less than $\pi/4$. Thus $\dot{\omega}_{grav}$ is reasonably insensitive to β near β_{max}; the requirement that β remain constant reduces to that involved in using the angular position of the table as a measure of the angular position of the small mass system. In other words, the requirement for knowing accurately the distance between a small mass and a large mass is transferred to the requirement for knowing ℓ_1 accurately (or, more generally, all of the radial distances in the system).

In eq. (1) the value of the small mass m obviously is missing. In this simple model the torque and the moment of inertia of the small mass system are proportional to m, so that $\dot{\omega}_{grav}$ is independent of m. In a real system of given geometry, $\dot{\omega}_{grav}$ will be independent of the density of the small mass system if the density is constant.

On the assumption that the large masses are spheres placed as close as feasible to the symmetry point, for the radius of a large mass we may write $R = \ell_1 - r_1 - \delta$, so that the angular acceleration becomes

$$\dot{\omega}_{grav} = \frac{4}{3}\pi\rho_M G \left(1 - x - \frac{\delta}{\ell_1}\right)^3 \frac{\sin\beta}{x} \left\{ [1 + x^2 - 2x\cos\beta]^{-3/2} - [1 + x^2 + 2x\cos\beta]^{-3/2} \right\};$$

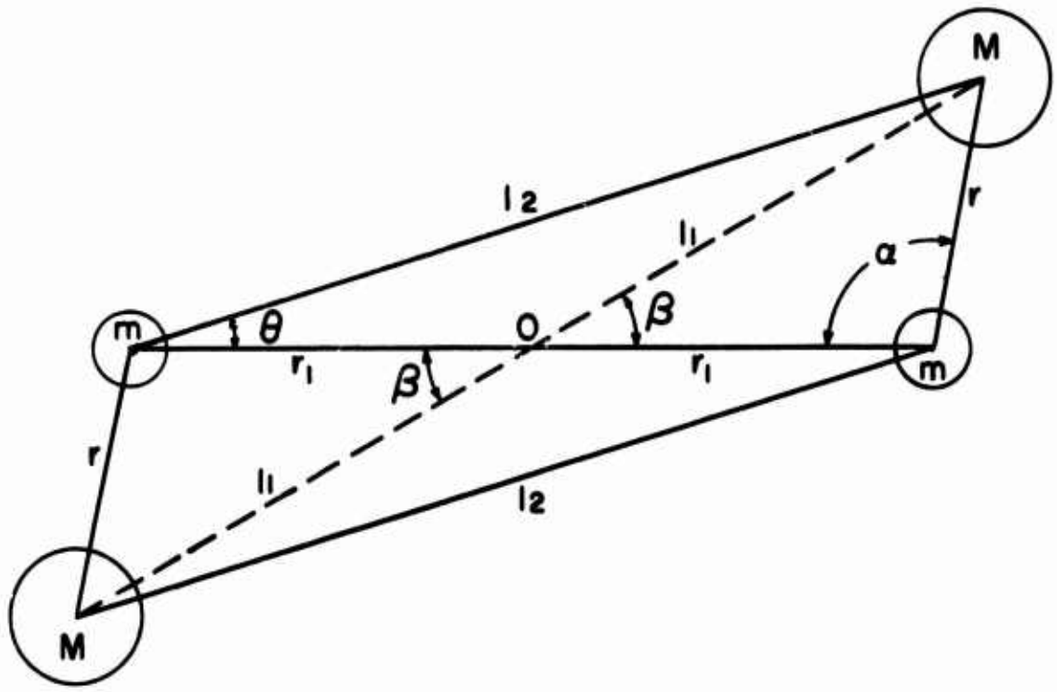

Fig. E-2. Geometry for discussion of gravitational torque.

we can conclude that except for practical limitations on δ (a measure of working space between small and large masses), $\dot{\omega}_{grav}$ is independent of the size of the system. Furthermore, it is obviously desirable that the large masses have large densities. Practical aspects (e.g., the desirability of enclosing the small mass system in a low pressure chamber with the large masses outside) dictate that $x = (r_1/\ell_1)$ be significantly less than unity. Calculations for reasonable values of δ show that as x decreases, $\dot{\omega}_{grav}$ increases. In the limit of small x, $\dot{\omega}_{grav}$ becomes

$$\dot{\omega}_{grav} = 4\pi \rho_M G \left(1 - x - \frac{\delta}{\ell_1}\right)^3 \frac{\sin 2\beta}{(1 + x^2)^{5/2}} \left\{1 + \frac{35}{6} \frac{x^2 \cos^2\beta}{(1 + x^2)^2} + \ldots\right\}. \tag{2}$$

It is interesting that the small x limit

$$(\dot{\omega}_{grav})_{x=o} = 4\pi \rho_M G \approx 0.8 \times 10^{-6} \rho_M \text{ rad/sec}^2 \ (\rho_M \text{ in g/cm}^3)$$

is an upper bound on the gravitational acceleration for this method.

PRECEDING PAGE BLANK - NOT FILMED.

III. SIMPLIFIED THEORY OF MEASUREMENT

A basic postulate for the following discussion is that the direct measurements are the time intervals corresponding to consecutive whole numbers of revolutions. The current experiment is so arranged. It is possible (with considerably more effort and expense) to arrange a finer observation grid (i.e., times corresponding to smaller angular displacements) but it was thought that observations at whole numbers of revolutions would not impose a limitation on accuracy.

The simplifying assumption is that the angular acceleration is constant; hopefully, this is close to reality, but of course it cannot be exactly true. Nevertheless, it should serve as a good basis for a crude accuracy analysis. If $\ddot{\theta} = a = \text{constant}$ where a is either the tare acceleration or $\dot{\omega}_{grav}$ plus the tare acceleration (and $\dot{\omega}_{grav}$ is at least of the same order as the tare acceleration) the usual constant acceleration expressions result:

$$\dot{\theta} = \omega_o + at \quad ; \quad \theta = \omega_o t + \frac{1}{2} at^2$$

where

$$\dot{\theta} = \omega_o \ , \quad \theta = 0 \ \text{ at } \ t = 0 \ .$$

If

$$\theta = 2\pi n \quad \text{for} \quad t = t_n \ ,$$

then

$$t_n = \frac{\omega_o}{a}\left\{\sqrt{1 + \frac{4\pi a n}{\omega_o^2}} - 1\right\} \ ;$$

if $(4\pi an/\omega_o^2)$ is small,

$$t_n \approx \frac{2\pi}{\omega_o}\left\{n - \left(\frac{\pi a}{\omega_o^2}\right)n^2 + 2\left(\frac{\pi a}{\omega_o^2}\right)^2 n^3 + \ldots\right\}$$

$$\Delta t_n = t_n - t_{n-1} = \frac{2\pi}{\omega_o}\left\{1 - \left(\frac{\pi a}{\omega_o^2}\right)(2n - 1) + 2\left(\frac{\pi a}{\omega_o^2}\right)^2 (3n^2 - 3n + 1) + \ldots\right\} .$$

The raw data consist of n, Δt_n pairs from which n, t_n may, if desired, be constructed. Since the acceleration is constant, it may be calculated as follows:

$$a = \frac{\frac{2\pi}{\Delta t_2} - \frac{2\pi}{\Delta t_1}}{\frac{1}{2}(\Delta t_2 + \Delta t_1)} = \frac{4\pi(\Delta t_1 - \Delta t_2)}{\Delta t_1 \Delta t_2 (\Delta t_1 + \Delta t_2)}$$

for consecutive revolutions, or

$$a = \frac{2\pi(\Delta t_n - \Delta t_{n+m})}{\Delta t_n \Delta t_{n+m}\left[t_{n+m} - t_{n-1} - \frac{1}{2}(\Delta t_{n+m} + \Delta t_n)\right]}$$

for the n^{th} and the $n + m^{th}$ revolutions. In order to obtain numbers, we assume that $a \sim 2 \times 10^{-6}$ (rad/sec^2) (a reasonable value for $\dot{\omega}_{grav}$) and $\omega_o \sim 0.1$ rad/sec (which has appeared to be an appropriate value, though the angular speed at which one operates is definitely an important adjustable parameter for the experiment). Let us examine two simple cases.

A. TWO CONSECUTIVE REVOLUTIONS

$$\Delta t_1 = \frac{2\pi}{0.1}\left\{1 - (2\pi \times 10^{-4}) + 2(2\pi \times 10^{-4})^2(1) \ldots\right\} \sim 20\pi = 62.8 \text{ sec}$$

$$\Delta t_2 = \frac{2\pi}{0.1}\left\{1 - (2\pi \times 10^{-4})(3) + 2(2\pi \times 10^{-4})^2(7) \ldots\right\} \sim 20\pi = 62.8 \text{ sec}$$

$$\Delta t_1 - \Delta t_2 = \frac{2\pi}{0.1}\left\{2(2\pi \times 10^{-4}) - 12(2\pi \times 10^{-4})^2 + \ldots\right\} \sim 80\pi^2 \times 10^{-4} = 0.079 \text{ sec}.$$

Obviously the error in

$$a = \frac{4\pi(\Delta t_1 - \Delta t_2)}{\Delta t_1 \Delta t_2 (\Delta t_1 + \Delta t_2)}$$

is dominated by the error in $\Delta t_1 - \Delta t_2$. For times of about 1 min, time intervals can be measured to a few microseconds. The determination of precise revolutions is more difficult. Let us assume that the angular

position sensor can distinguish 10^{-6} revolution (angles to $\sim 6 \times 10^{-6}$ rad). Then the error in Δt_1 and Δt_2 is about 10^{-6} of a period, and

$$\frac{\text{error } (\Delta t_1 - \Delta t_2)}{\Delta t_1 - \Delta t_2} \sim \frac{10^{-6}\,(60)}{0.08} \sim \frac{7.5}{104} ,$$

or about one part in 10^3, which is not a particularly precise result. Operation at a lower angular velocity, allowing a longer time for "at" to accumulate and allowing a smaller initial velocity for comparison, improves the precision. For example, for $a = 2 \times 10^{-6}$, $\omega_o = 0.01$ rad/sec ($\sim$0.1 rpm), $\Delta t_1, \Delta t_2 \sim 600$ sec, $\Delta t_1 - \Delta t_2 = 79$ sec error in Δt_1, $\Delta t_2 \sim 10^{-6}\,(600) = 6 \times 10^{-4}$ and

$$\frac{\text{error } (\Delta t_1 - \Delta t_2)}{\Delta t_1 - \Delta t_2} \sim \frac{10^{-6}\,(600)}{80} = \frac{7.5}{10^6} ,$$

or one part in about 10^5. This simple example indicates the basic desirability of operating at the smallest feasible angular velocities.

B. A LARGE NUMBER OF REVOLUTIONS INTERVAL

Again with $a = 2 \times 10^{-6}$ rad/sec^2 and $\omega_o = 0.1$ rad/sec, let us examine the second expression for a with $n = 1$ and $n + m = 50$ (i.e., a 50 revolution interval):

$$\Delta t_1 = t_1 = \frac{2\pi}{\omega_o}\left\{1 - \left(\frac{\pi a}{\omega_o^2}\right)(1) \ldots\right\} \sim 20\,\pi \text{ sec} = 62.8 \text{ sec}$$

$$t_{50} = \frac{\omega_o}{a}\left\{\sqrt{1 + \frac{4\pi a(50)}{\omega_o^2}} - 1\right\} \sim 3 \times 10^3 \text{ sec}$$

$$t_{50} = \frac{2\pi}{\omega_o}\left\{1 - \left(\frac{\pi a}{\omega_o^2}\right)(2n - 1) + 2\left(\frac{\pi a}{\omega_o^2}\right)^2 (3n^2 - 3n + 1) \ldots\right\} \cong 59.3 \text{ sec}$$

$$\frac{\text{error (a)}}{a} \approx \frac{\text{error } (\Delta t_1 - \Delta t_{50})}{\Delta t_1 - \Delta t_{50}} \approx \frac{10^{-6}\,(60)}{3.5} \sim \frac{2}{10^5} .$$

Fifty revolutions with $\omega_o = 0.1$ rad/sec corresponds to an operating time of about 1 hour, which is not unreasonable. Assuming that the angular position sensor corresponds to the limit of accuracy (10^{-6} rev), a lower angular velocity again improves the precision. For example, $a = 2 \times 10^{-6}$, $\omega_o = 0.02$, $n = 1$, $n + m = 10$ (for about the same running time);

$$\Delta t_1 = t_1 = \frac{2\pi}{\omega_o}\left\{1 - \left(\frac{\pi a}{\omega_o^2}\right)(1) + \ldots\right\} \sim 100\,\pi \text{ sec} = 314 \text{ sec}$$

$$t_{10} = \frac{\omega_o}{a}\left\{\sqrt{1 + \frac{4\pi a\,(10)}{\omega_o^2}} - 1\right\} \sim 2750 \text{ sec}; \; t_g \cong 2510 \text{ sec}$$

$$\Delta t_{10} \cong 240 \text{ sec}; \quad \Delta t_1 - \Delta t_{10} \cong 74 \text{ sec}$$

$$\frac{\text{error (a)}}{a} \approx \frac{\text{error } (\Delta t_1 - \Delta t_{10})}{\Delta t_1 - \Delta t_{10}} \cong \frac{10^{-6}\,(314)}{74} \approx \frac{4.2}{10^6} .$$

These simple considerations provide a basic idea of the error involved in the method and clarify the role played by the angular velocity.

IV. TYPES OF SMALL MASS SYSTEM SUPPORTS

It is appropriate to discuss here the various types of supports which have been considered for the small mass system. From the beginning of the experiment the University of Virginia group has believed that a magnetic support system would probably be superior, though it was recognized that certain aspects of a typical magnetic support system are reasonably uncertain. Specifically, bodies supported in one dimensional magnetic systems have been observed to execute slow oscillatory rotational motion about a vertical axis even in the most quiescent state. This lack of axial symmetry of the supporting magnet and supported body undoubtedly arises from the properties of real bodies and systems. To our knowledge, there has been no serious study of this effect nor any serious attempt to minimize it. Assuming that conservative and/or dissipative torques will exist about the vertical axis of the small mass system when a magnetic support is used, the magnitude of the effect and the ability to control it adequately must be of primary importance. For example, it might be of considerable importance whether the support magnet is attached to the rotating table or fixed in the laboratory. With the magnet fixed, a conservative torque would be periodic and would therefore tend to cancel out; a dissipative torque, however, would always be in the same direction. With the magnet attached to the table, the torque would be constant (assuming β constant); however, it might be difficult to determine the position or positions in which the torque is as small as desirable and varies with angular position as slowly as desirable. The apparatus is now being modified to use a magnetic support, and both methods of fixing the magnet will be tested.

The other basic method of small mass system support, used in the preliminary effort, is the use of a small torsion fiber (a tungsten fiber was used first, and then a quartz fiber). There are two basic difficulties with this method. (1) It is difficult to minimize the change in the torque on the small mass system resulting from the twist in the fiber; even if the fiber torsion constant were really constant (perhaps a good assumption for a quartz fiber) the fiber torque would impose a serious limitation on the allowable changes in angle β. (2) Misalignment of the top fiber support point from the table rotation axis and misalignment where the fiber is attached to the small mass system produce a centrifugal twist in the fiber, resulting in a torque which is proportional to the square of the angular speed.

PRECEDING PAGE BLANK - NOT FILMED.

V. GEOMETRY OF SMALL AND LARGE MASS SYSTEMS

Several geometries have been considered for the basic mass systems. Spheres and right circular cylinders have been considered for the large masses; dumbbells, cylinders, and discs have been considered at least casually for the small mass system. The most important concern is ease of precision fabrication and associated density homogeneity; ease of calculating the gravitational interaction is also important. For the large masses, metallurgists consider it more feasible to fabricate precise spheres than right circular cylinders; in addition, calculations are easier with spheres. For the small mass system, real dumbbells are difficult to fabricate, and calculations must include corrections for the connecting mass. It was concluded that the cylindrical shape shows the most promise.

The current precision experiment will use sintered tungsten spheres for the large masses*; the small mass system will use a quartz cylinder, with the rest of the system close to and axially symmetrical about the vertical axis. The parts of the small mass system other than the quartz cylinder will have relatively small contributions to the moment of inertia and the gravitational torque and these can be corrected for adequately. Fortunately, the gravitational interaction between a cylinder and two point (spherical) masses is not difficult to calculate, and this has been done. The procedure involves the calculation of the gravitational potential at any point in space resulting from and outside of a right circular cylinder starting with a circular ring element of the cylinder† and integration over the volume of the cylinder. The result is a series of Legendre polynomials. The force on a point mass can then be found by taking the gradient of the potential, and the torque on the cylinder can be calculated. The angular acceleration of the cylinder is (in the precision expression the contributions of the rest of the small mass system would be included)

$$\dot{\omega} = 24\,\frac{MG}{RL^2}\left[1 + 3\left(\frac{a}{L}\right)^2\right]^{-1} \sum_{\ell=0}^{\infty} \sum_{k=0}^{\ell} \sum_{j=1}^{k+1} A_{jk\ell} \left(\frac{2a}{L}\right)^{2(j-1)} \left(\frac{L}{2R}\right)^{\ell} \frac{2}{2\theta}\left[P_e\,(\cos\theta)\right] \; ; \qquad (3)$$

*Supplied by Union Carbide, Y-12 plant, Oak Ridge, Tennessee.

†J.D. Jackson, Classical Electrodynamics (Wiley, New York, 1962), p. 64.

here

$M \equiv$ mass of one (each) of the large masses

$R \equiv$ distance of a large mass from the center of the cylinder

$L \equiv$ length of the cylinder

$a \equiv$ radius of the cylinder

$\theta \equiv$ angle between the cylinder symmetry axis and the line from the center of the cylinder to a large mass (same for both masses).

The sum over ℓ includes only even integers of ℓ. It is estimated that about five terms in this series will be required for accuracy of one part in 10^6. Equation (3) corresponds to an ideal situation: equal M's, perfect geometry, etc. The construction of appropriate expressions for unequal masses, additional contributions to small mass system moment of inertia, etc., is straightforward. It is also interesting that the value of θ ($\theta = \beta$, used earlier) where $\dot{\omega}$ is maximum is closer to $\pi/4$ than for the dumbbell model.

VI. THE MOTION PROBLEM

In the actual experiment, of course, the motion of the small mass system will not be a constant acceleration. However, with the anticipated abundant data for each experimental run – n, Δt_n pairs for a reasonably large number of revolutions – it is hoped that the data can be reduced so that maximum precision may be extracted. With some type of least squares procedure anticipated, it is obviously desirable to know the form of the solution of the equation of motion. Two effects on motion have been studied in considerable detail.

A. FIXED MASS EFFECT

Early in the study it was recognized that the masses fixed in the laboratory and nearby would have an effect on motion. Rough estimates indicate that a 200 lb man at a distance of about 20 ft exerts a peak torque on the small mass system which is approximately equal to the torque corresponding to a precision of one part in 10^5. It may be clearly shown that the fixed mass torque in the laboratory is as $\sin 2\theta$ where θ is the angular position of the small mass system (first term in the expansion of eq. (3)). Moreover, with the support magnet fixed in the laboratory the conservative support magnet torque is expected to behave as $\sin(m\theta)$, or as a sum of such terms, where m is an integer. Therefore, it becomes interesting to examine a motion equation of the form $\ddot{\theta} = a + A \sin(m\theta + m\phi)$. We shall not attempt to narrate in detail the considerable effort devoted to the solution of this motion problem, but will merely summarize the current state of the investigation. The first integral of this equation (the "energy" equation) is

$$\dot{\theta}^2 = \dot{\theta}_o^2 + 2a\theta - \frac{2A}{m}\left\{\cos(m\theta + m\phi) - \cos m\phi\right\}. \qquad (4)$$

The next integral cannot be found in closed form. Furthermore, since we are concerned with large values of θ (at integral multiples of whole revolutions), small angle approximations are useless. An expansion of the pertinent quantities shows that the time for n revolutions t_n may be written in the form

$$t_n = \frac{\omega_o}{a}\left\{\sqrt{1 + \frac{4\pi a n}{\omega_o^2}} - 1\right\} + K_1 n + K_2 n^2 + \ldots$$

where K_i is a function of A, a, ω_o, ϕ.

An inspection of (4) is interesting, however. Consider the value of $\dot{\theta}^2$ at $\theta = 2\pi n$. The A term on the right always has the same value (i.e., zero), even though the time average of the velocity over one revolution

$$\bar{\dot{\theta}}_n = \frac{2\pi}{\Delta t_n}$$

(a direct result of the data) is a nonzero function of the parameter A.

If $\dot{\theta}^2$ is the energy, the constant acceleration a clearly corresponds to a linear increase in energy with angular displacement. The periodic acceleration (A term) corresponds to a periodic (in θ) oscillation of energy, i.e., transfer of energy to and from the small mass system. The space (angular displacement) average energy, which changes with time, must then result from the altered energy distribution in time, since the period is continually and monotonically changing. Therefore, if data actually containing some fixed mass effect were reduced as if the effect were absent, little error would be expected. This reasoning led to the following computer experiments.

If values of a, ω_o, A, ϕ, m are given, eq. (4) can be used to calculate Δt_n (single numerical integration), the time for the n^{th} revolution. These n, Δt_n pairs then constitute the data. If constant acceleration is assumed, the acceleration for two consecutive revolutions can be calculated

$$\bar{a} = \frac{4\pi\,(\Delta t_{n-1} - \Delta t_n)}{\Delta t_n\,\Delta t_{n-1}\,(\Delta t_n + \Delta t_{n-1})}$$

and compared with the original acceleration a.

$$fDa = \frac{\bar{a} - a}{a} \quad .$$

Some preliminary results are given in Table E-1.

Because of the integration error in evaluating the integral for Δt_n, values of $fDa = (\bar{a} - a/a)$ which are less than about 10^{-7} are not significant. Very roughly, the error in $\bar{a}$ appears to be proportional to A^2/ω_o^2, decreasing slightly as a increases. Obviously, the calculation of an acceleration $\bar{a}$ from two consecutive real data points, as we have done here, can give no indication of the actual error existing in $\bar{a}$. (In this numerical experiment, a is known.) These numerical experiments are continuing in an effort to (1) refine the error dependences, and (2) investigate the possibilities when runs of many data points are reduced.

TABLE E-1

Preliminary Results of Computer Experiments

ω_o, rad/sec	n	a, rad/sec^2	A, rad/sec^2	ϕ	m	fDa = $\frac{\bar{a} - a}{a}$
0.1	10	2×10^{-6}	10^{-3}	0	1	2.96×10^{-3}
0.1	10	2×10^{-6}	10^{-3}	π	1	4.4×10^{-3}
0.1	10	2×10^{-6}	10^{-3}	0	2	2.97×10^{-3}
0.1	10	2×10^{-6}	10^{-3}	$\pi/2$	2	4.39×10^{-3}
0.1	10	2×10^{-6}	10^{-4}	$\pi/8$	2	3.3×10^{-5}
0.1	10	2×10^{-6}	10^{-6}	$\pi/4$	2	-2.3×10^{-8}
0.1	10	10^{-4}	10^{-6}	0	2	6×10^{-9}
0.4	10	2×10^{-6}	10^{-3}	$\pi/8$	2	1.4×10^{-5}
0.2	10	2×10^{-6}	10^{-3}	$\pi/8$	2	2.22×10^{-4}
0.05	10	2×10^{-6}	10^{-3}	$\pi/8$	2	3.28×10^{-2}
0.025	10	2×10^{-6}	10^{-3}	$\pi/8$	2	2.10×10^{-1}

Even the most preliminary results are illuminating, however. Considering the laboratory fixed mass effect, an upper bound on A may be determined as follows. The entire space external to the rotating table system may be considered either occupied by mass of density ρ_{av} or empty; we then look for a mass distribution that would produce the maximum A. It is entirely reasonable that this configuration is two spheres placed symmetrically on either side of the system and of infinite radius ($x \rightarrow 0$). The acceleration (simple dumbbell model for the small mass system) for this configuration is $A = 4\pi \rho_{av} G$. If $\rho_{av} = 3.5$ g/cm^3 is taken as reasonable, the result is $A = 3 \times 10^{-6}$ rad/sec^2. Therefore, 3×10^{-6} rad/sec^2 is an absolute upper bound on A for a laboratory fixed mass effect; a more practical value would be two or more orders of magnitude less than this. It appears unlikely that a laboratory fixed mass effect will be significant, except possibly for operation at extremely small angular velocities.

An $A \sin(m\theta + m\phi)$ effect is expected for the magnetic suspension arrangement in the laboratory fixed magnet case; here there is no way to determine theoretically an upper limit on A. However, limits on A may be determined experimentally if the oscillatory motion is observed when the small mass system is suspended magnetically.

It is important to recall that G will be determined by comparing the motions with and without the large masses. Thus it is very likely that additional cancellation of errors will occur and can be demonstrated. These ideas are also included in the continuing numerical experiments.

B. CENTRIFUGAL EFFECT

When the small mass system (model dumbbell or actual cylinder) is connected to the support point (table — or magnetic sphere in the magnetic suspension case) by a very flexible fiber, misalignment in the attachments of the fiber and the position of the top support point generally produce a bending and twisting of the fiber as it deflects outward in the centrifugal field. Although it is hoped that these errors will be small, they are nonzero and are not accurately measurable. The result is an additional torque and hence an angular acceleration of the small mass system which is proportional to the square of the angular speed. An equation of motion of the form $\ddot{\theta} = a + k\dot{\theta}^2$ has been derived. Two cases result when a and k have the same and opposite signs. Clearly, for $a > 0$, $k > 0$,

$$e^{-k\theta} = \sqrt{1 + \omega_o^2 \, k/a} \;\; \cos\left[\sqrt{ak}\, t + \phi\right]; \quad \tan\phi = \cos\sqrt{k/a}$$

and for $a > 0$, $k < 0$,

$$e^{-k\theta} = \sqrt{1 + \omega_o^2 \, k/a} \;\; \cosh\left[\sqrt{-ak}\, t + \phi\right]; \quad \tan h\phi = \omega_o \sqrt{-\, k/a} \;;$$

in each case $\theta = 0$, $\dot{\theta} = \omega_o$ at $t = 0$. Numerical experiments have been performed for the first case ($a > 0$, $k > 0$). Times for N revolutions t_N were calculated from the solution (the expression was arranged carefully to avoid excessive dropout at small values of k), and the resulting perfect data were reduced as if the motion were constant acceleration motion. The resulting values of $\bar{a}$, each derived from two consecutive revolutions, changed (increased) with the number of revolutions, and were least squares fitted to an expression of the form $\bar{a} = c_o + c_1 \theta^2$;

here $\dot{\theta}$ is also calculated as if the acceleration were constant. The fitted values of C_o and C_1 were compared with a and k, respectively. Some preliminary results are shown in Table II, where N is the total number of revolutions (N - 1 is the number of values of $\bar{a}$ reduced), fDa = $(c_o - a)/a$, and fDk = $(c_1 - k)/k$.

TABLE E-II

Preliminary Results of Numerical Experiments

N	a	k	ω_o	fDa	fDk
10	2×10^{-6}	10^{-4}	0.1	-1.9×10^{-6}	3.47×10^{-6}
30	2×10^{-6}	10^{-4}	0.1	-1.89×10^{-7}	-1.20×10^{-8}
10	2×10^{-6}	10^{-4}	0.05	-2.05×10^{-7}	2.65×10^{-7}
10	2×10^{-6}	10^{-4}	0.5	-9.0×10^{-5}	7.14×10^{-6}
10	8×10^{-6}	10^{-4}	0.1	-1.08×10^{-7}	-2.83×10^{-7}

The obvious qualitative results from these experiments are the following:

1. The centrifugal term mustnot dominate the constant term (for accurate reduction), and thus low angular velocities are indicated.

2. For larger data sets (N = number of revolutions), the reduction is better.

3. The centrifugal effect is easily seen in the results which are reduced on the basis that the acceleration is constant.

4. A sizable centrifugal effect can be tolerated and the constant term may still be extracted with reasonable accuracy.

More detailed numerical experiments are in progress.

C. COMBINED FIXED MASS AND CENTRIFUGAL EFFECTS

Very recently a motion equation of the form $\ddot{\theta} = a + k\dot{\theta}^2 + A \sin (m\theta + m\phi)$ was integrated once to give

$$\dot{\theta}^2 = \omega_o^2 e^{2k\theta} - \frac{a}{k}(1 - e^{2k\theta}) + \frac{2A}{m\left(1 + \frac{4k^2}{a^2}\right)} \left\{ \left[-\frac{2k}{m} \sin (m\theta + m\phi) - \cos (m\theta + m\phi) \right] + e^{2k\theta} \left[2\frac{k}{m} \sin m\phi + \cos m\phi \right] \right\};$$

this can be used to calculate (with one numerical integration) the time for the n^{th} revolution, and thus perfect data can be generated for a combined fixed mass and centrifugal effect case. The perfect data may be reduced as if the acceleration were constant, and they may be fitted to appropriate forms to determine how well the parameters (particularly a) can be recovered and how the error depends on the values of a, k, A. It is anticipated that this case will not be drastically different from that for the centrifugal effect alone.

It should be noted that a considerable effort has been devoted to the motion problem. We believe the above type of analysis (or similar analyses if a different type of acceleration component is found) forms a sound basis for the study of real data. We believe that the noise level of real data at least can be demonstrated.

VII. MISALIGNMENT ERROR

Ideally, the center of symmetry of the small mass system should lie at the midpoint of the line joining the centers of the two (equal) large masses, and this point should lie on the axis of rotation of the table. Departures from this ideal arrangement naturally will result in errors. There are at least two types of errors which may be encountered: (1) error in the gravitational torque, because of the misalignment; (2) dynamical effects.

The change in the torque as a result of geometrical error is of second order in the linear displacements. For example, consider the situation sketched below:

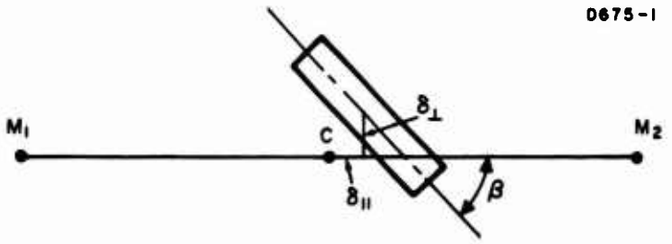

here an error $\delta_{||}$ and $\delta_{\perp}$ is assumed in the position of the center of symmetry of the small mass cylinder, and no error is assumed in the angle β. A simple analysis of the first term of $\dot{\omega}$ ($\sim$95% of $\dot{\omega}$) shows that the fractional change in $\dot{\omega}$ is proportional to $(\delta/R)^2$, with coefficients of +6 for $\delta_{||}$ and -7/2 for $\delta_{\perp}$. If R $\sim$ 8 cm, errors of $\sim$ 1 mil for $\delta_{\perp}$ and $\delta_{||}$ correspond to changes of one part in 10^6 for the torque. Since interferometric methods are to be used to measure distances and to monitor (and hopefully adjust) alignments and since 1 mil is about 40 wavelengths, we hope misalignments can be maintained below this level.

The situation is similar for errors in the vertical position. The large sphere centers and the cylinder's symmetry axis ideally lie in the same horizontal plane. The torque behaves as the cosine of the angles with a mean plane, and therefore the fractional changes are as $(\delta/R)^2$. Vertical positioning to less than 1 mil should be possible.

The dynamical effect is more subtle. A basic point of departure is as follows. Assume that the support point and the center of mass of the small mass system do not coincide with the rotation axis of the table. If a frame rotating with the table is used instead of an inertial reference frame and constant angular velocity is assumed, a (fictitious, inertial) centrifual gravitational field must be added. We can show clearly that the radial centrifugal field $(\omega^2 \bar{r})$ gives a resultant force on a body (at rest in the rotating frame) which is equal to the resultant force if all the mass were concentrated at its center of mass. Moreover, the moment of the centrifugal force about the center of mass has no component parallel to

the angular velocity and the perpendicular components vanish if the body is a lamina in a plane perpendicular to $\vec{\omega}$ or if certain products of inertia are zero. Thus the most obvious source of a dynamical effect arises from the detailed manner in which the force for balancing the centrifugal force is applied to the body. Observing again from the nonrotating frame, we may say that if the force for producing the centripetal acceleration of the center of mass of the rotating body is not effectively applied along a line through the center of mass, it will also produce a moment of force about the center of mass and will tend to contribute an additional angular acceleration.

The following description applies for the small mass system. First, consider the case in which a very flexible fiber connects the cylinder (probably with a vertical, rigid stem) to a support point, either a magnetically supported body or a point rigidly attached to the table. If the top support point does not lie exactly on the table's rotation axis, the bottom of the small mass system (the cylinder) will deflect outward as the table and small mass system rotate. If the bottom of the fiber is not perfectly aligned with the center of mass of the cylinder and stem, the centripetal force on the cylinder is applied off center and a torque results on the cylinder. Note that the servo system driving the table (ideally) prevents any angular displacement of the cylinder relative to the table. Such a misalignment of the top and bottom of the flexible (but not perfectly flexible) fiber generally produces an angular acceleration of the small mass system proportional to the square of the angular speed. Although an analysis has been made (Timoshenko's problem of the compressively loaded column can easily be converted to a tension loaded column), the results are of limited value, since the important misalignment parameters cannot be evaluated accurately. The most important result is that we can conclude that misalignment errors on the order of 1 mil, with the contemplated angular speeds (and the contemplated weak fibers) should give centrifugal angular accelerations which are one or two orders of magnitude smaller than that resulting from gravitational interaction. Of greater importance, assuming a fixed small mass system arrangement, an angular acceleration component proportional to ω^2 can be accurately separated out of the data, as demonstrated in the computer experiments described elsewhere.

It should be noted that if the entire small mass system is rigid (i.e., if the flexible fiber is replaced with a rigid rod) and the top of the system is magnetically supported, then for reasonable configurations the angular acceleration resulting from the centrifugal effect is expected to be virtually zero, even when the top support point is displaced from the axis of rotation. Here it might be noted that the first magnetically supported system to be used contains a flexible fiber (100 μ quartz, a fairly stiff fiber), and a centrifugal effect is expected.

The preliminary conclusion is that misalignment errors should not be a major source of final error, if the interferometric techniques for observing and adjusting alignment are developed successfully. Positioning accuracy of 1 mil does not appear prohibitively difficult.

PRECEDING PAGE BLANK - NOT FILMED.

VIII. ACCURACY ANALYSIS FOR THE G DETERMINATION

G will be determined from an expression of the following form:

$$\dot{\omega}_{grav} = \frac{GM}{R^3 \frac{I}{mL^2}} f\left(\beta, \frac{a}{L}, \frac{L}{R}\right) . \qquad (5)$$

For the present purpose, assume that the two large masses are identical. If they were not quite identical, $\dot{\omega}_{grav}$ would be written as the sum of two terms similar to that of (5), and no significant change would occur in the accuracy considerations. With a cylinder for the basic small mass system (where the other parts have 90^o rotational symmetry), the function f is the series in derivatives of the even Legendre polynomials, with coefficients which are series in $(a/L)^2$, as indicated earlier. R is the distance of the center of a large mass from the center of the cylinder. I is the moment of inertia of the small system and a and L are the radius and length, respectively, of the cylinder. $\dot{\omega}_{grav}$ is the measured angular acceleration of the small mass system resulting from the gravitational interaction with the large mass system. In deriving the equation, the ideal geometry of the small and large mass system is assumed.

If the expression is solved for G, the variation is taken for all the quantities whose values must be found (measured or calculated), and the resulting expression is divided by the original one, the following results:

$$\frac{\delta G}{G} = \frac{\delta\dot{\omega}_{grav}}{\dot{\omega}_{grav}} + \frac{3\delta R}{R} - \frac{\delta M}{M} + \frac{\delta(I/mL^2)}{I/mL^2} - \frac{\delta f}{f} .$$

If f is a function of β, (L/R), and a/L; if the first two terms of f are sufficient (one term for the $(\delta R/R)$ part); if I is taken as the moment of inertia of the cylinder alone; and if reasonable and expected values are used for the various quantities, we obtain

$$\frac{\delta G}{G} = \frac{\delta\dot{\omega}_{grav}}{\dot{\omega}_{grav}} + \frac{3\delta R}{R} - \frac{\delta M}{M} + 0.052\,\frac{\delta a}{a} - 0.052\,\frac{\delta L}{L} - \frac{(\partial f/\partial\beta)\,\delta\beta}{f} .$$

We may see the direct sources of error in the determination of G. If the variations are called errors and if it is assumed that the errors have normal distributions, the fractional error in G will be given by the square root of the sum of the individual fractional errors. We shall consider the error sources by type.

A. METROLOGY: ((δR/R), (δM/M), (δa/a), (δL/L))

1. δa/a, δL/L

The diameter 2a and length of the quartz cylinder to be used for the small mass system will be approximately 1/4 in. and 1.5 in., respectively; the density is assumed constant. If a is constant, an error of 1 wavelength of light (5×10^{-5} cm) in the diameter gives $0.052\ (\delta a/a) \sim 0.82 \times 10^{-5}$. Similarly, if L is constant (a better prospect), an error of 1λ in the length gives $0.052\ (\delta L/L) \sim 0.7 \times 10^{-6}$. Therefore, a measurement of the cylinder dimensions, especially the cylinder diameter, is probably important. The details of this problem have not been worked out. It should be noted that departures from a cylindrical shape indirectly induce other errors through the influence on the gravitational torque and moment of inertia. When these errors are determined or their limits are determined, limits on the indirect errors may be established. The supplier is attempting to make a fused quartz cylinder with a diameter which is constant to one part in 10^5.

2. δM/M

It is expected that the Bureau of Standards will determine the mass of the large sintered tungsten spheres and that an accuracy of better than one part in 10^6 will be achieved. The large mass supplier (the Y-12 group) expects to achieve sphericity to about 5 μin. It is hoped that the absolute diameter may be measured to about the same order of accuracy.

3. δR/R

Interferometric techniques are being developed for measuring the distance between the most distant surfaces of the two large spheres after they have been positioned on a quartz plate on the table. R will be deduced from this measurement and from the known diameters of the spheres. Fortunately, the positioning and aligning errors are not critical (see below). An error in R corresponding to one fringe shift gives $(\delta R/R) \sim 0.3 \times 10^{-5}$.

B. TECHNIQUE AND PROCEDURE: $\left(\frac{\frac{\partial f}{\partial \beta}\delta\beta}{f}, \frac{\delta\dot{\omega}_{grav}}{\dot{\omega}_{grav}}\right)$

1. $[(\delta f/d\beta)\,\delta\beta]/f$

The function $f(\beta, (L/R)\,a/L)$ has a maximum with respect to β at an angle just slightly less than 45^{o} (estimates using the first two terms of f and the cited values of a and L give $44^{o}\ 17'$). Since a precision method of measuring β has not been devised, and since f changes slowly around its maximum value, it is anticipated that $\dot{\omega}_{grav}$ will be measured with reasonable accuracy in β ranging across β_{max}, and that the value at β_{max} will be inferred. An accuracy of 1 mil in adjusting a sensor at 5 in. radius should be sufficient to yield the maximum $\dot{\omega}_{grav}$ to an accuracy of one part in 10^{6}.

2. $\delta\dot{\omega}_{grav}/\dot{\omega}_{grav}$

The majority of the experimental, operative errors are found in the term $\delta\dot{\omega}_{grav}/\dot{\omega}_{grav}$. The recognized pertinent factors in determining this term are the following:

a. The basic procedure for extracting the angular acceleration resulting from the gravitational interaction between the large and small mass systems is to compare two runs (or portions of two runs), one with the large masses in place and one with the large masses removed. The critical factor in this procedure is the validity of the necessary assumption that all other accelerations present (the tare accelerations) are identical for both runs. It is anticipated that a comparison of many such pairs of runs (and the values of $\dot{\omega}_{grav}$ extracted) will provide a suitable basis for an accurate analysis of ω_{grav}.

b. Errors in alignment of the apparatus cause errors in the measured acceleration. As indicated earlier, it is fortunate that the error is of second order in the linear misalignment. Alignment procedures have been developed which are expected to reduce the misalignments to less than 1 mil (errors of less than 1 or 2×10^{-6}). The testing of these procedures will provide verification of the misalignment effects. No difficulty is anticipated here.

c. The time measurement is more than adequate for the determination of the times for consecutive revolutions of the table. The sensing of precise revolutions is more critical. The present sensing system utilizes 0.01 in. circular apertures at a radius of about 100 in., giving an optical signal width of about 10^{-4} rad; with another order of magnitude derived from the constancy of the signal level triggering, this results in a resolution of about 10^{-5} rad. The configuration is being changed (slit rather than circular aperture); with other refinements, this is expected to result in angular position sensing to better than one part in 10^6 ($2\pi \times 10^{-6}$ rad in 2π rad).

d. A remaining (and serious) error results because the motion of the small system is not completely synchronous with that of the table. The system which detects the changes in the relative angular position of the small mass system and the table can easily sense $\Delta\beta$ of the order of 10^{-6} rad; it furnishes the error signal for the control system which drives the table. This error signal is plotted on a strip recorder as a part of the experimental data, and it can be calibrated with reasonable accuracy in terms of changes in the angle β. However, the present table has lubricated ball bearings and the table driving torque is largely (almost completely, since the accelerations are small) that required to balance the bearing friction torque. Moreover, the friction is not constant. In addition to exhibiting a variation of about 10% with a period equal to that of the table, the friction has an appreciable variation component with a period twice that of the table as well as appreciable higher frequency components. The offset for driving the table in one direction is about 50×10^{-6} rad.

If the $\Delta\beta$ offset (between the small mass system and the table) were really constant during a run, no error would result from it. However, the variation in the $\Delta\beta$ does produce an error. This is particularly true of the $\Delta\beta$ variation component, which has a period twice that of the table when the data are reduced by considering consecutive single revolutions. One solution (which was demonstrated for some crude data) is to calculate accelerations by considering consecutive intervals of two revolutions each; this procedure doubtless will be utilized in the study of good data. It should be mentioned that an obvious improvement is to use a rotary table with less friction and less variation in the friction; gas bearings come to mind immediately.

e. The system is now being studied with the crude mass systems and a magnetic suspension for the small mass system (with the support magnet attached to and rotating with the table). An aluminum cylinder and stem are attached by a fairly long quartz fiber to a magnetically soft, magnetically supported sphere. It has been found that the small mass system (the sphere) experiences a torque about the vertical axis which varies with relative angular position of the sphere and the support magnet; at least initially, this torque was

uncomfortably large. Such a torque probably results from a combination of a lack of spherical (magnetic) symmetry of the sphere and a lack of axial symmetry of the support field. Minor alterations of the support magnet have decreased the torque; however, it is still doubtful whether the magnetic torque can be made sufficiently small and sufficiently stable without a major redesign and reconstruction of the magnetic support configuration. It is possible that the simple quartz fiber support from a point fixed to the table is capable of better accuracy than the present magnetic support system.

PRECEDING PAGE BLANK - NOT FILMED.

IX. ESTIMATION OF THE ACCURACY IN G IN THE PRESENT PROJECT

The University of Virginia group is concerned that the project to determine G has not progressed more rapidly. A logical intermediate objective, which corresponds to solving a major fraction of the real problems, has been defined, and a target date of September 1967 has been set. For a given small mass system (of nonprecisely known properties) and brass large masses (of nonprecisely known properties) in a fixed relative position, the intermediate objective is to demonstrate that the angular acceleration of the small mass system can be measured reproducibly with a precision appropriate to the final absolute determination of G. The intermediate objective is thus not concerned with

- The precise mass, sphericity, or homogeneity of the large masses.
- The precise dimensions, mass, or moment of inertia of the small mass system components.

It is concerned with

- Accurate repositioning of the brass spheres on the table or accurate measurement of repositioning errors.
- All problems associated with determining the angular acceleration of the small mass system because of gravitational interaction with the large masses.

In the final phase, with precision large and small mass systems and with certain properties (e.g., dimensions and masses) determined by independent measurements, other precision mass system properties (for example, the density homogeneity of the large masses) would be studied in table experiments. Reasonably accurate limits should then be obtained for the final absolute value of G.

Assuming that the present project for determining G will be restricted to the ball bearing high friction rotating table and assuming that the magnetic support system will not be completely redesigned, it seems reasonable to estimate, based on current experience, that G will be determined to an accuracy of about one part in 10^4. If certain problems (e.g., correction for $\Delta\beta$ variations) are solved suitably, a slightly better result may be obtained. If the constancy and measurability of the dimensions of the small mass quartz cylinder are not as anticipated, the result could be slightly worse.

PRECEDING PAGE BLANK - NOT FILMED.

X. ULTIMATE PRECISION OF THE METHOD

The ultimate precision of this method obviously cannot be predicted until this project is concluded. Nevertheless, some problem areas are already fairly well defined. Others are less clear. The effort to reach the ultimate potential precision of the method would clearly involve effort in the following areas.

Observation of precise revolutions (smaller angular displacements do not appear necessary) of the small mass system will be a problem. At least two alternative approaches may be used. We could attempt to observe the angular displacements (revolutions) of the small mass system directly, rather than observing the revolutions of the table. This would reduce by a large factor the errors resulting from $\Delta\beta$ variations, and additional modifications of course could be made to reduce the $\Delta\beta$ variations. Such an approach possibly would change the experimental configuration, but it should be feasible.

The second approach could involve concentrating on reducing the $\Delta\beta$ variations, continuing to observe table rotations with corrections for $\Delta\beta$ variations if necessary. This approach would certainly require a much smaller and more constant table friction torque (probably air bearing table), as well as a better control system. It probably would also involve additional capital investment.

The necessity of having a constant tare acceleration for runs with and without the large masses in place is a serious problem with our method, and only limited experience with this problem has been accumulated. In a larger sense the problem is that of comparing data from two runs for identical physical configurations (except that one is with and one without the large masses), certain properties of which are precisely known. In addition to such effects as drifts in temperature, alignment, etc., an obviously important problem involves the stability of the acceleration of the small mass system as a result of interaction with the support system. It is difficult to predict whether a quartz fiber support or a magnetic support system is potentially superior. Quartz is certainly one of the most stable materials; the demonstration that $A \sin(m\theta + m\phi)$ terms in the motion equation introduce such small errors makes the quartz fiber support much more attractive than thought originally. On the other hand, with suitable design care it may be possible to produce a magnetic suspension system which gives very much less torque than a fiber support, and perhaps a very stable torque as well.

These two problem areas are associated with the measurement of the acceleration of the small mass system resulting from the gravitational interaction between the small and large mass systems. We speculate that the measurement of $\dot{\omega}_{grav}$ would not be the limit of

accuracy in the ultimate experiment. Instead, the uncertainties in the relative geometry, dimensions, and mass distributions of the interacting systems probably would determine the limit of accuracy in the ultimate experiment. A probable limiting factor is the dimensions of the small mass system (essentially the quartz cylinder in the present project). Density inhomogeneities also represent an area of uncertainty, both from the point of view of fabrication and that of detecting and correcting for their effects. For example, assume that a large mass is not quite perfectly spherical and has a significant variation in density. The existence of the effect would then be detected by taking measurements with the sphere in different orientations on the table. Once the effect was detected, it must be corrected. Although a corrective procedure might be feasible, it would probably be involved and tedious. Density inhomogeneities in the small mass system, though probably of less importance because acceleration is the ratio of torque to moment of inertia, are more difficult to study experimentally.

In conclusion it should be noted that temperature variations and drifts, external vibrations, and alignment may present problems in an ultimate experiment, although they should be solvable with sufficient effort. Thermal noise levels are believed to be smaller sources of error.

We anticipate that a reasonable ultimate experiment should attain accuracies greater than one part in 10^5, perhaps approaching one part in 10^6.

APPENDIX F

DISCUSSION AND ANALYSIS OF THE ROTATING FLAT PLATE NEWTONIAN GRAVITATIONAL CONSTANT EXPERIMENT

(Prepared by D. Berman)

SUMMARY

This scientific report covers one portion of a program to find a new experimental method of improving our knowledge of the Newtonian gravitational constant (G). According to the NBS Technical News Bulletin (October 1963) the presently accepted value is $6.670 \pm 0.015 \times 10^{-11}$ $m^3 kg^{-1} sec^{-2}$ (three standard deviations). The rotating flat plate experiment utilizes the gravitational interaction between two optically flat and parallel rectangular solids, one of which is rotating at constant speed and the other in a resonant mount. The experimental system schematic consists of a torsional suspension system for the resonant plate, a suspension system and drive for the rotating plate, an optical detection system to measure the angular deflection of the resonant plate, an optical interferometer system to measure the relative positions of the rotating plate and the resonant plate, and a vacuum and external vibration isolation system for the entire apparatus. The analysis establishes that the gravitational interaction between the two plates is a second order gravitational gradient and that the dynamic interaction will be at twice the rotation frequency of the rotating plate. The magnitude of this gravitational gradient is of the order of 10^{-8} sec^{-2} and depends only on the density of the plate for fixed dimension ratios. Similar experiments have already been carried out and it has been found possible to eliminate all external sources of dynamic noise from the detecting system except for the internal thermal noise. An error analysis has been carried out on all the primary system parameters to determine their required precision. Most of the technology required in this experiment has been developed in previous gravitational experiments. We conclude that if the interferometer techniques are successful and the noise isolation techniques can be extended so that the instrument noise is predominantly thermal noise, accuracies approaching one part in 10^6 should be obtained in the measurement of the gravitational constant. To reach this level of accuracy requires an experiment time or instrument response time of half a day. The primary limitations of this experiment will be density inhomogeneities in the plates, the stability of the mechanical damping constant, and the nonlinearities and drift in the suspension system.

I. INTRODUCTION

The gravitational constant G currently is known to one part in 500 (three standard deviations). The most accurate of the various experiments to determine G to date is the "time of swing method" of Heyl.[1] This experiment consists of two concentric torsion balances and is similar to the Cavendish apparatus (see Fig. F-1). One balance is held stationary while the other is excited into a pendulum torsional mode oscillation. When the two balances are aligned in parallel, the period of swing is less than when they are aligned at right angles. In the former position, the gravitational attraction between the two balances adds to the torsional spring restoring force; in the latter position, it subtracts from it. The gravitational constant is obtained from measurement of the difference in periods between the near and far positions. The periods were on the order of a half hour, and could be measured to 0.1 sec.

A method of determining G to higher accuracy currently is being tested at the University of Virginia.[2] (See Appendix F of this report.) This experiment is designed to improve the knowledge of G to one part in 10^4; with future versions, accuracies greater than one part in 10^5, and possibly one part in 10^6, should be allowable. It also consists of two concentric torsional balances. One balance is free to rotate under the attraction of the second, while the second is motor-driven and servo-controlled to maintain constant angular position with respect to the first. Hence, both balances will rotate through 360^o, while a constant torque is being maintained on the free balance. The angular displacement, after many hours, determines the gravitational constant.

In trying to push the determination of the gravitational constant to higher accuracy, all of the various possible experiments ultimately approach the limitation of precision in determining the relative position of the masses in the system and the homogeneity of density within the masses themselves. In addition, many experiments are affected by spurious nongravitational forces or stray gravitational effects of nearby masses which are difficult to separate from the desired gravitational interaction forces between the source masses and the detecting masses.

In an attempt to overcome some of these problems, we have investigated a dynamic Cavendish experiment design which utilizes the gravitational interaction between two optically flat and parallel rectangular solids. The generator plate is rotated at a constant speed, and the detector plate is allowed to vibrate on a mount that is resonant at twice the rotation frequency of the generator. The principle of operation is

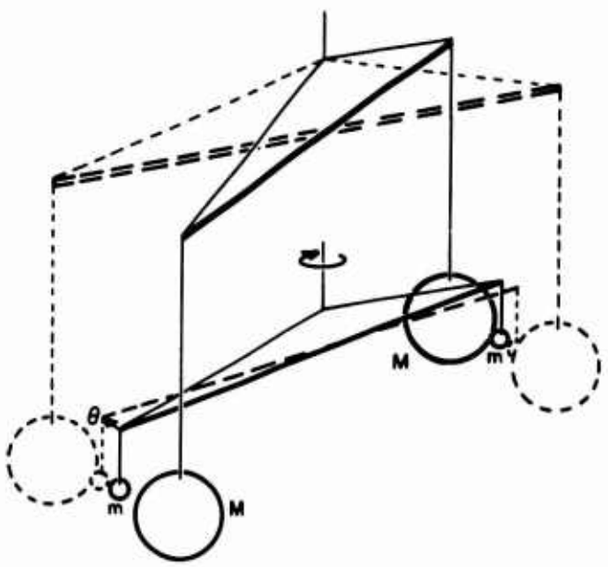

Fig. F-1. Cavendish type coaxial torsion balance system.

basically that used by Forward and Miller[3] (see also Appendix). Our preliminary analysis indicated, however, that the four-element mass octupole resonant structure used for the detector element in that experiment is not suitable for a high precision experiment. The detecting structure proposed is a plate with a mass quadrupole moment on a resonant torsional suspension. This type of detector is similar to that used in Zahradnicek's resonance experiment.[4]

Zahradnicek's apparatus consists of the usual two coaxial torsion balances of the Cavendish type. One balance is excited into simple harmonic motion at the same frequency as the resonant frequency of the second balance. In both the proposed experiment and Zahradnicek's experiment, the resonant response of the second balance builds up in amplitude many times that of an equivalent static Cavendish system, thus allowing more accurate measurements. Also, both methods are not susceptible to errors due to the presence of nearby stationary objects. Since the detector is a resonant system, the response depends only on the generator masses which are moving at the proper frequency.

The advantages of the proposed experiment over Zahradnicek's experiment are: (1) the relative position of all the interacting masses can be measured accurately with interferometer techniques (even during the experiment, if required), (2) flat optically clear plates can be machined to greater precision dimensionally, and can be controlled with respect to density homogeneity, and (3) the generating masses are moving at half the frequency of the detector resonant response, and therefore, predominantly all of the nongravitational noise produced by the generator is at a frequency that is outside the detector response frequency.

PRECEDING PAGE BLANK - NOT FILMED.

II. SYSTEM DESCRIPTION

The system is shown schematically in Fig. F-2. The heart of the system is two precision machined plates which have optically flat and parallel sides. The upper plate is suspended by a torsional mount, whose stiffness is determined very precisely by prior independent measurement of the torsional natural frequency. Such techniques of stiffness determination are well established, since they are used in all of the important gravitational constant experiments described in Section I. The accuracy required is discussed in Section V. The torsional fiber is subsequently mounted to a platform which is vibrationally isolated from external disturbances. The lower plate is connected to the rotor of a magnetically suspended rotor, which is driven at constant angular speed by a servo-controlled motor.

Precision alignment of the two plates is obtained by interferometer techniques. Thus, the plates must be translucent, and silver coated on one side. Using these techniques, distances can be established to an accuracy of 5×10^{-7} cm.[5]

Measurement of angular displacement can be accomplished by recording the deflection of a light beam off a mirror mounted at the center of the resonant plate. Here, too, the methods have been used before in the experiments cited above. In particular, the apparatus developed by Dicke and Roll[6] gives an accuracy of 10^{-9} rad. In that experiment, the source of light for the optical detector was a flashlight bulb. The light was focused through a narrow slit, reflected off the torsion balance, and focused again on a very narrow wire. The wire was made to oscillate at its resonant frequency, and a photomultiplier was placed behind it. When the diffraction pattern centered exactly on the equilibrium position of the oscillating wire, the photomultiplier detected only the even harmonics of the wire fundamental frequency. When the torsion balance rotated slightly, shifting the diffraction pattern off center, the fundamental frequency became detectable in the photomultiplier output. The output then passed through stages of amplification and filtering. Thus, the amplitude was proportional to the angular displacement, for very small angles.

The entire system, including motor, is enclosed in a vacuum system. This is necessary to avoid acoustic coupling from external sources, and also to avoid air currents.

It is obvious that in order to detect the very weak dynamic gravitational forces being generated by the rotating plate, the generator and detector must be well shielded to prevent acoustic and electromagnetic coupling. The detector is highly sensitive to acoustic noise with a frequency component at its resonance frequency, but experience has shown that the acoustic noise can be eliminated by placing the detector in a vacuum chamber at a few milliTorr.

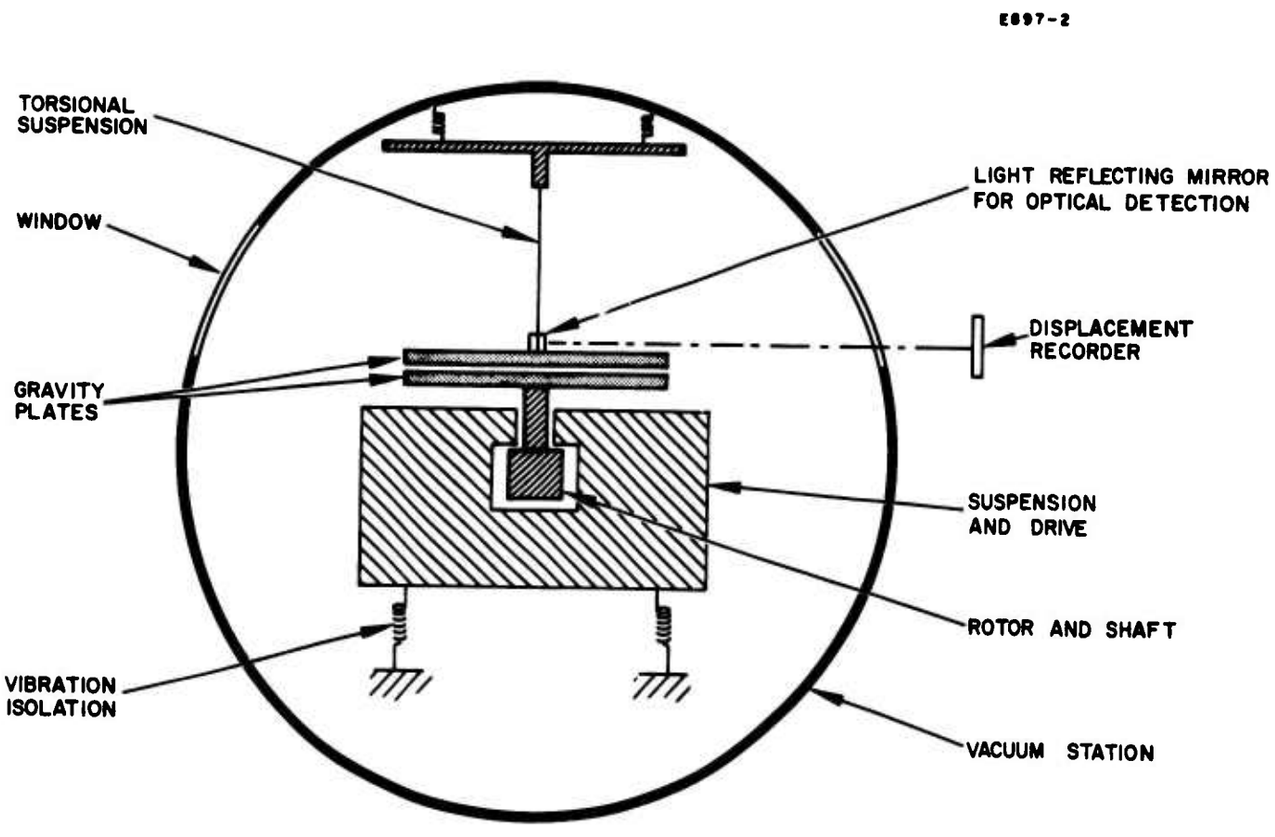

Fig. F-2. System schematic.

Although an ideal detector is theoretically insensitive to vibrations of the mounting structure, in practice a small amount of the vibrations in the mount leak into the gradient-sensing mode. Because of this, an effort must be made to keep the detector-mount vibrations at a low level. This is accomplished by suspending the detector in the chamber with a spring. The generator is isolated from the workbench by compression springs.

Electromagnetic coupling can occur by direct interaction of the rotating magnetic fields of the motor with the arms of the detector. Direct coupling of the rotating magnetic fields is eliminated by using a phase-locked asynchronous drive. In this mode of operation of the generator, the generator motor is driven by currents at some higher frequency so that they do not excite the detector resonant mode. The amplitude of the drive voltage is controlled by a servo loop so that the rotor remains at a constant speed. The servo loop can be made so tight that both the frequency and the phase of the rotor can be held tightly to the phase of a reference signal from a precise oscillator.[1]

Dynamic gravity devices which are similar to this experiment in many ways, have been operated successfully at Hughes Research Laboratories[1] (see Appendix). These devices have been perfected to the sensitivity level of thermal noise; all other sources of external disturbances have been reduced to less than this. Because of the similarities in design, we expect that with sufficient effort the noise disturbances of the flat-plate Cavendish experiment also will be determined predominantly by thermal noise.

PRECEDING PAGE BLANK - NOT FILMED.

III. GRAVITATIONAL INTERACTION

The determination of G requires a precise calculation of the gravitational interaction of the two plates. This calculation involves integrating the effect of each element of mass of the rotating plate on the elements of the resonant plate. The tangential component of the gravitational force gives the torsional coupling, from which the response (and therefore G) is determined.

The configuration for calculating the gravitational interaction is shown in Fig. 3. The gravitational potential $\mathcal{G}$ at r due to all mass in V' is:

$$\mathcal{G} = \int_{V'} \frac{G\rho \, dV'}{|r - r'|} \tag{1}$$

where r' is a function of θ as the plate rotates.

The tangential component of the gravitational force is given by

$$dF = \left[\nabla \int \frac{G\rho \, dV'}{|r - r'|}\right] \cdot i\,\hat{\theta} \tag{2}$$

where $\hat{\theta}$ = unit vector in direction of rotation.

The integral over all r on the plate gives the total interaction:

$$F = G\rho \iint \nabla \left|\frac{1}{r - r'}\right| dV' \, dV \tag{3}$$

In this paper, we do not propose to carry out the integration indicated in eqs. (1) through (3). We shall assume that the mathematics may be carried out with any desired degree of accuracy, and that the experiment will be limited only by laboratory measurement.

In order to estimate the gravitational interaction of the two plates, we shall consider only their gravitational quadrupole moments. Thus, we lump the mass of each as shown in the configuration of Fig. 4.

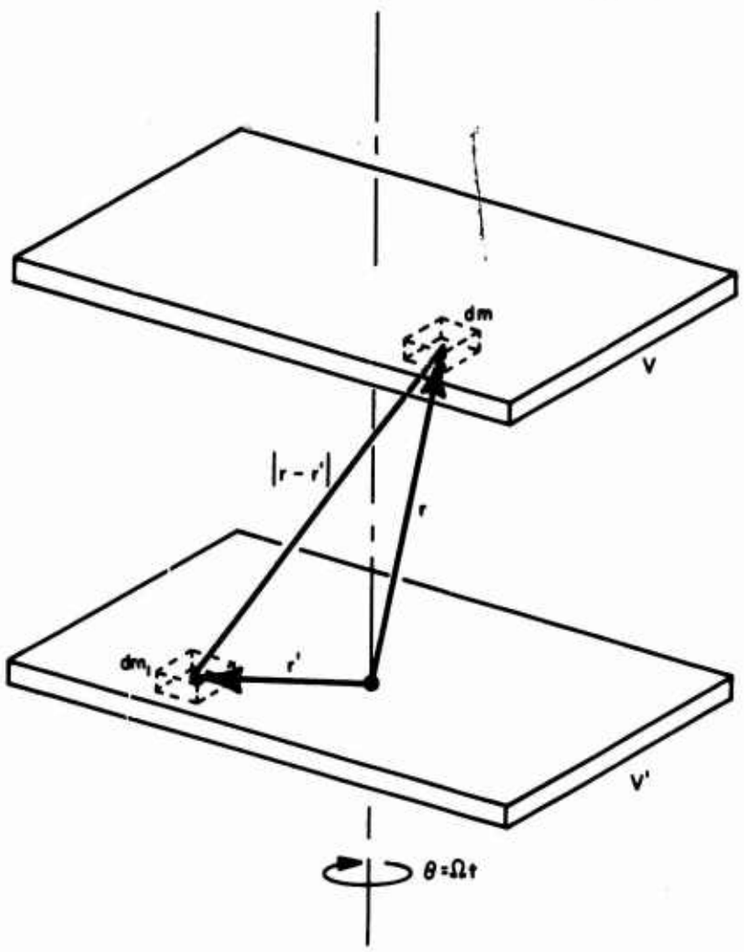

Fig. F-3. Calculation of gravitational force by integration over all elements and taking tangential components.

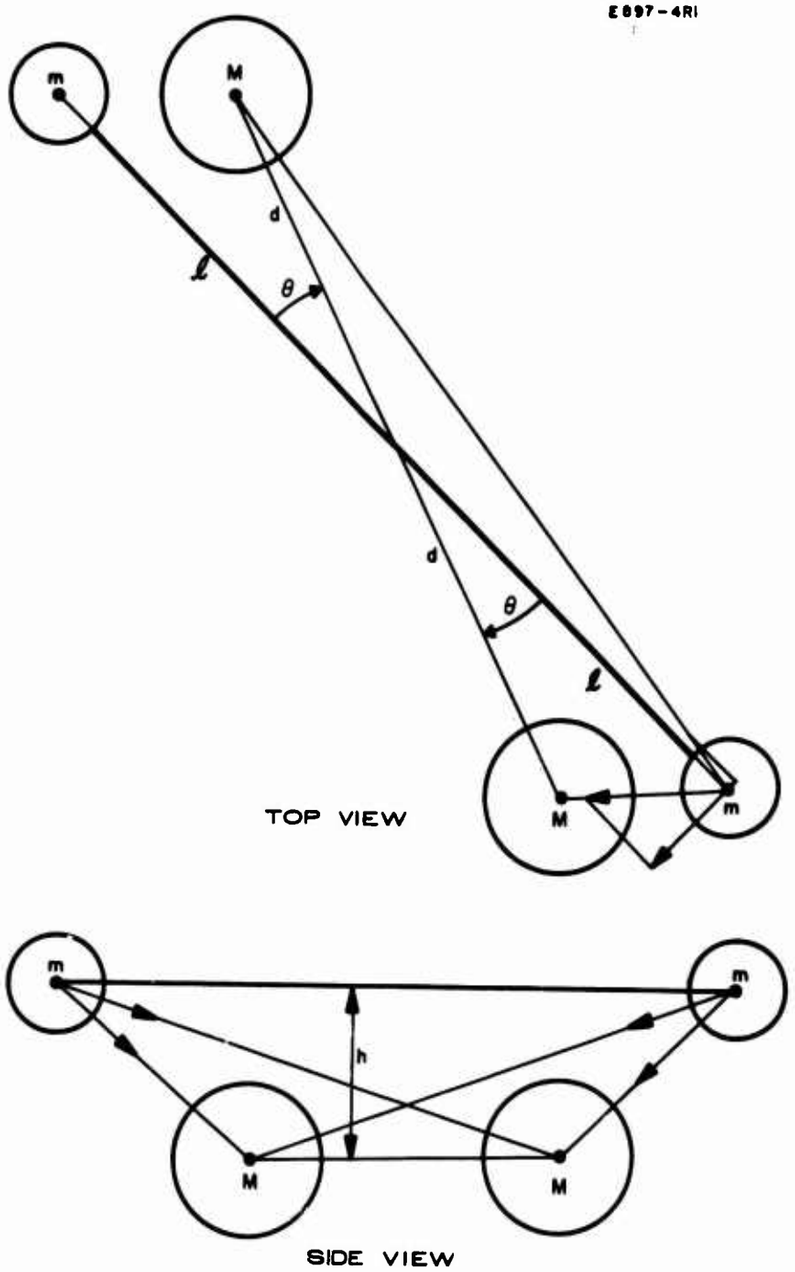

Fig. F-4. Model for gravitational-interaction calculation.

In the appendix, it has been shown that a quadrupole gravitational detector is excited by a quadrupole generator. The excitation is given by:

$$F = (GMm\, d/R^3)\left[6\Lambda \cos\theta + 35\Lambda^3 \cos^3\theta + \frac{693}{4}\Lambda^5 \cos^5\theta + \frac{6435}{8}\Lambda^7 \cos^7\theta + \ldots\right] \sin\theta \qquad (4)$$

where $\Lambda = \ell d/R^2$; $R = \ell^2 + d^2 + h^2$; M = generator mass, m = detector mass. $\theta = \Omega t$ is the rotational angle, for constant angular frequency Ω. To simplify, we invoke the trigonometric identities:

$$\begin{aligned} 8\cos^3\theta \sin\theta &= \sin 4\theta + 2\sin 2\theta \\ 32\cos^5\theta \sin\theta &= \sin 6\theta + 4\sin 4\theta + 11\sin 2\theta \\ &\vdots \\ &\text{etc.} \end{aligned} \qquad (5)$$

Substituting these into (4) yields:

$$F = (GMm\, d/R^3)\, 3\Lambda\left[1 + \frac{35}{12}\Lambda^2 + \frac{1155}{128}\Lambda^4 + \ldots\right] \sin 2\Omega t \qquad (6)$$

We have dropped the higher order terms in Ω, keeping only the lowest at 2Ω. Hence, the dominant driving force on the detector will be at a frequency that is twice the generator rotation frequency. For very close distances between generator and detector, h is small compared with d and ℓ, and we have as the limiting value of Λ (for $\ell = d$):

$$\Lambda = \ell d/R^2 \approx \frac{\ell d}{\ell^2 + d^2} = \frac{1}{2} .$$

For $\Lambda = 0.5$, the series indicated in eq. (6) converges to 4.0. The excitation then becomes:

$$F = (6\, GMmd/R^3) \sin 2\Omega t \approx \frac{2GMm}{d^2} \sin 2\Omega t. \qquad (7)$$

With the driving force given by eq. (7), we may calculate the detector response from the second order equation for a damped harmonic oscillator:

$$\ddot{\alpha} + \frac{1}{2\tau}\,\dot{\alpha} + \omega_o^2\,\alpha = T/I \equiv \Gamma \sin 2\Omega t \qquad (8)$$

where

α ≡ displacement angle

ω_o ≡ resonant frequency

τ ≡ detector time constant

T ≡ torque = Fd

I ≡ moment of inertia = $2md^2$

Γ ≡ gravitational gradient.

Evaluating the driving term

$$\Gamma = \frac{GM}{d^3} \qquad (9)$$

which has the units of $\sec^{-2}$ and which depends on the mass and size of the generator (which is the same size as the detector). These quantities are related, of course, so that we can reduce (9) to be a function only of density for a plate of fixed proportions.

Figure F-5 demonstrates the meaning of the parameters in our quadrupole model of a flat plate. We fix the relative proportions to be such that the plates are ten times longer than wide, and one tenth as thick. The first relative dimension assures a dominant quadrupole moment, and also allows us to ignore the noninteracting circular mass distribution in the center. The second dimensional criterion (thickness) assures that the mass separation distance is negligible. Hence, the following relations hold for large dimension L

$$M = \rho\,(L/2)\,(L/10)\,(L/100)$$

$$= \rho\,L^3/2000$$

(where ρ is the specific density of the plate), since M corresponds to half the quadrupole moment. Also, $d = L/4$ since the average mass is approximately this distance from the axis of rotation.

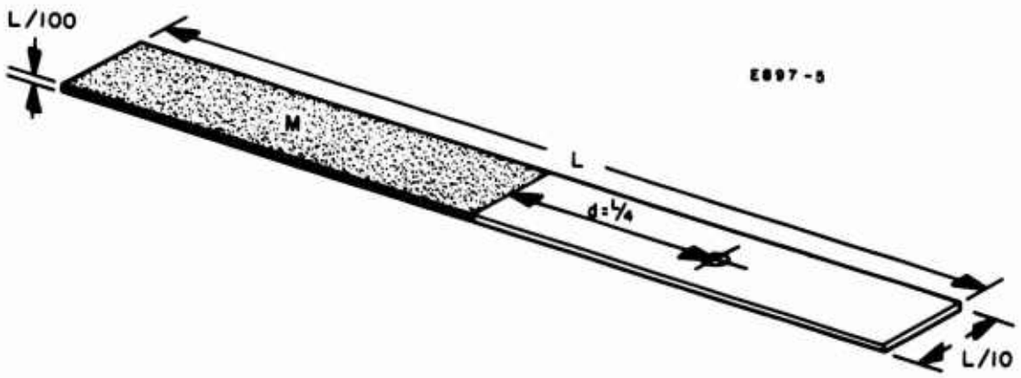

Fig. F-5. Parameters of flat plate.

Substituting these values into (9) yields:

$$\Gamma = G\rho\,(L^3/2000)/(L^3/64)$$

$$= 0.03\ G\rho = 2\rho\ \text{E.U.} \qquad (10)$$

This indicates that the gravitational interaction is predominantly a function of the density of the material used in the generator. Because the material used must be nonconductive, nonmagnetic, and transparent, we shall be limited to densities of the various glasses. There are glasses such as lead oxide with a specific density of 9.5. However, the most dimensionally stable glass is fused quartz with 2.3. By proper choice of material we can hope to maintain dimensional stability while maximizing density. In this way, we can expect to obtain gradients on the order of $\Gamma = 10$ E.U.

The deflection due to a gravitational excitation is found from the solution to eq. (8): at resonance (for zero initial conditions):

$$a = (2\Gamma\tau/\omega_o)\,(1 - e^{-t/\tau})\,\sin\omega_o t \ . \qquad (11)$$

Equation (11) is plotted in Fig. F-6 for the special case where the time constant equals 10 times the natural period, $\tau = 10(2\pi/\omega_o)$. We see that to maximize the resonator deflection, the amplitude must build up over a number of cycles of oscillation. For a fixed time constant τ, the amplitude for fully developed oscillation is inversely proportional to the natural frequency ω_o. It is therefore advantageous to use as low an ω_o as possible, from the standpoint of optical measurement of the deflection angle (Section II). The lower limit to ω_o is determined by the ability to support the resonant plate in a 1 g environment.

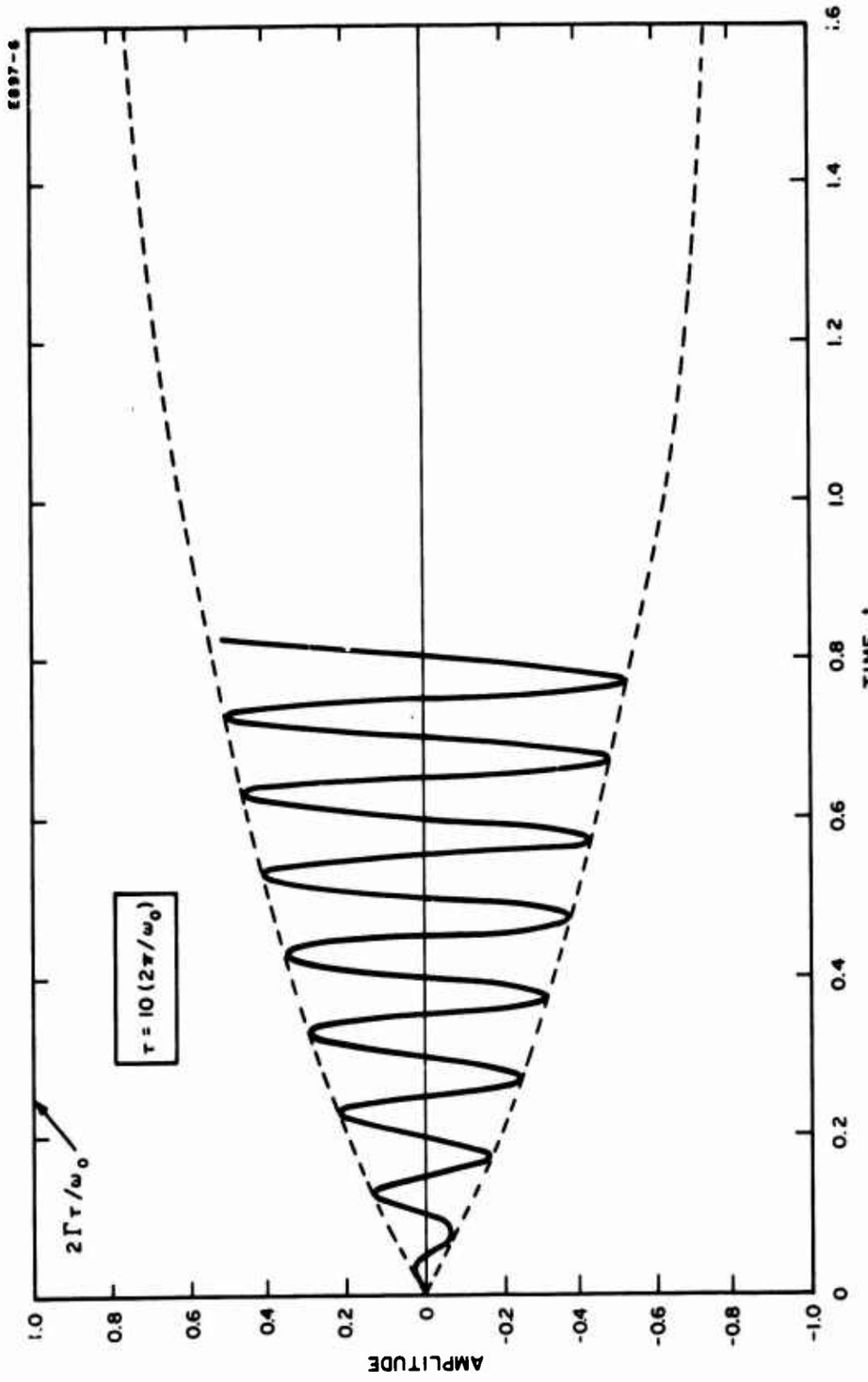

Fig. F-6. Time response of resonant plate.

IV. SIGNAL-TO-NOISE

The magnitude of angular deflection of the resonant plate due to gravitational coupling depends on the natural frequency and time constant τ (see eq. (11)). This amplitude must be large enough to dominate any nongravitational disturbance coupling by the factor of precision required in the experiment; in this case we consider a signal-to-noise ratio of 10^9.

In the previous dynamic gravitational experiments described in the Appendix, all sources of vibrational, acoustic, electromagnetic, etc., noise were negligible compared with the thermal noise in the device. This thermal noise is the limiting sensitivity in any instrument, because it is a thermodynamic molecular motion and depends only on temperature.

In order to determine the angular deflection of the gravitational detector due to the excitation of thermal noise, we will calculate the stored energy in a resonant harmonic oscillator. The energy is stored partly in the kinetic energy and partly in the potential energy of the spring:

$$E = KE + PE = \frac{1}{2} I \dot{\alpha}^2 + \frac{1}{2} \omega_o^2 \alpha^2 \quad . \tag{12}$$

The deflection α is obtained from the solution of eq. (8) at steady state:

$$\alpha = \alpha_n \sin 2\Omega t \, . \tag{13}$$

Substituting (13) into (12) yields (at $\omega_o = 2\Omega$):

$$E = \frac{1}{2} I (\omega^2 \alpha_n^2 \cos^2 \omega_o t) + \frac{1}{2} I \omega^2 \alpha_n^2 \sin^2 \omega_o t = \frac{1}{2} I \omega_o^2 \alpha_n^2 \quad . \tag{14}$$

The amplitude α_n of the oscillations, when the total energy in the vibrational mode is just the thermal energy (kT) required by the equipartition theorem, is:

$$\alpha_n = \left(\frac{2\,kT}{I\omega_o^2}\right)^{1/2} = \left(\frac{2\,kT}{M}\right)^{1/2} \frac{1}{\omega_o d} = \left(\frac{1000\,kT}{\rho}\right)^{1/2} \frac{8}{\omega_o L^5} \, . \tag{15}$$

Thus, the deflection due to thermal noise depends inversely on detector size and natural frequency.

To compare the thermal noise response with the gravitational response, we express the amplitude of (11) as:

$$a_g = 2\Gamma\tau/\omega_o . \qquad (16)$$

The signal-to-noise ratio is then obtained by dividing (16) by (15):

$$a_g/a_n \doteq \frac{\Gamma\tau}{4}\left(\frac{\rho}{1000\,kT}\right)^{1/2} L^{5/2} . \qquad (17)$$

We see that a_g/a_n is proportional to the time constant and independent of natural frequency.

To obtain an accuracy of one part in 10^6, for example, we must have $a_g/a_n = 10^6$. Using this value, and a nominal dimension of $L = 50$ cm, we solve (17) for τ. The result is $\tau = 6 \times 10^4$ sec, or about half a day. This amount of time is a typical requirement for conducting a gravitational constant experiment,[7] and it is not unreasonable to maintain stability of the system parameters for that length of time.

When attempting to make ω_o as low as possible, the limit is determined by the ability of the sensitive torsion fiber to support the resonant plate in a 1 g environment. In the literature we find that natural periods of 1000 sec ($\omega_o \approx 0.01$ rad/sec) are common for torsional balances on the order of 100 g. A system with $L = 50$ cm weighs 625 g, which is not unreasonable for a low ω_o suspension.

Returning to (16) and using the values

$$\tau = 6 \times 10^4 \text{ sec}$$

$$\Gamma = 10 \text{ EU} = 10 \times 10^{-9} \text{ sec}^{-2}$$

$$\omega_o = 0.01 \text{ rad/sec},$$

we calculate the gravitationally induced deflection of the resonator:

$$\alpha_g = \frac{(2)(10 \times 10^{-9})(6 \times 10^{4})}{(.01)} \approx 0.1 \text{ rad}$$

which is a fairly large angle. However, for the measurement to be precise to 10^{-6} implies a detection sensitivity of 10^{-7} rad. Using techniques described in Section II, we can expect to obtain this accuracy.

PRECEDING PAGE BLANK - NOT FILMED.

V. ERROR ANALYSIS

Equation (16) expresses the deflected angle as a function of the gravitational gradient, where $\Gamma = GM/d^3$ for the ideal mass quadrupole model. In the real case, the gravitational mass is not lumped at two discrete points, but instead is distributed over the extended dimensions of the plate. Thus, the values M and d represent the effective gravitational quadrupole moment of the rectangular mass distribution. These values must be calculated by techniques discussed in Section III (eq. (3)), following a precise measurement of the physical plate dimensions and total mass. However, it is of primary importance to facilitate a precise physical measurement. The mathematical conversion can always (in theory) be accomplished with any desired accuracy. Because of the flat-plate geometry, we can measure dimensions to greater accuracies than other geometries by using interferometer techniques. In this way, we can measure the dimensions and displacements to 5×10^{-7} cm.

To estimate the achievable accuracy of this flat plate dynamic Cavendish experiment, let us solve (16) for G (using (10)):

$$G = a_g d^3 \omega_o / 2 \tau M \quad . \tag{18}$$

The percentage error in d will be $5 \times 10^{-7}/50 = 10^{-8}$, well within an accuracy of one part in 10^6. Also, since $M \approx 10^3$ g, the necessary precision requires only the measurement of milligrams, and this should not be limiting. Of course, the uniformity of density over the extended plate dimensions must also be accurate to one part in 10^6, but here again, because of the flat plate geometry and transparent materials, we can use optical techniques such as measuring the index of refraction.

We have already stipulated that for a_g to be measured to an accuracy of 10^{-6}, the amplitude must build up over many resonant oscillations to a value of 0.1 rad. (This required a system time constant of half a day.) Therefore, the accuracy of angular measurement should not be limiting. In addition, the system time constant τ is on the order of 10^5 sec, and thus needs to be accurately known only to 0.1 for the required experimental precision.

In addition to the above, this experimental method also requires the accurate determination of the resonant frequency ω_o. Even though the natural period $(2\pi/\omega_o)$ is very large (1000 sec), a 10^{-6} requirement would mean that it must be accurate to 1 msec.

The separation distance is an implied parameter because, from (4), $R^2 = 2d^2 + h^2$. Thus, when $h \ll d$, as in the present case, h is only a second order consideration. For very closely spaced plates of several millimeters thickness, $h \sim 0.2$, whereas $d \sim 10$ cm.

The separation distance h is not as critical a parameter as may have been expected. This may be seen by the following:

$$R = \left[2d^2 + h^2\right]^{1/2} \approx \sqrt{2}d \left(1 + h^2/4d^2\right).$$

Evaluating, $h^2/4d^2 \approx 10^{-4}$, which need be known only to three significant places. To measure h to three significant figures requires an accuracy of only 10^{-3} cm.

VI. CONCLUSIONS

The proposed "Dynamic Cavendish Experiment" is similar to the "Resonance Method" of Zahradnicek, but with the important exceptions of flat-plate geometry and second-harmonic gravitational excitation. In pushing the gravitational constant to higher and higher accuracy, more precision is required in the measurements of the system parameters. Flat-plate geometry lends itself to dimensional measurements by interferometer techniques, and thus removes the accuracy limitations imposed in conventional techniques. The use of second-harmonic excitation eliminates a potentially troublesome source of noise.

In this report, we have estimated the gravitational interaction, and calculated the signal-to-noise ratio for the flat-plate experiment. We have established all primary system parameters, as well as their required precision. Most of the technology required in this experiment has been developed in previous gravitational constant experiments. Thus we conclude that if interferometer techniques are successful, an accuracy of 10^{-6} can be obtained.

PRECEDING PAGE BLANK - NOT FILMED.

REFERENCES

1. P. R. Heyl, "A redetermination of the constant of gravitation," Bur. Std. J. Res. 5, 1243 (1930).

2. J. W. Beams, A. R. Kuhlthay, R. Q. Lowry, and H. M. Parker, "Determination of Newton's Gravitational Constant G, with Improved Precision," University of Virginia Proposal EP-NSF-125-64U (1964).

3. R. L. Forward and L. R. Miller, "Generation and detection of dynamic gravitational field," J. Appl. Phys. 38, 512 (1967).

4. V. J. Zahradnicek, Z. Physik. 34, 126 (1933).

5. L. Jenkins and B. White, Fundamentals of Optics (McGraw-Hill, New York, 1957), pp. 253-259.

6. P. G. Roll, R. Krotkov, and R. H. Dicke, Ann. Phys. 26, 442 (1964).

7. "Gravitation," in Encyclopedia Britannica (Chicago, 1958), Vol. 10.

Appendix to Appendix F

Generation and Detection of Dynamic Gravitational-Gradient Fields

PRECEDING PAGE BLANK - NOT FILMED.

Reprinted from JOURNAL OF APPLIED PHYSICS, Vol. 38, No. 2, 512-518, February 1967
Copyright 1967 by the American Institute of Physics
Printed in U. S. A.

Generation and Detection of Dynamic Gravitational-Gradient Fields*†

ROBERT L. FORWARD AND LARRY R. MILLER‡
Hughes Research Laboratories, Malibu, California
(Received 5 August 1966)

We have constructed a generator of dynamic Newtonian gravitational-force-gradient fields and used it as a signal generator to calibrate the response of the gravitational-gradient detectors being developed in our research work on gravitational-mass sensors. The gravitational-gradient-field generator is a flat aluminum cylinder 14 cm in diameter, with four holes than can be filled with slugs of different density to create a rotating mass-quadrupole moment. The generator is mounted on an air-bearing-supported motor and rotated at a nominal speed of 44 rps (2640 rpm). Because of the bisymmetric mass distribution, the dynamic gravitational-gradient fields generated have a frequency of 88 Hz, or twice the rotation frequency. The detector is a 12-cm-diam cruciform-shaped structure which responds to 88 Hz gravitational-gradient forces. The small (10^{-11} cm) motions induced in the detector arms are sensed by piezoelectric strain transducers attached to the arms near the point of maximum strain. A simple vacuum system, an iron shield plate, and spring mounts suffice for acoustic and magnetic isolation, since most of the nongravitational noises were generated at 44 Hz, the rotation frequency, rather than at 88 Hz, the gravitational-gradient frequency. Data taken with four different mass distributions varying from 0 to 1000 g and separation distances varying from 4.8 to 12 cm agree well with the theory, indicating that only gravitational energy was being transmitted from the generator to the detector. The minimum dynamic gravitational-gradient field observed during this test was 6×10^{-9} sec^{-2} or 0.002 of the earth's gradient. The equivalent differential acceleration exerted on the sensor arms by this field was 3×10^{-11} g's.

INTRODUCTION

WE are engaged in a program to design, construct, and test a research model of a gravitational-mass sensor which can measure the mass of an object at a distance by using a rotating system of masses and springs (see Fig. 1) to detect the gravitational-force-gradient field of the object.[1,2] The ultimate objective of our work is to develop a small, rugged sensor to be used on spinning lunar orbiters to measure the mass distribution of the moon and on spinning deep space probes to measure the mass of the asteroids.

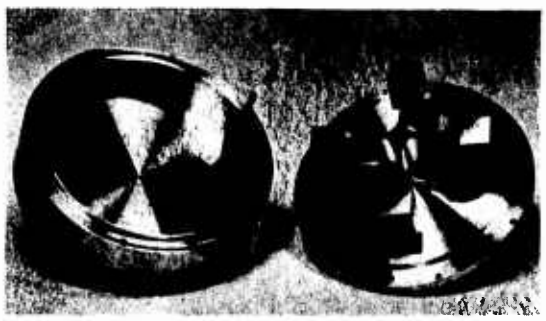

FIG. 1. Five-in.-diam cruciform gravitational-mass sensor.

Our primary goal in this research project is to develop methods of rotating the gravitational-mass-sensor structures without introducing large amounts of noise into the gravitational-gradient sensing mode, so that we can demonstrate the required degree of sensitivity in the laboratory without requiring flight tests to prove engineering feasibility. At present, we have demonstrated that we can measure accelerations down to 2×10^{-7} g's while operating in a 450-g rotational environment and a 1-g gravitational environment. The force level due to the earth's gravitational gradient is one order of magnitude below this. The noise problems are not fundamental and work is continuing on methods for lowering the noise level to the point where static gravitational gradients from laboratory masses can be seen.

A concurrent objective of our work is to learn enough about these structures to be able to predict their response to gravitational-gradient fields. The theoretical portion of this work is largely completed and was reported at the AIAA Second Annual Meeting.[3] In order to verify the equations experimentally and to develop a test system for calibrating the gravitational-gradient response of the various sensors, we have constructed a rotating generator of dynamic Newtonian gravitational-force-gradient fields and have measured the response of one of our sensors to these fields.[4] This work is similar to that of Weber *et al.* at the University of Maryland,[5] who utilized a vibrating rod to generate 1.6-kHz dynamic gravitational fields for calibration of a gravitation radiation detector.[6]

* Work partially supported by the National Aeronautics and Space Administration.
† Presented at A.P.S. Summer Meeting, Minneapolis, Minn., 20–22 June 1966; also Gravity Research Foundation Essay, New Boston, N.H., 15 April 1966.
‡ Presently on leave of absence on a Hughes Master of Science Fellowship at the University of California, Berkeley, Calif.
[1] R. L. Forward, in *Proceedings of the Symposium on Unconventional Inertial Sensors* (Republic Aviation Corp., Farmingdale, New York, 1963), pp. 36–60.
[2] R. L. Forward, *Proc.* AIAA *Unmanned Spacecraft Meeting* (AIAA, New York, N. Y., 1965), pp. 346–351.
[3] C. C. Bell, R. L. Forward, and J. R. Morris, "Mass Detection by Means of Measuring Gravity Gradients," presented at AIAA Second Annual Meeting, San Francisco, Calif., 26–29 July 1965; also AIAA Paper 65–403.
[4] R. L. Forward and L. R. Miller, Bull. Am. Phys. Soc. 11, 445 (1966).
[5] J. Sinsky, J. Weber, D. M. Zipoy, and R. L. Forward, Bull. Am. Phys. Soc. 11, 445 (1966).
[6] J. Weber, "Gravitational Waves," in *Gravitation and Relativity*, H.-Y. Chiu and W. F. Hoffman, Eds. (W. A. Benjamin, Inc., New York, 1964), p. 100, Chap. 5.

DYNAMIC GRAVITATIONAL-GRADIENT-FIELD GENERATOR

The generator of the dynamic gravitational-gradient fields is shown in Fig. 2. The drive unit for the generator is an air-bearing support and drive which was originally designed to rotate a sensor structure. The bearing table supports an aluminum mass holder 14 cm in diameter with four holes, 5.0 cm in diameter and 3.5 cm deep, on a radius of 4.0 cm. Opposite pairs of holes can be filled with either aluminum, brass, or tungsten slugs which slip fit into the holes. The various pairs of mass slugs were trimmed so that static and dynamic balance of the generator was achieved even though the mass holder has a mass-quadrupole moment. When balanced, the motor–generator combination is silent under all combinations of speed and mass-quadrupole loading, except for a slight, high-frequency hiss of the support air passing through the bearing. The motor can be operated in either a synchronous drive mode or a phase-locked asynchronous mode. The readout of the generator rotation speed and phase is obtained through a photoelectric pickoff which detects paint marks on the rotor. This photoelectric signal is used as the reference signal for a lock-in amplifier, and in the asynchronous mode can also be used to supply pulses for the asynchronous drive controller.

The masses of the various slugs used are

Tungsten	1212.0 g,
Brass	606.0 g,
Aluminum	200.0 g.

If four aluminum slugs are used, the generator has no mass-quadrupole moment. The maximum mass-quadrupole moment of 3.8×10^4 g·cm² is obtained when two tungsten slugs are used and the other two holes are left empty. When the opposing pair of holes is filled, the effective mass is just the mass difference. The various combinations possible with our present setup are listed below.

Holes 1 and 3	*Holes 2 and 4*	*Effective Mass, g*
Tungsten	Empty	1212.0
Tungsten	Aluminum	1012.0
Tungsten	Brass	606.0
Brass	Empty	606.0
Brass	Aluminum	406.0
Aluminum	Empty	200.0
Aluminum	Aluminum	0.0

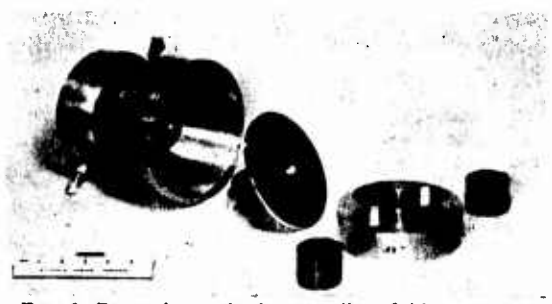

FIG. 2. Dynamic gravitational-gradient-field generator.

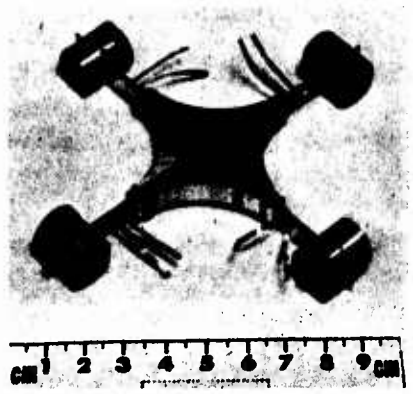

FIG. 3. Adjustable sensor.

The generator rotates at a nominal speed of 44 rps (2640 rpm); because of the bilateral or tensorial character of the mass-quadrupole generators, the ac gravitational-gradient fields generated are at 88 Hz, or *twice* the rotation frequency. (See Appendix.)

DETECTOR

The detector used in this first test was one of our adjustable sensors (see Fig. 3). The sensing masses of the detector are 20-g brass weights attached to the sensor arms by a screw-clamp arrangement. The weights have an eccentric cam arrangement which allows for small position adjustments on the arms. The arms are cantilever beams of aluminum with a 0.125-in.-thick base where they fasten to the hub and an outer bending portion 0.030 in. thick and about 0.70 in. long. The aluminum hub is designed to clamp the arms rigidly for good cross coupling and yet allow the arm-mass assembly to be moved in and out for mass balance of the final assembly.

The detector has a resonant frequency of 88.45 Hz in the dual tuning fork or gravity-gradient sensing mode (see Fig. 7 in the Appendix), a Q of 120 and an arm length of $l=5.0$ cm. Under the influence of a gravitational gradient of $\Gamma\sin2\Omega t$, the arms respond with a vibrational amplitude of [see Eq. (A21) of the Appendix]

$$\Delta=[Ql/(2\Omega)^2]\Gamma\cos2\Omega t=1.95\times10^{-3}\ \text{cm/sec}^2\ \Gamma\cos2\Omega t, \tag{1}$$

where $2\Omega=2\pi\times88.45$ rad/sec.

The readout of the detector vibrations is accomplished by sensing the dynamic strains of the detector arms with barium titanate strain transducers. (Gulton Ind. type SC-2). A pair of transducers were reversed from the arrangement shown in Fig. 3 so that opposing pairs of transducers would produce a differential output voltage which could be fed into the differential input of a Princeton Applied Research HR-8 lock-in amplifier.

The dynamic strain in the arms due to their deflection is a strong function of the details of the design of the detector arms, and is difficult to calculate accurately because of the complex mechanical structure used. The

relationship predicted in Ref. 3 is

$$\epsilon=[(b+L)c/(\tfrac{1}{3}L^3+bL^2+b^2L)]\Delta=0.026\ \text{cm}^{-1}\Delta, \quad (2)$$

where $b=0.3$ cm is the radius of the end mass, $L=1.8$ cm is the length of the arm, and $c=0.038$ cm is the half-thickness of the arm.

The barium titanate strain transducers extend over a considerable portion of the arm; therefore, they measure an averaged value of the strain, which is a maximum at the hub and zero at the end. This average measured strain was estimated as

$$\epsilon_t=0.6\epsilon=0.016\ \text{cm}^{-1}\Delta. \quad (3)$$

The transducers used on the detector had been calibrated on a test setup which compared them with a resistive strain gauge using pure longitudinal strains at 1600 Hz. The transducer factor obtained under these conditions was about $\sigma=0.7\times10^5$ V/unit strain. Thus the voltage output from this sensor should be approximately

$$V=\sigma\epsilon_t=1.1\times10^3\ \text{V/cm}\ \Delta=2.2\ \text{V}\cdot\text{sec}^2\ \Gamma\cos2\Omega t. \quad (4)$$

NONGRAVITATIONAL COUPLING

It is obvious that in order to detect the very weak dynamic gravitational forces being generated by the rotating mass quadrupole, the generator and detector must be well shielded from each other to prevent acoustic and electromagnetic coupling. The detector is highly sensitive to acoustic noise with a frequency component at its resonance frequency, but experience has shown that the acoustic noise can be eliminated by placing the detector in a vacuum chamber at a few mTorr.

Although an ideal detector is theoretically insensitive to vibrations of the mounting structure,[3] in practice a small amount of the vibrations in the mount leak into the gradient-sensing mode. Because of this, an effort must be made to keep the detector-mount vibrations at a low level. This was accomplished by suspending the detector in the chamber with a spring, and the chamber from the ceiling by another spring. The generator was isolated from the workbench by compression springs, and the iron-shield plate was vibrationally isolated from both the generator and detector by its own support springs (see Fig. 4).

Electromagnetic coupling can occur in two ways: (1) by direct interaction of the rotating magnetic fields of the motor with the arms of the detector; (2) by stray electromagnetic voltages or currents entering the detector output leads or the preamplifier. The electromagnetic coupling into the output electronics is easily checked, since it is independent of the resonant response of the detector and was found to be unobservable even in the single-ended mode of operation, although all data were taken with a differential input to insure that pickup was not a problem.

Direct coupling of the rotating magnetic fields around the generator motor into the detector was found to be a major problem. At first it was not well understood, since the detector arms were of aluminum and the detector masses of brass. This interaction was originally eliminated by using a phase-locked asynchronous drive. In this mode of operation of the generator, the generator motor is driven by currents at some higher frequency, typically 200 Hz, so they do not excite the detector resonant mode. The amplitude of the drive voltage is controlled by a servo loop so that the rotor remains at a constant speed of 44 rps. The servo loop is so tight that both the frequency and the phase of the rotor are held tightly to the phase of a reference signal from a precise oscillator (General Radio frequency synthesizer). It was later discovered that the detector had been assembled with stainless steel screws; when they were replaced by brass screws, the magnetic coupling was eliminated and it was possible to take good data using synchronous drive on the generator.

One important factor aided greatly in the problem of eliminating the nongravitational coupling between the generator and the detector. Because of the double mass in the mass quadrupole, the generator is rotated at *half* of the detector frequency. Therefore, predominantly all of the acoustic and electromagnetic energy produced by the generator is at a frequency which is outside the detector-response frequency; only that small portion of the energy which is harmonically generated at twice the rotation frequency must be shielded against.

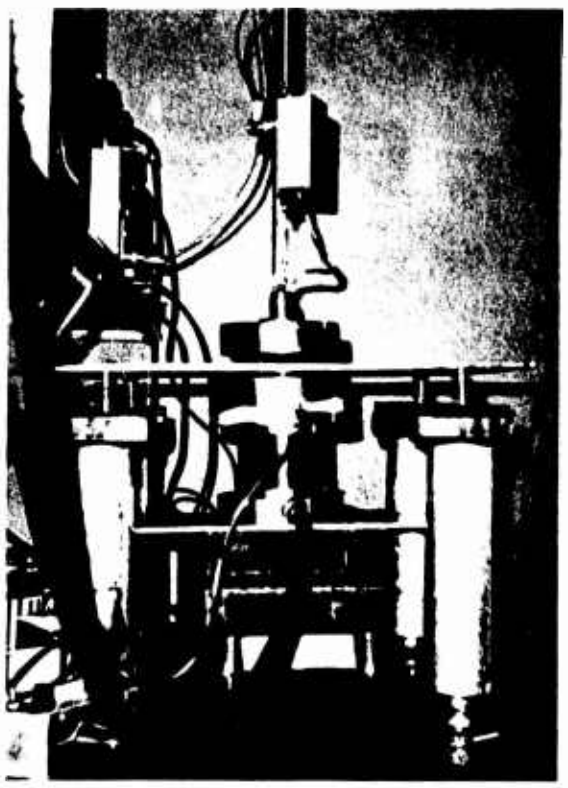

FIG. 4. Relative position of generator and detector.

The generator was designed specifically for the problem of determining the nongravitational-coupling effects. If four aluminum slugs are put in the mass holder, the generator has no time-varying mass-quadrupole moment and therefore no dynamic gravitational-gradient field; however, it still retains all of its electromagnetic and acoustic properties. A test run was made at 5 cm separation distance using the four aluminum slugs. The generator speed was varied from 43 to 45 rps, so that the detector-mode frequency of 88 Hz was not missed. The detector output remained at 0 ± 4 nV. The rotor was then deliberately unbalanced so that the acoustic output was noticeably increased and the test was rerun, with the same results. These experiments demonstrated that the response of the detector structure and sensor electronics to nongravitational forces arising from all sources, including the generator, was less than 4 nV.

DETECTOR CALIBRATION

After the test for nongravitational coupling, two of the aluminum slugs were replaced with tungsten slugs, resulting in a mass difference of 1012 g. The rotor was rebalanced and the generator and detector were placed 5 cm apart. The theoretical calculations presented in the Appendix indicate that at this distance, and with this size detector, a 1012-g effective mass should produce an equivalent gravitational-force gradient of

$$\Gamma \sin 2\Omega t = 1.25\times10^{-7} \sin 2\Omega t \text{ sec}^{-2}. \quad (5)$$

The dynamic gradient has an amplitude of about 0.04 of the earth's static gravitational-force gradient.

From the theory of operation of the sensors,[3] this gradient should cause the gravitational-gradient sensing mode of the detector to oscillate with an amplitude of [see Eq. (1)]

$$\Delta = 2.5\times10^{-10} \cos 2\Omega t \text{ cm}. \quad (6)$$

Although the amplitude of these motions is extremely small, of the order of 0.01 of the diameter of an atom, they are easily measured if piezoelectric strain transducers are used. Similar sensing techniques used on the gravitational radiation detectors at the University of Maryland[5,6] have measured motions down to 10^{-14} cm.

The motion induced in the detector causes an average strain in the arms of [see Eq. (3)]

$$\epsilon_t = 3.9\times10^{-12} \cos 2\Omega t. \quad (7)$$

If we assume that the transducer calibration is $\sigma = 0.7\times10^{5}$ V/strain, the predicted output of these sensors under excitation by a generator with a 1-kg mass difference at a 5-cm separation distance would be [see Eq. (4)]

$$V = 2.2 \text{ V/sec}^2\ \Gamma \cos 2\Omega t$$
$$= 270 \cos 2\Omega t \text{ nV (predicted)}, \quad (8)$$

or an rms voltage of 190 nV.

When the test was run, the actual measured output voltage of one arm of the sensor under these conditions was 97 ± 3 nV (rms). This is much larger than the output-voltage fluctuations of ±4 nV under the control conditions using the four aluminum masses, and is almost exactly half the predicted output. The reason for this lower output is not known. It is assumed that it is a result of the difficulty in obtaining an accurate calibration of the strain transducers, or in calculating the strain from the deflection Δ. Further experiments are in progress to resolve the question. The gravity-gradient input to detector-voltage output relationship for the adjustable detector obtained from this calibration is

$$V = 1.1 \text{ V/sec}^2\ \Gamma \cos 2\Omega t. \quad (9)$$

VERIFICATION OF GRAVITATIONAL COUPLING

Although the control experiments with the four aluminum slugs and the balanced and unbalanced rotor indicated that the nongravitational coupling was negligible, it was still possible that the replacement of the aluminum slugs with the tungsten slugs could change the magnetic moment or balance of the generator and cause nongravitational coupling. In order to further insure that the voltage output seen was caused only by gravitational-gradient coupling, a run of data was taken at various separation distances and with various mass-quadrupole moments. (One of the aluminum slugs froze in its hole in the generator during the preliminary work so it was possible to try only four different mass-quadrupole arrangements.)

At the start of the experiment, the phase of the lock-in detector was adjusted to give a maximum output with the tungsten slugs and was not adjusted or peaked during the remainder of the data run. The quadrature voltage was monitored periodically to insure the detection of any phase shift in the signal induced by any variation in the relative strength of the gravitational coupling and any synchronous nongravitational coupling. No quadrature component was detected during the data runs.

With the tungsten slugs in the generator, a set of data was taken while the separation distance was varied from 4.8 cm to 12 cm. The generator was then stopped and the tungsten slugs replaced with brass slugs, resulting in an effective mass difference of 406.0 g. Without adjustment to the sensor electronics, a second set of data was taken from 4.8 to 10 cm. The generator was again stopped and the brass slugs removed, leaving a void or relative mass difference of -200 g. The phase knob of the lock-in detector was switched exactly 180° to account for the effective negative mass, or 180° signal-phase difference, and the third set of data taken from 4.8 cm to 8 cm. When aluminum slugs were placed in all four holes, the output was 0 ± 3 nV. The data are plotted in Fig. 5.

Curves of detector output versus separation distance were then calculated and plotted in Fig. 5 for various

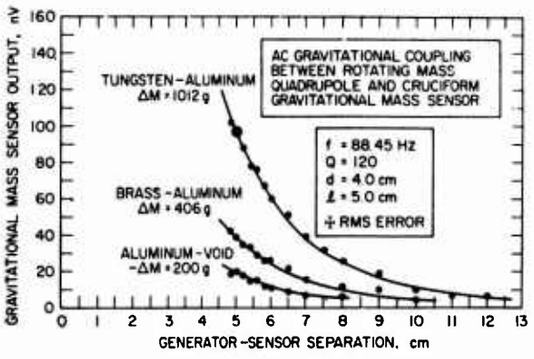

FIG. 5. Dynamic gravitational coupling between rotating mass quadrupole and cruciform gravitational-mass sensor.

mass-quadrupole moments using the theoretical Eqs. (A-15) and (A-16) derived in the Appendix. For conversion of the calculated equivalent gravitational-gradient field to sensor-voltage output, we used the calibration point at 5 cm and 97 nV (larger data point). The two lower curves are the upper curve multiplied by 0.4 and 0.2, respectively.

The excellent agreement of the data with the theoretical predictions in amplitude and phase for various conditions of mass-quadrupole moment and separation distance indicates that only gravitational energy was being transmitted from the generator to the detector. The minimum dynamic gravitational-gradient field observed during this test was about 6×10^{-9} sec^{-2} (6 Eötvös units) or 0.002 of the earth's gradient. The effective differential acceleration on the 5-cm-long detector arms due to this field was

$$a=\Gamma l=3\times10^{-8}\ \text{cm/sec}^2=3\times10^{-11}\ g\text{'s}, \qquad (10)$$

and the effective force level on the 20-g detector masses was

$$F=ma=6\times10^{-7}\ \text{dyn}. \qquad (11)$$

SUMMARY

We have constructed a generator of 88-Hz gravitational-gradient fields and used the fields to calibrate the response of a dynamic gravitational-gradient sensor. The test involved the transmission of gravitational energy over distances up to 12 cm by means of dynamic Newtonian gravitational-gradient fields.

APPENDIX: GRAVITATIONAL INTERACTIONS BETWEEN A CRUCIFORM DETECTOR AND A ROTATING-MASS QUADRUPOLE

The model which we will use to calculate the gravitational interaction between a rotating-mass quadrupole and a resonant cruciform gravitational-mass sensor is shown in Fig. 6. The generator is assumed to be two spherical masses of mass M separated by a distance $2d$ and rotated about their center of mass at a constant angular frequency $\dot{\theta}=\Omega$. The detector is assumed to be four spherical masses of mass m on orthogonally disposed massless arms of length l. The sensor is supported from above so that its center of mass is at a height h directly above the center of mass of the generator. The particular mode of the sensor used to sense the gravitational-gradient forces is the dual tuning-fork mode (see Fig. 7). It was shown in previous analyses[3] that this mode does not respond to vibrational forces at the mount nor to the direct gravitational force field, but only to the gradient of the gravitational force field.

The forces on the sensor resulting from the gravitational interaction between the rotating masses M_c and the sensor masses m_i typically consist of

$$F_{ic}=-GMm/R_{ic}^2, \quad i=1\text{ to }4,\ c=a,b,\ m_i=m,\ M_c=M, \qquad (A1)$$

where

$$R_{ic}^2=h^2+r_{ic}^2, \qquad (A2)$$

and

$$\begin{aligned} r_{3a}^2&=r_{1a}^2=l^2+d^2-2ld\cos\theta,\\ r_{3b}^2&=r_{1b}^2=l^2+d^2+2ld\cos\theta,\\ r_{4a}^2&=r_{2a}^2=l^2+d^2-2ld\sin\theta,\\ r_{4b}^2&=r_{2b}^2=l^2+d^2+2ld\sin\theta. \end{aligned} \qquad (A3)$$

However, the components of the forces which drive the sensing mode of the detector are the tangential

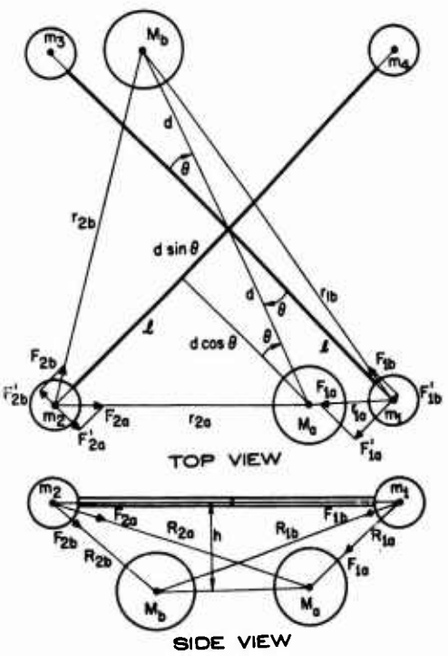

FIG. 6. Model for gravitational-interaction calculation.

components of the forces F_{ic}

$$F_{3a}' = F_{1a}' = (GMm/R_{1a}^3)d\sin\theta,$$
$$F_{3b}' = F_{1b}' = -(GMm/R_{1b}^3)d\sin\theta,$$
$$F_{4a}' = F_{2a}' = -(GMm/R_{2a}^3)d\cos\theta,$$
$$F_{4b}' = F_{2b}' = (GMm/R_{2b}^3)d\cos\theta, \qquad \text{(A4)}$$

where the sense of the forces is taken to be positive in the clockwise direction.

The resultant force F_i' on each of the arms due to the forces F_{ic}' is given by

$$F_3' = F_1' = F_{1a}' + F_{1b}'$$
$$= GMmd[(1/R_{1a}^3) - (1/R_{1b}^3)]\sin\theta,$$
$$F_4' = F_2' = F_{2a}' + F_{2b}'$$
$$= -GMmd[(1/R_{2a}^3) - (1/R_{2b}^3)]\cos\theta. \qquad \text{(A5)}$$

The response of the detector arms to these resultant forces has been presented in a previous work by Bell, Forward, and Morris.[3] Taking a simplified version of their Eqs. (38) through (41), we obtain

$$m\ddot{\Delta}_i + d\dot{\Delta}_i + k\Delta_i = F_i', \qquad i = 1\text{–}4, \qquad \text{(A6)}$$

where Δ_i is the deflection of the ith arm, k is the spring constant, and d is the damping.

These four equations (A6) describe the individual motions of the four arms; however, the vibrations of interest are the motions of the gravity-gradient sensing mode (see Fig. 7). The equation for this mode is obtained by the following linear combination of the individual arm motions[7]

$$\Delta_g = \tfrac{1}{2}(\Delta_1 - \Delta_2 + \Delta_3 - \Delta_4), \qquad \text{(A7)}$$

where the normalization factor of $\frac{1}{2}$ is used so that the detector energy expressed in terms of the four arm amplitudes is equivalent to the detector energy expressed in terms of the four vibrational mode amplitudes (gravity gradient, torsional, and two translational).[7]

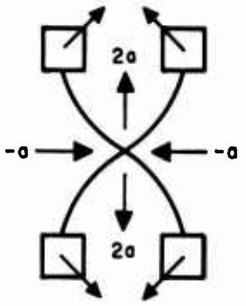

FIG. 7. Gravity-gradient sensing mode.

If we add the equations for the four arm motions [Eqs. (A6)] in this manner, we obtain the equation of motion for the gravity-gradient sensing mode

$$m\ddot{\Delta}_g + d\dot{\Delta}_g + k\Delta_g = \tfrac{1}{2}(F_1' - F_2' + F_3' - F_4') = F_g, \qquad \text{(A8)}$$

where

$$F_g = GMmd\{[(1/R_{1a}^3) - (1/R_{1b}^3)]\sin\theta + [(1/R_{2a}^3) - (1/R_{2b}^3)]\cos\theta\}. \qquad \text{(A9)}$$

Because R_{ic} is a function of the angle θ, the resultant force F_g has a complex behavior with the angle of rotation. To calculate the components of the resultant force as a function of frequency, we will expand the terms in R_{ic}^{-3}. Letting

$$R^2 = l^2 + d^2 + h^2, \qquad \text{(A10)}$$

we can write the resultant force F_g as

$$F_g = GMmd\{[(R^2 - 2ld\cos\theta)^{-3/2} - (R^2 + 2ld\cos\theta)^{-3/2}]\sin\theta + [(R^2 - 2ld\sin\theta)^{-3/2} - (R^2 + 2ld\sin\theta)^{-3/2}]\cos\theta\}. \qquad \text{(A11)}$$

Bringing R^2 out from the denominator and letting $\Lambda = (ld/R^2)$, we obtain

$$F_g = (GMmd/R^3)\{[(1 - 2\Lambda\cos\theta)^{-3/2} - (1 + 2\Lambda\cos\theta)^{-3/2}]\sin\theta + [(1 - 2\Lambda\sin\theta)^{-3/2} - (1 + 2\Lambda\sin\theta)^{-3/2}]\cos\theta\}. \qquad \text{(A12)}$$

We now expand each term using the binomial expansion theorem; however, because the expansion parameter Λ can be as high as $\frac{1}{3}$ when the generator and detector are separated by 4.5 cm, it is necessary to take the expansion out to the seventh order.

$$F_g = (GMmd/R^3)\{[6\Lambda\cos\theta + 35\Lambda^3\cos^3\theta + \tfrac{693}{4}\Lambda^5\cos^5\theta + \tfrac{6435}{8}\Lambda^7\cos^7\theta]\sin\theta$$
$$+ [6\Lambda\sin\theta + 35\Lambda^3\sin^3\theta + \tfrac{693}{4}\Lambda^5\sin^5\theta + \tfrac{6435}{8}\Lambda^7\sin^7\theta]\cos\theta\}. \qquad \text{(A13)}$$

(The even order terms drop out because of the symmetry.) If we rearrange the above equation and use the trigonometric identities

$$2\sin\theta\cos\theta = \sin 2\theta,$$
$$2(\cos^3\theta\sin\theta + \sin^3\theta\cos\theta) = \sin 2\theta,$$
$$16(\cos^5\theta\sin\theta + \sin^5\theta\cos\theta) = 5\sin 2\theta + \sin 6\theta,$$
$$32(\cos^7\theta\sin\theta + \sin^7\theta\cos\theta) = 7\sin 2\theta + 3\sin 6\theta, \qquad \text{(A14)}$$

we can obtain the expression

$$F_g = (6GMmld^2/R^5)\{(1 + \tfrac{35}{12}\Lambda^2 + \tfrac{1155}{128}\Lambda^4 + \tfrac{15015}{512}\Lambda^6)\sin 2\Omega t + (\tfrac{231}{128}\Lambda^4 + \tfrac{6435}{512}\Lambda^6)\sin 6\Omega t\}, \qquad \text{(A15)}$$

[7] C. C. Bell, J. R. Morris, J. M. Richardson, and R. L. Forward, "Vibrational Mode Behavior of Rotating Gravitational Gradient Sensors" (to be published).

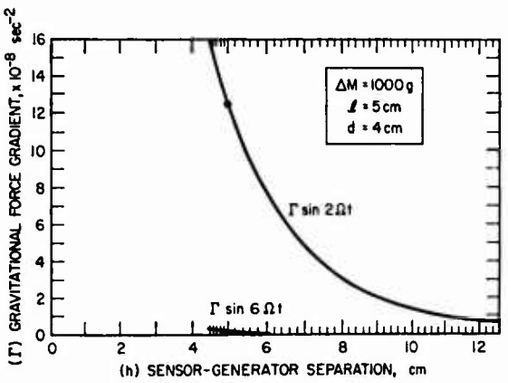

FIG. 8. Calculated equivalent gravitational-force gradient.

where we brought out a factor of $6\Lambda = 6ld/R^2$ from behind the brackets. This expression shows that the interaction force between the generator and detector is complicated at close distances of separation and depends upon the sizes of the generator and detector, as well as the separation distance. This expression also shows that in addition to responding to the gravitational-force gradient or the second-order gradient of the potential at 2Ω, the detector will also respond to the sixth-order gradient of the potential at 6Ω. Because of the symmetry of the generator–detector combination, the intermediate higher-order gradients are not observable.

In order to relate the equation for the effective force on the gravitational-gradient sensing mode of the detector [Eq. (A15)] to the previous work, we define an equivalent gravitational-force gradient by the relation

$$\Gamma = F_0/2ml, \tag{A16}$$

where m is the effective mass and $2l$ is the effective length of the gravitational-gradient sensing mode.

The effective gravitational-force gradient [Eq. (A16)] was computer calculated for various values of the separation distance h, and the results for the amplitudes of the two frequency components are plotted in Fig. 8. For this curve it was assumed that the detector had an effective radius of 5 cm, and the generator consisted of two 1-kg masses on a radius of 4 cm. At the nominal separation distance of 5 cm, the effective gravitational-force gradient resulting from the generator is 1.24×10^{-7} sec^{-2}. This is about 0.04 of the earth's gradient. These two relatively small masses have a relatively large gradient because we are able to bring the center of mass of the detector very close to the center of mass of the generator.

At distances greater than 12 cm, the only important term in Eq. (A16) is the first, and the effective gravitational gradient is given by the formula

$$\Gamma = 3GMd^2 \sin2\Omega t/(h^2+d^2+l^2)^{5/2} \approx (3GMd^2/h^5)\sin2\Omega t. \tag{A17}$$

The gradient is falling off as d^2/h^5 rather than as $1/h^3$ because the detector is only sensitive to the dynamic gradient being generated by the rotating mass-quadrupole moment of the generator and is not sensitive to the static gradient of its monopole moment which does fall off as $1/h^3$.

If we choose the rotation speed Ω of the generator so that the detector senses the gravitational-force gradient fields being generated at twice the rotation speed

$$k/m = (2\Omega)^2, \tag{A18}$$

then the gravitational forces at 2Ω are seen to be driving terms in the equation of motion of the vibrational mode [Eq. (A8)]:

$$\ddot{\Delta}_0 + (d/m)\dot{\Delta}_0 + (2\Omega)^2\Delta_0 = 2\Gamma l \sin2\Omega t. \tag{A19}$$

The solution to this equation is well known as

$$\Delta_0 = -2\Gamma l[Q/(2\Omega)^2]\cos2\Omega t, \tag{A20}$$

where Δ_0 is the amplitude of the vibrational mode and $Q = 2\Omega m/d$ is the quality factor of the resonance.

In practice we do not measure the mode amplitude directly, but instead measure the amplitude of one of the arms

$$\Delta_1 = \tfrac{1}{2}\Delta_0 = -\Gamma l[Q/(2\Omega)^2]\cos2\Omega t. \tag{A21}$$

APPENDIX G

DISCUSSION AND ANALYSIS OF THE VERTICALLY TUNNELED SPHERE-NEWTONIAN GRAVITATIONAL CONSTANT EXPERIMENT

(Prepared by D. Berman)

SUMMARY

This scientific report covers one portion of a program to find a new experimental method of improving our knowledge of the Newtonian gravitational constant (G). According to the NBS Technical News Bulletin (October 1963) the presently accepted value is $6.670 \pm 0.015 \times 10^{-11}$ $m^3\ kg^{-1}\ sec^{-2}$ (three standard deviations). The vertically tunneled sphere experiment is based on a suggestion of Professor J. W. M. DuMond of the California Institute of Technology. The experiment utilizes the fact that a mass moving freely through a tunnel bored in a sphere will oscillate about the midpoint of the tunnel at a period determined by the density of the sphere. To counteract the large forces of the earth in the vertical position, it is necessary to bore two tunnels and measure the net response of two masses suspended from the level arm of a balance. A measurement of the change in the period of the balance when the sphere is put in place will then be proportional to the density of the sphere. The accuracy of the experiment will be limited by precision in the manufacturing of the balance, sphere, and tunnels, as well as the ability to detect extremely small changes in period. The analysis indicates that presently attainable accuracies in the manufacture of the experimental apparatus will introduce measurement errors of appreciable magnitude. It does not appear that this experiment, in the analyzed configuration, can significantly improve our knowledge of the Newtonian gravitational constant.

I. INTRODUCTION

The gravitational constant G currently is known to one part in 500 (three standard deviations). The most accurate of the various experiments to determine G to date is the "time of swing" method of Heyl.[1] This experiment consists of two concentric torsion balances and is similar to the Cavendish apparatus (see Fig. G-1). One balance is held stationary while the other is excited into a pendulum torsional mode oscillation. When the two balances are aligned in parallel, the period of swing is less than when they are aligned at right angles. In the former position, the gravitational attraction between the two balances adds to the torsional spring restoring force; in the latter position, it subtracts from it. The gravitational constant is obtained from measurement of the difference in periods between the near and far positions. The periods were on the order of a half hour, and could be measured to 0.1 sec.

A method of determining G to higher accuracy currently is being tested at the University of Virginia.[2] (See Appendix E of this report.) This experiment is designed to improve the knowledge of G to one part in 10^4; with future versions, accuracies greater than one part in 10^5 and possibly one part in 10^6 should be attainable. It also consists of two concentric torsional balances. One balance is free to rotate under the attraction of the second, while the second is motor-driven and servo-controlled to maintain constant angular position with respect to the first. Hence, both balances will rotate through 360°, while a constant torque is being maintained on the free balance. The angular displacement, after many hours, determines the gravitational constant.

In trying to push the gravitational constant to higher accuracy, we ultimately approach the limitation of precision in the determination of mass separation distances and homogeneity of density within the masses themselves.

Professor DuMond has suggested that a new "time of swing" experiment can be performed. A vertical torsion balance (Fig. G-2) may be constructed such that the suspended masses move freely through each of two tunnels bored in a sphere. The period of oscillation for an ideal system is on the order of one hour. He has also suggested that the sphere can be hollow and filled with liquids of various densities. The primary advantage of the tunneled sphere experiment is that to first order we do not need to know the position of the tunnels in the sphere or the positions of the suspended masses in the tunnels. It also has the advantage that the gravitational force measurement has been converted directly into a frequency measurement, and these can be made with high accuracy.

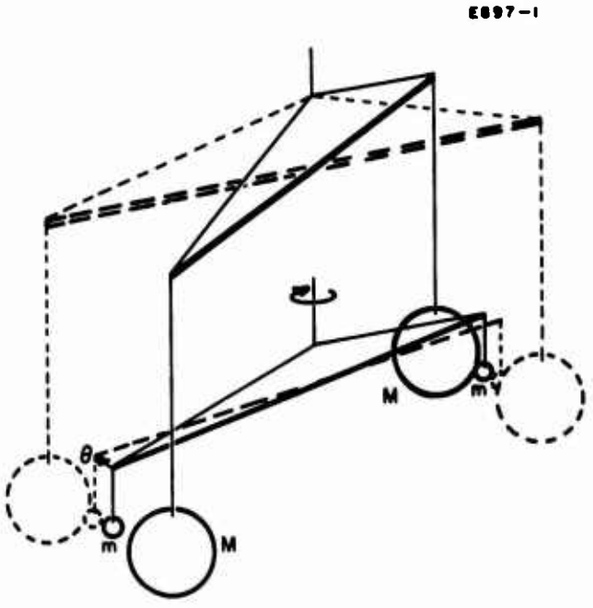

Fig. G-1. Cavendish type coaxial torsion balance system.

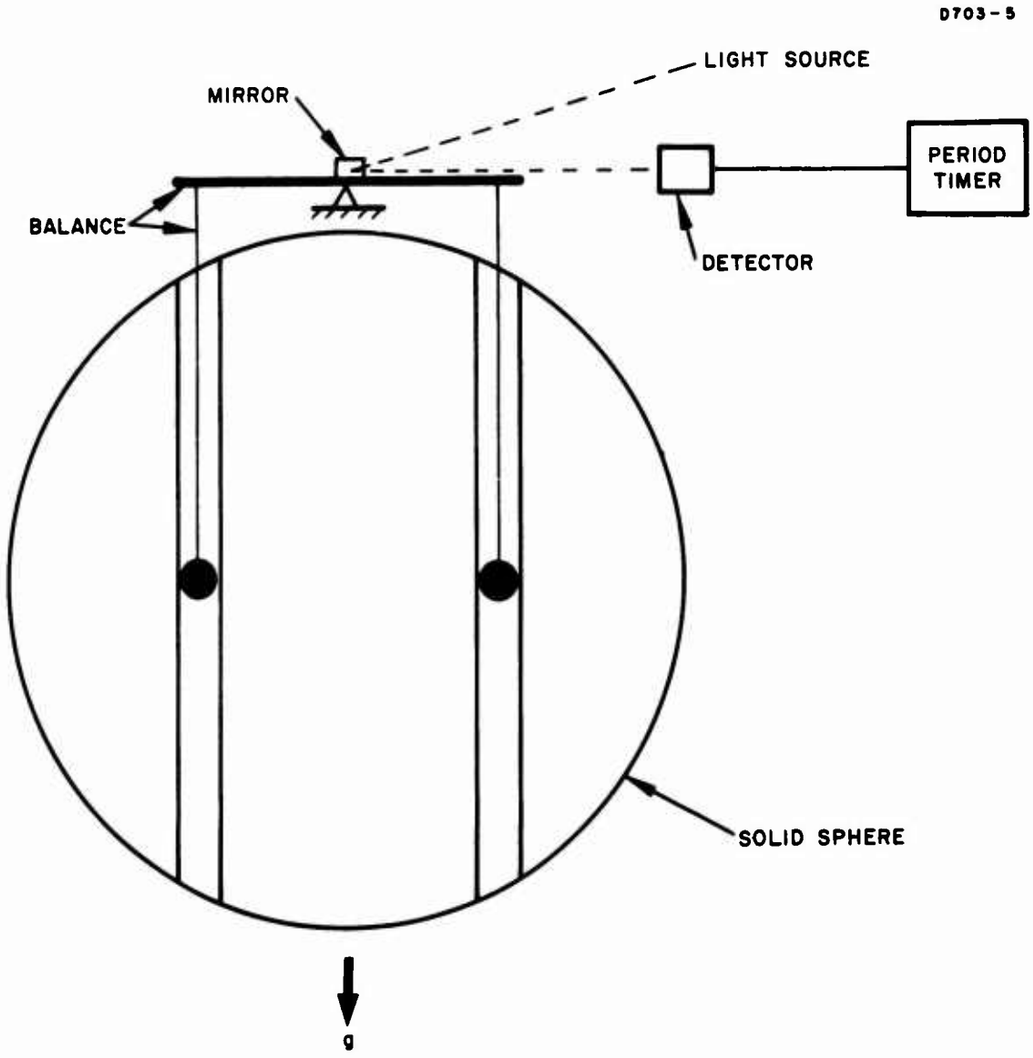

Fig. G-2. System schematic.

PRECEDING PAGE BLANK - NOT FILMED.

II. SYSTEM DESCRIPTION

An operational system could be as shown schematically in Fig. G-2. The main component is a large solid sphere, precision machined to within tolerances of eccentricity as defined in Section IV. Two parallel tunnels are drilled in the sphere. A vertical balance is constructed such that two identical masses are suspended into the tunnels from the ends of fine wires. The balance is initially adjusted to an equilibrium position, such that the masses rest at the line passing through the center of the sphere and parallel to the horizontal bar of the balance.

Attached to the center of the balance is a small mirror, which deflects a steady light beam onto a detector. The angular motion of the balance is observed in this way. The timing of the period of the balance can be accomplished by standard period measurement techniques using precise electronic counters.

The balance system must be operated in a vacuum in order to decrease the damping and eliminate connection disturbances. It is also advantageous to shield the system magnetically, as this has been found necessary in previous gravitational experiments even when the apparatus was made of nonferromagnetic material.

Initially, the balance is adjusted to an equilibrium position in order to cancel out the constant torque due to mechanical imperfections. Then the oscillations are induced by manipulating the balance. The induced motion is continued in resonance until the desired amplitude of deflection is attained.

PRECEDING PAGE BLANK - NOT FILMED.

III. GRAVITATIONAL INTERACTION: IDEAL BALANCE

The gravitational potential at a point is given by the Poisson equation:

$$\nabla^2 \phi = - 4\pi G\rho \tag{1}$$

where

ϕ = the gravitational potential

ρ = local density

G = gravitational constant = 6.67×10^{-8} (cgs) (2)

In spherical coordinates and for spherical symmetry, equation (1) becomes ($\phi = \phi(r)$)

$$\frac{d}{dr}\left(r^2 \frac{d\phi}{dr}\right) = - 4\pi G\rho r^2 \tag{3}$$

To find the attractive force (per unit mass) inside a uniform sphere of constant density, integrate both sides

$$F_r = \frac{d\phi}{dr} = - \frac{4}{3} \pi G \rho r \tag{4}$$

The force is in the radial direction, toward the center of the sphere, and proportional to the distance from it.

Consider next a tunnel through the sphere, not necessarily passing through its center (Fig. G-3). The component of force parallel to the tunnel is easily seen to be proportional to x, the displacement from the center of the tunnel. The tunnel itself will have no gravitational effect in the direction parallel to it.

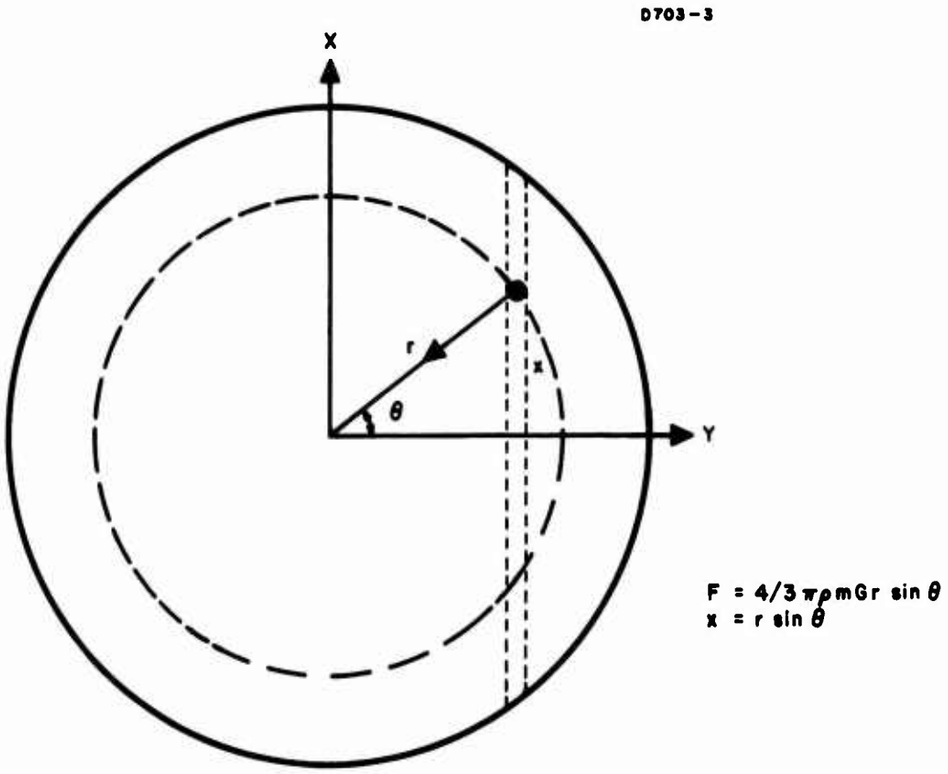

Fig. G-3. Components of gravitational attraction inside the tunnel of a solid sphere.

The differential equation for the motion of a test mass m along the tunnel (undamped) is readily written

$$m\ddot{x} + \frac{4}{3}\pi G\rho m x = 0 \tag{5}$$

such that its natural period is given by:

$$\omega_o^2 = \frac{4}{3}\pi G\rho \tag{6}$$

and the period by:

$$\tau = \frac{2\pi}{\omega_o} = (3\pi/G\rho)^{1/2} . \tag{7}$$

Thus, the gravitational constant G is available by measurement of the period of oscillation τ and knowledge of the density ρ. Solving (7)

$$G = 3\pi/\rho\tau^2 . \tag{8}$$

Hence, we must know ρ and τ with the precision that we hope to determine G.

To estimate the order of magnitude of the periods involved in this experiment, substitute into (8) $G = 6.67 \times 10^{-8}$ (cgs); and $\rho = 13.5$ (the density of Hg). The result is, $\tau = 3000$ sec, or 50 min.

So far in the analysis, we have not considered the gravitational attraction of the earth in the calculation of the motion of the test mass. The second tunnel shown in Fig. G-2, with the balance arrangement of the second mass, cancels out the large gravitational acceleration due to the earth for an ideal balance. However, the gradient due to the earth will affect the period.

With respect to Fig. G-4, let x_1 and x_2 be the vertical distance of the two masses from the center of the sphere. Consider the earth as spherical, with center at distance R. The vertical force on mass one,

due to both the surrounding sphere (F_s) and the earth (F_e), is given by: $F_1 = F_s + F_e$

$$F_1 = mG \left[\frac{4}{3} \pi \rho x_1 + \frac{M}{(R + x_1)^2} \right] \tag{9}$$

where M = mass of earth.

For the spherical earth, we may write

$$M = \frac{4}{3} \pi R^3 \rho_e \tag{10}$$

where ρ_e = density of the earth. Because $x_1 \ll R_1$, F_e becomes

$$F_e = m \frac{4}{3} \pi G \rho_e (R - 2x_1) \ . \tag{11}$$

Using this result, equation (9) becomes

$$F_1 = m \frac{4}{3} \pi G \left[\rho x_1 + \rho_e (R - 2x_1) \right] \ . \tag{12}$$

Similarly, the forces on mass two are

$$F_2 = m \frac{4}{3} \pi G \left[\rho x_2 + \rho_e (R - 2x_2) \right] \ . \tag{13}$$

The total torque acting on the over-all balance system is

$$T = a(F_2 - F_1) \tag{14}$$

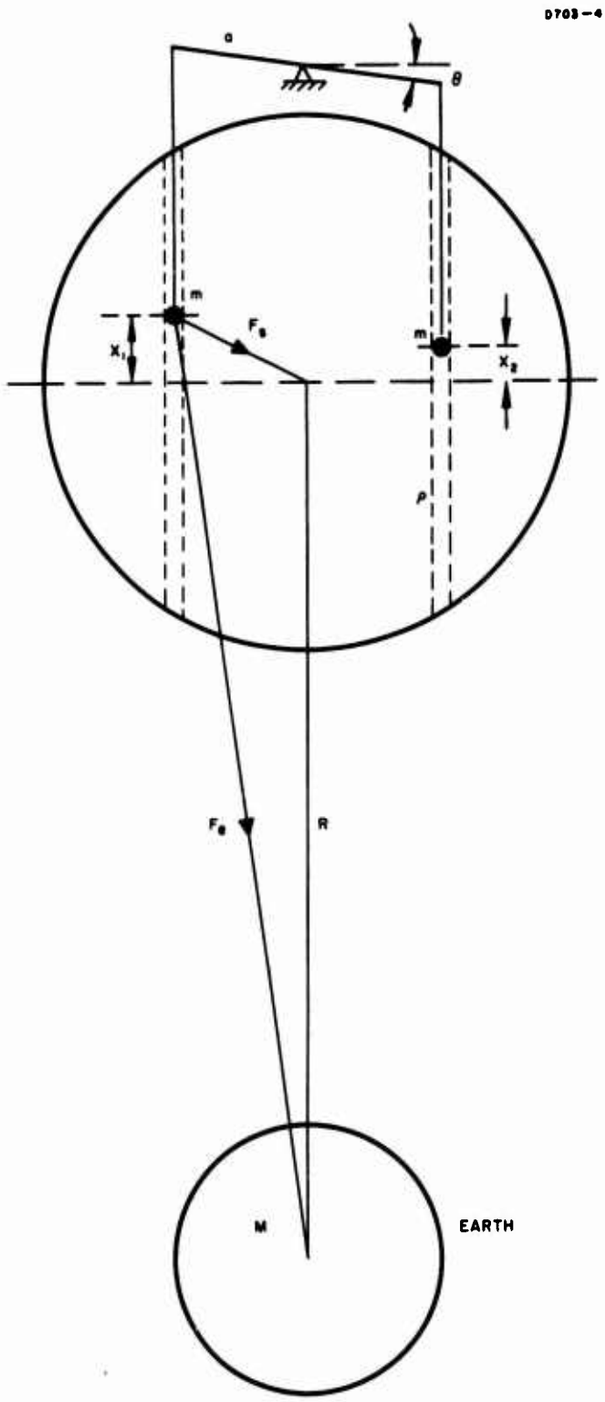

Fig. G-4. System schematic showing effect of earth's gradient.

where a = lever arm. Substituting (12) and (13) into (14) yields

$$T = ma \frac{4}{3} \pi G (2\rho_e - \rho)(x_1 - x_2) \quad . \tag{15}$$

The differential vertical displacement $(x_1 - x_2)$ is related to the balance angular deflection θ by (Fig. 4)

$$(x_1 - x_2) = 2a \sin \theta \quad . \tag{16}$$

Using (16), equation (15) becomes

$$T = \frac{8}{3} \pi m a^2 G (2\rho_e - \rho) \theta = - k\theta \tag{17}$$

for small θ.

The differential equation for angular motion of the balance is written

$$I\ddot{\theta} + k\theta = 0 \tag{18}$$

where I = moment of inertia = $2ma^2$. Thus, the natural frequency of the system is

$$k/I = \frac{4}{3} \pi G (\rho - 2\rho_e) \tag{19}$$

with the corresponding natural period

$$\tau = \left[\frac{3\pi}{G(\rho - 2\rho_e)} \right]^{1/2} \quad . \tag{20}$$

Comparison with (7) shows that the effect of the earth is to replace the sphere density by a combination of sphere density and earth density.*

*If we had not assumed a spherical earth, ρ_e would be replaced by the earth's vertical gradient at the surface.

Thus, the earth's density must be known to the same accuracy with which we want to determine G (from equation (20)).

A solution to this problem would be to conduct two identical experiments at the identical point on the earth's surface, but using spheres of different densities. Then the density of the earth may be found from solving (20) simultaneously, yielding

$$\rho_e = \frac{1}{2}\left[\frac{\tau_1^2\rho_1 - \tau_2^2\rho_2}{\tau_1^2 - \tau_2^2}\right] \tag{21}$$

where τ_1 and τ_2 are the measured periods using two spheres of different densities ρ_1 and ρ_2.

Then G would be solved from (20)

$$G = \frac{3\pi(\tau_1^2 - \tau_2^2)}{\tau_1^2\tau_2^2(\rho_2 - \rho_1)} \; . \tag{22}$$

From equation (20) if $2\rho_e = \rho$, the period is infinite; i.e., there is no oscillation. Moreover, if

$$\rho < 2\rho_e \tag{23}$$

the system is unstable. However, these results are for a perfect balance. In the following section, we will show that an imperfect balance gives rise to a period much less than that indicated by (20), and G must be found by an extremely sensitive frequency measurement.

PRECEDING PAGE BLANK - NOT FILMED.

IV. SOURCES OF ERROR

In Section III, we derived the equation of motion of the balance assuming perfect manufacturing of all system components. In this section, we shall re-derive these equations, accounting for a nonspherical sphere (spheroid) and an imperfect balance. It will be shown that the required tolerances are quite severe, and that this experiment will therefore be difficult to perform.

We now consider the imperfect balance. As shown in Fig. G-5, the lever arm is not straight, but warped by an angle β. This effect causes the balance to restore to an equilibrium position, thus interfering with the gravitational attraction due to the sphere. The period of oscillation even for a highly balanced system, will be much less than that predicted by (7). Writing the forces in the two masses (Fig. G-5),

$$F_1 = Gm \left\{ \left[\sin(\theta + \beta) - \sin\beta\right] \left(\frac{2M}{R^3} - \frac{4}{3}\pi\rho\right) a + \frac{M}{R^2} \right\} a \cos(\theta + \beta) \tag{24}$$

$$F_2 = Gm \left\{ \left[\sin(\theta + \beta) - \sin\beta\right] \left(-\frac{2M}{R^3} + \frac{4}{3}\pi\rho\right) a + \frac{M}{R^2} \right\} a \cos(\theta - \beta) . \tag{25}$$

The torque is obtained from

$$T = a\cos(\theta + \beta) F_1 - a\cos(\theta - \beta) F_2 . \tag{26}$$

Substituting (24) and (25) into (26) for small θ and β

$$T = 2G\, ma^2 \left[\left(\frac{2M}{R^3} - \frac{4}{3}\pi\rho\right) + \frac{M\beta}{aR^2} \right] \theta . \tag{27}$$

The natural frequency (from 19), using $M = (4/3)\pi R^3 \rho_e$, is

$$\omega^2 = \frac{4}{3}\pi G (2\rho_e - \rho) + \beta g/a \tag{28}$$

where $g = 980$ cm/sec^2.

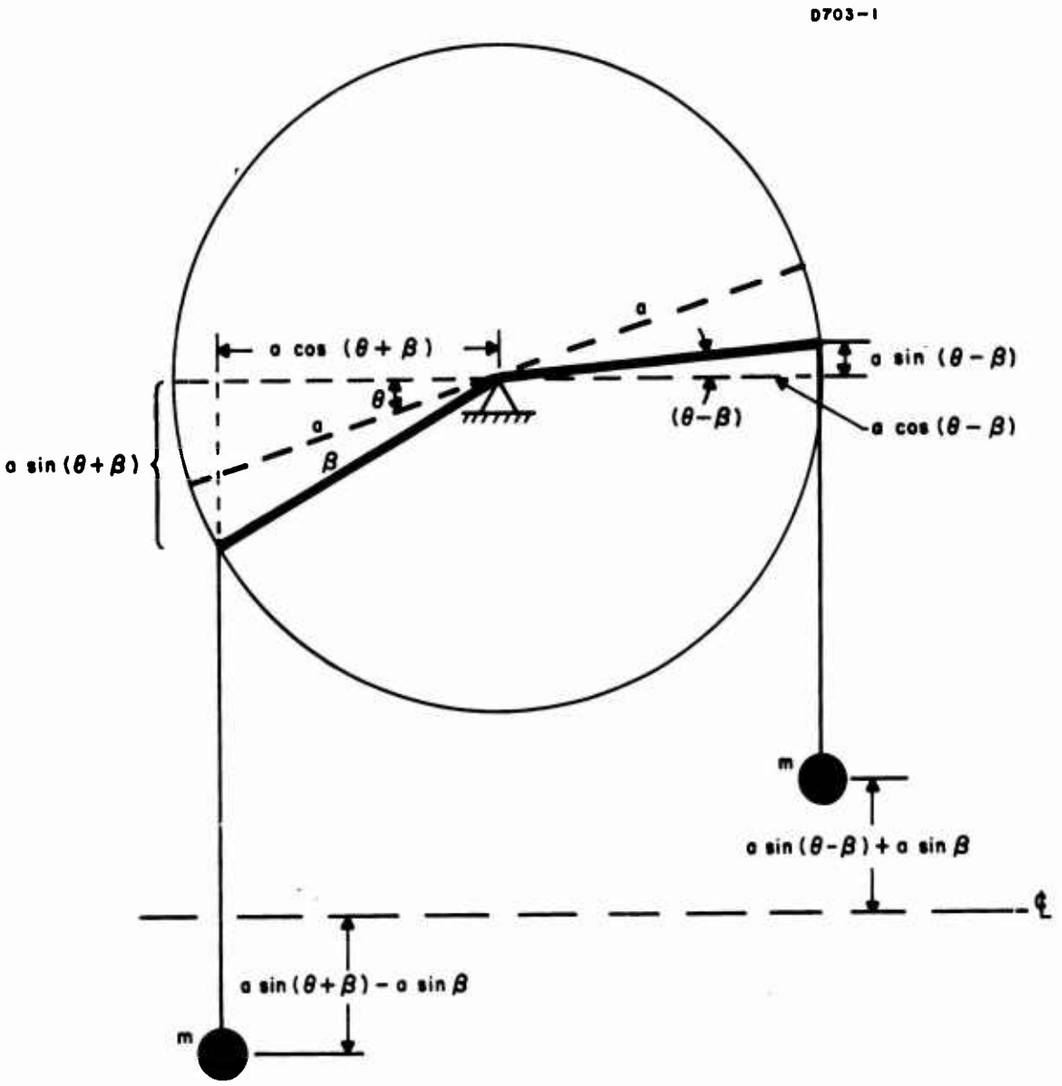

Fig. G-5. Imperfect pendulum.

We recognize the first term as the natural frequency (squared) of the ideal balance (see eq. (19)). The second term is dependent on the imperfection of the balance lever arm, and is present even in the absence of the sphere. Rewriting (28)

$$\omega^2 = \omega_o^2 + \omega_\beta^2 \tag{29}$$

where $\omega_\beta^2 = \beta g/a$. The period is

$$\tau_\beta = \frac{2\pi}{(\beta g/a)^{1/2}} = 2\pi a/(g\Delta)^{1/2} \tag{30}$$

where $\Delta = a\beta$, the alignment of the suspension points at the end of the lever arm (see Fig. G-6). To increase the period to 3000 sec to be comparable to the ideal period, requires making adjustments to 10^{-7} cm. On the other hand, if we allow a larger value of Δ, for example $\Delta = 10^{-4}$ cm, then $\tau_\beta = 200$ sec. This is 15 times less than the natural period of the ideal system, and, in order to obtain an accuracy of 10^{-6} in the measurement of G, must be measurable to one part in $(10^6)(15)^2 \approx 2 \times 10^8$. In other words, there is a trade-off between either a very critical adjustment capability, or a very sensitive frequency determination. Precision timing references up to one part in 10^{11} are available and previous experiments have obtained such measurements approaching one part in 10^5. The question is whether these techniques could be refined to measure frequency to the required precision.

We next consider the effect of a nonperfect sphere (spheroid). Inside a nearly spherical ellipsoid, the attractive force in the vertical direction is[3]

$$F = \frac{4}{3}\pi G\rho \left(1 - \frac{6}{5}\,\frac{b-k}{k}\right) x \approx \frac{4}{3}\pi G\rho\,(1+\epsilon)\,x \tag{31}$$

where k = average sphere radius, b = vertical major axis, and ϵ = fractional deviation of radius from mean. Comparison of eq. (31) with (4) and (8) shows that the error in determination of G is directly proportional to the tolerance with which the sphere is manufactured. To obtain an accuracy of 10^{-6}, for example, requires that the circumferential variation in sphere radius from the mean be no greater than 0.0001%. A ten inch sphere requires a machining accuracy of ten millionths. This level of manufacturing precision is very difficult to attain, especially in the large spheres required for this experiment.

We conclude that this experiment would be difficult to carry out in the form considered herein, primarily because of the difficulty in fabricating the experimental apparatus to the required tolerances.

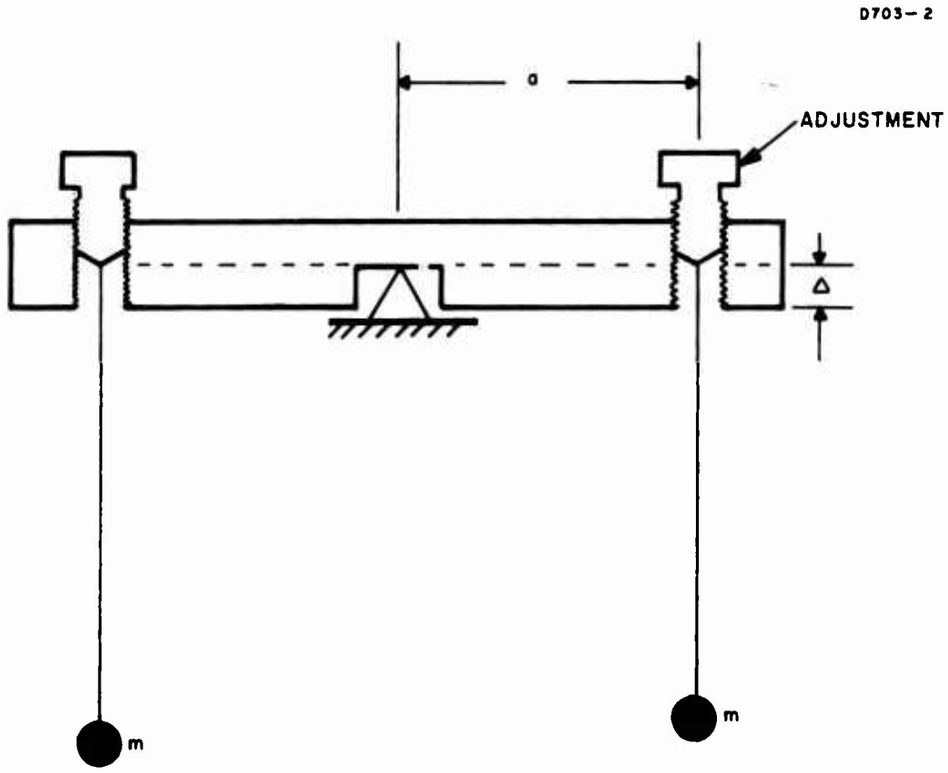

Fig. G-6. Schematic of balance with adjustable mass position.

REFERENCES

1 P. R. Heyl, "A Redetermination of the Constant of Gravitation," Bureau of Stand. J. Research., 5 1243 (1930).

2 J. W. Beams, A. R. Kuhlthay, R. A. Lowry, and H. M. Parker, "Determination of Newton's Gravitational Constant G, with Improved Precision," University of Virginia, Proposal EP-NSF-125-64U (1964).

3 A. S. Ramsey, Newtonian Attraction, Cambridge University Press, (1961).

APPENDIX H

AERIAL APPLICATIONS OF GRADIOMETERS

Prepared by

E. Hose

Aerospace Group
Hughes Aircraft Company

LIST OF SYMBOLS

$\vec{a}_f$	Unit vector in the direction of the vector $\vec{f}$
$\vec{a}_F$	Unit vector in the direction of the vector $\vec{F}$
$\vec{a}_v$	Unit vector in the direction of azimuth A
$\vec{a}_t$	Unit vector in the direction of $A + \frac{R}{2}$
$\vec{a}_g$	Unit vector in the direction of the vector g
$\vec{a}_\psi$	Unit vector in the direction of the azimuth ψ
A	Flight azimuth angle
$E[\ ]$	The expected value operator
$\frac{d}{dt}[X]_I$	Time derivative of X in the inertial coordinate system
$\vec{f}$	The gradient field vector
f	The intensity (magnitude) of $\vec{f}$
$\vec{F}$	The inertial field vector
$\vec{g}$	The gravity vector
g	Intensity of gravity
g_i	a resolvable component of a gravity intensity measurement $g = \frac{1}{I} \sum_{i=1}^{I} g_i$
Δg_q	Gravity anomaly at point q
$\vec{G}$	The gravitation vector
k	The universal gravitation constant
ℓ	Length of arc traveled in time τ
M	Effective mass of the earth

N	Height anomaly of the geop with respect to the spherop or the geoid with respect to the international spheroid
N_p	N at point p
$\vec{p}$	The fixed field vector
Q	The point of measurement
r	Radius vector of the geopotential in azimuth A
$\vec{R}$	Position vector to the geocenter
U	The gravity potential
$\vec{V} = \left[\frac{d\vec{R}}{dt}\right]_E$	Geodetic velocity
$\vec{V}_P = \left[\frac{d\vec{R}}{dt}\right]_p$	Platform velocity
$\Gamma = \frac{\Gamma_\rho + \Gamma_\nu}{2}$	Average vertical gradient of g
Γ_A	Vertical gradient of g in the plane of azimuth A
Γ_i	The average vertical gradient of g_i
$\Delta\Gamma$	Bias error in the gradiometer
Γ_ρ	Vertical gradient of g in the major principal section the geop
Γ_ν	Vertical gradient of g in the minor principal section of the geop
η_a	Astronomical east deflection of vertical
η_g	Gravimetric east deflection of vertical
ν	Radius of curvature of minor geop section
ξ_a	Astronomical north deflection of vertical
ξ_g	Gravimetric north deflection of vertical
ρ	Radius of curvature of major geop section
$\sigma\Gamma$	Standard deviation of the gradiometer errors

τ	Averaging or integration time of the instrument
χ_t	Deflection of vertical in the direction of $A + \frac{R}{2}$
ψ	Azimuth of the major geop section
$\vec{\omega} = \vec{\omega}_{PE}$	Precession of the platform with respect to the earth
$\vec{\Omega} = \vec{\Omega}_{EI}$	Precession of the earth with respect to inertial space

PRECEDING PAGE BLANK - NOT FILMED.

I. INTRODUCTION

A gradiometer is a differential accelerometer which measures differences in the specific force vectors at two different points in space. The inertial field vectors at these points can be decomposed into three othogonal components — one along the line connecting the two points and two in the plane normal to it. The class of instruments of interest here senses the gradient of the field in one direction in the orthogonal plane. Two crossed mass quadrupoles connected together at their centers by a flexural pivot form such an instrument. The orthogonal gradient in the plane of the sensor causes a torque in each quadrupole. The difference in torques between the two quadrupoles flexes the pivot; the strain in the pivot is thus related to the gradients of the inertial field at the plane of the sensor.

Static gradiometers are sensitive to the stabilities of all the instrumental components which carry the signal during a measurement. The problems are no different from those encountered in the design of accelerometers or gravitometers. At present, the state of the art in these devices falls short of the accuracy requirements for useful gradient measurements. Fortunately, gradiometers naturally overcome this limitation.

The magnitudes of the gradients of the field vary with direction. These variations are in the nature of angle function modulation of the field constant. A periodic change in the orientation of the dipoles in the plane of the quadrupole causes the space angle function to time modulate the sensed gradients. The time variable component of the measurement is proportional to the field constant. An estimate of the field can thus be derived from the periodic component of the measurement. This estimate is affected only by instrumental drifts which occur during the scan period. These drifts are negligible, permitting accuracies and threshold sensitivities which approach the theoretical performance limit. Thus, dynamic gradiometers, by angle scanning the field at the point of measurement, can achieve sensitivities which are beyond the state of the art of static specific force sensors.

Dynamic gradiometers can employ a number of types of angle scans. The type which has received the most attention to date is rotation at a constant rate. The rotating gradiometer has been under development at Hughes Research Laboratories for a number of years. Its development up to April 1966 is summarized in Ref. 1, and current concepts and plans are described in Ref. 2 and the final report of the subject contract, of which this report is a part.

Investigations to establish the potential of the rotating gradiometer in aerial geodesy have led to the conclusion that it can be used to level a moving platform. Inturn, this has led to the discovery of a new gradient sensing mode which is possible in a modified form of the quadrupole sensor. This gradient level mode resonates at the driving frequency, while the vertical gradient mode resonates at twice the driving frequency.

The gradient level mode is the key to the concept of the nutating gradient level. This level and the analysis leading to its invention are described in Ref. 3. In addition to measuring level, the nutating gradiometer is capable of measuring simultaneously the vertical gradient in two orthogonal planes. These planes are aligned with the principal sections of the geopotential by sensing the variations of the vertical gradients with azimuth. Thus, a single device can sense the level direction of the geopotential surface as well as the azimuths and the vertical gradient of its principal sections.

This report is an outgrowth of two research studies in the field of aerial geodesy. One is concerned with aerial gravity measurements, and the other with establishing the geodetic altitude of an airborne camera. The nutating gradiometer, or an aggregate of other gradiometers having the same capabilities, promised to have applications in both problems. At first the two problems appeared totally different, belonging to two separate disciplines of geodesy. As the latent capabilities of the gradiometer became evident, they were applied differently to the two problems. Later it proved that the solutions to one problem enhanced the solutions to the other. Thus, the simultaneous considerations of both proved profitable.

The aim of this presentation is to explain the aerial capabilities of gradiometers. Gradiometers sense the parameters of the gravity field. Their measurements, therefore, result in information about the field which can be used to map it. Every gradiometer application is in effect a mapping process. Here this process is described from the point of view of physical geodesy. The primary objective is the improvement in accuracy and resolution of aerial measurements of gravity, as well as their reduction to the map of the geoid.

The direct application of gradient measurements to aerial measurements of gravity was analyzed under the subject contract. The analyses of the capabilities of the gradiometers, their application to aerial sectioning of the geopotentials, and the manner by which sectioning can improve the map of the geoid were the result of a separate investigation. This investigation, "Altitude Deviation Study," is performed under contract with the Research Institute for Geodetic Sciences, USA/ETL (U.S. Army Engineer Topographic Laboratories), Contract No. DAAK-02-67-C-0262.

II. LEVELING OF A MOVING PLATFORM

The inertial field of a point of measurement is described by its equation of motion in inertial space. The equation of motion of a point Q in the vicinity of the earth is derived in Ref. 4, paragraph 2.4, and, in a simplified form in Ref. 5. The expression for the inertial field vector depends on the coordinate systems in which the variables are expressed. Transformations of variables between the coordinate systems are described by the Coriolis theorem. Let Q be a point of measurement fixed on a platform which is translating and rotating with respect to the earth. The inertial field at Q may be expressed in the platform coordinate system by

$$\vec{F} = \underbrace{\left[\frac{d\vec{V}_P}{dt}\right]_P}_{\text{acceleration}} + \underbrace{2\vec{\Omega} \times \vec{V}_P + 2\vec{\omega} \times \vec{V}_P}_{\text{Coriolis effect}}$$

$$\text{specific force} = \text{acceleration} + \text{Coriolis effect}$$

$$- \vec{G} + \vec{\Omega} \times \vec{\Omega} \times \vec{R} \qquad (1)$$

$$\underbrace{\text{gravitation} + \text{centrifugal force}}_{\text{+ gravity}}$$

$$\underbrace{+ 2\vec{\Omega} \times \vec{\omega} \times \vec{R} + \vec{\omega} \times \vec{\omega} \times \vec{R}}_{\text{+ Eötvös effect}}$$

$$\underbrace{+ \left[\frac{d\vec{\omega}}{dt}\right]_P \times \vec{R}}_{\text{+ angular acceleration}}$$

where

$\vec{F} = \vec{F}_P \equiv$ total specific force at Q

$\vec{V}_P = \left[\frac{d\vec{R}}{dt}\right]_P \equiv$ platform velocity of Q with respect to the geocenter

$\vec{\Omega} = \vec{\Omega}_{EI} \equiv$ earth rotation with respect to inertial space

$\vec{R} = \vec{R}_P \equiv$ position vector of Q from the geocenter

$\vec{\omega} = \vec{\omega}_{PE} \equiv$ rotation of the platform with respect to the earth

$\vec{G} = \vec{G}_Q \equiv$ gravitation at Q

$\vec{g} = \vec{G}_Q - \vec{\Omega} \times \vec{\Omega} \times \vec{R} \equiv$ gravity at point Q

$\left[\frac{d}{dt}\right]_P \equiv$ time derivative in the platform coordinate system.

The inertial field vector consists of two major components, the constant field $\vec{p}$ and the gradient field $\vec{f}$. $\vec{p}$ is independent of $\vec{R}$, while $\vec{f}$ is a function of $\vec{R}$. Thus,

$$\vec{F} = \vec{p} + \vec{f} \tag{2}$$

where

$$\vec{p} = \left[\frac{d\vec{V}_p}{dt}\right]_P + 2\vec{\Omega} \times \vec{V}_P + 2\vec{\omega} \times \vec{V}p \tag{3}$$

and

$$\vec{f} = \vec{G} + (\vec{\Omega} + \vec{\omega}) \times (\vec{\Omega} + \vec{\omega}) \times \vec{R} + \left[\frac{d\vec{\omega}}{dt}\right]_P \times \vec{R} + (\vec{\Omega} \times \vec{\omega}) \times \vec{R} \ . \tag{4}$$

Let $\vec{a}_g$ be a unit vector in the direction of $\vec{g}$. $\vec{a}_g$ is then the direction of the vertical which is the perpendicular to the geopotential at Q. Leveling involves aligning in the direction of the vertical.

When the platform is stationary with respect to the earth, then $\vec{V}_p = 0$, $[d\vec{V}_p/dt]_p = 0$, $\vec{\omega} = 0$, and $[d\vec{\omega}/dt]_p = 0$. As a result, $\vec{F} = \vec{f} = \vec{g}$, and the inertial force field is equal to the gradient field, which in turn is equal to the gravity field. The direction of the gravity vertical or the direction of $\vec{g}$ can then be determined either with an inertial level, which measures the direction of $\vec{F}$, or a gradient level,[3] which measures the direction of $\vec{f}$.

A two-axis force sensor (such as a bubble level) constitutes an inertial level. In the conventional bubble level the bubble is under a curved surface, and it is centered only when its base plane is perpendicular to the inertial force $\vec{F}$. Uncertainties in measuring the bubble position limits it to sensitivities of 10^{-6} rad. In the limiting case, as the radius of curvature goes to infinity and the surface of the bubble becomes an optical flat, the bubble is stationary only when the optical flat is perpendicular to the inertial field, and the slightest tilt accelerates the bubble. Measurement of the motion of the bubble rather than its position has led to inertial bubble levels with sensitivities better than 10^{-9} rad (Ref. 6).

The bubble level loses its effectiveness on a moving platform. The instantaneous inertial field vector now deviates widely from the gravity field vector as a result of platform accelerations. This causes severe dynamic tracking problems, which result in lag errors and possibly, in extreme cases, in bubble breakdown. So long as the bubble can be kept intact and the lag errors within bound, it is possible to measure the long term average direction of the inertial field. This is facilitated in situations where $\overline{(d\vec{V}_p/dt)_p} = 0$. In that case,

$$\overline{(\vec{F})} = \overline{(2\vec{\Omega} \times \vec{V}_p)} + \overline{(2\vec{\omega} \times \vec{V}_p)} - \overline{(\vec{g})} + \overline{(2\vec{\Omega} \times \vec{\omega} \times \vec{R})} + \overline{(\vec{\omega} \times \vec{\omega} \times \vec{R})} \quad ; \quad (5)$$

When the motional terms are known, $\overline{(\vec{a}_g)}$ can be derived from $\overline{(\vec{a}_F)}$. Pure inertial leveling of a moving platform is difficult to implement; in addition, it requires a very long average distance, which limits its accuracy.

An alternative approach to inertial leveling by long term averaging is possible when independent estimates of $\vec{V}_p$ are available. To eliminate the breakup problem, the bubble is replaced with two crossed accelerometers. The level direction is computed from (1) using the measured values of $\vec{F}_p(t)$ and $\vec{V}_p(t)$. This technique, Doppler-inertial leveling, is discussed further in Ref. 7.

The gradient level is not sensitive to frame accelerations. The direction of the orthogonal gradient field vector therefore does not vary significantly from the vertical. The required averaging time is the same as in stationary operation. As a result, the gradient level is just as effective on a moving platform as in stationary measurements.

Rewriting (4) yields

$$\vec{g} = 2\vec{\Omega} \times \vec{\omega} \times \vec{R} + \vec{\omega} \times \vec{\omega} \times \vec{R} + \left[\frac{d\vec{\omega}}{dt}\right]_P \times \vec{R} - \vec{f} \; ; \qquad (6)$$

$\vec{a}_g$ can be shown to be equal to $\bar{a}_f$ when only the orthogonal component of $\bar{f}$ is measured.

When the frame of measurements is in orbit, $\vec{F} = 0$. As a result, it is impossible to measure $\vec{a}_g$ by inertial leveling. The gradient field, on the other hand, remains unmodified. Equation (6) still applies, and the gradient level will work. This extends the utility of the device to orbital operations.

This new independent capability for accurately leveling a moving platform on earth or in space is important to navigation and geodesy. The navigation applications of the gradient level are discussed in Ref. 7. This report explores its application to geodesy with emphasis on aerial physical geodesy.

III. MEASURING THE CURVATURE OF THE GEOPOTENTIALS

The geoid (mean sea level) and the geopotentials above it are solid surfaces which undulate about an ellipsoid of revolution.[8] Assume that any small region of the geopotential can be approximated by an ellipsoid of revolution. In that case the geopotential at any point can be defined by its two principal radii of curvature ρ and ν and by the azimuth ψ of the section whose radius is ρ (Ref. 9, p. 8.03). The azimuth of the section whose radius is ν is $\psi + (\pi/2)$. The curvature of the section whose azimuth is A is given by Euler's theorem[9]:

$$\frac{1}{r} = \frac{\cos^2(\psi - A)}{\rho} + \frac{\sin^2(\psi - A)}{\nu} \; . \qquad (7)$$

This section describes two techniques for measuring r. One makes use of a level sensor on a moving platform. The other requires the measurements of gravity intensity and the vertical gradient of gravity. This technique is also applicable to stationary measurements.

Let a measurement platform travel along a level surface with velocity $V = [d\vec{R}/dt]_E$ in the direction of azimuth A. Let a level sensor such as the gradient level operate on the measurement platform. The angular rotation of the level with respect to the earth is given by

$$\vec{\omega} = \vec{a}_t \cdot \left(\frac{V}{r}\right) + \vec{a}_v \cdot \left(\frac{d\chi}{dt}\right)_E + \vec{a}_g \cdot \left(\frac{dA}{dt}\right)_E \qquad (8)$$

where $\vec{a}_v$, $\vec{a}_t$, $\vec{a}_g$ form a right handed coordinate system; $\vec{a}_t$ is in the level plane with azimuth $(A + (R/2))$; $\vec{a}_v$ is in the level plane with azimuth A; and a_g is always in the direction of the vertical; r is the instantaneous radius of curvature of the geopotential section along the line of flight. $\chi = -\xi \sin A + \eta \cos A$ - the deflection of vertical in the direction of $A + (R/2)$.

$\vec{V}$ can be measured independently by Doppler radar or accelerometers. $\vec{\omega} \cdot \vec{a}_v \cdot (d\chi/dt)_E$ and $\vec{a}_g (dA/dt)_E$ can be measured by reference to an inertial platform. Substituting the measured values in (8) results in an estimate of r along the line of flight.

The measurement of r in any section, including the line of flight, is also possible with a vertical gradiometer. The two-dimensional gravity model in any section is circular. That is,

$$U = \frac{kM}{r}$$

$$g = -\frac{kM}{r^2}$$

$$\Gamma_A = \frac{\partial g}{\partial r} = \frac{2kM}{r^3} \qquad (9)$$

where

U ≡ gravity potential number

k ≡ universal gravitational constant

M ≡ effective mass of the earth along the section

Γ_A ≡ vertical gradient of gravity in the direction of azimuth A.

g is measured with a gavitometer, and Γ_A is measured with a vertical gradiometer whose plane coincides with A. On a moving platform the gradiometer measures the gradient in the direction of A along the line of flight. The corresponding average radius of curvature is computed from

$$r = - \frac{2g}{\Gamma_A} \quad . \tag{10}$$

For the purposes of vertical continuation the vertical gradient is taken as the average of the gradients in the directions of the principal sections (Ref. 9, pp. 7.26):

$$\Gamma = - g \left(\frac{1}{\rho} + \frac{1}{\nu} \right) \quad . \tag{11}$$

This model also applies to the decomposition of a single measurement of g into its component values (see Section V).

IV. CURVATURE AIDED LEVELING

The nutating gradiometer of Ref. 3 can perform the functions of a number of single plane gradiometers. It is in fact capable of simultaneously measuring Γ_ρ, Γ_ν, $\vec{a}_g$ and $\vec{a}_\psi$. The last section of Ref. 3 pointed out that the radius of curvature along the line of flight can be estimated either from Γ_A or from the angular rate of $\vec{a}_g$ along the line of flight. The estimate of r is more sensitive to pointing errors than to proportional errors in Γ_A (Ref. 10). At the same time, the threshold sensitivities for both modes of operation in the nutating gradiometer are the same.[3] These two conditions can be used to enhance the resolution of the gradient level while retaining its accuracy.

The threshold sensitivity of a gradiometer is a function of its quadrupole constants (mass of the pole and length of the quadrupole arm), and the integration time. In the nutating gradiometer the quadrupole constants are the same in both modes. When the integration time is the same in both modes, the estimate of curvature from the vertical gradient is more accurate than its estimate from the level rate. When the integration time of the vertical mode is reduced, to give curvature estimates which are equal in accuracy to the estimates from the level rate, the resolution of the measurements increases. The increase in resolution is by $(\sqrt{6}/\pi)(r/\ell)$ where ℓ is the length of arc traveled during the integration time of the level mode.[10] This accommodates higher frequency undulations in the geopotential without aliasing errors.

The techniques of physical geodesy were originally developed for gravity measurements taken on the earth surface. High cost and complicated logistics preclude the attainment of adequate coverage of the globe with surface measurements in the near future.[11] Aerial measurements of gravity offer an alternative to surface measurements. They have the advantage of speed, mobility, and access to remote areas, and thus overcome many of the problems of surface measurements.

The most advanced system for airborne measurement of gravity is now under evaluation by the gravity branch of the AFCRL Terrestrial Sciences Laboratories. This system is described in some detail in Ref. 12. Figure 1 describes the operational profile of the system.

The aircraft attempts to fly a constant heading course on a single geopotential. The actual flight altitude differs from the desired course because of the characteristics of the autopilot. This needs to be compensated for in the data reduction. The system employs barometric means for sensing the altitude deviations from the geopotential. The isobaric section does not coincide with the geopotential section. An estimate of its deviation from the geop is computed during data reduction. The three major error sources in this process are the compensated height uncertainty, the uncertainty in the estimate of the isobaric height deviations from the geop, and the representation error which results from aliasing the high frequency unmodulations of the geop.

The airborne gravitometer is a special purpose single axis integrating accelerometer, designed for stability and accuracy over a limited range of g values. It measures the average component of the inertial field $(\vec{F})$ in the direction in which it is pointing. The inertial field at a point occupied by the gravitometer is given by (1). The average measurement is given by (5). Equation (5) can be further simplified by taking note that $E[(\vec{V}_p)] \rightarrow 0$. The gravitometer is always pointed in the direction of $\vec{a}_R$ by the navigation system. Estimates of $(\vec{R})$ and $(\vec{\omega}) = (\vec{V} \times \vec{a}_R/R)$ are also derived from the navigation system. This procedure is similar in nature to the pure inertial leveling of a moving platform discussed in Section II. Errors in this measurement are introduced by the following sources: gravitometer errors, residual vertical acceleration due to $(d\vec{V}_p/dt)_p \neq 0$, level errors due to $\overline{a_R} \neq \overline{a_g}$, and navigation errors as reflected in the Eötvös correction.

To map the geoid, the measured values of the external gravity field must be continued downward to sea level. The techniques for vertical continuation involve spatial correlation of measurements.[13] They all depend on the estimate of the geopotential height and a standard model of the external field. This provides two other sources of error in the final result. The first is the uncertainty in height, and the second results from local variations of the field.

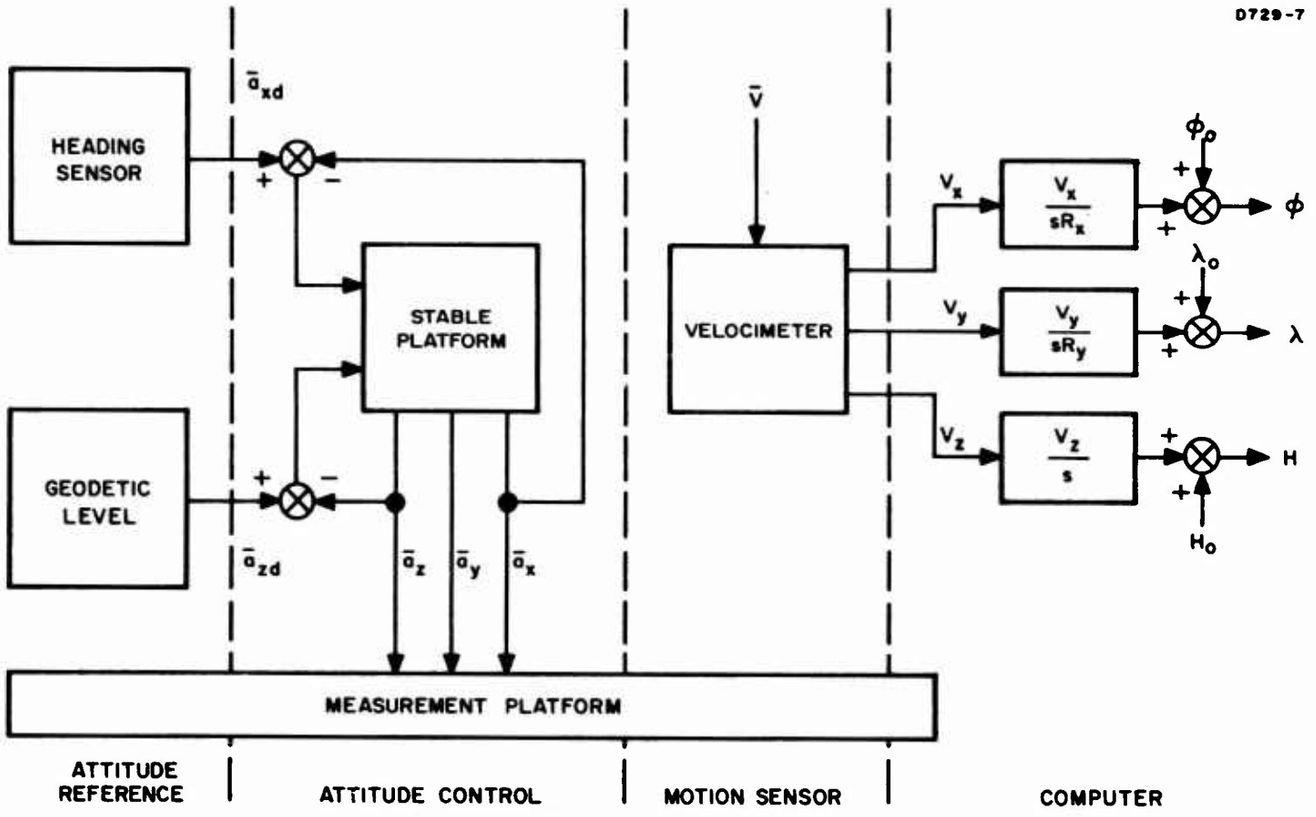

Fig. H-1. Conceptual diagram of a dead reckoning navigation system.

When leveling a moving platform, the instrument senses the average error from true level. The true level direction changes as the instrument moves in space during the averaging time. When the integrating time is short compared with the time behavior of the scanned undulations of the geopotential, the curvature of the geopotential can be predicted from the level rate. This predicted curvature is then used to precess the level during the averaging time. This compensates for the motion of the level.

The curvature estimates from the vertical gradient mode can also be used to precess the level during its averaging time. The required integrating time of the curvature estimates is smaller than the level integrating time. This permits the removal of effects of high frequency undulations which cannot be directly tracked by the level mode. The resulting estimate of the level error is free from aliasing errors. The level at all times actually points in the proper direction as determined by instantaneous curvature. The process is in effect equivalent to increasing the frequency response of a low pass filter by the addition of a parallel band-pass filter.

Curvature aided leveling along the line of flight improves the resolution in one dimension of a two-dimensional situation. Unfortunately, the "twist rate" or precession normal to the line of flight cannot be estimated from the curvature. Therefore, it is not possible to improve the spatial resolution in that direction without a priori mapping. Fortunately, in most applications level accuracy along the line of flight is more important than level accuracy in the transverse direction.

V. AERIAL MEASUREMENTS OF GRAVITY

Two important problems in geodesy are the mapping of the external gravity field and the determination of the shape of the geoid. The two problems are interrelated because one can be estimated from the other by vertical continuation.

Physical geodesy provides one of the more promising approaches to this mapping problem.[8, 9] In this method the geometrical parameters of the geoid at any point are determined by the correlation of gravity intensity measurements taken all over the globe. The measured values are reduced to mean sea level and the gravity anomalies Δg's, the differences between the reduced values and those computed from the standard gravity formula, are derived. The height anomaly N at any point is computed by means of the Stoke's formula. The gravimetric deflections of vertical at that point ξ_g and η_g are computed by means of the Vening Meinesz formula (ibid).

Conceptually, gradiometers can directly improve the accuracy of aerial gravity measurements in three ways:

1. Eliminate leveling errors.

2. Improve the local model of the external field by vertical gradient measurements. This should improve the accuracy of downward continuation to the geoid and the height compensation of the gravitometer.

3. Reduce representation errors by estimating the true radii of curvature of the geopotential from vertical gradient measurements. Vertical gradient measurements can be done faster than gravity measurements. When done to a commensurate precision they permit the resolution of the average gravitometer measurement to its components.

The procedure for reducing the representation error by vertical gradient measurements is based on the following two relationships:

$$g_i = \sqrt{-\frac{U\Gamma_i}{2}} \qquad (12)$$

and

$$\sqrt{-\frac{U}{2}} = \frac{g}{\frac{1}{I}\sum_{i=1}^{I} (\Gamma_i)^{1/2}} \quad . \qquad (13)$$

Here g is the measured average value of gravity intensity,

$$\Gamma_i = \frac{\Gamma_{\rho_i} + \Gamma_{\nu_i}}{2}$$

is the average vertical gradient of the i^{th} spatial component, g_i is the gravity intensity of the i^{th} component and

$$g = \frac{1}{I}\sum_{i=1}^{I} g_i \quad .$$

Assume that each vertical gradient measurement is limited by a random error, and that the expected rms value of this error is the same in all measurements. Under these conditions the estimate of the rms fractional error in g_i is given by

$$\left(\frac{\sigma g_i}{g_i}\right) = \sqrt{2}\left[\left(\frac{\sigma g}{g}\right)^2 + \left(\frac{\sigma \Gamma_i}{\Gamma_i}\right)^2 \left(1 + \frac{1}{I}\right)\right]^{1/2} . \qquad (14)$$

Thus if

$$\frac{\sigma \Gamma_i}{\Gamma_i} \leq \frac{\sigma g}{g}$$

it is possible to improve the resolution of the gravitometer without decreasing its averaging time. The averaging time determines the uncertainty in gravity measurements due to residual vertical accelerations of the gravitometer. This error source depends on aircraft control characteristics and aerodynamics and is very difficult to reduce by means other than long term averaging. This is why the possibility of improving the measurements with gradiometer measurements is of interest.

A gradiometer, accurate enough to improve the resolution of gravity measurements directly, presents a very difficult design problem. The main concern is with linear dynamic range. A scanning gradiometer is always modulated by the full magnitude of the gradient. This precludes the biased mode of operation which is used to extend the sensitivity of gravitometers. On the other hand, small gravity gradients are easy to generate accurately. This may permit a time shared mode of operation which calibrates a small range around a fixed but unknown value. Unfortunately, such a device is not useful for accurately decomposing g, except perhaps, at very high altitudes.

Gradiometers, in addition to the direct improvements in accuracies of aerial gravity measurements, can also help indirectly. They are useful to a number of other systems which can reduce the errors in the measurements. In particular, the class of systems described in Ref. 7 can reduce all errors related to level navigation. The class of systems described in Ref. 10 can, in addition, compensate the flight to the true geopotential section to a very high accuracy, reduce

$$E\left[\left(\frac{d\vec{V}_p}{dt}\right)_p\right]^2 ,$$

and measure the height of the geopotential more accurately. Thus, with the aid of gradiometers, it becomes possible to reduce the errors from all the sources limiting the present system.

VI. GEOPOTENTIAL SECTIONING

Gradient measurements make possible another method for mapping the external gravity field. This method is aerial sectioning of the geopotentials. The method is equivalent conceptually to surface astrogeodesy (Refs. 8 and 9). A number of system configurations which can derive geopotential section lines are described in Ref. 10. These systems fall into two categories: the first operates in a manner analogous to surface astrogeodetic measurements; the second reconstructs the section line from curvature measurements. For simplicity, the concept will be explained in terms of the first category of systems.

This astrogeodetic method employs a level and an inertial attitude reference (a star tracker or a stable platform) to determine the astronomical deflections of vertical ξ_a and η_a. The station latitude and longitude of the measurement must be known to an angular accuracy commensurate with the measurement accuracy. As a result, surface stations must be precisely surveyed, whereas aerial systems require precise navigation. The measurements are used to plot geopotential sections in the local datum coordinate system.

Surface astrogeodesy is at present confined to land areas. Therefore, it is limited by the necessity for dependence on local datum coordinates. Aerial sectioning, on the other hand, can be extended to gird the globe. As a result it should be possible to completely map the geoid or other geopotentials using a single datum. This possibility is particularly attractive with orbital surveying systems.

A satellite-borne sectioning system is capable of covering the globe in a short period of time. Its potential accuracy is better than that of present day satellite geodesy, which estimates the spherical harmonics of the external gravity field from orbital tracking.[14] Measurements made by this method should supplement and enhance the results of physical geodesy. They should also provide the best map of the field in near space.

The required gradiometer accuracies for a sectioning are commensurate with those of the curvature aided leveling. The level accuracies are directly comparable to proportional g accuracies but the vertical gradient accuracies are considerably more relaxed. As a result, high resolution sectioning presents a simpler instrumentation problem than high resolution measurements of gravity. In orbit there may not be a need for curvature aiding, as a result the measurements of angles transverse to the orbit are as accurate as the measurement along the orbit. Aerial measurements of angles on the other hand are more accurate along the line of flight because of curvature aiding. As a result sectioning by curvature is preferred whenever curvature aiding is required.

The Stokes formula for estimating the height anomaly N from the gravity anomalies Δg_q's may also be used in reverse to estimate the high resolution Δg_q's from N_p values obtained by sectioning. This reverse capability provides an alternative to high resolution measurements of gravity. It trades off a difficult instrumentation problem for a much increased computational load.

The Stokes formula is a linear equation in Δg_q's. A set of such equations is required to derive the height anomalies N_p's in a given area. Conceptually, it is possible to employ linear algebra and determinant manipulations to derive a set of linear equations which express Δg_q in terms of the N_p's. The values of Δg_q will depend on N_o of the datum system used for deriving the N_p's. Using statistical estimation techniques it is possible to change N_o of the datum system so the computed values of

$$\left(\frac{1}{I}\sum_{i=1}^{I}\Delta g_i\right)$$

agree most closely with the measured Δg's. The N_p values which provide the best fit are those which would be computed from direct measurements of the Δg_i's by the technique of Section V. Thus, the two methods are equivalent.

Similarly, the Vening Meinesz formula which relates the deflections of vertical ξ and η from Δg_g is also a linear equation. It too can be reversed and used to compute Δg_q from ξ_p and η_p. Statistical estimating techniques will remove ξ_o and η_o of the ^{p} datum, thus resulting in ξ_g and η_g, the gravimetric deflections of vertical.

The adjustment of the datum system to agree with results of the gravity measurements results in a geopotential map which is referenced to the international ellipsoid.[8] This adjustment may be carried at the geopotential which is being mapped. By repeating the process at different altitudes it is possible to map the true vertical profile of the external field. This should improve the accuracy of vertical continuation in either direction, and improve the map of the geoid.

PRECEDING PAGE BLANK - NOT FILMED.

REFERENCES

1. R.L. Forward, C.C. Bell, J.R. Morris, L.R. Miller, D. Berman, and J.M. Richardson, "Research on Gravitational Mass Sensors," Final Report, Contract NASW 1035, Hughes Research Laboratories, Malibu, California, June 1966.

2. "Vertical Gravity Gradiometer Development," Proposal No 67M-7497/B1104-1, Hughes Research Laboratories, Malibu, California, April 1967.

3. E. Hose, "The Nutating Gradient Level," IDC 2766/74, Hughes Aircraft Company, Culver City, California, September 1967.

4. G.R. Macomber and M. Fernandez, Inertial Guidance Engineering (Prentice-Hall, Englewood Cliffs, N.J., 1962).

5. C.F. Edge, "DDA's Versus GP Digital Computers for Schuler-Tuned Inertial Navigation Systems," IEEE Trans. MIL-7, 23 (1963).

6. "Digital Tiltmeter Model DTM-10," Applications Brochure, Hughes Research Laboratories, Malibu, California, 1966.

7. E. Hose, "Level Navigation," IDC 2766/89, Hughes Aircraft Company, February 1968.

8. W.A. Heiskanen, The American Institute of Physics Handbook 2nd ed. (McGraw-Hill, New York, 1963), Section 2i, "Geodesy."

9. G. Bomford, Geodesy (Oxford University Press, New York, 1962).

10. E. Hose, "Aerial Terrain Height Determination," IDC 2766/80, Hughes Aircraft Company, Culver City, California, 10 November 1967.

11. R.K. Burkard, "Geodesy for the Layman," Aeronautical Chart and Information Center, St. Louis, Mo., November 1964, AD-617530.

12. L.G.D. Thompson and C.S. Hawkins, Advances in Aerial Gravity 1963 - 1964 (American Geophysical Union, Washington, D.C., 1966).

13. H. Moritz, "Methods for Downward Continuation of Gravity," AFCRL, Bedford, Mass., Dept. of Geodetic Sciences, Report No. 67, April 1966.

14. W.M. Kaula, Theory of Satellite Geodesy (Blaisdell, Waltham, Mass., 1966).

Unclassified
Security Classification

DOCUMENT CONTROL DATA - R&D
(Security classification of title, body of abstract and indexing annotation must be entered when the overall report is classified)

1. ORIGINATING ACTIVITY (Corporate author)	2a. REPORT SECURITY CLASSIFICATION
Hughes Research Laboratories 3011 Malibu Canyon Road Malibu, California 90265	Unclassified
	2b. GROUP N/A

3. REPORT TITLE

RESEARCH TOWARD FEASIBILITY OF AN INSTRUMENT FOR MEASURING VERTICAL GRADIENTS OF GRAVITY

4. DESCRIPTIVE NOTES (Type of report and inclusive dates)

Final Report, 15 July 1966 through 15 September 1967

5. AUTHOR(S) (Last name, first name, initial)

Forward, Robert L.

6. REPORT DATE	7a. TOTAL NO. OF PAGES	7b. NO. OF REFS
October 1967		0

8a. CONTRACT OR GRANT NO.	9a. ORIGINATOR'S REPORT NUMBER(S)
AF 19(628)-6134 b. PROJECT NO. 8607 c. d.	N/A 9b. OTHER REPORT NO(S) (Any other numbers that may be assigned this report)

10. AVAILABILITY/LIMITATION NOTICES

11. SUPPLEMENTARY NOTES	12. SPONSORING MILITARY ACTIVITY
	AFCRL Office of Aerospace Research L. G. Hanscom Field, Bedford, Mass.

13. ABSTRACT

The theories for the determination of the Newtonian gravitation constant (G) and the earth's gravitational constant (GM) have been examined. Two experiments have been considered for determining the Newtonian constant, one of which appears to be capable of improving the accuracy of measurement of G by at least one order of magnitude. Measurement of GM by gradient techniques does not, however, appear to yield any improved accuracy.

Experimental tests have demonstrated that the rotating gravitational gradient sensor concept is capable of measuring static gravitational gradients in the 1 g environment of the earth and that the sensor designs have the accuracy needed for useful measurements (~~0.5 x 10⁻⁹ sec⁻²~~). A design of a prototype transportable gradiometer system has been completed and a program for fabrication and test has been established.

A study of sensor applications indicates that these sensors can aid in airborne gravimetry surveys by improving the guidance system performance and by obtaining a real time measurement of local gravity anomalies.

(5 to the minus 9th power/square sec)

DD FORM 1 JAN 64 1473

Unclassified
Security Classification

14 KEY WORDS	LINK A		LINK B		LINK C	
	ROLE	WT	ROLE	WT	ROLE	WT
Newtonian gravitational constant Gravitational mass sensor Gravitational gradient sensor Earth's gravitational constant Navigation Gravity mapping Gravity gradiometer						

INSTRUCTIONS

1. ORIGINATING ACTIVITY: Enter the name and address of the contractor, subcontractor, grantee, Department of Defense activity or other organization *(corporate author)* issuing the report.

2a. REPORT SECURITY CLASSIFICATION: Enter the overall security classification of the report. Indicate whether "Restricted Data" is included. Marking is to be in accordance with appropriate security regulations.

2b. GROUP: Automatic downgrading is specified in DoD Directive 5200.10 and Armed Forces Industrial Manual. Enter the group number. Also, when applicable, show that optional markings have been used for Group 3 and Group 4 as authorized.

3. REPORT TITLE: Enter the complete report title in all capital letters. Titles in all cases should be unclassified. If a meaningful title cannot be selected without classification, show title classification in all capitals in parenthesis immediately following the title.

4. DESCRIPTIVE NOTES: If appropriate, enter the type of report, e.g., interim, progress, summary, annual, or final. Give the inclusive dates when a specific reporting period is covered.

5. AUTHOR(S): Enter the name(s) of author(s) as shown on or in the report. Enter last name, first name, middle initial. If military, show rank and branch of service. The name of the principal author is an absolute minimum requirement.

6. REPORT DATE: Enter the date of the report as day, month, year; or month, year. If more than one date appears on the report, use date of publication.

7a. TOTAL NUMBER OF PAGES: The total page count should follow normal pagination procedures, i.e., enter the number of pages containing information.

7b. NUMBER OF REFERENCES: Enter the total number of references cited in the report.

8a. CONTRACT OR GRANT NUMBER: If appropriate, enter the applicable number of the contract or grant under which the report was written.

8b, 8c, & 8d. PROJECT NUMBER: Enter the appropriate military department identification, such as project number, subproject number, system numbers, task number, etc.

9a. ORIGINATOR'S REPORT NUMBER(S): Enter the official report number by which the document will be identified and controlled by the originating activity. This number must be unique to this report.

9b. OTHER REPORT NUMBER(S): If the report has been assigned any other report numbers *(either by the originator or by the sponsor)*, also enter this number(s).

10. AVAILABILITY/LIMITATION NOTICES: Enter any limitations on further dissemination of the report, other than those imposed by security classification, using standard statements such as:

(1) "Qualified requesters may obtain copies of this report from DDC."

(2) "Foreign announcement and dissemination of this report by DDC is not authorized."

(3) "U. S. Government agencies may obtain copies of this report directly from DDC. Other qualified DDC users shall request through _____."

(4) "U. S. military agencies may obtain copies of this report directly from DDC. Other qualified users shall request through _____."

(5) "All distribution of this report is controlled. Qualified DDC users shall request through _____."

If the report has been furnished to the Office of Technical Services, Department of Commerce, for sale to the public, indicate this fact and enter the price, if known.

11. SUPPLEMENTARY NOTES: Use for additional explanatory notes.

12. SPONSORING MILITARY ACTIVITY: Enter the name of the departmental project office or laboratory sponsoring *(paying for)* the research and development. Include address.

13. ABSTRACT: Enter an abstract giving a brief and factual summary of the document indicative of the report, even though it may also appear elsewhere in the body of the technical report. If additional space is required, a continuation sheet shall be attached.

It is highly desirable that the abstract of classified reports be unclassified. Each paragraph of the abstract shall end with an indication of the military security classification of the information in the paragraph, represented as *(TS), (S), (C), or (U)*.

There is no limitation on the length of the abstract. However, the suggested length is from 150 to 225 words.

14. KEY WORDS: Key words are technically meaningful terms or short phrases that characterize a report and may be used as index entries for cataloging the report. Key words must be selected so that no security classification is required. Identifiers, such as equipment model designation, trade name, military project code name, geographic location, may be used as key words but will be followed by an indication of technical context. The assignment of links, rules, and weights is optional.

GPO 886-551

SUPPLEMENTARY

INFORMATION

AD-828 853

HUGHES *Research Laboratories*
A DIVISION OF HUGHES AIRCRAFT COMPANY
3011 MALIBU CANYON ROAD
MALIBU, CALIFORNIA

ERRATA

Research Toward Feasibility of an Instrument for Measuring Vertical Gradients of Gravity

Final Report
Contract No. AF 19(628)-6134
AFCRL-67-0631
dated October 1967

1. Page iii

   III Determination of the Earth's Gravitational Constant (G)

   should read

   III Determination of the Earth's Gravitational Constant (GM)

2. Page H-1, line 4

   $\vec{a}_t$ Unit vector in the direction of $A + \frac{R}{2}$

   should read

   $\vec{a}_t$ Unit vector in the direction of $A + \frac{\pi}{2}$

3. Page H-10, line 8

   $\vec{a}_g$ can be shown to be equal to $\bar{a}_f$ ...

   should read

   $\vec{a}_g$ can thus be computed from $\bar{a}_f$ ...

4. Page H-11, line 8

   ... the level plane with azimuth $(A + (R/2))$; $\bar{a}_v$ is in the level plane with azimuth A; and a_g is always in the direction of the vertical;...

should read

...the level plane with azimuth $(A + (\pi/2))$; $\bar{a}_v$ is in the level plane with azimuth A; and $\vec{a}_g$ is always in the direction of the vertical;...

5. Page H-11, line 12

... direction of $A + (R/2)$.

should read

... direction of $A + (\pi/2)$.

6. Page H-12, line 16

delete ... of Ref. 3 ...

7. Page H-13

renumber to Page H-14

8. Page H-14

replace Fig. 1 with attached Figure 1 and renumber as Page H-15

9. Page H-15

renumber to Page H-13

10. Page H-17, last line

$$E\left[\left(\frac{\overrightarrow{dV_p}}{dt}\right)_p\right]^2$$

should read

$$E\left[\left(\frac{\overrightarrow{dV_p}}{dt}\right)^2_p\right]$$

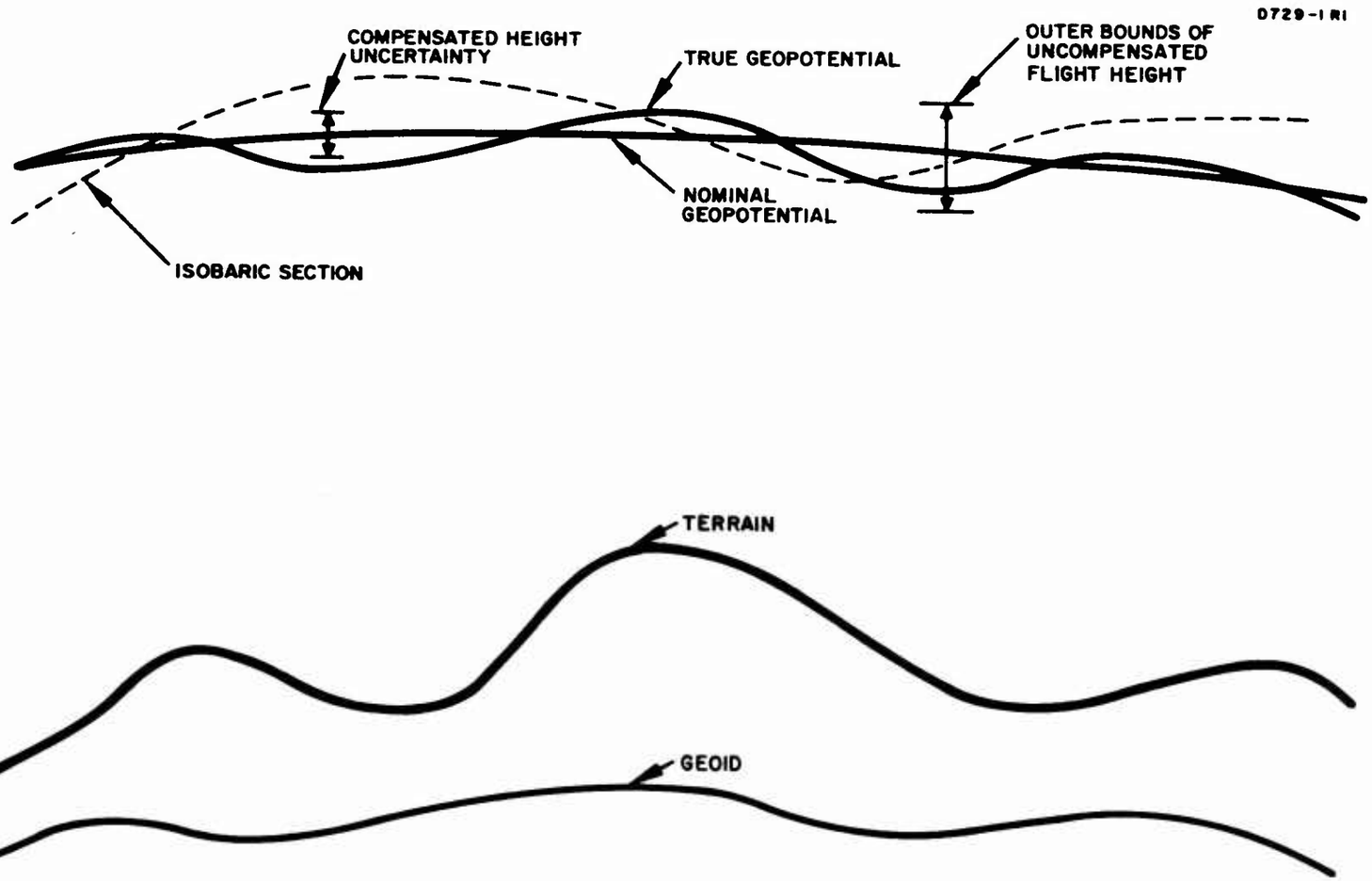

Fig. H-1. Operational profile of the present system for airborne measurements of the geopotential.

SUPPLEMENTARY

INFORMATION

IDENTIFICATION	FORMER STATEMENT	NEW STATEMENT	AUTHORITY
AD-828 853L Hughes Research Labs., Malibu, Calif. Final rept. 15 Jul 66-14 Sep 67. Rept. no. AFCRL-67-0631 Oct 67 Contract AF 19(628)-6134	Controlled: all requests to Air Force Cambridge Research Labs., Attn: CRUL, L. G. Hanscom Field, Bedford, Mass.	No limitation	AFCRL ltr, 29 Apr 69